Institut für Geowissenschaften, Universität Potsdam, Deutschland

Laboratoire PEPS, UMR 5125, Université Claude Bernard – Lyon 1, France

Doctoral thesis

Presented to obtain the Academic Degrees

"Doktor der Naturwissenschaften an der Universität Potsdam"

and

"Docteur de l'Université Claude Bernard – Lyon 1"

under the convention of

"Gemeinsam Betreute Promotion"

"Cotutelle de thèse"

Speciality: Geology

THE ARAL SEA: A PALAEOCLIMATE ARCHIVE

by

Philippe SORREL

Defended in Potsdam 13 July 2006

Joined German-French examination committee

Roland OBERHÄNSLI, Universität Potsdam	**PhD supervisor**, reviewer
Jean-Pierre SUC, Université C. Bernard-Lyon I	**PhD supervisor**
Christophe LÉCUYER, Université C. Bernard-Lyon I	Reviewer
Volker MOSBRUGGER, Forschungsinstitut Senckenberg	Reviewer
Gerald HAUG, GeoForschungsZentrum Potsdam	Examination
Hedwig OBERHÄNSLI, GeoForschungsZentrum Potsdam	Examination
Martin HEAD, Brock University, Canada	Examination
Spéranta-Maria POPESCU, Université C. Bernard-Lyon I	Examination
Axel BRONSTERT, Universität Potsdam	Examination

Institut für Geowissenschaften, Universität Potsdam, Deutschland

Laboratoire PEPS, UMR 5125, Université Claude Bernard – Lyon 1, France

Doctoral thesis

Presented to obtain the Academic Degrees

"Doktor der Naturwissenschaften an der Universität Potsdam"

and

"Docteur de l'Université Claude Bernard – Lyon 1"

under the convention of

"Gemeinsam Betreute Promotion"

"Cotutelle de thèse"

Speciality: Geology

THE ARAL SEA: A PALAEOCLIMATE ARCHIVE

by

Philippe SORREL

Defended in Potsdam 13 July 2006

Joined German-French examination committee

Roland OBERHÄNSLI, Universität Potsdam	**PhD supervisor**, reviewer
Jean-Pierre SUC, Université C. Bernard-Lyon I	**PhD supervisor**
Christophe LÉCUYER, Université C. Bernard-Lyon I	Reviewer
Volker MOSBRUGGER, Forschungsinstitut Senckenberg	Reviewer
Gerald HAUG, GeoForschungsZentrum Potsdam	Examination
Hedwig OBERHÄNSLI, GeoForschungsZentrum Potsdam	Examination
Martin HEAD, Brock University, Canada	Examination
Spéranta-Maria POPESCU, Université C. Bernard-Lyon I	Examination
Axel BRONSTERT, Universität Potsdam	Examination

Acknowledgments

Since beginning of 2003, this PhD thesis under the German-French convention of "Gemeinsam Betreute Promotion" / "Co-tutelle de thèse" offered me the opportunity to share my time between the GeoForschungsZentrum Potsdam, the University Claude Bernard of Lyon and the University of Potsdam. Today I would like to thank all the people who contributed to the progress of this thesis, as well as all those that I have met since the 4th of November 2002 and who have enriched me a lot, both scientifically and personally.

I gratefully acknowledge the project CLIMAN, from where this thesis outcomes. This work was supported by the INTAS organization of the European Union (Project N° Aral 00-1030) and the German Science Foundation (DeutscheForschungGemeinshaft, under contract 436 RUS 111/663 – OB 86/4). I also acknowledge the GFZ Potsdam and the University of Lyon 1 for providing me all the scientific, infrastructural and friendly contributions during these last three years.

First of all, I would like to warmly thank Dr. Hedi Oberhänsli, my supervisor at the GFZ Potsdam and the initiator of the project CLIMAN, who gave me the opportunity to be involved in a wonderful international team, and entrusted me with this PhD thesis. She was a great mentor, provided me countless fruitful ideas and the required support on my work. She was always trustful with my initiatives and every day extremely motivated.

To similar regards, I warmly thank Prof. Dr. Jean-Pierre Suc and Dr. Speranta-Maria Popescu from the University of Lyon, for the considerable support they provided me day after day. They were formidable supervisors. I thank Jean-Pierre Suc for his precious and great experience on pollen grain taxonomy and his fruitful ideas. He also made my participation to several congresses possible and highly encouraged me to present my results during internal seminars at the University of Lyon. I warmly thank Speranta-Maria Popescu for introducing me to the identification of dinoflagellate cysts, for her great kindness and her black coffee. She was a wonderful roommate.

Particular thanks are addressed to my two supervisors in chief, Prof. Dr Roland Oberhänsli (University of Potsdam) and Prof. Dr. Jean-Pierre Suc (University Claude Bernard-Lyon 1) who made this collaboration between respective institutions possible. I acknowledge the administration staff from both universities for their fast and pleasant way in solving problems. They were of great help.

I would like to gratefully thank Dr Stefan Klotz (University of Tübingen) who introduced me to the "probability mutual climatic spheres" (PCS) method. Many thanks also for our countless discussions and for his contributions to this work. He was also a very good friend, who always enjoyed the idea to share a beer at the "Palais de la bière" of Lyon, sometimes late in the night.

Prof. Dr. Martin Head (Brock University, Canada) is kindly acknowledged for his precious help during my first steps in learning taxonomy of dinoflagellate cysts. I also thank him for his kindness in inviting me three days at the Geographical Institute of Cambridge, and for his hospitality. I had the great opportunity to share his house and to meet his sweet family.

Acknowledgments

I warmly thank Prof. Gerald Haug (GFZ Potsdam, Universität Potsdam) for his precious advices, his enthusiasm and his support during my PhD.

I would like to thank Dr. Nick Boroffka (GFZ Potsdam) for his help and his kindness during the CLIMAN expedition in the delta of the Amu Darya in summer 2003. He was always very patient with me and often supported my bad character. He is someone that I will not forget, and receives my sincere admiration. I also thank him for the fruitful scientific discussions we had together, both on the field and later in Potsdam.

Thanks to all members of the CLIMAN project from various horizons, especially Patrick Austin and Dr. Anson Mackay (Univeristy College of London), Dr. Danis Nourgaliev (Kazan University), Dr. Jana Friedrich (AWI Bremerhaven) Dr. Sergey Krivonogov (RAS Novosibirsk) and Dr. Dietmar Keyser (University of Hamburg). Thanks to all members of the NATO project for the very pleasant time we had in Moscow in October 2005, especially Dr. Peter Zavialov and Dr. Phil Sapozhnikov (Shirshov Institute of Oceanology, Moscow) and Christine Heim (AWI Bremerhaven).

I would like to warmly thank Prof. Gerald Haug and Prof. Axel Bronstert (Universität Potsdam) for their presence in the examination committee, as well as Prof. Roland Oberhänsli (Universität Potsdam), Prof. Volker Mosbrugger (Forschungsinstitut Senckenberg Frankfurt), Prof. Christophe Lécuyer (Université Claude Bernard-Lyon 1) and Prof. Martin Head (Brock University) for accepting to evaluate this work.

Another big thank to Dominique Barbe and Sophie Passot for their tremendous help in printing the manuscripts, and above all, for their kindness and availability.

I especially gratefully thank Dr. Francois Demory (University of Marseille) for his countless advices during the first year of my PhD. He always helped me when my scientific competence reached its borders. He was a nice flatmate in Potsdam too. I thank his wife, Dr. Juliette Lamarche (University of Marseille) for her daily good mood and for her recommendable “tarte au Maroilles”.

Many thanks to Matthias Zopperitsch for his friendship during the 3 years of this PhD and Samuel Jaccard (ETH Zürich) for the nice moments we had together in Bremen. Great thanks to Christophe Pelosi for being a wonderful flatmate in Potsdam.

Thanks are adressed to Andrew Cavanagh, Hans von Suchodoletz, Fabien Magri, Youri Maystrenko, Judith Sippel, Leni, Sushma Prasad, Björn Lewerenz, Andrea Rieser and Katka Novotna for their good mood and the nice moments at the 4th level of GFZ Potsdam.

Thanks to Sam, Matt and Tof for being true friends. Thanks to my father for his disponibility and his patience during the stressful period of writing.

Je remercie enfin du fond du coeur Cloé, ainsi que ma mère, pour leur soutien permanent et pour avoir supporté mes accès d’humeur, mes découragements. Merci à toi Cloé de m’avoir accompagné jusqu’au bout, même jusqu’à Potsdam. Ce travail est dédié à ma mère, qui a toujours cru en moi et qui a suivi avec passion chaque étape, chaque moment de ce travail au cours des 3 dernières années. Un immense merci à vous.

Abstract

The intracontinental endorheic Aral Sea, remote from oceanic influences, represents an excellent sedimentary archive in Central Asia that can be used for high-resolution palaeoclimate studies. We performed palynological, microfacies and geochemical analyses on sediment cores retrieved from Chernyshov Bay, in the NW part of the modern Large Aral Sea. The most complete sedimentary sequence, whose total length is 11 m, covers approximately the past 2000 years of the late Holocene.

High-resolution palynological analyses, conducted on both dinoflagellate cysts assemblages and pollen grains, evidenced prominent environmental change in the Aral Sea and in the catchment area. The diversity and the distribution of dinoflagellate cysts within the assemblages characterized the sequence of salinity and lake-level changes during the past 2000 years *(Chapter III)*. Due to the strong dependence of the Aral Sea hydrology to inputs from its tributaries, the lake levels are ultimately linked to fluctuations in meltwater discharges during spring. As the amplitude of glacial meltwater inputs is largely controlled by temperature variations in the Tien Shan and Pamir Mountains during the melting season, salinity and lake-level changes of the Aral Sea reflect temperature fluctuations in the high catchment area during the past 2000 years. Dinoflagellate cyst assemblages document lake lowstands and hypersaline conditions during ca. 0–425 AD, 920–1230 AD, 1500 AD, 1600–1650 AD, 1800 AD and since the 1960s, whereas oligosaline conditions and higher lake levels prevailed during the intervening periods. Besides, reworked dinoflagellate cysts from Palaeogene and Neogene deposits happened to be a valuable proxy for extreme sheet-wash events, when precipitation is enhanced over the Aral Sea Basin as during 1230–1450 AD. We propose that the recorded environmental changes are related primarily to climate, but may have been possibly amplified during extreme conditions by human-controlled irrigation activities or military conflicts *(Chapter VI)*. Additionally, salinity levels and variations in solar activity show striking similarities over the past millennium, as during 1000–1300 AD, 1450–1550 and 1600–1700 AD when low lake levels match well with an increase in solar activity thus suggesting that an increase in the net radiative forcing reinforced past Aral Sea's regressions.

On the other hand, we used pollen analyses to quantify changes in moisture conditions in the Aral Sea Basin *(Chapter IV)*. High-resolution reconstruction of precipitation (mean annual) and temperature (mean annual, coldest versus warmest month) parameters are performed using the "probability mutual climatic spheres" method, providing the sequence of

climate change for the past 2000 years in western Central Asia. Cold and arid conditions prevailed during ca. 0–400 AD, 900–1150 AD and 1500–1650 AD with the extension of xeric vegetation dominated by steppe elements. Conversely, warmer and less arid conditions occurred during ca. 400–900 AD and 1150–1450 AD, where steppe vegetation was enriched in plants requiring moister conditions. Change in the precipitation pattern over the Aral Sea Basin is shown to be predominantly controlled by the Eastern Mediterranean (EM) cyclonic system, which provides humidity to the Middle East and western Central Asia during winter and early spring. As the EM is significantly regulated by pressure modulations of the North Atlantic Oscillation (NAO) when the system is in a negative phase, a relationship between humidity over western Central Asia and the NAO is proposed.

Besides, laminated sediments record shifts in sedimentary processes during the late Holocene that reflect pronounced changes in taphonomic dynamics *(Chapter V)*. In Central Asia, the frequency of dust storms occurring during spring when the continent is heating up is mostly controlled by the intensity and the position of the Siberian High (SH) Pressure System. Using titanium (Ti) content in laminated sediments as a proxy for aeolian detrital inputs, changes in wind dynamics over Central Asia is documented for the past 1500 years, offering the longest reconstruction of SH variability to date. Based on high Ti content, stronger wind dynamics are reported from 450–700 AD, 1210–1265 AD, 1350–1750 AD and 1800–1975 AD, reporting a stronger SH during spring. In contrast, lower Ti content from 1750–1800 AD and 1980–1985 AD reflect a diminished influence of the SH and a reduced atmospheric circulation. During 1180–1210 AD and 1265–1310 AD, considerably weakened atmospheric circulation is evidenced.

As a whole, though climate dynamics controlled environmental changes and ultimately modulated changes in the western Central Asia's climate system, it is likely that changes in solar activity also had an impact by influencing to some extent the Aral Sea's hydrology balance and also regional temperature patterns in the past *(Chapter VI)*.

Résumé

La Mer intracontinentale endoréique de l'Aral, éloignée de toute influence océanique, constitue en Asie Centrale une excellente archive sédimentaire pour des études paléoclimatiques à haute résolution. Nous avons effectué une analyse palynologique, sédimentologique et géochimique sur des carottages sédimentaires effectués dans la Baie de Chernyshov, située au nord-ouest de l'actuelle Grande Mer d'Aral. La séquence sédimentaire la plus complète mesure 11 m et représente les 2000 dernières années de l'Holocène terminal.

L'étude palynologique, conduite conjointement sur des assemblages de kystes de dinoflagellés et de grains de pollen, a mis en évidence de profonds changements environnementaux en Mer d'Aral, ainsi que dans le bassin Aralien. Les variations d'assemblages de kystes de dinoflagellés (diversité, distribution des espèces) ont permis d'établir la séquence des variations de salinité et du niveau du lac au cours des 2000 dernières années *(Chapitre III)*. En raison de l'étroite dépendence de l'hydrologie de la Mer d'Aral aux apports fluviaux de l'Amu Darya et de la Syr Darya, les variations de niveau du lac sont étroitement liées à l'apport d'eaux résultant de la fonte des neiges en altitude au printemps. Or, l'amplitude de ces apports étant principalement contrôlée par les variations de température printanières dans les massifs du Tien Shan et du Pamir au cours de la fonte, les variations de salinité et de niveau de la Mer d'Aral traduisent essentiellement des fluctuations de température dans le bassin versant au cours des 2000 dernières années. Ainsi, les assemblages de kystes de dinoflagellés caractérisent des épisodes de bas niveau de la Mer d'Aral accompagnés d'une forte augmentation de la salinité au cours des périodes 0–425, 900–1230, 1500, 1600–1650 et 1800 après J.C., ainsi qu'après les années 1960. Inversement, un retour vers des conditions de faible salinité associées à une hausse du niveau du lac est documenté pour les périodes intermédiaires. Par ailleurs, la présence de kystes de dinoflagellés remaniés des dépôts Paléogène et Néogène alentours caractérise des évènements de désagrégation intense des berges lors d'une hausse significative des précipitations sur le bassin Aralien, notamment au cours de la période 1230–1450 après J.C. Nous proposons que les changements environnementaux enregistrés sont principalement liés à des changements climatiques mais qu'ils ont également pu être amplifiés par l'homme lors de conditions extrêmes, via une irrigation non-maîtrisée et/ou des conflits militaires *(Chapitre VI)*. En outre, les variations de salinité montrent de fortes similitudes avec celles de l'activité solaire au cours du dernier millénaire, notamment pour les périodes 1000–1300, 1450–1550 et 1600–1700 après J.C. où les périodes de bas niveau du lac correspondent à une activité solaire accrue, suggérant qu'une augmentation du bilan radiatif ait renforcé les régressions de la Mer d'Aral dans le passé.

Parallèlement, le contenu du sédiment en grains de pollen a été analysé afin de mettre en évidence des changements environnementaux, et notamment des variations d'humidité dans le bassin Aralien au cours des 2000 dernières années *(Chapitre IV)*. Une reconstruction quantitative à haute résolution du taux de précipitation (moyenne annuelle) et des températures (moyenne annuelle, mois le plus froid versus le plus chaud) a été réalisée à l'aide de la méthode dite de "probabilité des sphères climatiques mutuelles", permettant d'obtenir la séquence chronologique des changements climatiques en Asie Centrale. Un climat froid et aride domine au cours des périodes 0–400, 900–1150 et 1500–1650 après J.C., caractérisé par l'extension d'une végétation de type désertique avec des éléments de steppe. En revanche, un climat plus chaud et moins sec apparaît au cours des périodes 400–900 et 1150–1450 après J.C., caractérisé par une végétation steppique enrichie en plantes exigeant des conditions d'humidité plus élevées. Les variations de précipitation enregistrées dans le bassin Aralien au cours des 2000 dernières années sont principalement contrôlées par le système cyclonique de la Méditerranée Orientale qui fournit l'humidité nécessaire au Moyen Orient et en Asie Centrale à la transition hiver–printemps. Ce système cyclonique étant étroitement lié aux modulations de pression régulées par l'Oscillation de l'Atlantique Nord (NAO), une relation entre humidité en Asie Centrale et le NAO en phase négative est proposée.

Enfin, les sédiments laminés des carottages étudiés ont enregistré des changements marqués de la sédimentation au cours de l'Holocène terminal qui révèlent des bouleversements importants de la dynamique d'apports du matériel sédimentaire *(Chapitre V)*. En Asie Centrale, la fréquence des tempêtes de poussières s'intensifie au printemps lorsque le continent se réchauffe, et est ainsi principalement contrôlée par l'intensité et la position de l'anticyclone Sibérien sur le continent. Une analyse semi-quantitative du contenu du sédiment en Titanium, révélateur fiable d'apports détritiques d'origine éolienne, a permis d'établir la séquence chronologique des variations de la dynamique éolienne en Asie Centrale au cours des 1500 dernières années, représentant aussi la plus longue reconstruction dans le temps de l'intensité de l'anticyclone Sibérien établie jusqu'ici. Ainsi, une intensification de la dynamique éolienne est documentée pour les périodes 450–700, 1210–1265, 1350–1750 et 1800–1975 après J.C. En revanche, de faibles concentrations en Titanium (1750–1800 ; 1980–1985 après J.C.) caractérisent une réduction significative de l'intensité de l'anticyclone Sibérien et une circulation atmosphérique plus stable. Au cours des périodes 1180–1210 et 1265–1310 après J.C., une profonde modification de la circulation atmosphérique s'installe en Asie Centrale. En Mer d'Aral, elle se caractérise par une réduction considérable des apports détritiques éoliens.

En définitive, si l'ensemble des intéractions entre différents systèmes climatiques ont contrôlé les changements environnementaux en Asie Centrale et modulé les variations climatiques au cours de l'Holocène terminal, il est probable que les variations de l'activité solaire aient eu un impact notable sur l'évolution du bilan hydrique de la Mer d'Aral au cours des 1000 dernières années (*Chapitre VI)*.

Zusammenfassung

Der Aralsee ist ein intrakontinental gelegenes endorheisches Gewässer fernab von ozeanischen Einflüssen, welches ein exzellentes sedimentäres Archiv für hochauflösende Paläoklimastudien in Zentralasien darstellt. In der vorliegenden Studie wurden umfangreiche palynologische, mikrofazielle und geochemische Analysen anhand von mehreren Bohrkernen aus der Chernyshov-Bucht im NW des heutigen Großen Aralsees durchgeführt. Die vollständigste der erbohrten Sequenzen weist dabei eine Länge von 11 m auf und beinhaltet näherungsweise die letzten 2000 Jahre des Holozän.

Die hochauflösenden palynologischen Analysen der Studie, welche sowohl die Untersuchung von Dinoflagellatenzysten als auch Pollen beinhaltet, zeugen von einschneidenden Umweltveränderungen im Aralsee und seinem Einzugsgebiet. Die Untersuchung von Diversität und räumlicher Verbreitung der fossilen Dinoflagellatenzysten vermittelt dabei ein genaues Bild von den Salinitäts- und Seespiegeländerungen der letzten 2000 Jahre (Kapitel III). Aufgrund der weitgehenden Abhängigkeit der hydrologischen Verhältnisse des Aralsees von der Wasserführung seinen tributären Flüsse, hängt sein Seespiegel unmittelbar von den Schmelzwasserzuflüssen im Frühjahr ab. Da der Schmelzwasserzufluss seinerseits mit den Temperaturveränderungen im Tien Shan und Pamir während der Schneeschmelze in Verbindung steht, spiegeln die Paläo-Salinität und der Paläo-Seespiegel des Aralsees folglich die Temperaturveränderungen im hochgelegenen Einzugsgebiet des Aralsees wider. Die Untersuchung der fossilen Dinoflagellatenzysten belegt besonders niedrige Seestände und hypersaline Bedingungen während der Perioden 0–425 AD, 920–1230 AD, 1500 AD, 1600 AD, 1800 AD und seit 1960, wohingegen oligohaline Bedingungen und höhere Seestände zwischen diesen Phasen dokumentiert sind. Ferner stellen umgelagerte Dinoflagellatenzysten aus Paläogenen und Neogenen Ablagerungen wertvolle Proxies für den Beleg von extremen Flächenspülereignissen dar, wie sie beispielsweise 1230–1450 AD aufgetreten und durch sehr hohe Niederschläge dokumentiert sind. Anhand der in der Studie erarbeiteten Daten ist davon auszugehen, dass die am Aralsee nachgewiesenen Umweltveränderungen im Wesentlichen von klimatischen Änderungen induziert wurden, durch historischen Bewässerungsfeldbau oder militärischen Konflikten jedoch noch verstärkt werden konnten (Kapitel VI). Darüber hinaus zeigen die Seestandsveränderungen eine sehr hohe Korrelation mit der Sonnenaktivität im letzten Jahrtausend, wie etwa während den Perioden 1000–1300 AD, 1450–1550 und 1600–1700 AD. Hierbei korrespondieren niedrige Seestände und regressive Phasen mit zunehmender Sonnenaktivität und daher mit erhöhter Nettostrahlung.

Komplementär zu der Untersuchung von Dinoflagellatenzysten liefert die Pollenanalyse wertvolle Klimadaten für das Becken des Aralsees (Kapitel VI). Verschiedene Temperatur- (Jahresmittel,

kältester gegen wärmster Monat) und Niederschlagsparameter wurden mit Hilfe der Methode der „probability mutual climatic spheres“ quantitative ausgewertet, womit die Klimaentwicklung im westlichen Zentralasien der letzten 2000 Jahre nachvollzogen werden konnte. Kalte und aride Bedingungen wiesen demnach die durch trockenangepasste Vegetation und Steppenelementen geprägten Perioden 0–400 AD, 900–1150 AD und 1500–1650 AD auf. Andererseits traten warme und weniger aride Klimabedingungen in den durch niederschlagsbedürftigere Pflanzen gekennzeichneten Zeiträumen 400–900 AD and 1150–1450 AD in den Vordergrund. Die Studie zeigt für das Becken des Aralsees, dass die Veränderungen im Niederschlagsmuster hauptsächlich vom zyklonalen System des östlichen Mittelmeergebietes (EM) gesteuert werden, welches den nahen Osten und das westliche Zentralasien mit Feuchtigkeit im Winter und Frühjahr versorgt. Da seinerseits das EM maßgeblich von Luftdruckänderungen der Nordatlantischen Oszillation (NAO) während seiner negativen Phase reguliert wird, ist ein Zusammenhang zwischen der Feuchtigkeit im westlichen Zentralasien und dem NAO anzunehmen.

Außerdem belegen die laminierten Sedimente Veränderungen in den Sedimentationsprozessen während des späten Holozän, sowie ausgeprägte Änderungen im taphonomischen Verhalten (Kapitel V). In Zentralasien hängt die Häufigkeit der im Frühjahr auftretenden Staubstürme hauptsächlich von der Intensität und der Position des Sibirienhochs (SH) ab. Der Gehalt an Titanium (Ti) als Proxy für äolischen Eintrag in den laminierten Sedimenten erlaubt die Rekonstruktion von winddynamischen Veränderungen in Zentralasien in den letzten 1500 Jahren. Die Studie beinhaltet daher die bislang längste Analyse der Variabilität des SH. Hohe Titaniumwerte sprechen für eine stärkere Winddynamik während den Perioden 450–700 AD, 1210–1265 AD, 1350–1750 AD und 1800–1975 AD, und dokumentieren demzufolge eine stärker ausgeprägtes SH während des Frühjahrs. Umgekehrt belegen geringe Titaniumwerte für die Zeit von 1180–1210 AD, 1265–1310 AD, 1750–1800 AD und 1980–1985 AD einen reduzierten Einfluss des SH.

Zusammengefasst, obgleich die allgemeinen klimadynamischen Prozesse natürliche Umweltveränderungen bedingen und letztlich auch Modulationen des westlichen zentralasiatischen Klimasystem bewirken, ist es dennoch wahrscheinlich, dass Veränderungen der Solaraktivität gleichsam einen Einfluss hatten und bis zu einem gewissen Grad die Wasserbilanz am Aral See sowie die regionale Temperaturen in der Vergangenheit veränderten (Kapitel VI).

Contents

List of Figures

List of tables

Chapter I: Introduction

Reconstruction of past climate from palaeoclimate proxy data is important for improving constraints on the role and the scope of natural climate variability onto environments. A number of efforts have been made to reconstruct variations in Northern Hemisphere temperature within the past millennium using well-dated, high-resolution proxy records (e.g. Overpeck et al., 1997; Jones et al., 1998, 2001; Mann et al., 1998, 1999; Pfister, 1999; Bradley, 2000, 2003; Briffa, 2000; Briffa et al., 2001, 2002; Crowley, 2000; Folland et al., 2001; Esper et al., 2002a; Crowley and Lowery, 2003; Mann and Jones, 2003; Cook et al., 2004; von Storch et al., 2004; Moberg et al., 2005). Most of the climate shift events over the past 1500 years often coincided with reorganisations of human societies (Buckland et al., 1995; Cullen et al., 2000; de Menocal, 2001; Haug et al., 2003). Detailed high-resolution temporal and spatial patterns of climate change are available for Europe over the last 300–600 years (e.g. Appenzeller et al., 1998; Luterbacher et al., 2001, 2002; 2004; Büntgen et al., 2005; Pauling et al., 2005; Casty et al., 2005a, 2005b, 2005c; Jacobeit et al., 2003; Slonosky et al., 2000, 2001), in the Artic region (Overpeck et al., 1997) and in northern Asia over the past 2000–4000 years (Naurzbaev et al., 2002; Hantemirov and Shiyatov, 2002). However, hemispheric-scale reconstructions provide little information about regional scale anomalies in both temperature and precipitation. Therefore, studies focusing on reconstruction of specific regions are also necessary. To date reconstructions of climate variability during the late Holocene are rather scarce for Central Asian areas. They are limited in time (ca. 1000–1300 yr BP) and often restricted to temperature changes, as based on tree-ring width analyses (Esper, 2000; Esper et al, 2002b; 2003).

I.1. Aims of the study

Due to the unsustainable diversion of water resources for irrigation purposes associated to a preoccupant degradation and pollution of its ecosystem, the Aral Sea recently became the focus of international environmental concerns. The Aral Sea (Fig. 1.1) represents one of the few Eurasian continental sites with a complete sedimentary archive that can be used for high-resolution palaeoclimate studies. Its remote location in the continental interior of western Asia, where different climate systems (e.g. the Subpolar Westerly Jet Stream, the Siberian High Pressure Cell, the North Atlantic Oscillation) are interlinking, is crucial for unraveling

their respective influence on the hydrology in western Central Asia. The hydrological balance of the endorheic Aral Sea is strongly dependent on the fluvial inputs from the Amu Darya and the Syr Darya, its two main tributaries in the Aral Sea Basin (Fig. 1.1), which account for ca. 80% of the hydrological input into the Aral Sea. As for comparison, between 1911 and 1960, the mean river discharge to the Aral Sea represented 56 km^3/year (4.2 km^3/year during 1981–1990), while precipitation totalled only 9 km^3/year, groundwater discharges 0–5 km^3/year (Jarsjö and Destouni, 2004), and the mean evaporation rate 66 km^3/year (Zavialov, 2005). At a regional scale, past climate variability in the arid Aral Sea Basin may be an important key for understanding future climate change, which may affect even more drastically such arid and semi-arid regions. Also, understanding past climate change is of great importance to evaluate the anthropogenic impact on present-day and future climates in this highly sensitive semi-arid region.

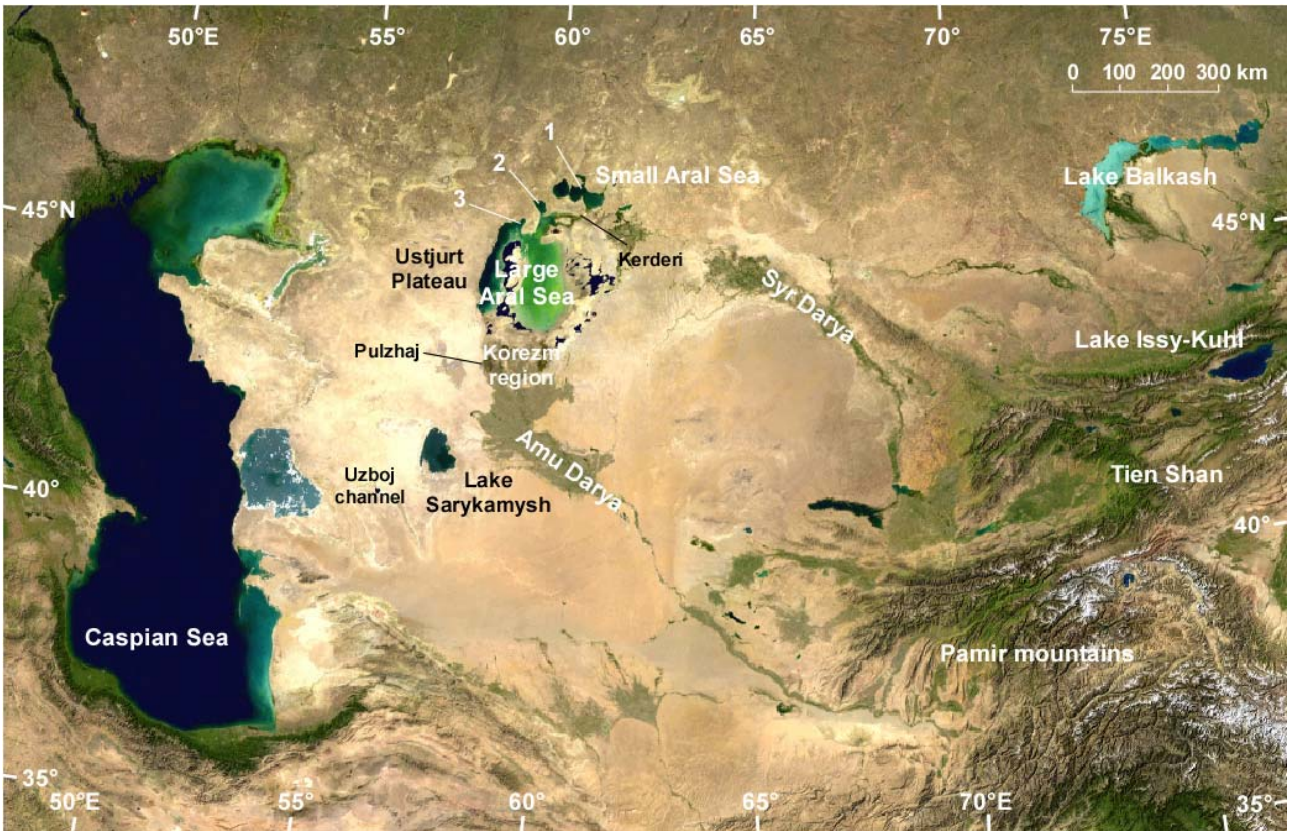

Figure 1.1: *The Aral Sea, located in Central Asia, with the main tributaries Amu Darya and Syr Darya, and the coring locations. 1: Tastubek Bay; 2: Tschebas Bay; 3: Chernyshov Bay. Map extracted from NASA World Wind 1.3.*

This thesis is embedded in the international collaborative research project CLIMAN (Holocene CLImate variability and the evolution of HUMan settlement in the Aral Sea Basin). The project aims to investigate the following tasks:

- Determine the sequence of lake-level changes of the Aral Sea during the late Holocene. This requires a close collaboration between geoscientists (remote sensing), geomorphologists (field observations) and archaeologists (field observations);
- Assess a robust chronology of climate change in the Aral Sea Basin based on a multi-proxy approach, i.e., organic- and inorganic sediment core proxies recording environmental change at high resolutions;
- Evaluate the underlying forcing factors regulating climate variability in the Aral Sea Basin by comparing with other Eurasian climate records and so, searching for atmosphere–biosphere interactions in order to improve our understanding of the Eurasian and the Northern Hemisphere climate system;
- With climate as the dominant forcing factor, assess the history of human adaptation in response to environmental change in Central Asia.

In this study, we mainly focus on the second and third tasks of the project CLIMAN. Three main purposes were defined:

- Establish a reliable age model as based on AMS ^{14}C dating from sediment core macroremains;
- Establish a multi-proxy dataset from biotic and abiotic proxies for reconstructing lake-level changes and hydrological conditions in the Aral Sea, moisture conditions in the hinterland associated with vegetation cover, and wind dynamics determining detrital inputs in the Aral Sea Basin;
- Evaluate the main seasonal patterns of past climate variability over western Central Asia. Climate variability in the Aral Sea Basin may highlight the climatic affinity and possible teleconnections between Central Asia and other Eurasian climate regimes.

Past climate variability can be reconstructed using both proxy-based correlations and climate quantification methods. However, investigating climatic change as recorded in lake sediments is still a challenge. One of the difficulties is to establish reliable age models for lake sediments. Additionnally, because (i) each lacustrine environment is basically unique and (ii)

various local to regional influences may overprint primary signals, proxy records from lake sediments must often be considered differently and transfer models must be recalibrated from one ecosystem to the other.

I.2. Climate variability over the Eurasian continent and its influence on Central Asia and the Aral Sea Basin

Within the global climate system, the Central Asian sector defined in this study as the area from 30°N–55°N to 50°E–70°E in the Eurasian continent (30°N–70°N to 10°W–90°E), constitutes an issue of particular concern within the context of regional and global climate variability. The Asian continent exerts a strong influence on global circulation patterns, being a region of unambiguous warming during the last decades (Hansen et al., 1988). The dominant synoptic systems which control and determine seasonal pressure, temperature gradients and precipitation in Asia are the Mediterranean Low-pressure Cell, the Siberian High pressure Cell and the locally-driven surface highs (lows) during winter (summer).

The Mediterranean Low-pressure Cell

The Mediterranean basin is considered to be the most cyclogenetic area in the world usually favouring development of weak low-pressure systems. The depressions occurring over the Mediterranean and associated cyclonic tracks to the NE have been subject of extensive climatological research (Alpert et al., 1990a; Chang, 1972; Karaca et al., 2000; Katsoulis, 1980; Maheras, 1983a, 1983b, 2001, Wigley and Farmer, 1982). The formation of lows over this region in winter is associated with cold air invasion into the Mediterranean (Alpert and Reisin, 1986; Tayanç et al., 1997; Kahana et al., 2002; Ziv et al., 2006), being connected with positive vorticity advection at the upper levels (Kallos and Metaxas, 1980), and stems from a thermal contrast between the cold dry air and the relatively warmer seawaters. Regions of enhanced cyclone activity during winter and spring are the interior of the Asia Minor, the eastern edge of the Black Sea and the Caspian Sea (Maheras et al., 2001) (Fig. 1.2). Subsequently, maximum of precipitation is recorded during winter and spring over this area (see Fig. 1.4i).

Figure 1.2: *Low-pressure fields moving over the Middle East and western Central Asia, bringing showers and storms over these regions (26.03.2003). Map extracted from NOAA site* http://www.noaa.gov/

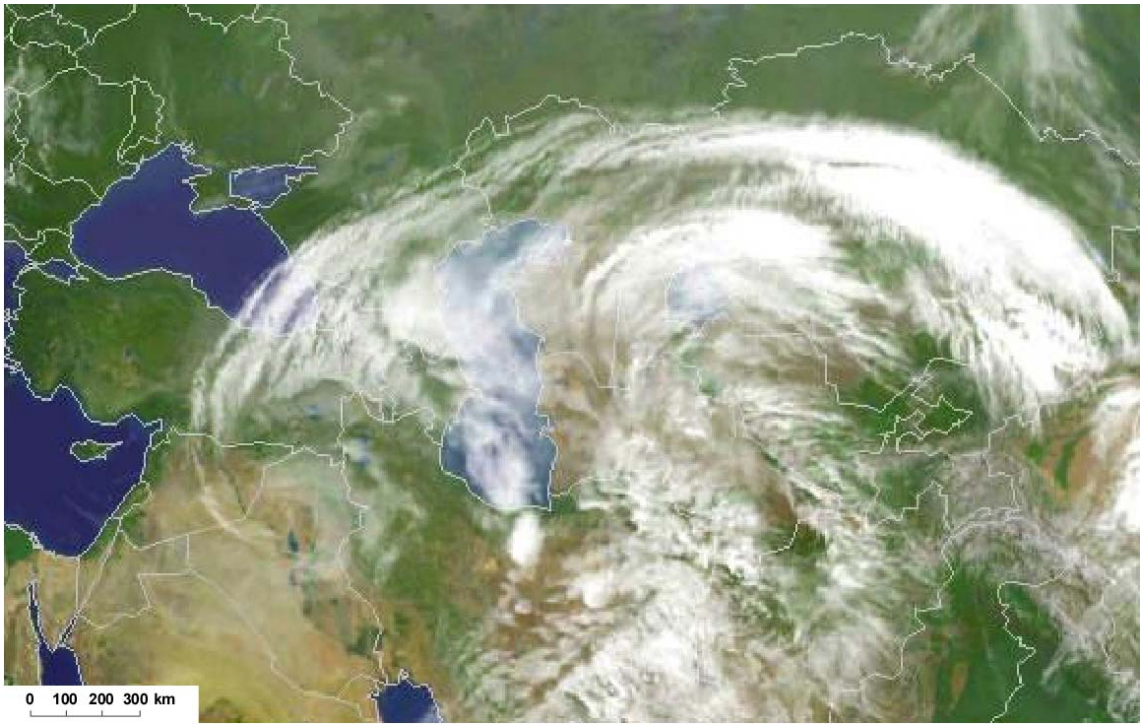

The Siberian High Pressure Cell

The Siberian High (SH) (Fig. 1.3) is a semi-permanent and quasi-stationary anticyclone usually centered over northern Mongolia, but often spreads over a very large part of Asia (Panagiotopoulos et al., 2005) including the Aral Sea Basin (Fig. 1.3a). It is the coldest and most extensive centre of action of winter-time (October–April) general circulation of the atmosphere (Lydolf, 1977; Sahsamanoglou et al., 1991). The SH is characterized by a maximum in the winter mean sea-level pressure (SLP) in the Northern Hemisphere (Fig. 1.3b). However, it shows no strong relationship to other climatological SLP centers, apart a weak negative correlation with southern Europe (Fig. 1.3b) where a stronger SH enhances cyclogenesis in the Mediterranean region. The SH originates predominantly from the intensive radiative cooling of the lower troposphere above the snow-covered of Asia, and its intensity correlates closely with sea-surface temperature (Panagiotopoulos et al., 2005). Correlation between the SH index and different wind tropospheric fields evidences that the Aral Sea Basin is significantly influenced by the extension and strength of the SH (Fig. 1.3c). According to Panagiotopoulos et al. (2005), significant teleconnections exist as well between the SH and westerly jet streams on one hand, and with the winter East Asian monsoon on the other hand as further reported from Takaya and Nakamura (2004). Its influence on the Eurasian snow cover has been, however, controversially discussed (Clark et al., 1999; Cohen and Entekhabi, 1999). Whereas an intensification of the SH since the 1960s has been suggested by Mokhov and Petukhov (1999), Sahsamanoglou et al. (1991) and more recently

Panagiotopoulos et al. (2005) provided compelling information that document a clear decreasing trend in the SH intensity during the past 30 years. According to Gillett et al. (2003), this trend may be even strengthened in near future due to increased concentrations in greenhouse gases.

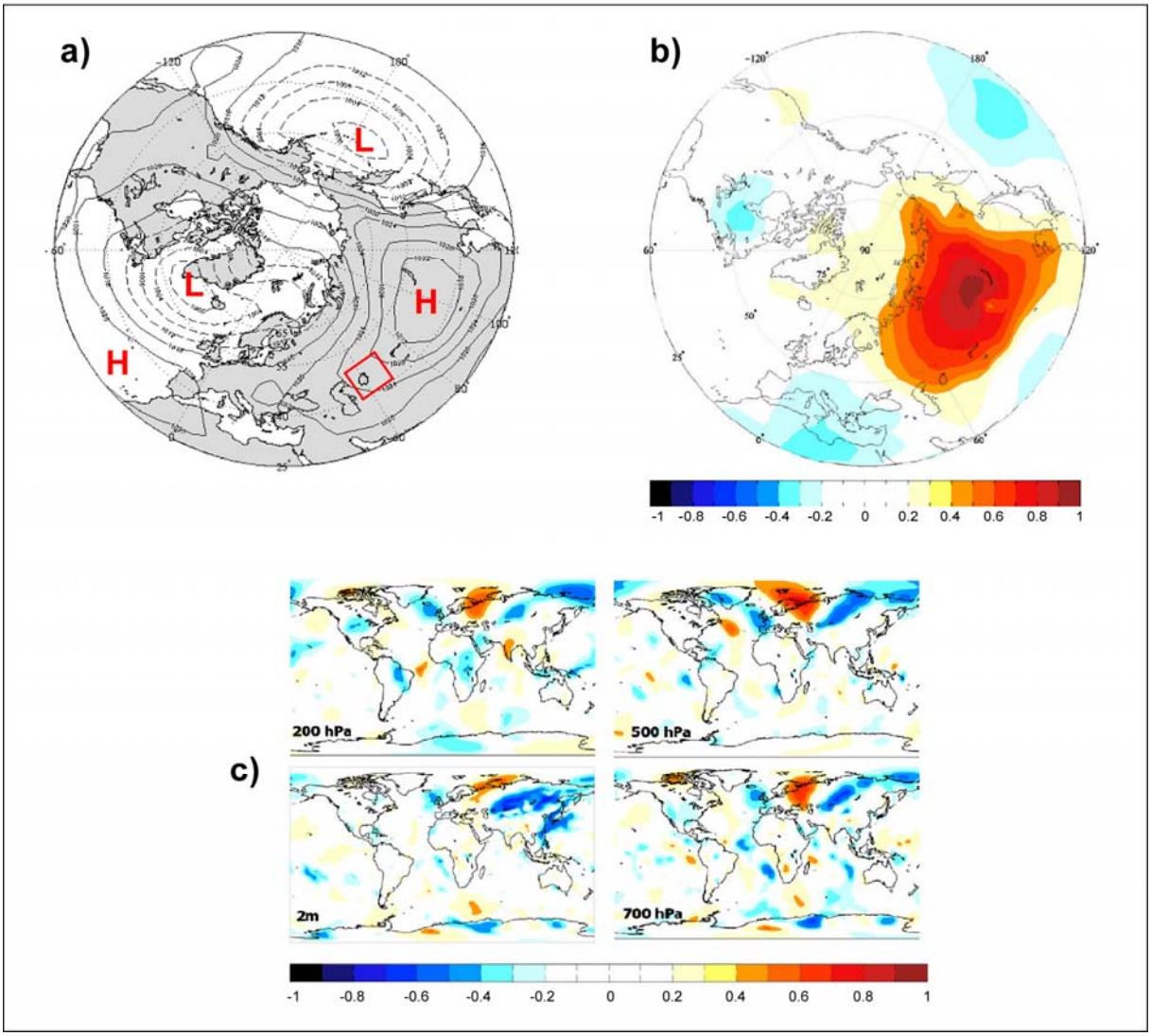

Figure 1.3: *The Siberian High Pressure Cell (modified after Panagiotopoulos et al., 2005). a: Winter (DJF) sea-level pressure (SLP) in January averaged over 1900–2001. b: Correlation of Siberian High index with sea-level pressure (Trenberth, 1899–2001). c: Correlation of the SH index (mean SLP) and meridional winds at different levels of the troposphere from NCAR/NCEP (1948–1998).*

With the purpose to describe the climatology of the main climate variables for the Central Asian sector, Figure 1.4 presents observed surface climate data for the winter and summer temperature (a–b), global radiation (c–d), wind speed (e), number of frost / wet days per month (f, i–j), cloud cover (g–h) and precipitation (k–l) during the second half of the 20th century (1961–1990).

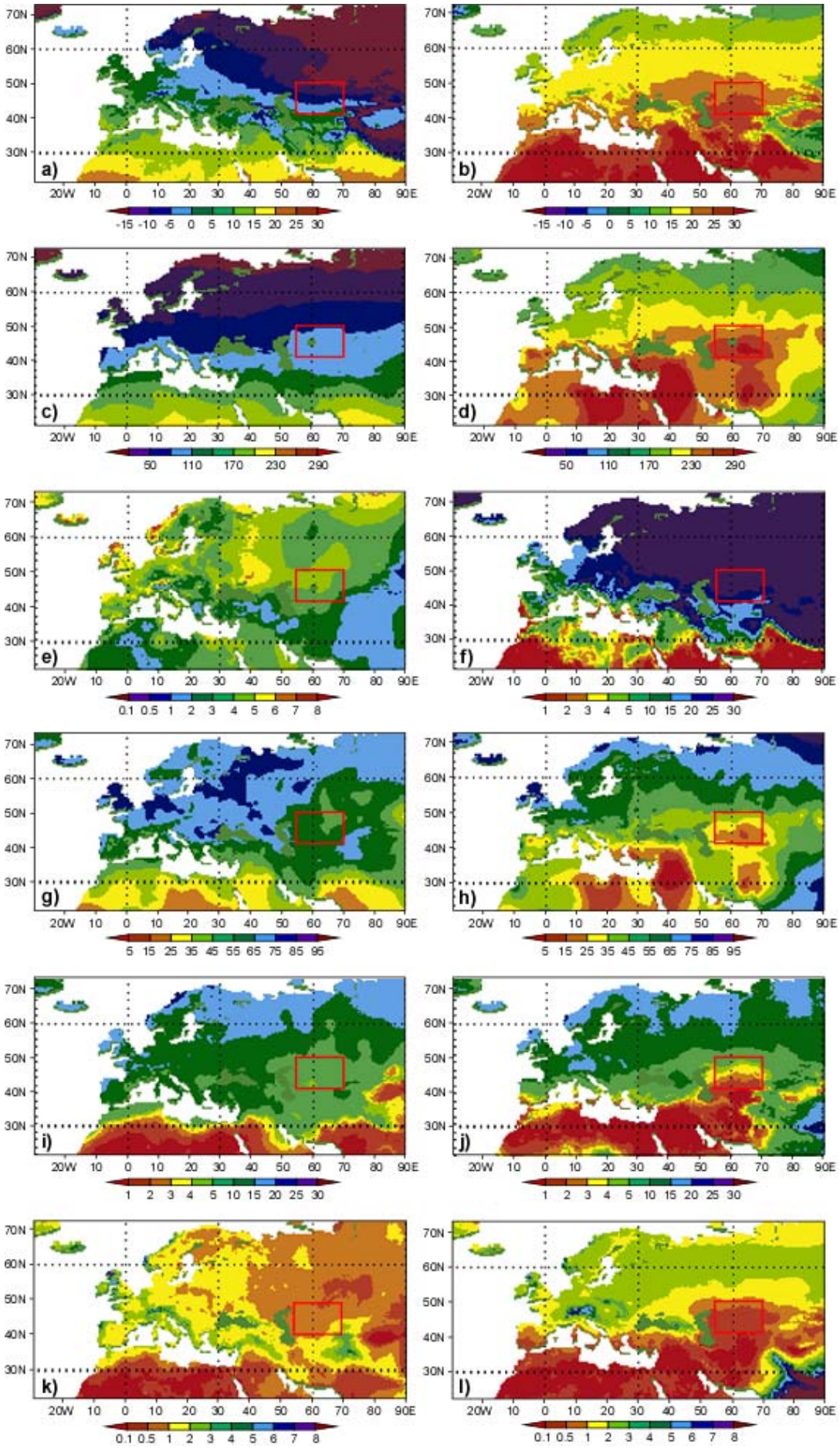
a)
b)
c)
d)
e)
f)
g)
h)
i)
j)
k)
l)
70N
60N
50N
40N
30N
20W 10 0 10 20 30 40 50 60 70 80 90E
-15 -10 -5 0 5 10 15 20 25 30
50 110 170 230 290
0.1 0.5 1 2 3 4 5 6 7 8
1 2 3 4 5 10 15 20 25 30
5 15 25 35 45 55 65 75 85 95

Figure 1.4: *Temperature, global radiation, wind speed, number of frost / wet days per month, cloud cover and precipitation climatologies for winters (DJF) and summers (JJA) over the Eurasian sector. a–b: Averaged land surface mean temperature 1961–1990 for DJF and JJA, respectively (shadings, in °C); c–d: Same as a–b but for averaged global radiation 1961–1990 (in W/m^2); e: Averaged wind speed 1961–1990 for DJF (in m/s); f: number of frost days per month 1961–1990 for DJF; g–h: Same as a–b but for cloud cover 1961–1990 (in %); i–j: Same as a–b but for the number of wet days per month 1961–1990; k–l: Same as a–b but for land surface precipitation 1961–1990 (in mm/day). The data are from http://ipcc-ddc.cru.uea.ac.uk/java/visualisation.html. The Aral Sea Basin (Central Asia) is marked with the red rectangle.*

The winter temperatures yield a northeast to southwest divide over the Eurasian continent, with warmer conditions in Western Europe and around the Mediterranean due to the influence of the surrounding water masses (Fig. 1.4a). The deserts and semi-deserts of Central Asia have a strong continental climate. The temperature pattern for winter is largely influenced by high pressure resulting from a cold anticyclone centered over eastern and northern Asia (i.e., the Siberian High) with pronounced negative temperatures from 0–-15°C in average up to -40°C for the minimal values (Lioubimtseva et al., 2005). This has been often associated to a prolonged period of freezing conditions with up to 25–30 frost days per month (Fig. 1.4f). At the transition between winter and spring, low temperature lead to a steepening of the pressure gradients (not shown here) which are responsible for enhanced wind dynamics (Fig. 1.4e) and numerous dust storms in Central Asia (Orlovsky et al., 2005). The global radiation is considerably reduced during winter as compared to the summer values (Fig. 1.4c–d), the highest in the whole Eurasian area. In the winter precipitation sketch (Fig. 1.4k), the Atlantic and Mediterranean region that are persistently influenced by the westerlies are wet regions. Precipitation in the deserts of Central Asia mostly occur between December and March–April (Fig. 1.4k). They depend highly on the position of the Siberian High and the mode of atmospheric circulation (Aizen et al., 2001; Lioubimtseva et al., 2005; Zavialov, 2005), and are largely controlled by shifts of the westerly cyclonic circulation. Rain is generally brought by the depressions which develop over the Eastern Mediterranean region during winter and spring (Maheras et al., 2001, Fig. 1.2), migrate northeastwards, and regenerate over the Caspian Sea (Lioubimtseva, 2002; Maheras et al., 2001). This results in an enhanced cloud cover in winter and early spring as seen in Fig. 1.4g and thus, a higher number of wet days (Fig. 1.4j). Over the past 20 years, a net deficit in monthly precipitation has been recorded in Western and Central Asia (Fig. 1.5). However, within the Aral Sea Basin, a great spatial variability in precipitation trends can be observed at the landscape scale between the different meteorological stations (Neronov, 1997), and seems to be controlled mostly by land use (irrigation) and land cover characteristics. Two other important controls on precipitation

changes over Central Asia are the levels of the Caspian and the Aral seas and their contribution of moisture and heat to the lower atmosphere, especially during summer when evaporation greatly intensifies (Lioubimtseva et al., 2005).

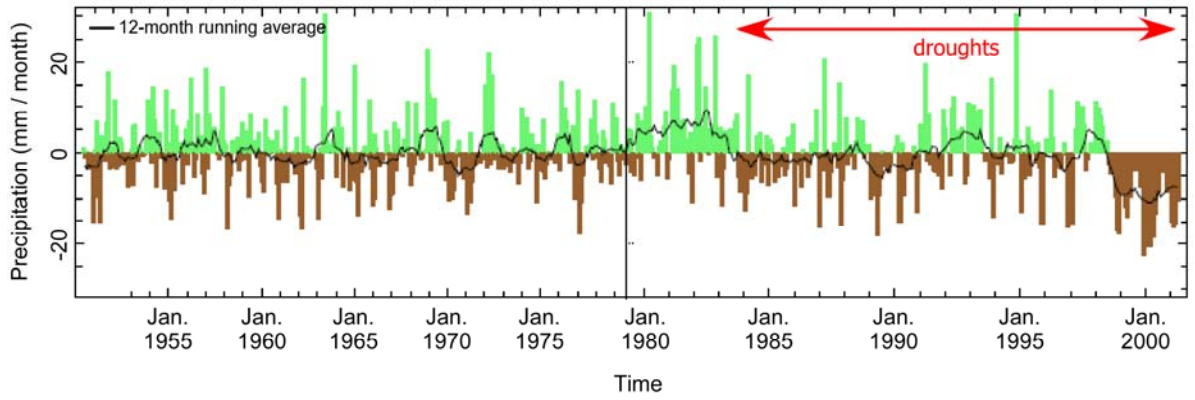

Figure 1.5: *Monthly precipitation anomalies over Central and Southwest Asia (25°N–42°N; 42°E–70°E) for the period January 1951–September 2001. Modified after Agrawala et al. (2001): IRI Special Report.*

During summer, the climate variability and pressure gradients are weaker, as the influence of the Siberian High diminishes. The temperature distribution yields relatively high averaged temperatures over continental Europe, and very high temperatures over Central Asia with values similar to those in northern Africa (25–30°C; Fig. 1.4b). Within the Aral Sea Basin, the average July temperatures are about 32°C with a maximum of 52°C in the eastern Kara Kum (Lioubimtseva et al., 2005). Meteorological data series show a steady increase of annual temperatures (1–2°C) over the region during the 20th century (see Figs. 2–3 in Lioubimtseva et al. (2005) for Tashkent, Repetek and Bayramaly stations). This increase is regarded as to be the result of a decreasing influence of the southwestern periphery of the Siberian High during winters and the intensification of summer thermal depressions over Central Asia. High summer temperatures probably stem also from a considerably increased radiative warming with highest values centered over the Aral Sea Basin (Fig. 1.4d). In the summer precipitation map (Fig. 1.4l), the wettest regions correspond to the British Islands and northern Europe, whereas the southern parts of Europe are relatively dry and influenced by the Azores subtropical High. In Central Asia, the cloud cover (Fig. 1.4h) is considerably weakened during summer. Coevally, precipitation are extremely low between June and August (Fig. 1.4l), resulting in a frequency of 1 to 4 wet days per month in average from 1961–1990 (Fig. 1.4j). For more details on the twentieth century climatology and current trends, we refer to Lioubimtseva et al. (2005).

I.3. Teleconnections

To evaluate the impact of broadly recognized modes of climate variability affecting the global system on the climatology of western Central Asia is still a challenge. NAO and ENSO predominantly affect climate variability within Europe and the Middle East, most particularly by determining seasonal distribution of temperature and precipitation (see Hurrell, 1995; Hurrell & van Loon, 1997; Thompson et al., 2003; Wanner et al., 2001 and Diaz et al., 2001 for a review). Such modes of climate variability can, therefore, be expected to exert an influence, even moderate, on the climate in Central Asia, and more likely on precipitation.

The North Atlantic Oscillation (NAO)

The impact of the NAO in the European weather system has been widely investigated (Hurrell, 1995; 1996; Hurrell & van Loon, 1997; Hurrell et al., 2001; Ulbrich & Christoph, 1999; Ulbrich et al., 1999; Xoplaki et al., 2004). However, its influence onto the climate in the Eastern Mediterranean (e.g. Ben-Gai et al., 2001; Eshel et al., 2000; Eshel & Farrell, 2001; Eshel, 2002; Ziv et al., 2006), the Middle East (Cullen & de Menocal, 2000; Touchan et al., 2003) and Central Asia (Aizen et al., 2001) is still intensively discussed. During low (negative phase) NAO winters, the sub-tropical sea-level pressure (SLP) gradient between the Iceland Low and the Azores High is weakened and Atlantic westerlies assume a more zonal trajectory, bringing moister and warmer conditions over the Mediterranean region (Hurrell, 1995; Hurrell & van Loon, 1997; Hurrell et al., 2001) and even further east towards the Caspian Sea (Cullen et al., 2002). Correlation analyses between atmospheric circulation patterns and regional-averaged precipitation showed that a negative (positive) difference in anomalies of sea-level pressure between the Azores and the Iceland is favourable (unfavourable) for precipitation development over the middle plains of Asia (Aizen et al., 2001). Mann (2002) further reported that NAO-related interdecadal to centennial-scale variability could play a principle role on the climatology of Middle Eastern regions.

The Arctic Oscillation (AO)

The influence of the Arctic Oscillation (AO), the leading mode in the Northern Hemisphere wintertime circulation pattern (Thompson & Wallace, 1998; 2000; Wallace &

Thompson, 2002), on climate change in Central Asia has not been thoroughly studied yet. However, relationship between AO variability and SST and surface wind over the Middle East during winter was evidenced by Rimbu et al. (2001) from winter time series of coral $\delta^{18}O$ record in the Red Sea. Along with strong continental conditions during a positive AO phase, the Red Sea and EM regions receive cold and dry air from the North (see also Fig. 8d in Aizen et al., 2001), leading to lower SST in respective areas.

Though the AO correlates strongly with the NAO (Serreze et al., 2000), the AO captures more of the hemispheric variability than the NAO does (Mac Donald et al., 2005). The AO is, therefore, strongly correlated with Eurasian temperatures (Thompson & Wallace, 2000). The relationship between winter AO and 1000 h-Pa air temperature over Central Asia is indeed strong for DJF, with $R > 0.4$ (significant at the 97% level) in the northern part of the Aral Sea Basin during the period 1958–2001 (Fig. 1.6A). This may have had important consequences on the precipitation of snow over the region during winter as for the duration of the cold season, thus controlling the onset of snow melt during spring. An increase in the AO index is indeed believed to result in negative snow-cover anomalies over Eurasia (Serreze et al., 2000), as reported for the period 1972–1997 when the snow cover in Eurasia sharply declined (Mac Donald et al., 2005). The snow-cover anomalies can in turn induce large-scale dynamical responses and affect winter-time circulation in the Northern Hemisphere (Cohen & Entekhabi, 2001), hence constituting feedbacks. Over half of the changes in surface air temperature observed in Eurasia since the 1970s have been ascribed to the AO (Serreze et al., 2000). These temperature changes are considered large enough to have an immediate effect on polar circulation (Morison et al., 2000), and thus on the Eurasian circulation downstream as shown on Fig. 1.6B. Correlation maps of surface and 1000 h-Pa (not shown) meridional wind (DJF) and winter AO time series for the period 1958–2001 are in accordance with the results of Rimbu et al. (2001). They show significant correlation ($R > 0.5$) over the Aral Sea Basin, reflecting the predominant influence of the AO during winter on midlatitudes from Central Asia. As for the air temperature correlation map above, the seasonal averaged variables used here were extracted from the NCEP/NCAR reanalysis archive, whereas the AO index time-series were taken from the NOAA site http://www.cdc.noaa.gov/correlation/.

Figure 1.6: *Correlation maps of different climate variables with Arctic Oscillation (AO) time series. A: Correlation of 1000-hPa air temperature for December–February (DJF) (1958–2001) with December–February AO. B: Correlation of surface meridional wind for December–February (DJF) (1958–2001) with December–February AO (extracted from http://www.cdc.noaa.gov/correlation/). See text for detail.*

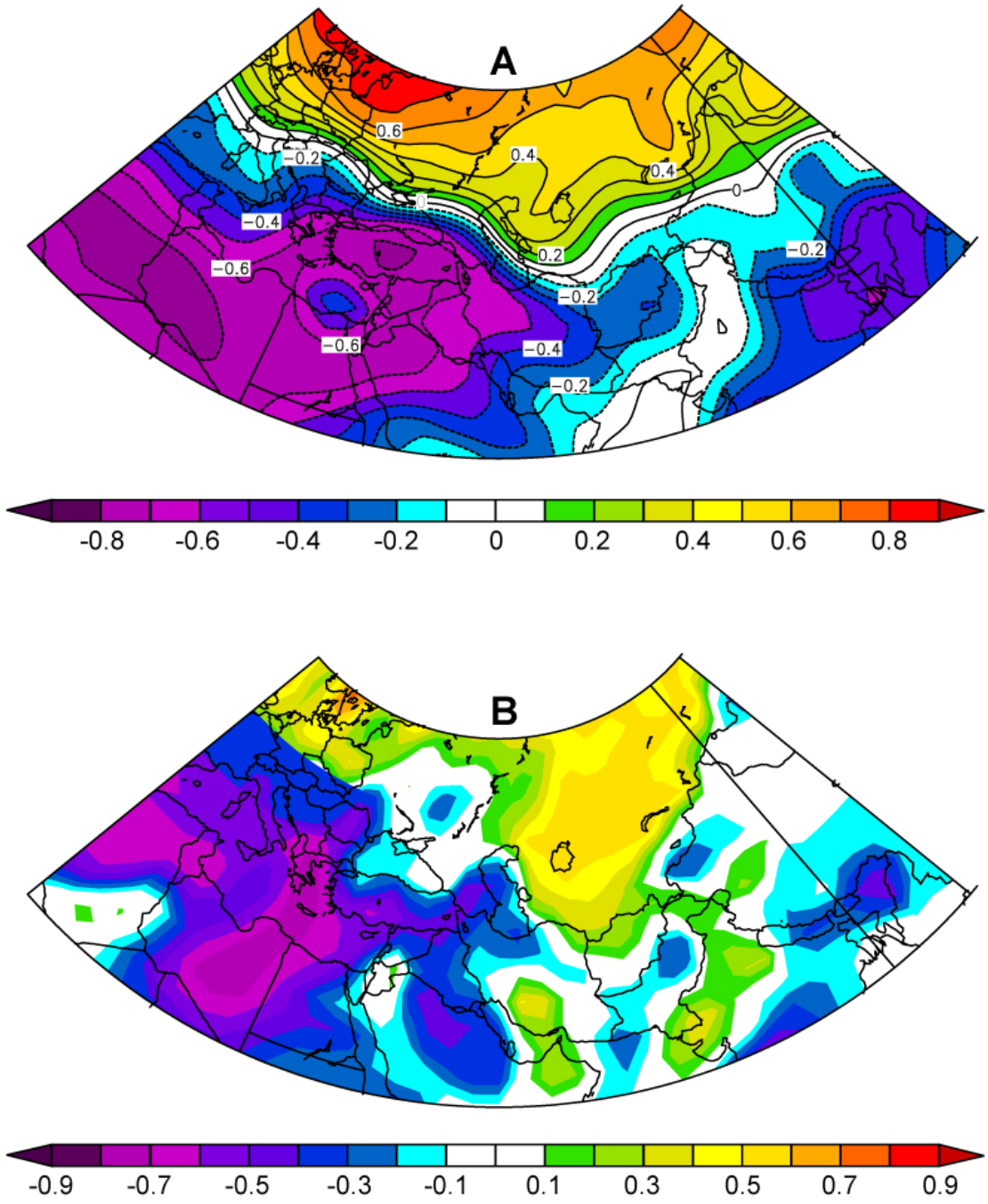

The El-Niño Southern Oscillation (ENSO)

The ENSO is recognized as a major source of global climate variability (Trenberth et al., 1998; Diaz et al., 2001). Several authors have attempted to assess the impact of ENSO on precipitation in the Eastern Mediterranean Sea and the Middle East (e.g. Kiladis & Diaz, 1989; Price et al., 1998), and especially in Turkey (Kadioğlu et al., 1999; Kahya & Karabörk, 2001). Within Central Asia, pionner studies which aimed to detect the influence of ENSO on the climate were undertaken by Gruza et al. (1999). According to these authors, the ENSO

signal in Central Asia is generally weak. However, statistical relationships based on wavelet analyses of daily observational air temperature data in the Aral Sea region reveals peaks in the frequency spectrum of 5–6 years which can be linked with ENSO (Khan et al., 2004). The relationship with ENSO is prominent in the northeastern part of the Aral Sea region, but much weaker in other parts of the region.

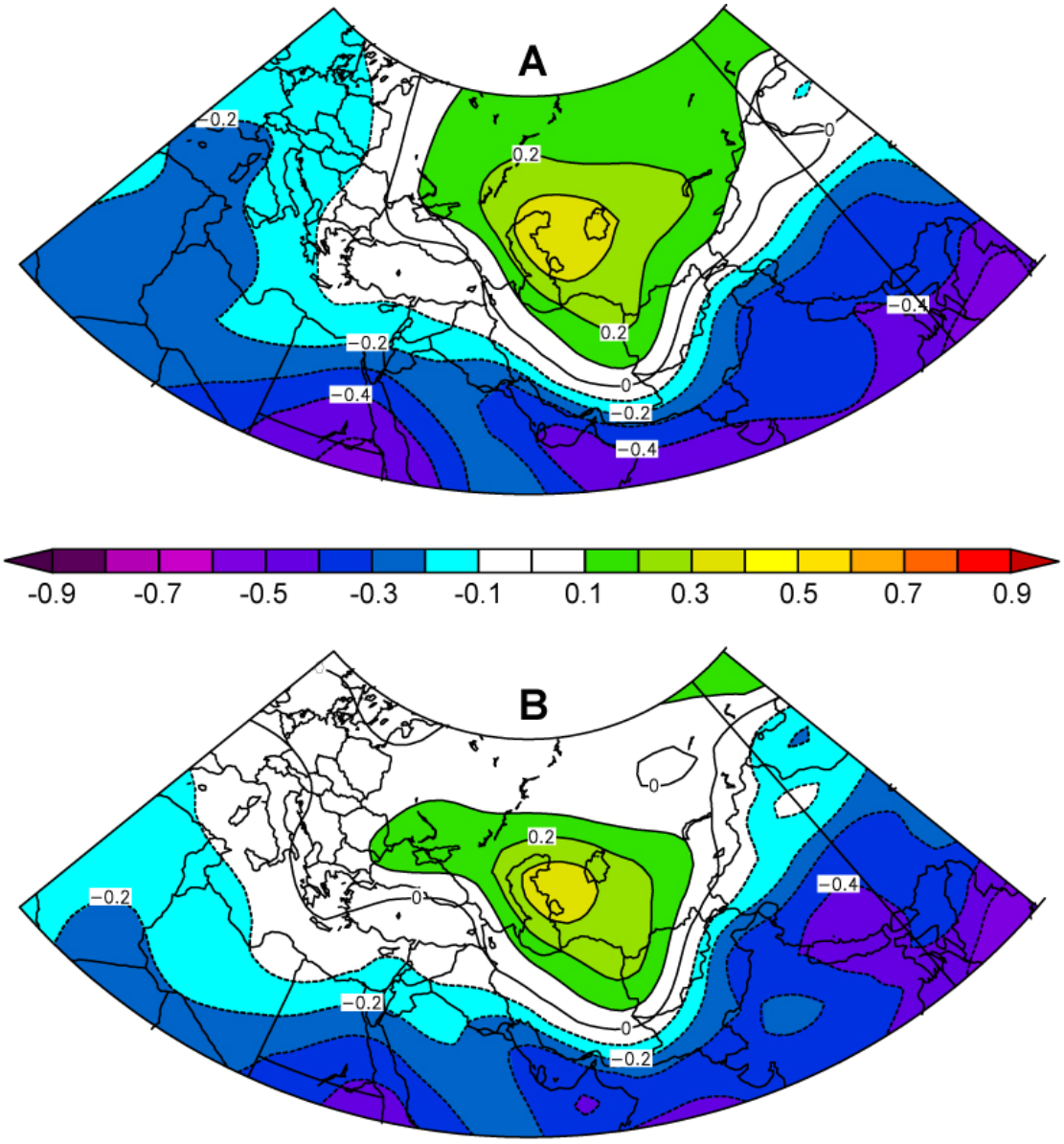

Figure 1.7: *Correlation maps of 1000-hPa geopotential height for December–February (DJF) (1949–2005) with Southern Oscillation Index (SOI) time series. Index leads by one month (November–January; A) and one season (September–November; B) (extracted from NOAA site http://www.cdc.noaa.gov/correlation/). See text for detail.*

To illustrate the connection between ENSO and different atmospheric fields within Central Asia, we use correlation maps based on midwinter month (i.e. December–February or DJF) averages, as the influence of ENSO on Middle Eastern climates is generally more pronounced during winter (Kiladis & Diaz, 1989; Kadioğlu et al., 1999; Karaca et al., 2000). The monthly / seasonal averaged variables used in this analysis were extracted from the NCEP/NCAR reanalysis archive (Kalnay et al., 1996; Kistler et al., 2001) and the Southern Oscillation Index (SOI) time-series were taken from NOAA site http://www.cdc.noaa.gov/correlation/. Regarding the study period (54 years) and assuming that the monthly / seasonal values of the atmospheric fields are not serially correlated, any correlation of $|R| > 0.3$ is significant at the 97% level. Figure 1.7 represents the correlation between SOI time series and 1000-hPa gph for the time period 1949–2003. It shows that the connection is more pronounced when a lead time of one month (NDJ) rather than of one season (SON) is applied, with a correlation center located over the Aral Sea basin ($R > 0.3$). Similar observations come up for sea-level pressure averages calculated across the interval 1949–2005 (not shown). The correlation maps show significant correlation ($R > 0.3$) over the Aral Sea Basin, reflecting the weak, but existing, influence of ENSO during winter on midlatitudes from Central Asia.

I.4. Structure of the thesis

The thesis is written in form of three papers (Chapters III, IV and V), preceded by two chapters setting the environmental context of this study.

Chapter II deals with a description of the coring sites where sediment cores were retrieved, the composition and lithological properties of the studied material. Methods related to inorganic and organic studies are briefly described. A review on previous dating obtained on sediment cores from the Aral Sea is given and the chronology established for the present study is explained in detail.

Chapter III is a paper published in Palaeogeography, Palaeoclimatology, Palaeoecology in 2006. It presents a high-resolution quantitative study on dinoflagellate cysts, the first one performed in the Aral Sea. Dinoflagellate cysts assemblages were used to reconstruct the sequence of lake-level and salinity variations both reflecting the hydrographic development of the Aral Sea during the past 2000 years. Changes in salinity levels in the Aral Sea are linked with changes in river run-off from the Pamir and Tien Shan moutains, reflecting temperature fluctuations in the high catchment area as revealed from comparison with other

reconstructions in Central Asia. The variability and remarkable events of lake-level change are further compared with historical reviews in order to unravel the respective impact of climate and human on the late Holocene history of environmental change in the Aral Sea.

Chapter IV is a publication accepted with revision in Quaternary Research. This chapter deals with a quantification of climatic parameters and a reconstruction of climate variability in the Aral Sea Basin during the late Holocene, as revealed from high-resolution pollen analyses. The quantification of climatic parameters is assessed based on the method of the "probability mutual climatic spheres" (PCS) method. This study allows to evidence significant changes in moisture conditions in the Aral Sea Basin during the past 2000 years. This variability appears to be mainly controlled by humidity brought on NE trajectories from the Mediterranean, as inferred from comparison with other records from the Eastern Mediterranean region and the Middle East.

Chapter V is a publication accepted with revision in Quaternary Research. It presents a coupled high-resolution geochemical and microfacies analysis aiming to detect changes in detrital input in the Aral Sea and its consequence on sedimentation. Effort is focused on the identification of the forcing controlling wind dynamics and their relation with general atmospheric circulation over Central Asia.

Chapter VI is the synthesis part. It is based first on the basis of a fourth paper "*Archaeology and Climate: Settlement and lake level change at the Aral Sea"* by Boroffka *et al.* (Geoarchaeology, in press) which discuss the role of human activities on the Aral Sea's water balance in the past based on new archaeological findings. Secondly, we expose the most important results of this thesis and discuss what kind of forcing is basically controlling environmental and climate change in western Central Asia during the past 2000 years.

In Chapter VII, conclusions are drawn, including a short outlook for future work.

A CD-ROM gathering dating measurements and different datasets (gamma-ray density, magnetic susceptibility and X-ray fluorescence data performed on all sediment cores investigated in the frame of the project CLIMAN) is joined to the thesis for data archive

Chapter II: Material and Methods – site location, sediment properties and chronology

II.1. Coring sites: the CLIMAN summer 2002 campaign

During the CLIMAN field campaign in July/August 2002 at the northern shore of the Aral Sea (http://climan.gfz-potsdam.de), sediment cores were retrieved at 3 different stations from the Small and the Large Aral Sea. Site selection was determined using a preliminary seismic survey looking for continuous sedimentation deprived of slumping features (Fig. 2.1).

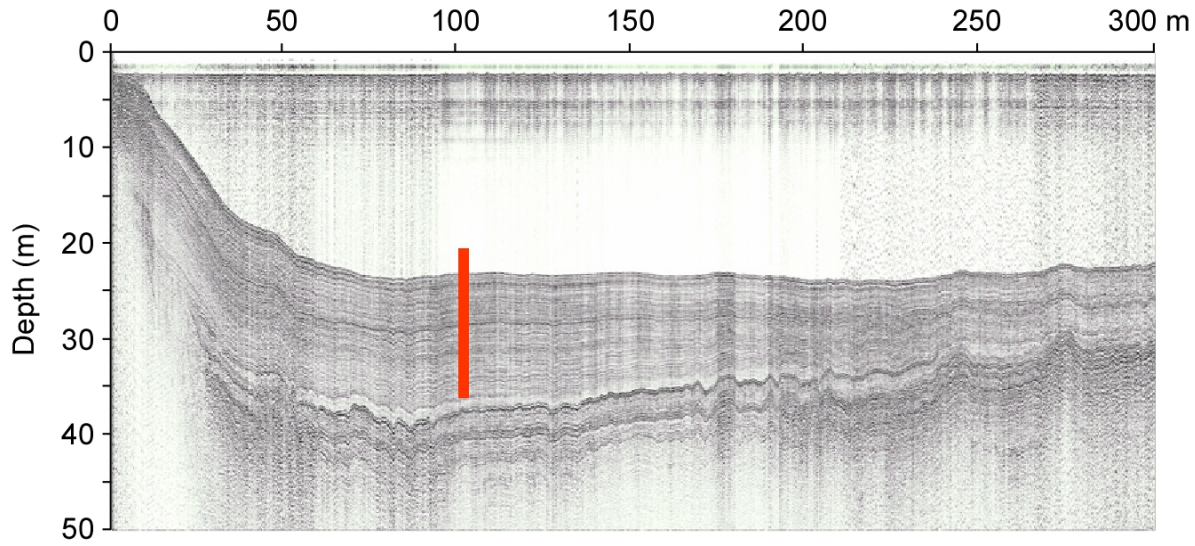

Figure 2.1: *Transversal seismic profile from Chernyshov Bay showing the coring location (N45°58'581"; E°59°14'461: Core CH1 and N45°58'528"; E°59°14'459: Core CH2) and sediment structures.*

It includes three sites offshore (Fig. 1.1): Tastubek Bay (N46°33'340"; E 60°42'298"; TAS1), Tschebas Bay (N46°17'868"; E°59°40'040: TSC1 and N46°18'266"; E°59°38'912: TSC2), Chernyshov Bay (N45°58'581"; E°59°14'461: CH1 and N45°58'528"; E°59°14'459: CH2). Two types of cores were retrieved from the drilling platform. The piston coring (http://www.uwitec.ut) allowed for retrieving a composite core up to 11 m in length, consisting in sediment cores of 3 m in length with overlapping sections of about 0.5 m. This technique, however, hampers in getting the topmost sediments. To complete the sedimentary sequence with surface sediments, we used a gravity corer covering for the uppermost 0.5 to 0.6 m with preserved sediment top features (Kelts, 1978).

Both piston and gravity cores were used for macro- and microsedimentology, micropalaeontology, XRF screening and radiocarbon dating (^{14}C). For the thesis, though lithological description and physical parameters measurements were performed on all sediment cores from the 3 coring locations, we only discuss palynological and sedimentological data gathered from the cores at Chernyshov Bay (Fig. 1.1) (CH1 and CH2), offering the longest sedimentary sequence by far available in the Aral Sea (see Chapters III, IV and V).

II.2. Sediment preservation and lithology

Lithological description, photographs and measurements of physical properties (Gamma-ray density, magnetic susceptibility) were performed directly after core opening on the surface of split core halves. Coring quality is generally good though disturbed laminations due to coring artefacts (e.g., sea roughness during drilling) may sometimes occur. Sediment lithology was described in detail on cores offshore from Chernyshov Bay (CH1 and CH2) (Fig. 2.2), Tschebas Bay (TSC1 and TSC2) and Tastubek Bay (TAS1). Sediment consists mostly of greyey silty clays and dark organic muds, occasionally with intercalated evaporites (gypsum, salt, sometimes mirabilite) revealed from observations on smear slides. Neither erosive discontinuity, nor features of bottom traction or turbiditic sediments were observed in the different coring sites. Moreover, no slumps, faults, or sediments loads have been recognized.

Chernyshov Bay is situated at the northern tip of the western basin of the Large Aral Sea. Echo sounding revealed a shallow bay that is followed by a sharp descent of the sea bottom to a 22 m-deep basin (Fig. 2.1). The most striking feature at this location is the occurrence of a strong pycnocline and the presence of a huge anoxic water body below it (Friedrich and Oberhänsli, 2004), preventing sedimentation from bioturbation. Accordingly, sediments from Chernyshov Bay show mostly well-preserved laminations. Cores CH1 and CH2 were collected 1m apart at about 1 km from the shoreline, at a water depth of 22 m. A detailed lithological description of Core CH1 (Fig. 2.1a), consisting in cores 21, 22, 23 [0–6.1 m] and 27, 28, 29 [6.1–11.05 m], is given in Chapter V.2.4. Core CH2 (Fig. 2.1b) consists in cores 30, 31 and 32 [0–6.2 m]. Splicing of cores 30, 31, 32 (Core CH2) and cores 27, 28, 29 with overlaps results in the composite section CH2/1, which was investigated for high-resolution palynological analyses.

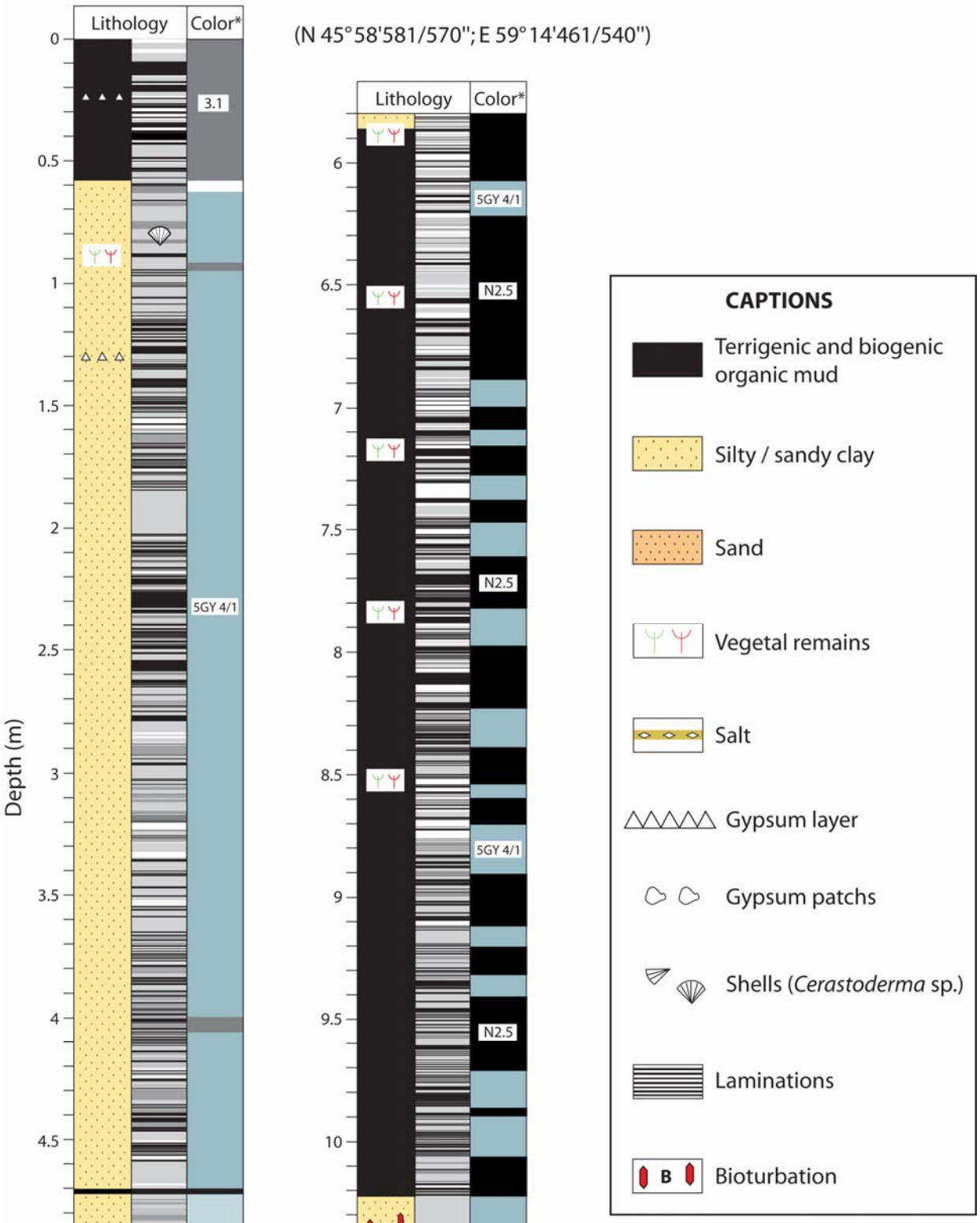

Figure 2.2a: *Lithology of sediment piston Cores CH1 with coordinates. Description of sediment colour is based upon the colour index of the Munsell® Soil Colour Chart. Core CH1 consists in the splicing of cores 21, 22, 23, 27, 28, 29.*

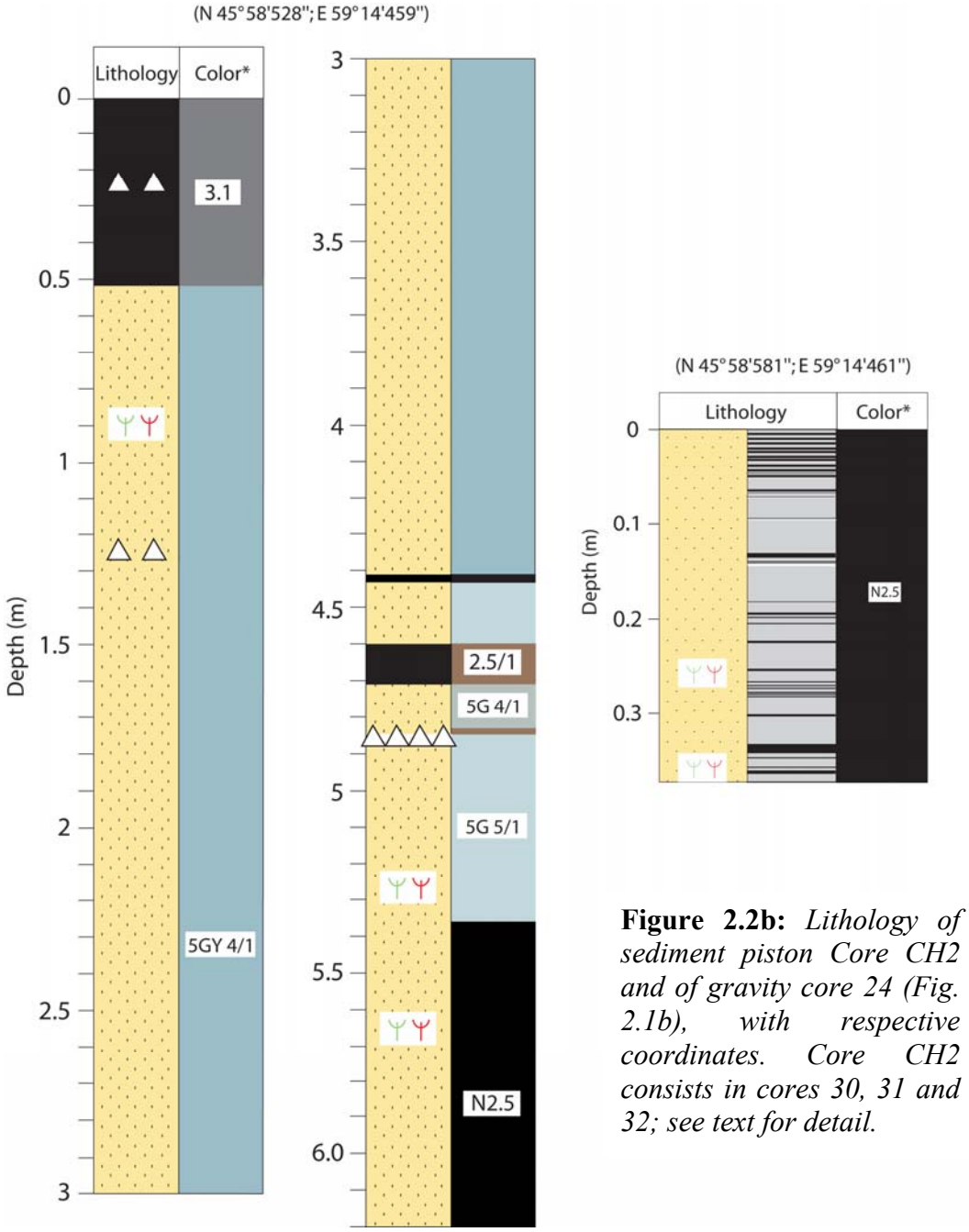

Figure 2.2b: *Lithology of sediment piston Core CH2 and of gravity core 24 (Fig. 2.1b), with respective coordinates. Core CH2 consists in cores 30, 31 and 32; see text for detail.*

A detailed lithological description of Core CH2/1 is given in Chapter III.1.1. The correlation between Cores CH1 and CH2 was performed by matching laminations using photographs, physical properties and X-Ray Fluorescence (XRF) scanning (Fig. 2.3). Sediment cores CH1 and CH2 were continuously sub-sampled for palynological investigations after splitting of the cores in two halves. 125 and 35 sediment samples were collected downcore for the analyses of dinoflagellates cysts and pollen grains at a resolution of about 10 cm and 40 cm, respectively, and stored within plastic boxes in a cool room at 4°C. Chemical treatments of sediment samples for extracting and condensing palynomorphs were conducted in the laboratory of the University Claude Bernard of Lyon (see Chapter II.3.2.1.).

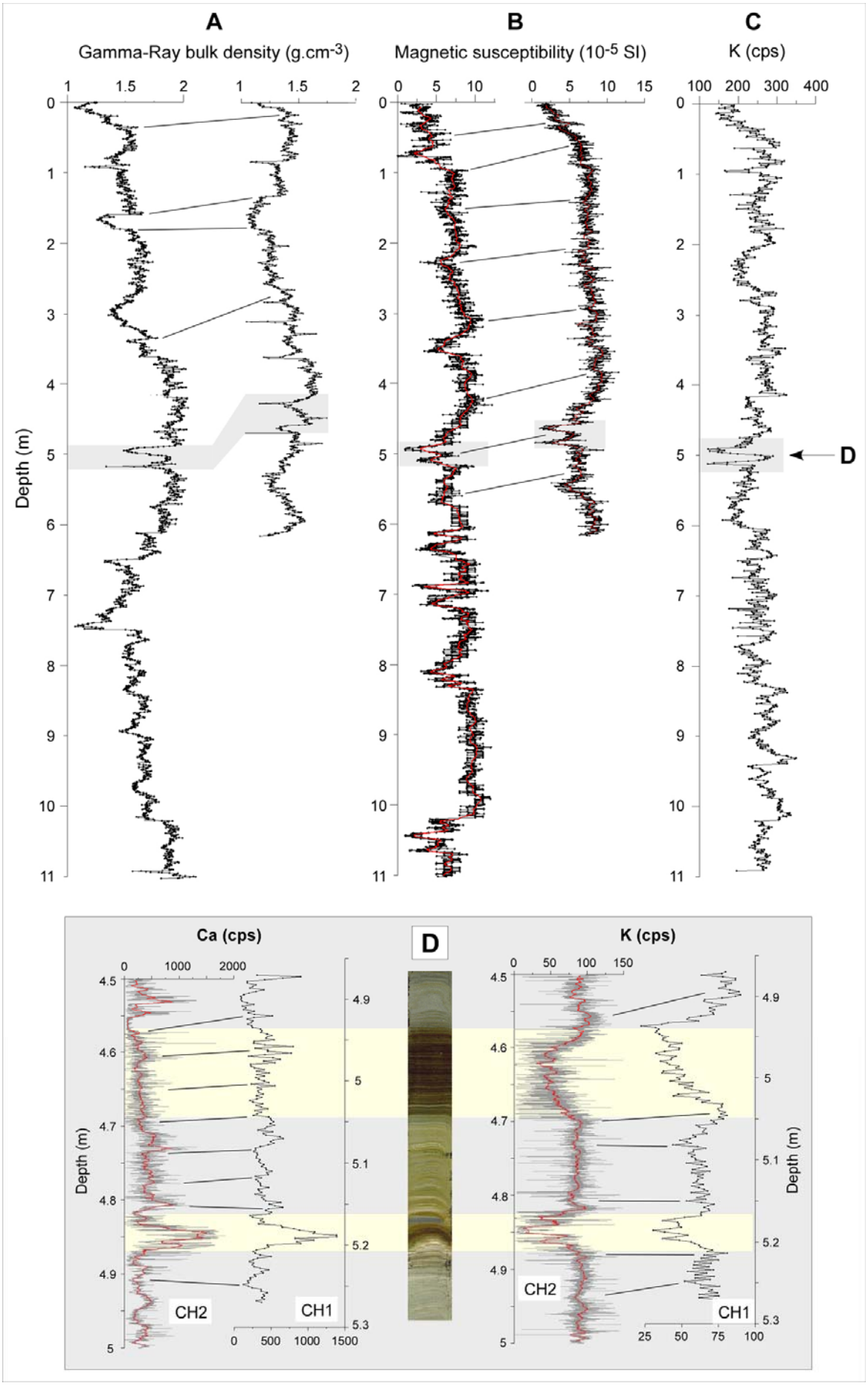
A
Gamma-Ray bulk density (g.cm-3)
B
Magnetic susceptibility (10-5 SI)
C
K (cps)
Depth (m)
D
Ca (cps)
K (cps)
CH2
CH1
Depth (m)

Figure 2.3: *Stacked downcore variations in Gamma-ray density (A) and magnetic susceptibility (B) showing correlating trends between Cores CH1 and CH2 from Chernyshov Bay. Gamma-ray plots are original data at resolution steps of 0.5 cm. MS plots are original data at resolution steps of 0.1 cm [608.2–837.6 cm; 1020.1–1102.1 cm] to 0.2 cm (black curves); red curves are smoothed data using a 51-point running average. C–D: X-Ray fluorescence analyses on Cores CH1 and CH2. C: stacked downcore variations in Potassium (K) in Core CH1, at scanning steps of 1 cm-resolution. D: close-up interval [4.5–5 m] in Core CH2 showing correlating features for K (upper panel) and Ca (lower panel) at different scanning steps: black curves 0.2 cm-; light-grey curves: 40 µm-resolution; red curves: smoothed data using a 101-point running average. Note the remarkable anti-correlation between K and Ca. The light-grey shading refers to the close-up interval.*

II.3. Inorganic proxies

II.3.1. Physical properties

Gamma ray natural radiation density

Gamma ray natural radiation of bulk sediment (Bodwaker, 1996) was measured using the GeoTek device (http://www.geotek.co.uk). We used this non-destructive method on split core halves to determine the gamma ray attenuation through the core. The GeoTek device is characterized by a gamma ray source and a detector which are mounted across the core on a sensor that aligns them with the centre of the split core (Fig. 2.4).

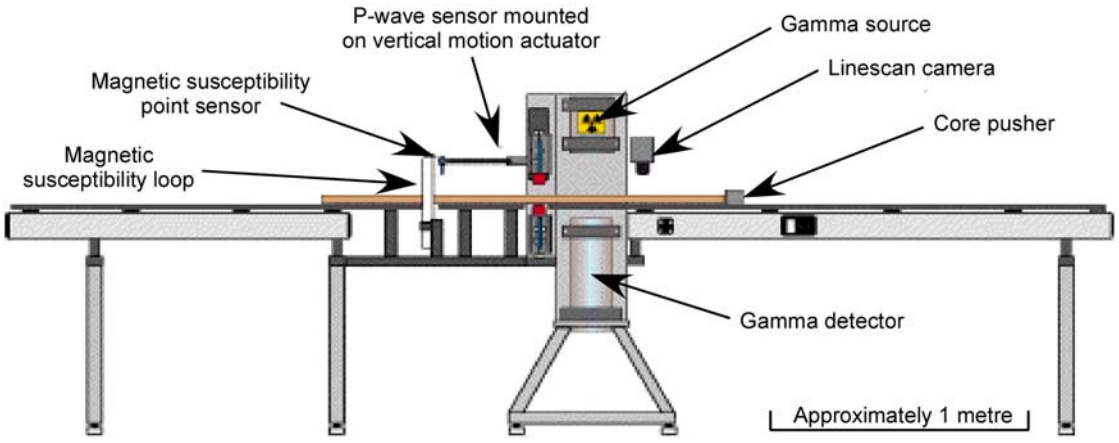

Figure 2.4: *Schematic representation of the GeoTek device (from http://www.geotek.co.uk).*

A narrow beam of gamma rays is emitted from a 10-milli-curie Cesium-137 source with energy mostly of 0.662 MeV. Photons from the ^{137}Cs emitting source pass through the core and are detected on the other side. The incident photons are scattered by the electrons in the core with a partial energy loss. The attenuation, therefore, is direcly related to the number of electrons in the gamma ray beam. By measuring the number of unscattered gamma photons

that pass through the core unattenuated, the density of the core can be determined. Gamma ray attenuation density measured on cores from Chernyshov Bay (CH1, CH2) was performed at a step-resolution of 0.5 cm, and compiled in a CD-ROM for data archive. In this study, Gamma ray attenuation density is mostly used for core-to-core correlation purposes (Fig. 2.3A).

Magnetic susceptibility

Magnetic susceptibility (MS expressed as χ) of lake sediments is controlled by the concentration and the grain size distribution of ferromagnetic minerals. It is a non-destructive method (Fig. 2.4), which provides a valuable tool for detailed correlation of sediment records (Thompson et al., 1975; Verosub and Roberts, 1995; Nowaczyk, 2001). The magnetic susceptibility is a measure of the ease with which sediments are magnetized when subjected to a magnetic field. Sediment that is rich, per unit volume, in magnetizable substances will show high readings. In contrast, sediment that is poor in magnetizable substances, and/or contain diamagnetic minerals (e.g. organic matter, quartz, feldspars, calcium carbonate) will yield low or negative values. Magnetizable minerals include the ferromagnetic minerals (strongly magnetizable as for instance magnetite, hematite, iron titanium oxides) and any of the paramagnetic minerals (moderately magnetizable including a broad panel of substances all of which contain Fe^{2+}, Fe^{3+}, or Mn^{2+} ions) and other substances. The paramagnetic minerals may include clay minerals (chlorite, smectite and glauconite), iron and manganese carbonates (siderite, rhodochrosite), ferromagnesian silicates (olivine, amphiboles, pyroxenes, etc.), as well as a variety of ferric-oxyhydroxide mineraloids. The magnetic assemblage in sediments is typically composed of particles originating from erosion in the catchment (detrital input), in-situ dissolution and authigenesis of magnetic carriers (Berner, 1980; Snowball, 1993; Williamson et al., 1998).

MS was measured directly after core opening on the surface of split core halves with a Bartington MS2E sensor (GFZ Potsdam) at a resolution of 1 to 2 mm. The Chernyshov Bay MS record shows moderate variations in amplitude and frequency, with generally low values that reflect the signature of the catchment area. Admittedly, the source area of the detritics is mainly confined to the surrounding Palaeogene marls which also have a very low content in magnetic particles (Bolle and Adatte, 2001). At Chernyshov Bay, the coring site is characterized by relatively high sedimentation rates within some sedimentary sequences (up to 3 cm/ yr) which mainly stem from the overwhelming presence of terrigenous material

throughout the core (see Chapter V). For this study, the MS record was applied for high-resolution core correlation (Fig. 2.3B).

II.3.2. X-Ray Fluorescence (XRF) spectrometry: a proxy of geochemical variability of sediments

XRF spectrometry consists in identifying and quantifying the elemental composition of a substance (Jenkins, 1999). In XRF spectrometry, high-energy primary X-ray photons are emitted from a source and strike the sample, involving the so-called "photoelectric effect". The energy of the emitted fluorescent X-ray photon is determined by the difference in energies between the initial and final orbitals of the individual transitions (K, L, or M), and is characteristic of a specific element. Therefore, this method enables a non-destructively measure of the elemental composition of a sediment. The energy required to knock out electrons from their initial orbital depends on the atomic number (N) of the element in the periodic table; i.e., the higher N, the higher primary energy required.

In sediment cores from the Aral Sea, XRF scanning was conducted on split cores at different scanning steps. 1cm-resolution runs were performed with a profiling X-ray fluorescence scanner (Jansen et al., 1998; Röhl and Abrams, 2000) for gaining the overall distribution in K, Ca, Ti, Mn, Fe and Sr on Cores CH1, TSC1 and TAS1 (CD-ROM). Additional running at 5 mm and 2 mm-resolution was applied on the same cores to (i) get a higher-resolution set of changes in elemental distribution within highly laminated intervals, (ii) match dominant trends of variability with prominent changes in sedimentation types and (iii) test the reproductibility of the method using different resolution steps (Fig. 2.5). Results show that though 1 cm-scanning step runs do not allow to get the resolution required in highly laminated intervals where the chemical composition is expected to vary from one sequence of laminae to the next, similar trends are obtained when comparing relative rather than absolute values at different resolutions. Besides, where a more detailed comparison between XRF and sedimentological data was required, scanning steps of 40µm were conducted on selected sediment intervals preserved in Araldite®-impregnated polished slabs. XRF measurements were used together with MS and microfacies data to infer changes in detrital inputs in Core CH1 (see Chapter V).

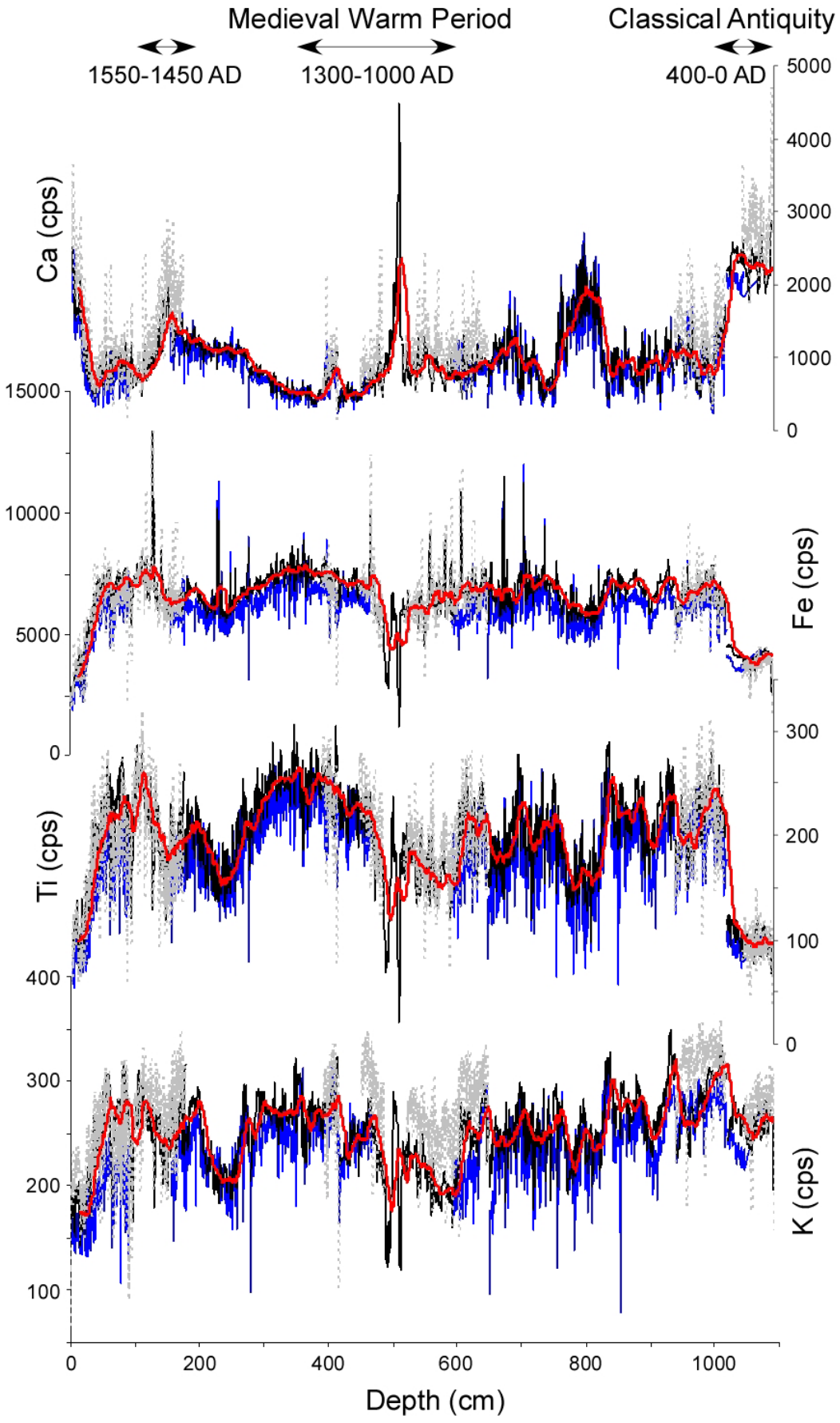

Figure 2.5: *Stacked downcore variations of K, Ti, Fe and Ca (cps) in Core CH1, respectively, at scanning steps of 1 cm- (black full line), 0.5 cm- (blue full line) and 0.2 cm-resolution (grey dashed line), showing similar trends. Red thick lines are smoothed curves using a 15-point running average.*

II.3.3. Microfacies analyses: a proxy of sedimentary dynamics

Microfacies analyses were conducted in selected laminated intervals only, with the aim to produce implemental high-resolution data to XRF measurements. From thin sections we determined semi-quantitatively changes in grain size, thickness of laminations and abundance of selected diatom species and searched for possible micro-disturbances in sedimentation. The confrontation between microfacies and geochemical data in highly laminated intervals at the scale to one-to-one lamination helps to (i) decipher the nature and type of sediments (organic, clastic or mixed sediments), and (ii) relate changes into the sedimentary dynamics to internal / external forcings of the sedimentary system. Material and methods used for microfacies analyses are given in Chapter V.2.2.

II.4. Organic proxies

II.4.1. Dinoflagellate cysts – a proxy of hydrological change

Dinoflagellates are microscopic, unicellular, flagellated and often photosynthetic protists generally involved in an asexual reproduction (Fensome et al., 1993). They represent a significant part of the primary planktonic production in both oceans and lakes (Wall and al., 1977). Within their life cycle, many dinoflagellates are characterized by two different states with distinct morphology (Fig. 2.6): a planktonic motile stage reflecting favourable environmental conditions (spring, summer) and a planktonic / benthic cyst stage which forms in autumn when lowered temperatures take place, and remain dormant on the sea floor in winter. Dinoflagellates can, however, remain in dormancy during prolonged periods of prevailing unfavourable cold conditions. The alternation between the motile and the encysted form is, therefore, primarily regulated by seasonal variability of environmental conditions, but not restricted to. The resting cyst, whose wall is generally very resistant to degradation, is preserved in sediments (Head, 1996).

Both heterotrophic and autotrophic dinoflagellates are known (Fensome et al., 1993). Whereas autotrophic species preferentially thrive in waters enriched in nutrients (delta mouths, upwelling currents), heterotrophic species generally feed on phytoplankton cells (diatom, dinoflagellates). Certain dinoflagellate species can stand both fresh and salt waters although the majority is marine and sensitive to changes in water mass, including temperature

and salinity (Marret and Zonneveld, 2003). As a whole, the dinoflagellates have a wide temperature (1–35° C) and salinity tolerance (0–50 psu) (e.g. Marret and Zonneveld, 2003).

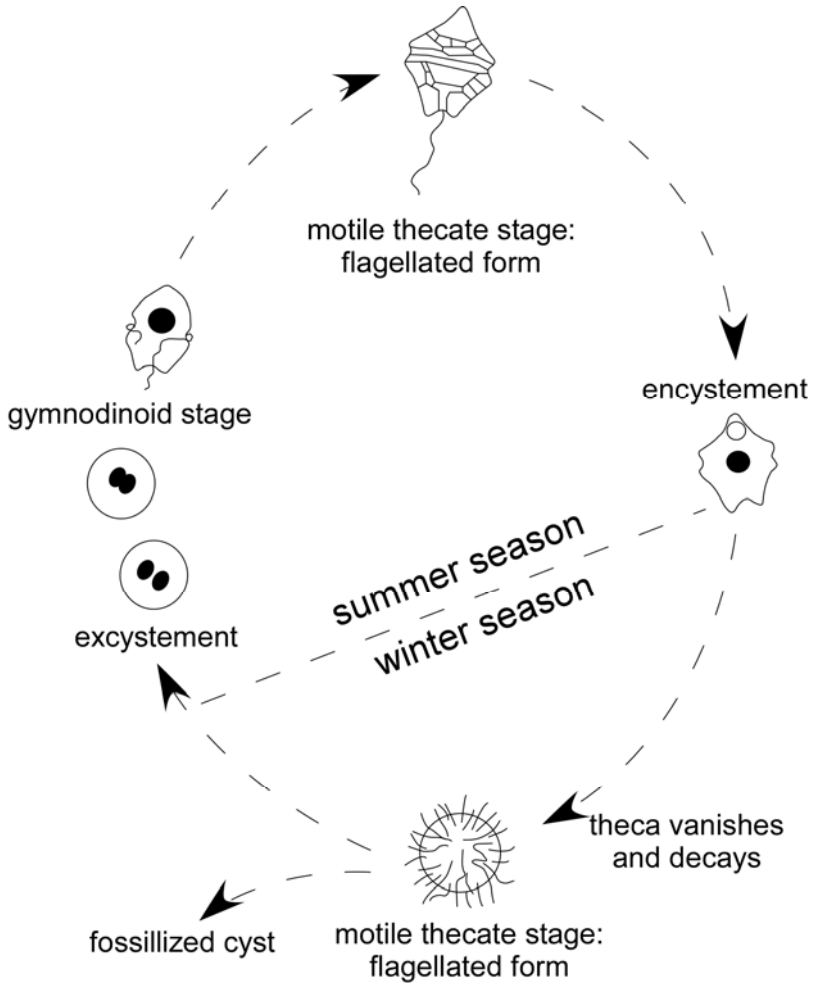

Figure 2.6: *Schematic diagramm representing the life cycle history of dinoflagellates.*

They can be used, therefore, as privileged indicators of changing environmental conditions. Numerous recent studies have used the dinoflagellate cysts to reconstruct sea-surface conditions (Dale, 1996; Rochon et al., 1999; Matthiessen and de Vernal, 2001; Dale and Dale, 2002). In this thesis, studies on dinoflagellates rely on the preservation of their cysts in late Holocene sediments from Chernyshov Bay. We focus on the ability of dinoflagellate cyst assemblages to identify climatically-induced salinity changes in the Aral Sea (Chapter III).

II.4.2. Pollen grains – a proxy of land moisture conditions

Many coniferous and flowering plants produce vast quantities of pollen as part of their reproductive cycle. Pollen grains are dispersed widely over the landscape, mainly by winds

and rivers over short and long distances. Most of pollen grains fall to the ground or are washed from the atmosphere by rain and ultimately become part of sedimentary particles accumulating on the floor of lakes. Because plants often have very specific climatic requirements and/or tolerances, knowing which plants were growing in an area at a particular time also gives reliable information on past climate and landscape conditions. The Aral Sea, located in the interior of the large Asian continent characterized by different latitudinal vegetation types (e.g. Tarasov *et al.*, 1998a; Tarasov *et al.*, 1998b), represents a privileged area for investigating past evolution of landscapes in relation with climate change during the late Holocene. However, the richness in pollen grains within recent and modern sediments is controlled by different factors: (i) the pollen production that varies from one plant producer to the other, (ii) their diffusion in the environment by local / regional transporting factors, and (iii) their preservation in sediments. The strategy and method used for pollen analyses must be, therefore, clearly assessed with respect to the aim of the study before leading to palaeoenvironmental and palaeoclimatic reconstructions.

Most pollen grains are extremely resistant to decay (Brooks and Shaw, 1968), which allows their preservation in large numbers in sediments. In order to extract the pollen grains, sediment samples must be chemically processed. The walls of pollen grains (or exine) are made of sporopollenin (Rowley and Southworth, 1967), one of the most resistant natural chemical substances known, imparting a high acid-proof to the exine and the preservation of its characteristic criteria for identification. The strategy used for the chemical treatment of samples has been adapted from the method described by Cour (1974). It basically aims to remove all organic and mineral components except the resistant palynomorphs (pollen grains, spores) and to concentrate them in a residue. The successive steps used for the chemical treatment of the pollen samples, together with the method used for the calculation of the richness in palynomorphs (Cour, 1974), are presented in detail separately to the thesis (CD-ROM: "*Preparation of palynological slides*"). Also given in the CD appendix is the method used for the identification and counting of pollen grains under the photonic microscop, following the concept of Erdtmann (1966).

II.4.3. Climate quantification and reconstruction based on pollen data

For a quantification of palaeoclimate signals recorded in plant remains, the "probability mutual climatic spheres" (PCS) method described in Klotz and Pross (1999) and Klotz *et al.*

(2003, 2004) is applied. Principles and proceedings of this method and the application of the PCS method to pollen grain data from Core CH2/1 are explained in Chapter IV.2.4. We then refer to this section for detailed information. Results are compiled separately to the thesis (CD-ROM for data archive).

II.5. Dating and chronology

Laminated lacustrine sediments are an important tool for studying the palaeoclimatic and palaeoenvironmental variability of continental regions because of the large panel of proxy data they provide. A prerequisite, however, is the establishment of a precise and reliable chronology which is basically crucial to compare data with other high-resolution records and to perform correlations. The assessment of a reliable age model for this unique archive of past climate that represents the Aral Sea was the first challenge of the thesis regarding the poorness of dating by now available on Holocene sediments.

A number of authors attempted to date palaeoshorelines from the Aral Sea using different analytical methods (see Boomer et al., 2000 and references herein for a review). Dating on lake sediments were mostly undertaken by Maev and Karpychev (1999) based on 40 radiocarbon age determinations from two cores (86 and 45) retrieved nearby the central and western parts of the Aral Sea, respectively, and Maev and Maeva (1991) from a number of cores taken in the central part of the basin (e.g. Boomer et al., 2000). Most of these data, however, concern early and mid-Holocene sequences and dating of late Holocene sediments (e.g. the past 2000 years) are rather scarce. Such dating have been commonly used for palaeontological (Aleshinskaya, 1991; Aleshinskaya et al., 1996), sedimentological (Ferronskii et al., 2003) and geochemical purposes (Le Callonec et al., 2005) at generally low time-resolution.

Recently, in the frame of the project CLIMAN, a series of new dating were conducted on piston and gravity cores from the Aral Sea. Based on ^{210}Pb and ^{137}Cs measurements, as time markers, and using the constant rate of supply (CRS) model (Appleby, 1997), Heim (2005) dated the gravity core 24 from Chernyshov Bay to the time frame [1905–2002]. A peak in ^{137}Cs, recorded both in the gravity core 24 and in core 30 (top Core CH2) at different depths, was regarded to be a good correlation tool, reflecting the bomb period at 1963–1964 AD. Therefore, by using both ^{137}Cs values and matching laminations, a correlation has been established between gravity core 24 and Cores CH1 / CH2, assuming a post-1964 AD age for

the upper 0.46 and 0.39 m in Cores CH1 and CH2, respectively. This is concurrent with ^{14}C dating obtained at 0.56 m (CH1) and 0.55 m (CH2) which indicate a post-1950 age (expressed in pMC) at sediment tops (Table I).

Sample name	Core depth (m)	Lab. no.	Age ^{14}C (BP)	Error bar	Calibrated age (yr BP)	Dated material
Tastubek Bay (Small Aral)						
Aral 3 10-12cm	0,11	Poz-4752	128.7 pMC	0.3	modern	*Vaucheria* sp. + mollusc shells
Tschebas Bay (Large Aral)						
Aral 16 163-167cm	1,33	Poz-4765	1105	30	982, 1035	mollusc shells
Aral 16 185-187cm	1,54	Poz-4763	3405	30	3700	*Vaucheria* sp.
Aral 16 200-201cm	1,685	Poz-11468	1125	35	1010, 1053	*Vaucheria* sp.
Aral 17 197-200cm	1,83	Poz-4754	2550	30	2710, 2730	*Vaucheria* sp.
Aral 17 219-221cm	2,05	Poz-4755	7070	90	7930	*Vaucheria* sp.
Chernyshov Bay (Large Aral)	*CH1 / CH2/1*					
Aral 30 53-57cm	0.55	Poz-12281	101.9 pMC	0.3	modern	*Vaucheria* sp.
Aral 21 55-57cm	0.56	Poz-4753	108.6 pMC	0.3	modern	*Vaucheria* sp.
Aral 22 34-36cm	1.41 / 1.3	Poz-4750	4320	80	4860	*Vaucheria* sp.
Aral 32 134.5-138.5cm	4.91 / 4.65	Poz-13511	815	30	730	TOC
Aral 32 146.5-149.3cm	5.015 / 4.77	Poz-13561	1340	100	1285	TOC
Aral 32 155.5-156 + 23 193.5-194.5cm	5.06 / 4.84	Poz-13512	1295	30	1265	TOC
Aral 23 200-205cm	5.145 / 4.925	Poz-9834	1240	200	1173	ostracods
Aral 27 70-72cm	5.16 / 4.97	Poz-12278	1290	80	1195, 1265	*Vaucheria* sp.
Aral 23 225-227cm	5.38 / 5.16	Poz-4756	1650	30	1540	*Vaucheria* sp.
Aral 23 275-277cm	5.88 / 5.66	Poz-4758	1225	30	1170	*Vaucheria* sp.
Aral 32 255-257cm	6.06 / 5.85	Poz-12282	1270	35	1185, 1205, 1240, 1255	*Vaucheria* sp.
Aral 27 167-167.5cm	6.125 / 5.93	Poz-4759	1655	30	1540	*Vaucheria* sp.
Aral 27 209-212cm	6.555 / 6.34	Poz-12279	1160	110	1062	*Vaucheria* sp.
Aral 27 269-271cm	7.15 / 6.93	Poz-4762	1395	30	1300	*Vaucheria* sp.
Aral 28 15.5-17.5cm	7.615 / 7.395	Poz-4764	1600	40	1521	*Vaucheria* sp.
Aral 28 40-45; 52-54cm	~7.95 / ~7.73	Poz-9662	1480	30	1355	ostracods
Aral 28 112-114cm	8.505 / 8.285	Poz-4760	1515	25	1395	*Vaucheria* sp.
Aral 28 229-231cm	9.675 / 9.46	Poz-12280	9930	60	11300	*Vaucheria* sp.
Aral 29 2-8.5cm	10.22 / 10.01	Poz-13559	3930	50	4420	TOC
Aral 29 51-58.5cm	10.72 / 10.505	Poz-13560	3245	35	3475	TOC

Table 1: *^{14}C dating measurements performed in this study for Tastubek Bay (Small Aral Sea), Tschebas Bay and Chernyshov Bay (Large Aral Sea). Measurements were conducted by Dr. Tomasz Goslar in the Poznań Radiocarbon Laboratory (Poland). Precision on the dated material is given. Shaded values correspond to reworked C_{org} material whereas green values are ^{14}C dating used in the age model.*

Another recent series of new dating was obtained on Cores Ar-7, Ar-8 and Ar-9 retrieved at Chernyshov Bay at about 50 m apart from Cores CH1 and CH2, using terrestrial macrofossils (Nourgaliev et al., 2003). The correlation between magnetic susceptibility (MS) data from Cores Ar-7, Ar-8, Ar-9 and Cores CH1, CH2 is remarkable (Fig. 2.7). Hence, by assuming a modern age at sediment tops, this correlation enables to establish a reliable age model for the 6-upper meters of Core CH1 (see Chapter V.2.5) and for the whole Core CH2 (see Chapter III.2.2). Radiocarbon analyses of drowned saxaul stumps near Barsakelmes Island gave an age of 287 ± 5 ^{14}C yr BP, corresponding to an important sea-level fall to about 41 m.a.s.l. (Boomer et al., 2000). This date comes to improve and validates our age model, as it corresponds to a noticeable increase in salinity levels (see Chapter III.4.2.).

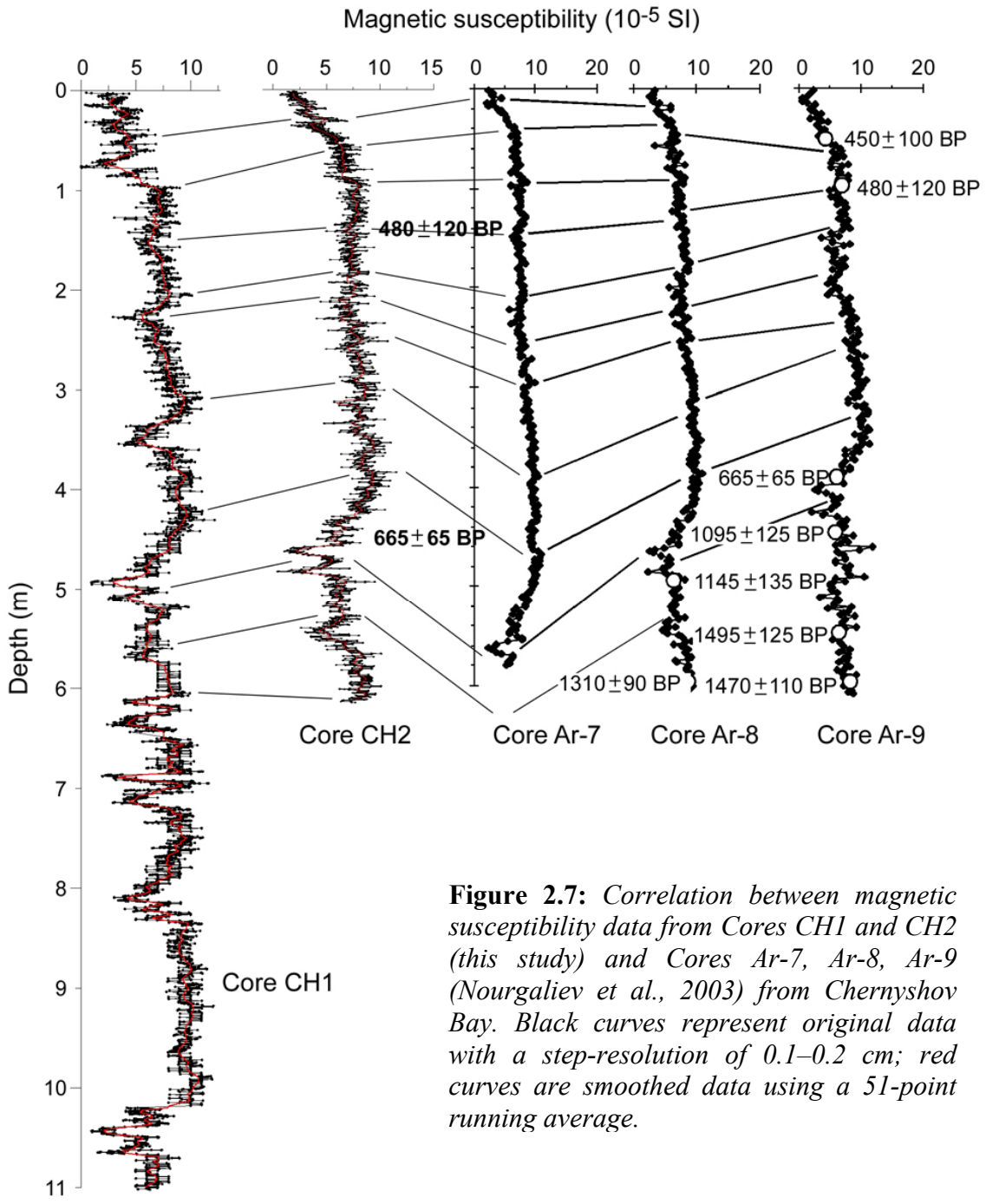

Figure 2.7: *Correlation between magnetic susceptibility data from Cores CH1 and CH2 (this study) and Cores Ar-7, Ar-8, Ar-9 (Nourgaliev et al., 2003) from Chernyshov Bay. Black curves represent original data with a step-resolution of 0.1–0.2 cm; red curves are smoothed data using a 51-point running average.*

To finalize our age model downcore, twenty additional AMS ^{14}C dating on undisturbed sediments from Chernyshov Bay were performed (Fig. 2.8). The material selected for dating is described in detail in Table 1. Absolute dating was calibrated using the IntCal04 terrestrial calibration curve of Reimer et al. (2004). They indicate values with 2 standard deviations (95% of confidence). The error bar for some data is quite large and probably stems from the small size of the sample. For assessing a reliable chronology below 6 m, dated intervals with reworked dead C_{org} material (see shadings in Table 1) were not included in our age model.

They probably reflect erosion of material washed-off from the catchment area during sheet-wash extremes. By extrapolation of sedimentation rates downcore, we propose that the basement of Core CH1 (and CH2/1) correspond to the beginning of the 1st millennium AD, and that, therefore, Cores CH1 and CH2/1 represent the past ca. 2000 years (Fig. 2.8). Our age model implies important changes in sedimentation rates for Cores CH2/1 (see Chapter III.2.2) and CH1 (see Chapter V.2.5).

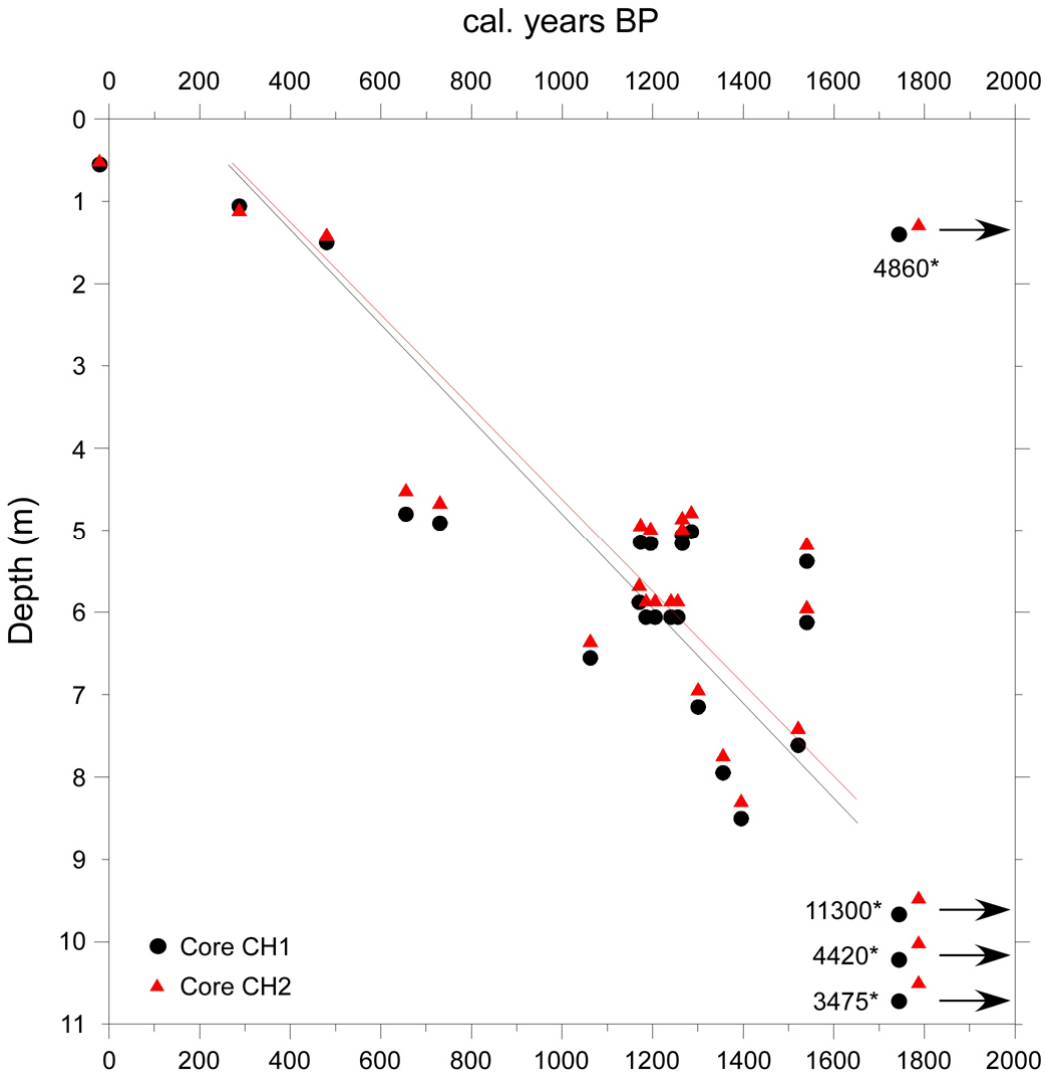

Figure 2.8: *Age-depth plot for Cores CH1 (black circles) and CH2/1 (red triangles). ^{14}C values marked with * indicate reworked material older than 2000 yr BP.*

Due to the lack of dating of living algae samples from the near-shore, no reservoir correction can be applied by now on sediments from the Aral Sea. This is presently still work in progress. However, regarding the overwhelming dominance of sulphates in the Aral Sea (Létolle and Mainguet, 2005) as compared to marine ecosystems where dissolved carbonates prevail, we would expect reservoir effects in the Aral Sea to be relatively small.

Chapter III: Hydrographic development of the Aral Sea during the last 2000 years based on a quantitative analysis of dinoflagellate cysts

P. **Sorrel** [1,2] , S.-M. **Popescu** [2], M.J. **Head** [3], J.P. **Suc** 2, S. **Klotz** [2, 4], H. **Oberhänsli** [1]

(1) GeoForschungsZentrum, Telegraphenberg, D-14473 Potsdam, Germany;
(2) Laboratoire PaléoEnvironnements et PaléobioSphère (UMR CNRS) 5125, Université Claude Bernard – Lyon 1, 27–43, boulevard du 11 Novembre, 69622 Villeurbanne Cedex, France;
(3) Department of Geography, University of Cambridge, Downing Place, Cambridge CB2 3EN, UK; present address: Department of Earth Sciences, Brock University, 500 Glenridge Avenue, St. Catharines, Ontario L2S 3A1, Canada;
(4) Institut für Geowissenschaften, Universität Tübingen, Sigwartstrasse 10, 72070 Tübingen, Germany.

In: *Palaeogeography, Palaeoclimatology, Palaeoecology* 234 (2–4), 304–327

Abstract

The Aral Sea Basin is a critical area for studying the influence of climate and anthropogenic impact on the development of hydrographic conditions in an endorheic basin. We present organic-walled dinoflagellate cyst analyses with a sampling resolution of 15 to 20 years from a core retrieved at Chernyshov Bay in the NW Large Aral Sea (Kazakhstan). Cysts are present throughout, but species richness is low (seven taxa). The dominant morphotypes are *Lingulodinium machaerophorum* with varied process length and *Impagidinium caspienense*, a species recently described from the Caspian Sea. Subordinate species are *Caspidinium rugosum*, *Romanodinium areolatum*, *Spiniferites cruciformis*, cysts of *Pentapharsodinium dalei*, and round brownish protoperidiniacean cysts. The chlorococcalean algae *Botryococcus* and *Pediastrum* are taken to represent freshwater inflow into the Aral Sea.

The data are used to reconstruct salinity as expressed in lake level changes during the past 2000 years. We quantify and date for the first time prominent salinity variations from the northern part of the Large Aral Sea. During high lake levels, *Impagidinium caspienense*, representing brackish conditions with salinities of about 10–15 g kg^{-1} or less, prevails. Assemblages dominated by *L. machaerophorum* document lake lowstands during approximately 0–425 AD (or 100? BC–425 AD),

920–1230 AD, 1500 AD, 1600–1650 AD, 1800 AD and since the 1960s. Because salinity in the Aral Sea is mostly controlled by meltwater discharges from the Syr Darya and Amu Darya rivers, we interpret changes in salinity levels as a proxy for temperature fluctuations in the Tien Shan Mountains that control snow melt. Significant erosion of marine Palaeogene and Neogene deposits in the hinterland, evidenced between 1230 AD and 1400 AD, is regarded as sheet-wash from shore. This is controlled by the low pressure system that develops over the Eastern Mediterranean and brings moist air to the Middle East and Central Asia during late winter and early spring. We propose that the recorded environmental changes are related primarily to climate, but perhaps to a lesser extent by human-controlled irrigation activities. Our results documenting climate change in western Central Asia are fairly consistent with reports elsewhere from Central Asia.

Keywords: Aral Sea hydrology; Late Holocene; Dinoflagellate cysts; lake level changes; glacial meltwater discharge; Mediterranean low-pressure system.

III.1. Introduction

The Aral Sea is a large saline lake in the Aral–Sarykamish depression in Central Asia and bordered by Kazakhstan and Uzbekistan (Fig. 3.1). After about 14 ka, when the Aral and Caspian seas became separated from one another (Tchepaliga, 2004), the Aral Sea level developed a strong dependence upon the inflow of its two main tributaries, the Syr Darya and Amu Darya rivers. These rivers originate from the highest part of the Pamir and Tien Shan mountains, 1500 km southeast of the Aral Sea. Nowadays, the Aral Sea is an endorheic lake with low freshwater inflow from rivers and low precipitation due to the extremely arid continental climate (~100 mm/yr on average; Létolle and Mainguet, 1993). As a result of extreme insolation-forced heating leading to desert conditions, the mechanical and chemical weathering of sediments is accentuated and erosional processes are enhanced.

During the past 40 years the Aral Sea, which was the fourth largest inland lake in the world, has suffered a dramatic reduction in size due to intensive irrigation activities in the hinterland (Boomer *et al.,* 2000). As a consequence, its area has diminished more than fourfold, and the volume more than tenfold. The lake level has in fact stabilised during the last three to four years, as irrigation has decreased (Zavialov, 2005). Nonetheless, the lake level dropped by 22.5 m from its value in 1965, and the Aral Sea became split into two major water bodies, namely the Large Aral Sea represented by its western and eastern basins which are connected only through a short (3 km) and shallow (8 m) channel (Nourgaliev, pers. comm. in Zavialov*,* 2005), and the Small Aral Sea in the North (Fig. 3.1). Today, the lake level is at 30.5 m above sea level (a.s.l.) (Zavialov et al*.,* 2003), whereas it was at 53 m a.s.l. in 1960 (Létolle and Mainguet, 1993). As a result of the considerable reduction in water volume and the reduced freshwater influx into the Aral Sea, salinity levels have increased more than eightfold.

Figure 3.1: *Location map of the present Aral Sea (in light blue) and the study area. The orange area represents the Aral Sea's surface and associated lake levels from the early 1960s, whereas the dashed lines represent the former courses of episodic local rivers (after Létolle and Mainguet, 1993).*

Surface-water salinity rose from 10.4 g kg^{-1} in 1960 to more than 80 g kg^{-1} in 2002–2003 (Zavialov et al., 2003; Friedrich and Oberhänsli, 2004). The salinification had recently considerable consequences for the flora and fauna (Mirabdullayev et al., 2004), thus showing that the Aral Sea represents an ecosystem highly sensitive to climate changes and anthropogenic impact.

The palaeoenvironmental development of the Aral Sea has been studied from sediments since the late 1960s. Maev and Karpychev (1999) dated changes in palaeoenvironmental conditions over the past 7000 years from two cores retrieved in the central part of the eastern basin. They reported phases of major regression during approximately 450–550 AD and 1550–1650 AD. This was further confirmed by Aleshinskaya et al. (1996) using palaeontological proxies and by Boroffka et al. (2005) from archaeological and geomorphological observations. Boroffka et al. (2005) also documented a low lake level from 800 AD to 1100 AD. However, interpretation remains ambiguous for the time window 1000–1500 AD. Aleshinskaya et al. (1996) suggested deep-water conditions between 1100 AD and

1500 AD, whereas historical data point to a severe (or even complete) drying-out of the lake between the 13th and the 16th centuries (Boroffka et al. 2005).

Regarding environmental changes during the Holocene, the present state of knowledge is fairly good for the region south of the Aral Sea but rather poor for the northern part. During a field campaign in the summer of 2002, sediment cores were retrieved for the first time from the northwest shore of the Large Aral Sea (Chernyshov Bay; Fig. 3.1) (www.CLIMAN.gfz-potsdam.de). Using this cored material, we present new palaeontological data covering the past 2000 years with a time resolution of 15 to 20 years. Based on a quantitative analysis of organic-walled dinoflagellate cysts, we provide evidence for large palaeosalinity and lake water level variations.

III.2. Material and methods

III.2.1. Sedimentological description

In August 2002, two piston cores (composite cores CH1 and CH2 with respective total lengths of 11.04 m and 6.0 m) taken with a Usinger piston corer (http://CLIMAN.gfz-potsdam.de) and six gravity cores were retrieved from Chernyshov Bay (Fig. 3.1). These cores were collected 1 km from the shoreline (45°58'528'' N, 59°14'459'' E) at a water depth of 22 m. Composite Core CH1 consists of sections 21, 22, 23, 27, 28 and 29, whereas composite core CH2 consists of sections 30, 31 and 32. Cores CH1 and CH2 were retrieved from the same coring location at about 1m apart. In this study, we conducted our analyses on sections 30, 31 and 32 from Core CH2 and on sections 27, 28 and 29 from Core CH1. We then named this composite core section CH2/1, whose total length is 10.79 m. The correlation between Cores CH1 and CH2 was performed by matching laminations using photographs, physical properties (bulk sediment density, magnetic susceptibility) and XRF scanning.

Sediments from this site (Fig. 3.2A) consist of greenish to greyish silty clays and dark water-saturated organic muds with sporadically-intercalated more sandy material. The sediments, which are finely laminated, comprise material of variable origin (terrigenous, biogenic and chemogenic) and size (from clay and fine silt to fine sand with mollusc shell fragments). Chemical precipitates, such as gypsum (G), occur both as dispersed microcrystals in the sediment (G_3, G_4; Fig. 3.2B) and as discrete layers (G_1, G_2). Neither erosive discontinuity, nor features of bottom traction are observed in the core. The laminated character of section CH2/1 indicates probable settling of various autochthonous and allochthonous particles from the water column during seasonally varying hydrographic conditions. Four lithological units are recognized. Between 0.0 and 4.5 m (Unit 1), the sediment is mostly silty to sandy clay with rare macrofossil remains although the uppermost part (0.0–0.5 m) consists of a dark, organic, finely laminated mud. Unit 2 is characterized by a horizon of laminated gypsum at its base (G_2: 1-cm thick) overlain by a 13-cm thick interval of yellowish thinly laminated sediments which in turn are abruptly interrupted by brownish laminated sediments (10.5-cm thick interval).

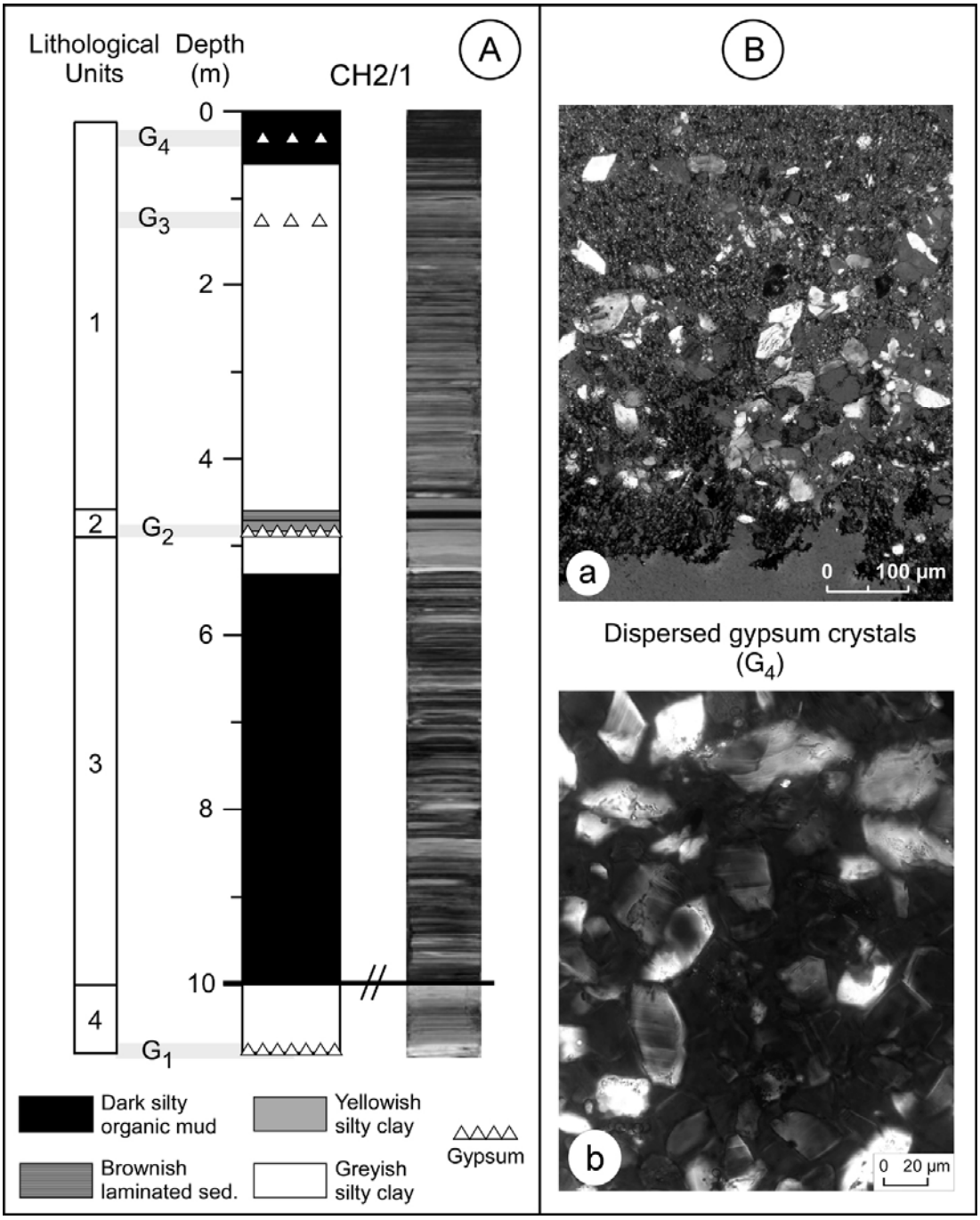

Figure 3.2: *A: Lithology of section CH2/1 (total depth = 10.79 m). Note the break in core between Units 3 and 4 corresponding to a coring gap of unknown extent. B: Microfacies photographs. a: Dispersed gypsum crystals in a fine clayey matrix (×200; G_4 [0.2–0.3 m]); b: Gypsum crystals showing characteristic monoclinic structures and cleavages (×400; G_4 [0.2–0.3 m]).*

Downcore, between 4.86 and 9.97 m depth (Unit 3), the sediments consist of a dark silty organic mud, often water-saturated and very rich in organic matter including allochthonous aquatic plant remains. The plant remains occur both as a dispersed phase in the matrix and as partly decayed fragments that constitute organic horizons. These sediments, which are characteristic of dysoxic to anoxic bottom-water conditions, are separated from a lower sequence (9.97–10.79 m, Unit 4) by a coring gap of unknown extent. Unit 4 consists of thinly laminated grey silty clays that include at the

base, laminated gypsum (G_1) interbedded with clayey layers. No turbiditic sediments have been recognized. The hydrochemical conditions at Chernyshov Bay today are very pronounced. A strong pycnocline has developed that maintains and stabilises an underlying body of anoxic deep-water (Friedrich and Oberhänsli, 2004) that in turn influences sedimentation by preventing bioturbation (except in the topmost part of the core [0.0–0.05 m]). Hence, sediments from Chernyshov Bay show well-preserved laminations (Friedrich and Oberhänsli, 2004).

III.2.2. Age model

In section CH2/1, AMS radiocarbon ages were determined using the filamentous green alga *Vaucheria* sp. and $CaCO_3$ from mollusc shells which were picked from the sediment sample and carefully washed. Algae were stored in water within a glass vessel. For each sample, AMS ^{14}C dating was performed using between 0.2 and 1.0 mg of pure extracted carbon. Radiocarbon ages were corrected to calibrated (cal) ages using the IntCal04 calibration curve published in Reimer et al. (2004). These determinations resulted in sedimentation rate estimates for the different lithological units. A preliminary age model for section CH2/1 is proposed in Figure 3.3.

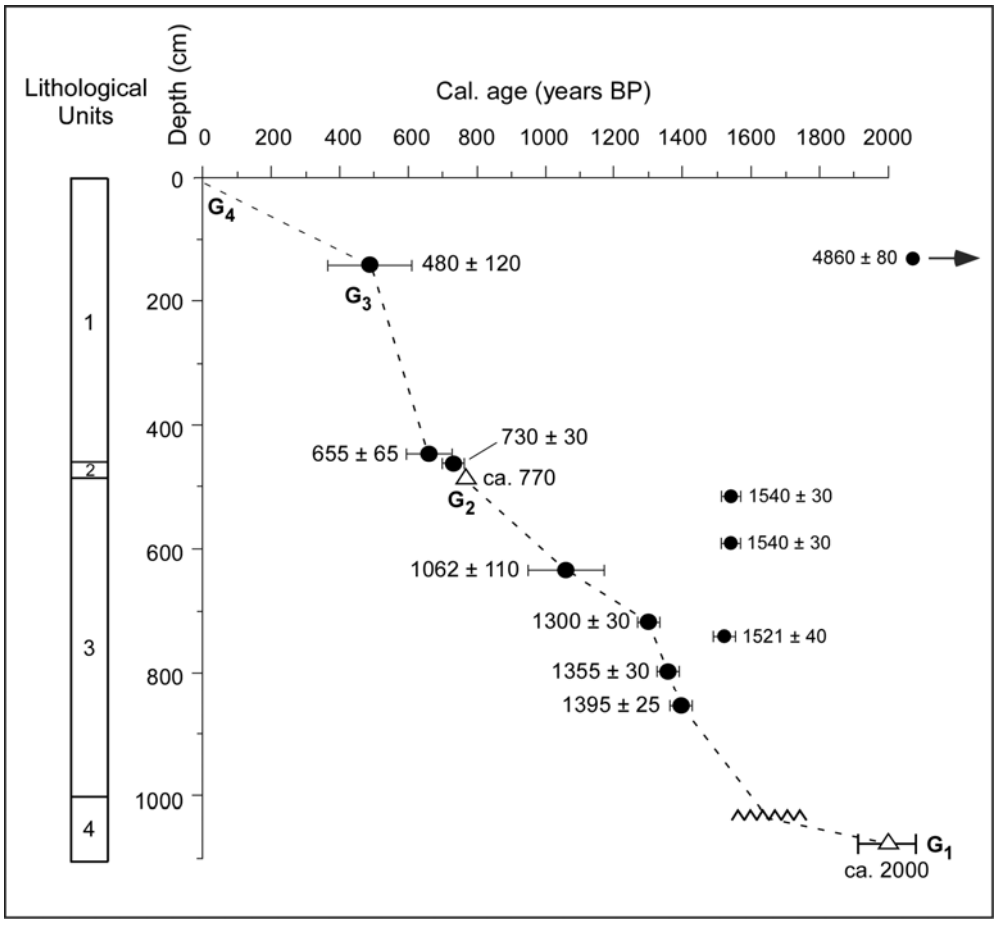

Figure 3.3: *Age model for section CH2/1 based on AMS ^{14}C dating on the filamentous green alga Vaucheria sp.: 480±120 cal. yr BP, 655±65 cal. yr BP (Nourgaliev et al., 2003); 108.6±0.3 pMC (Poz-4753), 1062±110 yr BP (Poz-12279), 1300±30 cal. yr BP (Poz-4762), 1395±25 cal. yr BP (Poz-4760), 1521±40 cal. yr BP (Poz-4764), 1540±30 cal. yr BP (Poz-4756/59), 4860±80 cal. yr BP (Poz-4760), on TOC: 730±30 yr BP (Poz-13511), and on $CaCo_3$ of mollusc shells: 1355±30 cal. yr BP (Poz-9662). AMS ^{14}C dating was measured in the Poznań Radiocarbon Laboratory (Poland).*

Reliable dating for the upper 6 m of section CH2/1 was obtained by correlation with the magnetic susceptibility record from parallel cores 7, 8 and 9 retrieved 50 m apart from the studied cores (Nourgaliev et al., 2003). AMS ^{14}C dating on cores 7, 8 and 9 was performed on the green alga *Vaucheria* sp. This correlation gives an age of 480±120 yr BP (cal. years) at 1.4 m depth for section CH2/1. In addition, the time interval represented by Unit 2 is temporally constrained between 655±65 yr BP (cal. years) at 4.5 m depth and 770 yr BP at 4.86 m for the laminated gypsum, as correlated to a decrease in tree-ring width from the Tien Shan Mountains (see Fig. 3.11). This time range is further constrained by an age of 730±30 yr BP (cal. years) at 4.65 m. These results imply high sedimentation rates during the deposition of Unit 1 (1.6 cm yr^{-1} from 1.36 m to 4.43 m) but conversely very low sedimentation rates for Unit 2 (~0.3 cm yr^{-1}). Supplementary ^{14}C dating performed on *Vaucheria* sp. provide an age of 1062±110 cal. yr BP at 6.34 m, 1300±30 cal. yr BP at 6.94 m and of 1395±25 cal. yr BP at 8.25 m, while ^{14}C dating from mollusc shells indicates an age of 1355±30 cal. yr BP at 7.73 m. Relatively high sedimentation rates are implied for Unit 3 (~1.4 cm yr^{-1} from 6.94 m to 10.36 m). Based on this adjustment, a linear extrapolation along Unit 3 would suggest an average age of ca. 2000 yr BP (100? BC to 100 AD) for the base of section CH2/1 (G_4) corresponding to a major lake level drop. This is consistent with others studies (see Aleshinskaya et al., 1996 on radiocarbon-dated cores 15 and 86 from the Large Aral, and Boomer et al., 2000, p. 1269) that report on an important lake regression at 2000 yr BP. Accordingly, a sampling interval of 10 cm, which represents a time resolution of 15 to 20 years, was selected. The top of the core (uppermost 40 cm) has been dated as post-1963, as based on a peak in ^{137}Cs at 0.46 m reflecting the climax of the bomb period (ca. 1963–1964 AD) (Heim, 2005) and this is confirmed by a date on *Vaucheria* sp. that reveals an age of 108.6±0.3 pMC at 0.56 m. The dates 4860±80 yr BP at 1.30 m, 1540±30 yr BP at 5.16 m, 1540±30 yr BP at 5.90 m and 1521±40 yr BP at 7.40 m, respectively, reflect reworking of older material from shore. This is confirmed by reworked dinoflagellate cysts that are conspicuously abundant at these depths (see Fig. 3.4). Ages between 1521 and 1540 yrs BP typically represent sediment ages of a high lake-level stand. Due to a lack of dating of living algae sampled from the near-shore, no reservoir correction can be applied yet. This is work in progress.

III.2.3. Sample processing and palynological analysis

For the study of dinoflagellate cysts, 125 sediment samples each consisting of 15 to 25 g dry weight were treated sequentially with cold HCl (35%), cold HF (70%) and cold HCl (35%) after Cour's method (1974). Denser particles were then separated from the organic residue using $ZnCl_2$ (density = 2.0). After additional washing with HCl and water, the samples were sieved at 150 µm to eliminate the coarser particles including macro-organic remains, and then sieved again at 10 µm following brief (about 30 s) sonication. The residue was then stained using safranin-o, homogenized,

and mounted onto microscope slides using glycerol. Finally, the coverslips were sealed with LMR histological glue**.**

Dinoflagellate cysts were identified and enumerated under a light microscope at ×1000 magnification. Between 200 and 400 dinoflagellate cysts were counted for intervals of elevated salinity since specimens are generally abundant in such intervals. In other slides, where dinoflagellate cysts occur very sparsely, a minimum of 100 dinoflagellate cysts per sample were counted. Light photomicrographs (LM) were taken using a Leica DMR microscope fitted with a Leica DC300 digital camera. For scanning electron micrographs, residues were sieved at 20 µm, washed with distilled water and air-dried onto small circular metal blocks for 2 h, mounted onto metal stubs, and sputter-coated with gold.

Calculation of dinoflagellate cyst concentrations per gram of dry sediment was performed according to Cour's method (1974). Dinoflagellate cysts were found in every sample examined and preservation varies from poor (crumpling of cysts) to very good in intervals of elevated salinity. The dinoflagellate cyst record is shown by relative abundances of each taxon in a detailed diagram to emphasize palaeoenvironmental changes in the core (Fig. 3.4). Also shown are concentrations of in-situ cysts (per gram dry weight), of other palynomorphs and of reworked taxa (Fig. 3.5). Counts are archived at the Laboratory 'PaléoEnvironnements et PaléobioSphère' (University Claude Bernard-Lyon 1, France). The dinoflagellate cyst zones (DC-a–DC-f; Figs. 3.4 and 3.5) have been established using Statistica 6.0 according to a canonical correspondence analysis performed on selected taxa representing variables, in order to determine major ecological trends across section CH2/1. In addition, to examine whether relative abundance could be biased by concentration values, a principal component analysis was performed on selected variables using the software "Past". The results revealed that no relevant link exists between the different variables.

III.2.4. Ecological groupings of dinoflagellate cysts and other palynomorphs

The in-situ dinoflagellate cyst flora is of low diversity and comprises the following taxa: *Impagidinium caspienense* (Fig. 3.6.1–4), cysts of *Pentapharsodinium dalei* (Fig. 3.6.5–6), protoperidiniacean cysts (Fig. 3.6.7–8), *Lingulodinium machaerophorum* (Figs. 3.6.13–20 and 3.9), *Caspidinium rugosum* (Figs. 3.7.1–4; 3.10.1–3)*, Spiniferites cruciformis* (Figs. 3.7.5–8; 3.10.4–7) and morphotypes assigned to *Romanodinium areolatum* (Fig. 3.8.1–5). The species are grouped according to their ecological preferences. Additional aquatic palynomorph taxa recorded are specimens of the chlorophycean (green algal) taxon *Botryococcus braunii*-type (Fig. 3.10.9) and *Pediastrum* sp.; the prasinophycean (green flagellate) species *Hexasterias* (al. *Polyasterias*) *problematica* (Fig. 3.7.20) and genus *Cymatiosphaera*; loricae of the ciliate order Tintinniida (Fig. 3.7.15–16); and incertae sedis taxa including *Micrhystridium* (a probable algal cyst), Incertae sedis sp. 1 (Fig. 3.7.17–18), Incertae sedis sp. 2 (Fig. 3.7.19) and *Radiosperma corbiferum* (Figs. 3.6.9–12; 3.10.9).

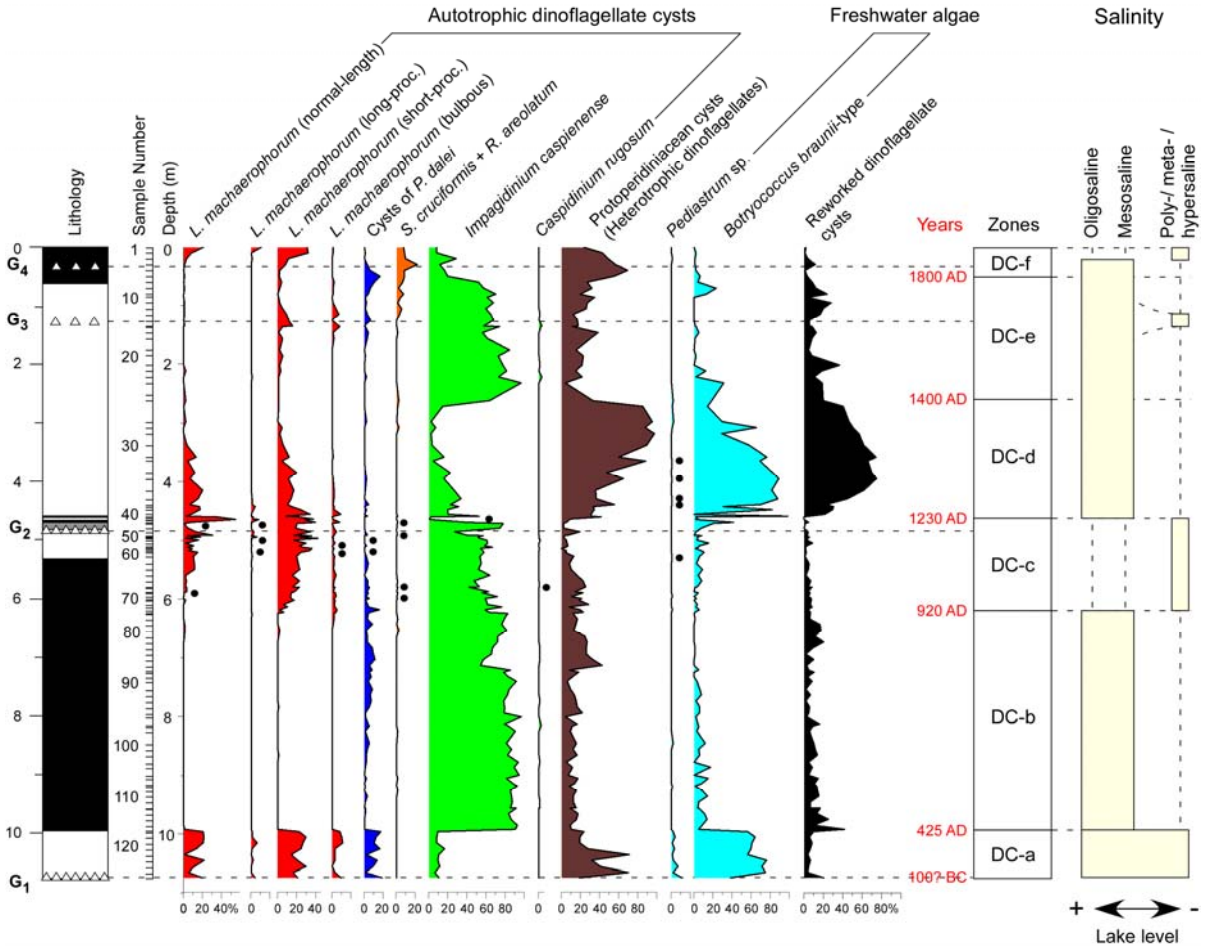

Figure 3.4: *Relative abundance of dinoflagellate cysts and freshwater algae from the Chernyshov Bay section CH2/1, ecostratigraphic zonation based on the dinoflagellate cysts, and schematic salinity fluctuations. Each species and morphotype is expressed as a proportion of the total in-situ dinoflagellate cysts. Pediastrum sp. and Botryococcus braunii-type are expressed as a proportion of the total in-situ dinoflagellate cysts plus freshwater taxa. Reworked dinoflagellate cysts are expressed as a proportion of total in-situ dinoflagellate cysts plus reworked dinoflagellate cysts. Solid dots indicate rare occurrence (0.5% or less). Each sample represents a ~10 cm interval of core and is plotted by its mean depth. Oligosaline conditions represent salinities of 0.5–5 g kg^{-1}; mesosaline conditions salinities of 5–20 g kg^{-1} and poly- to meta-/ hypersaline conditions salinities >20/30 g kg^{-1}. See Figure 2 for explanation of lithology.*

- *L. machaerophorum* (Figs. 3.6.13–20 and 3.9) is a euryhaline species that can tolerate salinities as low as about 10–15 g kg^{-1} (see Head et al., 2005, p. 24–25 for review) and as high as about 40 g kg^{-1} based on laboratory culturing studies (Lewis and Hallett, 1997), or indeed higher than 40 g kg^{-1} and approaching 50 g kg^{-1} as indicated by its distribution in surface sediments of the Persian Gulf (Bradford and Wall, 1984). The motile stage of this species blooms in late summer, and has a tropical to temperate distribution, with a late-summer minimum temperature limit of about 10–12°C (Dale, 1996; Lewis and Hallett, 1997). Since *L. machaerophorum* develops different morphotypes with respect to changing temperature (-3 to 29°C) and salinity of surface-waters, it is regarded as a reliable indicator of environmental changes in a water body. These morphotypes are characterized by large variations in process length and shape (Fig. 3.4). Up to 15 different process types have been found for

L. machaerophorum in previous studies (Wall et al., 1973; Harland, 1977; Kokinos and Anderson, 1995; Lewis and Hallett, 1997; Hallett, 1999). Most of these process types are also found in the late Holocene sediments of Chernyshov Bay. Typical specimens (Figs. 3.6.13–16; 3.9.7–8) have processes of moderate length (5–15 µm) that taper distally to points, while other specimens may have long processes (15–20 µm; Fig. 3.9.1–3) again tapering to points and often bearing small spinules at their distal ends. Some specimens with long, curved processes are also seen. Specimens with reduced processes (≤5µm; Fig. 3.9.4–6) are found with terminations that are columnar, pointed or bulbous (Figs. 3.6.17–20; 3.9.9).

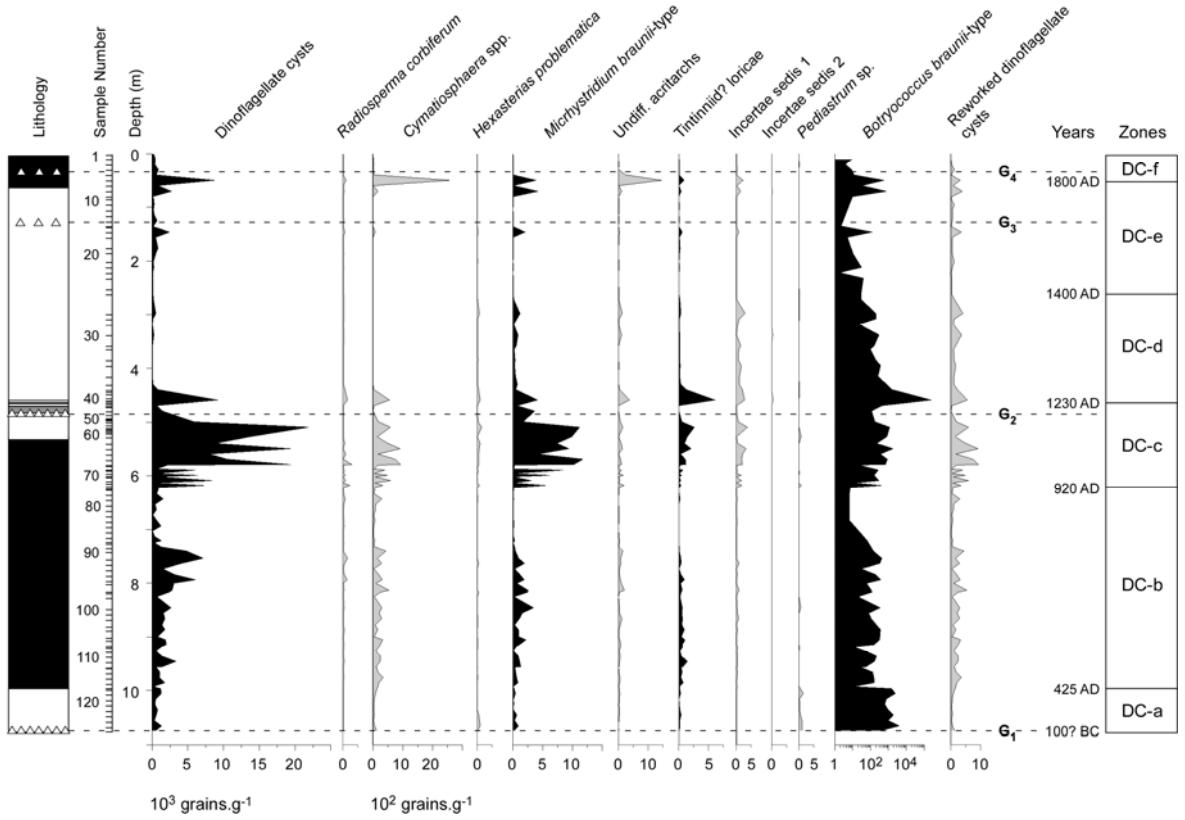

Figure 3.5: *Concentrations (per gram of dry sediment) of all aquatic palynomorphs counted in section CH2/1. Black-shaded curves: 10^3 grains g^{-1}. Grey-shaded curves: 10^2 grains g^{-1}. Note that concentrations of Botryococcus braunii-type are expressed in a logarithmic scale. Each sample represents a ~10 cm interval of core and is plotted by its mean depth. The zones refer to the dinoflagellate cyst ecostratigraphy described herein. See Figure 2 for explanation of lithology.*

- *P. dalei* (Fig. 3.6.5–6) is a spring-blooming species (Dale, 2001) most common in high northern latitudes (Rochon et al., 1999; de Vernal et al., 2001, Marret and Zonneveld, 2003). It tolerates a wide range of salinities (21–37 g kg^{-1}) and nutrient concentrations judging from a literature compilation of its cyst distribution (Marret and Zonneveld, 2003), although the small size and inconspicuous morphology of these cysts suggest the possibility of misidentification. Its presence in the Aral Sea core may be related to cool spring surface-waters resulting from cold winters (<0°C).

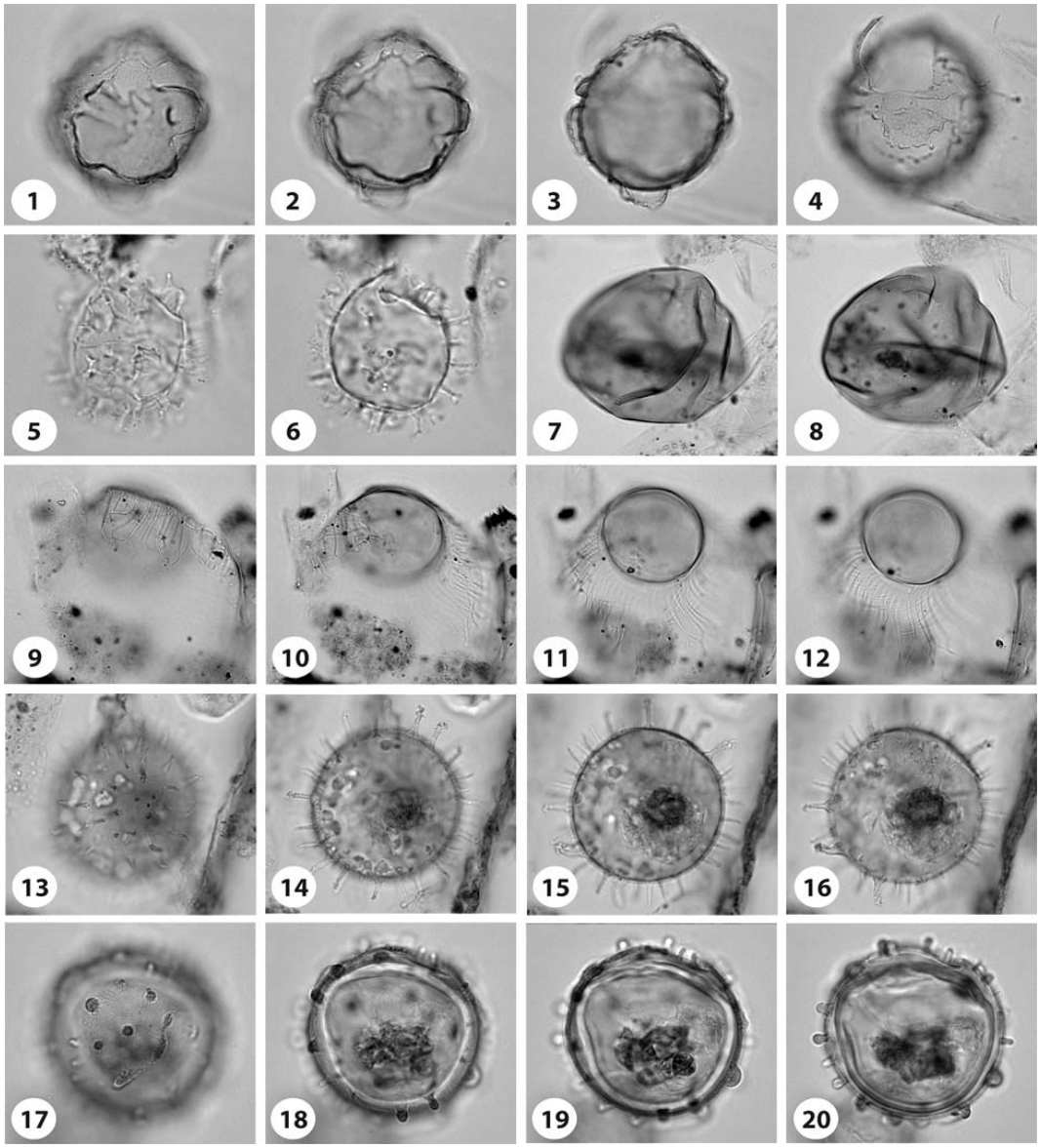

Figure 3.6: *Dinoflagellate cysts and other aquatic palynomorphs from Chernyshov Bay. Light micrographs in bright-field. An England Finder reference is given after the sample number. (1–4) Impagidinium caspienense Marret, 2004. Ventral view of ventral surface (1–2), mid-focus (3), and dorsal surface (4) showing archeopyle; max. dia. 45 µm; sample 1A (M20/3); depth 537.5–540.5 cm. (5–6) Cyst of Pentapharsodinium dalei (Indelicato and Loeblich, 1986), upper and mid foci; central body max. dia. 23 µm; sample 11A (K20/3); depth 507.5–510.5 cm. (7–8) Protoperidiniacean cyst, upper and low foci; max. dia. 44 µm; sample 9A (N43/3); depth 537.5–540.5 cm. (9–12) Radiosperma corbiferum Meunier, 1910 (= Sternhaarstatoplast of Hensen, 1887), upper (9–10), mid (11) and low (12) foci; central body max. dia. 38 µm; sample 9A (M10/0); depth 537.5–540.5 cm. (13–20) Lingulodinium machaerophorum (Deflandre and Cookson, 1955). (13–16) Specimen with processes of normal length (8–10 µm); upper (13–14), mid (15) and low (16) foci; central body max. dia. 51 µm; sample 9A (F35/4); depth 537.5–540.5 cm. (17–20) Specimen with bulbous processes; upper (17–18) and mid (19–20) foci; central body max. dia. 46 µm; sample 9A (J51/0); depth 537.5–540.5 cm.*

- *S. cruciformis* (Figs. 3.7.5–14; 3.10.4–7) in our section shows similar morphological variability to that described from the Holocene of the Black Sea by Wall et al. (1973) and Wall and Dale (1974), and as that described for modern and sub-modern specimens of the Caspian Sea (morphotypes A, B and C; Marret et al., 2004). *S. cruciformis* was first described from Late

Pleistocene to early Holocene (23 to 7 kyr BP) sediments from the Black Sea (Wall et al., 1973). The ecological affinities of *S. cruciformis* have already been discussed in several papers because this species has been found in other Eurasian water bodies, such as the Black, Marmara and Aegean seas (Aksu et al., 1995a, b; Mudie et al., 1998, 2001, 2002; Popescu, 2001), and the Caspian Sea (Marret et al., 2004), but also in Lake Kastoria sediments of Late Glacial and Holocene ages (Kouli et al., 2001). Its occurrence was also reported from Upper Miocene / Lower Pliocene sediments of the Paratethys (Popescu, 2001; Popescu, in press) and the Mediterranean realms (Kloosterboer-van Hoeve et al., 2001). The shape and size of sutural septa, ridges and processes have been all described as extremely variable (Wall et al., 1973; Mudie et al., 2001). Such variations may be linked to fluctuations in salinity (Dale, 1996). In this study, specimens assigned to *S. cruciformis* vary widely in body shape and degree of development of sutural septa and flanges. The size of the central body is rather similar between specimens (length 40–50 μm; width 30–40 μm). The central body is either cruciform or ellipsoidal to pentagonal in shape. The degree of variation in the development of the flanges / septa consists of: (1) no development (Fig. 3.10.7), (2) low, fenestrate septa and incipient flange development (Fig. 3.10.4), or (3) well-developed and perforate–fenestrate flanges and septa (Figs. 3.7.5–14; 3.10.5–6). However, there is a full range of intermediate variability. Specimens assignable to *R. areolatum* (Baltes, 1971a, b) are presented in Figure 8 (3.8.1–5). Because of the presence of morphologies intermediate between *S. cruciformis* and *R. areolatum* in our material, we have grouped these two species together in the counts (Fig. 3.4).

- *I. caspienense* (Figs. 3.6.1–4; 3.10.1–3) and *C. rugosum* (Fig. 3.7.1–4) have recently been described from surface and subsurface sediments of the Caspian Sea by Marret et al. (2004). These species are apparently endemic to Central Asian Seas. However, since they might respond to different controls, they were plotted separately (Fig. 3.4). *I. caspienense* is the most abundant species encountered in sediments from section CH2/1, although our detailed understanding of its ecological requirements is poor. It thrives in low salinity waters (Marret et al., 2004).

- Protoperidiniacean cysts are also frequent (Fig. 3.6.7–8). These are large, smooth, spherical to subspherical pale brownish cysts, often folded, and with a rarely visible archeopyle. They are considered heterotrophic, and their presence may be related to elevated nutrient levels from river inflow. Because they typically feed on diatoms and other primary producers, protoperidiniacean cysts, such as those of the genus *Protoperidinium*, are regarded as paleoproductivity indicators (Dale & Gjellsa, 1993; Dale, 1996). Moreover, since they are very sensitive to post-depositional oxygen-related decay, they give crucial information on past variations in bottom water and/or pore water circulation in the sediment (Zonneveld *et al.,* 2001). As we expect anoxic conditions (oxygen-depleted conditions) to have prevailed on the lake bottom during the time window studied (resulting from the highly stratified waters), we can therefore here use protoperidiniacean cysts as a paleoproductivity indicator.

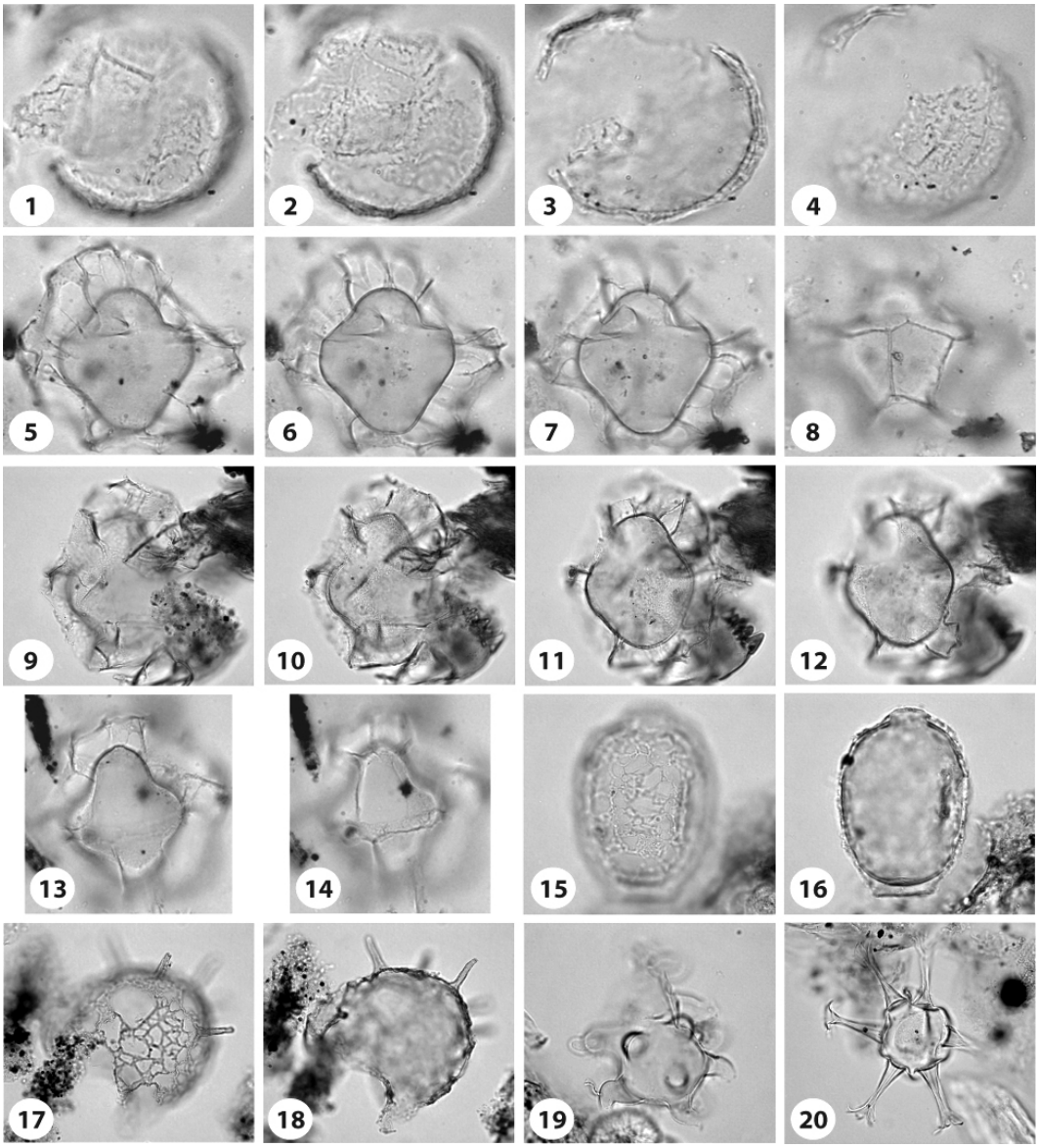

Figure 3.7: *Dinoflagellate cysts and other aquatic palynomorphs from Chernyshov Bay. Light micrographs in bright-field. An England Finder reference is given after the sample number. (1–4) Caspidinium rugosum Marret, 2004. Upper (1–2), mid (3) and low (4) foci; central body max. dia. 52 µm; sample 32A3; depth 607.5–610 cm. (5–8) Spiniferites cruciformis Wall et al., 1973, ventral view showing ventral surface (5), mid focus (6–7) and dorsal surface (8); sample 32A3; central body max. dia. 52µm; depth 587.5–590 cm. (9–12) S. cruciformis Wall et al., 1973, ventral view showing ventral surface (9–10), mid focus (11) and dorsal surface (12); central body length 51µm; sample 9A (J25/0); depth 537.5–540.5 cm. (13–14) S. cruciformis Wall et al., 1973, low focus (13) and slightly lower focus of the dorsal surface in ventral view (14) showing archeopyle; central body max. dia. 51 µm; sample 32A3; depth 547.5–550.5 cm. (15–16) Tintinniida? lorica, upper (15) and mid (16) foci; total length 53 µm; sample 1A (P27/0); depth 457.5–459.5 cm. (17–18) Incertae sedis 1, upper (17) and mid (18) foci; central body maximum diameter 77 µm; sample 1A (P27/0); depth 457.5–459.5 cm. (19) Incertae sedis 2, upper focus; total length 62 µm; sample 9A (M10/0); depth 537.5–540.5 cm. (20) Hexasterias problematica Cleve, 1900, mid-focus; central body max. dia. 38 µm; sample 11A (J31/3); depth 507.5–510.5 cm.*

- Freshwater algal taxa are represented by coenobia of the chlorococcalean (green algae) genus *Pediastrum*, and by colonies of the chlorococcalean *B. braunii*-type (Fig. 3.10.9). *Pediastrum* is a predominantly freshwater genus (Parra Barrientos, 1979; Bold and Wynne, 1985), although records

from brackish habitats are documented (Brenner, 2001). *Botryococcus* is mostly associated today with freshwater environments, although records from brackish habitats are also known (Batten and Grenfell, 1996). On the grounds of probability (see also Matthiessen et al., 2000), we regard *Pediastrum* and *B. braunii*-type as indicators of freshwater discharge into Chernyshov Bay.

In addition to the groups discussed above, other aquatic taxa occur in low quantities. The distributions of these taxa are listed individually on Figure 3.5.

- *Radiosperma corbiferum* (Figs. 3.6.9–12; 3.10.8) is a marine to brackish organism previously recorded from the living plankton of the South-Western Baltic Sea (as Sternhaarstatoblast in Hensen, 1887), Baltic Sea proper including the eastern Gulf of Finland where summer surface salinities are below 3 g kg^{-1} (Leegaard, 1920) and the Barents Sea (Meunier, 1910). It has been reported also from modern sediments of the brackish Baltic Sea where it occurs in nearly all samples from a transect representing low salinity (<6 g kg^{-1}) in the western Gulf of Finland to relatively high salinity (about 25 g kg^{-1}) in the Skagerrak (as Organismtype A in Gundersen, 1988, pl. 4, fig. 4). Highest concentrations were recorded in the central Baltic Sea where summer surface salinities are around 6–7 g kg^{-1}. Elsewhere, *R. corbiferum* has been reported from modern surface sediments of the Laptev Sea (Kunz-Pirrung, 1998, 1999), where this species has highest values north and east of the Lena delta and in front of the Yana river mouth (Kunz-Pirrung, 1999). It is also known from modern sediments of the Kiel Bight, South-Western Baltic Sea (as Sternhaarstatoblast of Hensen, 1887, in Nehring, 1994) and from sediments of Guanabara Bay at Rio de Janeiro, Brazil (Brenner, 2001). In the fossil record, *R. corbiferum* has been reported from Holocene deposits of the central Baltic Sea (Brenner, 2001) and Last Interglacial deposits of the South-Western Baltic Sea (Head et al., 2005). This distinctive but biologically enigmatic organism evidently has a broad salinity tolerance and, although it has been reported mostly from brackish-marine environments, factors additional to salinity may also control its distribution (Brenner, 2001).

- *Hexasterias* (al. *Polyasterias*) *problematica* (Fig. 3.7.20) has been recorded previously from Baffin Bay fjords where it is one of several species that increase towards the meltwater plumes (Mudie, 1992). It has also been found in modern sediments of the Laptev Sea (Kunz-Pirrung, 1998, 1999) and the plankton of the North Sea region (Cleve, 1900) as well as in the same general area (as "Röhrenstatoblast" in Hensen, 1887). It appears to be a brackish or euryhaline species (Matthiessen *et al.,* 2000).

- The other aquatic groups (Fig. 3.7.15–16; 3.7.17–18) here identified have either broad or uncertain environmental preferences.

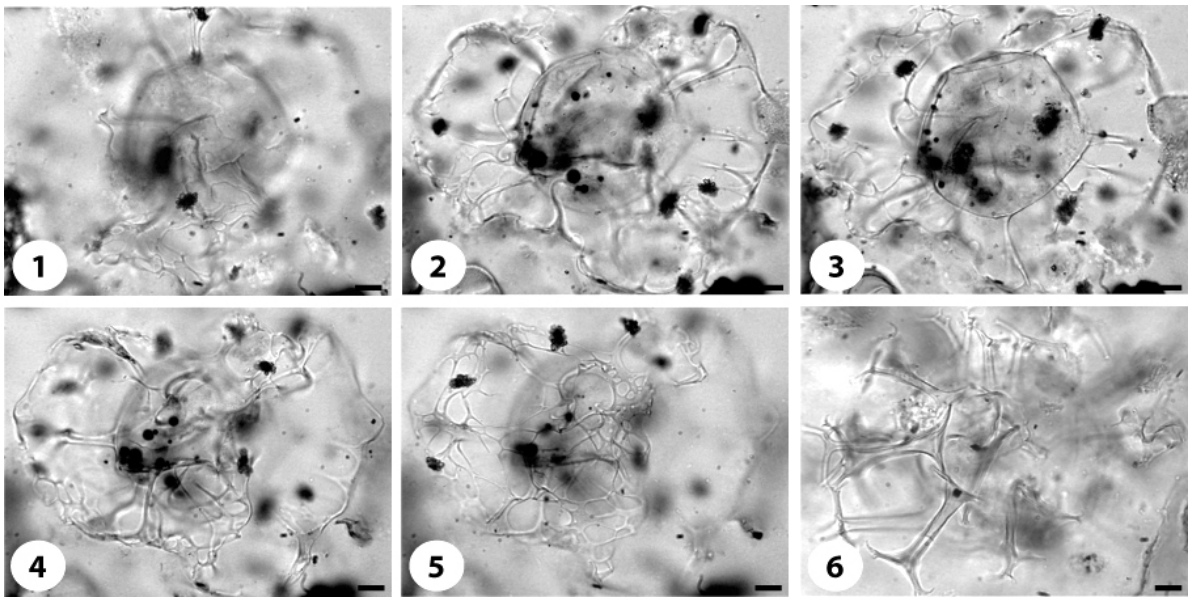

Figure 3.8: *Dinoflagellate cysts from Chernyshov Bay. Light micrographs in bright-field. (1–5) Romanodinium areolatum Baltes 1971b, upper (1–2), mid (3) and lower (4–5) foci; central body max. dia. 63 µm; sample 32A3; depth 587.5–590 cm. (6) Reworked specimen of Spiniferites validus Süto-Szentai, 1982 low focus; central body max. dia. 71µm sample 32A3; depth 607.5–610 cm.*

Reworked specimens were found to occur generally within intervals of increased freshwater inflow. One group includes *Charlesdownia coleothrypta, Enneadocysta arcuata, Deflandrea phosphoritica, Phthanoperidinium comatum, Dapsilidinium pseudocolligerum, Areosphaeridium diktyoplokum,* and *Spiniferites* spp. (Fig. 3.8.6), and represents Palaeogene reworking. These specimens are often distinguished by an increased absorption of safranin-o stain, which probably reflects the oxidation history of these reworked specimens. A second group of reworked taxa, notably *Spiniferites* cf. *falcipedius*, *S. bentorii* (a single specimen), *S. hyperacanthus*, *S. membranaceous*, *S. ramosus*, *S. bulloideus*, *Spiniferites* sp., *Operculodinium centrocarpum* sensu Wall and Dale, 1966, is characterized by thin-walled cysts generally not affected by the safranin-o stain. Most of these specimens (*Spiniferites* cf. *falcipedius*, *S. bentorii*, *S. hyperacanthus*, *O. centrocarpum* sensu Wall and Dale, 1966) represent a typical Mediterranean assemblage that occurs in peak frequencies when river transport is implicated. We therefore presume that they have been reworked from upper Neogene or Quaternary deposits, and their presence is probably linked to Plio–Pleistocene connections between the Aral, Caspian, Black and Mediterranean seas.

III.3. Results

Seven ecostratigraphic zones have been distinguished by statistically assessing major changes in the composition of the dinoflagellate cyst assemblages (Figs. 3.4 and 3.5). These ecostratigraphic zones mostly coincide with the lithological units previously defined.

Zone DC-a (10.75–9.97 m) is characterized by the dominance of *L. machaerophorum* as a whole, with maximum total values of 63% at 10.16 cm. Morphotypes bearing short- and normal-length processes are abundant (respectively up to 29% and 21% at 10.06 m) while specimens with long and bulbous processes are present (respectively up to 6% and 8% at 10.16 m). Frequencies of protoperidiniacean cysts fluctuate at relatively high numbers and oscillate between 18% at 9.97 m to 70% at 10.36 m. Note the reciprocating fluctuations in the frequencies of *L. machaerophorum* and protoperidiniacean cysts. Counts of *B. braunii*-type depict a somewhat decreasing trend through this zone, with relative abundances of 75% at 10.66 m to 57% at 9.97 m, as do numbers of *Pediastrum*, decreasing from 10.6% at 10.75 m to 1.7% at 9.97 m. Abundances of *I. caspienense* are relatively low throughout this zone where they average 10%, when frequencies in cysts of *P. dalei* display maximum values of 18% at 10.75 m. Reworked taxa are also present in low abundances, amounting to 20% at 10.75 m. Preservation is good throughout this zone and the dinoflagellate cyst concentration is relatively low (300–1,300 specimens g^{-1}). The abrupt shift that characterizes the upper limit of this zone at 9.97 cm is related not to natural causes but to a coring failure.

Zone DC-b (9.97–6.18 m) is dominated by the species *I. caspienense*, which averages 70% to 80% for most of the zone. The previously dominant species *L. machaerophorum* disappears almost totally at the base, but occurs discretely again upwards (10% in total at 6.22 m). Counts of protoperidiniacean cysts are relatively constant throughout this zone (10–20%) but nevertheless exhibit a marked increase around 7.13 m (41%). Freshwater taxa, as well as cysts of *P. dalei*, are present as well, the latter increasing in abundances from the lower part to the top, attaining 15% at 6.18 m. Low abundances of *C. rugosum* (up to 2%) are also recorded. Dinoflagellate cyst concentrations are medium (500–7,250 cysts g^{-1}) and the preservation is poor due to crumpling of cysts.

Zone DC-c (6.18–4.64 m) documents the co-occurrence of two dominant taxa: *L. machaerophorum* and *I. caspienense*. While *I. caspienense* values remain relatively constant throughout this interval (50–60% on average), relative abundances of *L. machaerophorum* depict a progressive increase from 14% at bottom up to 91% at 4.64 m in total (respectively minimal and maximal values of 0–30%, 0–6%, 0–41.5% and 0–8% from morphotypes with normal length, long, short and bulbous processes). Conversely, relative abundances of protoperidiniacean cysts decrease from 27% at 6.09 m to 2% at 4.71 cm (0% at 5.14 m). Also, cysts of *P. dalei* (0–5%) and freshwater taxa (<10% on average but 40% at 4.695m) occur in low numbers throughout this zone. *S. cruciformis* including *R. areolatum* is mostly found in the lowermost part (between 5.99 and 5.69 m; 1–2%) although they also occur in low frequencies near the top. *C. rugosum* is rare (up to 1.5%). Preservation is very good in this zone; correlatively the dinoflagellate cyst concentration is relatively high (from 800 to ca. 22,000 cysts.g^{-1}; Fig. 3.5). There is also a noticeable increase in the concentration of

Michrystridium braunii-type organisms throughout this zone (up to ca. 12,000 specimens g^{-1} at the top). The transition from Zone DC-c to DC-d coincides with the transition from lithological Unit 2 to 3 (Fig. 3.2).

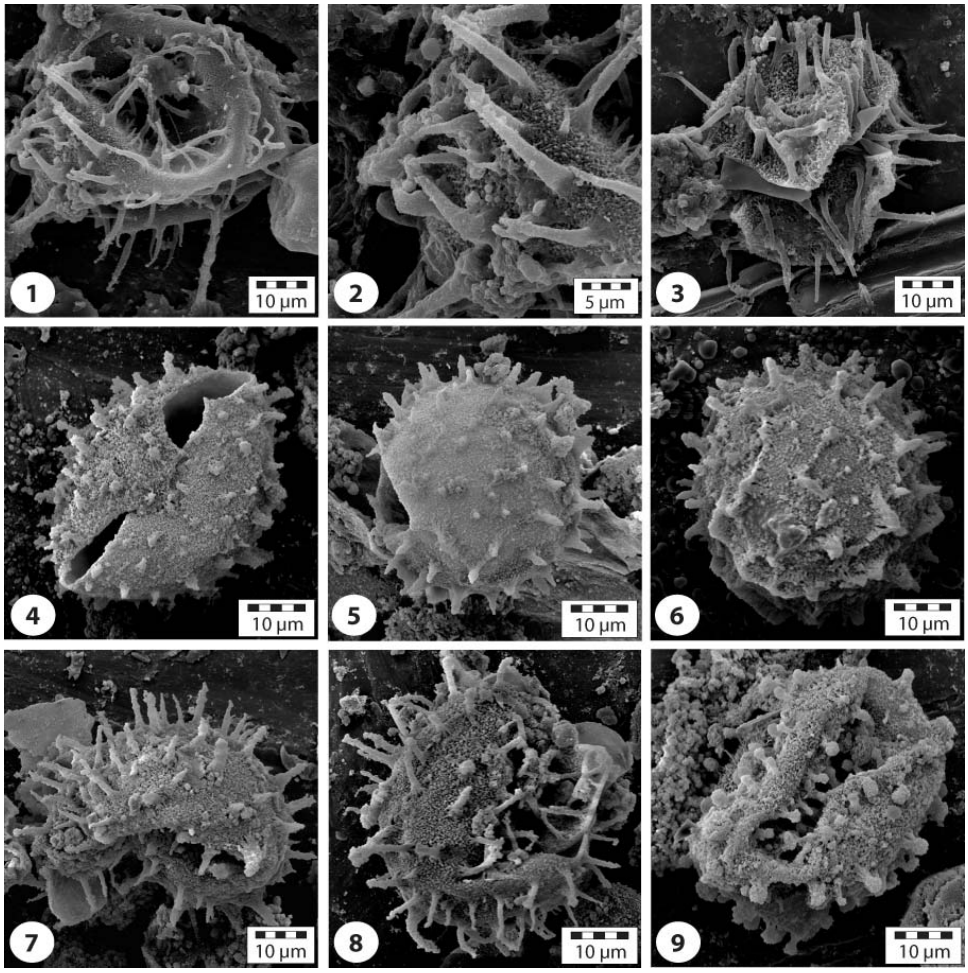

Figure 3.9: *Morphotypes of Lingulodinium machaerophorum from Chernyshov Bay. Scanning electron micrographs. (1–3) L. machaerophorum with long processes; sample 11A; depth 507.5–510.5 cm. (4–6) L. machaerophorum with reduced processes; sample 11A; depth 507.5–510.5 cm. (7–8) L. machaerophorum with processes of normal length; sample 11A; depth 507.5–510.5 cm. (9) L. machaerophorum with bulbous processes; sample 11A; depth 507.5–510.5 cm.*

Zone DC-d (4.64–2.62 m) is characterized by an abrupt increase in the relative abundance of protoperidiniacean cysts, with a maximum of 95.8% at 3.18 m and frequencies fluctuating around 70% between 3.95 m and 2.72 m. Correspondingly, after an abrupt increase in the frequencies of freshwater species (notably *B. braunii*-type) with average values increasing up to 96.5% at 4.59 m, the abundance shows a progressive decreasing trend upwards (18% at 2.62 m). Abundances of reworked dinoflagellate cysts are also high in this zone, increasing to 75% at 3.75 m and at 3.58 m, before progressively decreasing further upwards. Abundances of *L. machaerophorum* show a stepwise decrease from 91% at 4.64 m (ecozonal boundary Zones DC-c/d) to 1% at 2.72 m. Relative

abundances of cysts of *P. dalei* remain very low (<5%) in this zone. *S. cruciformis* including *R. areolatum* is found in low abundances (1–3%), mostly between 3.08 and 2.62 m. Also present are reworked specimens of *Spiniferites* species, including *S. ramosus* and *S. bulloideus,* which occur as smooth, thin-walled and delicate specimens. This zone is characterized by very low concentrations of dinoflagellate cysts (30–600 specimens g^{-1}) and poor preservation.

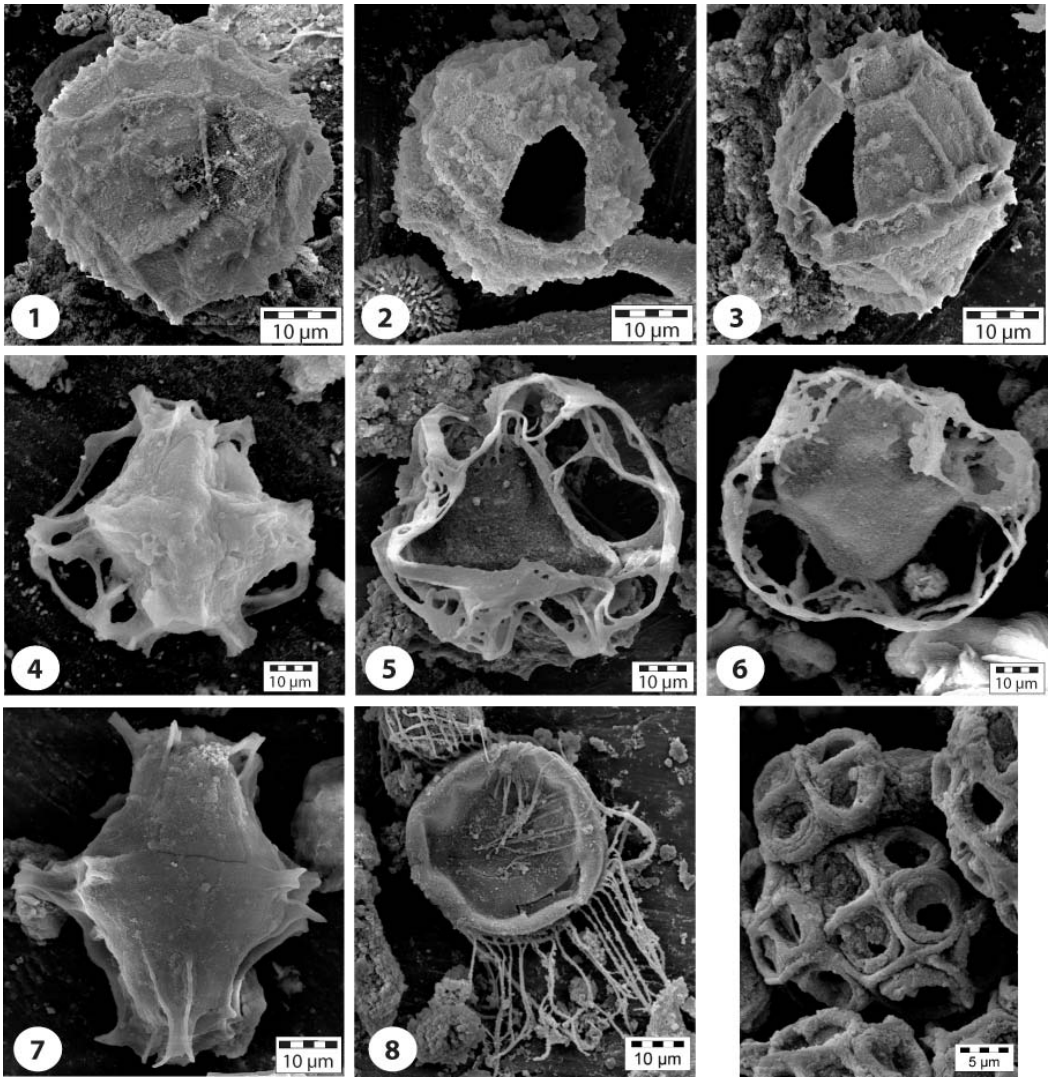

Figure 3.10: *Dinoflagellate cysts and other aquatic palynomorphs from Chernyshov Bay. Scanning electron micrographs. (1–3) Impagidinium caspienense Marret, 2004. Antapical view (1) and dorsal views showing archeopyle (2–3); sample 11A; depth 507.5–510.5 cm. (4–7) Spiniferites cruciformis Wall et al., 1973. (4) Cruciform / ellipsoidal body with a well-developed and perforated flange, ventral view; sample 24B; depth 49–51 cm. (5) Cruciform body with well-developed and perforated flange, ventral view; sample 24B; depth 49–51 cm. (6) Cruciform/ellipsoidal body with well-developed and perforated flange, ventral view; sample 24B; depth 49–51 cm. (7) Cruciform body with incipient flange formed by incomplete development of low septa, dorsal view; sample 24B; depth 49–51 cm. (8) Radiosperma corbiferum Meunier, 1910 (= Sternhaarstatoplast of Hensen, 1887), dorsal view showing pylome; sample 11A; depth 507.5–510.5 cm. (9) Botryococcus braunii-type; sample 11A; depth 507.5–510.5 cm.*

Zone DC-e (2.62–0.5 m) is characterized by the replacement of protoperidiniacean cysts (20% on average but 4% at 2.32 m) by *I. caspienense* that becomes conspicuously dominant, with average values amounting to 60%. Correspondingly, relative abundances of reworked taxa significantly decline (ca. 20% at 2.62 m to 8% at 0.6 m). Frequencies of *L. machaerophorum* are low throughout this zone, although a slight increase is noticeable between 1.36 m and 1.05 m (10–20%). *S. cruciformis* including *R. areolatum* is more scarcely represented in this zone with contributions never exceeding 2% of the dinoflagellate cyst assemblage. Relative abundances of cysts of *P. dalei* are relatively constant (~5%) but conspicuously increase at the top (16% at 0.5 m). Rare cysts of *C. rugosum* are also present (1–3%). Dinoflagellate cyst concentrations are again low (70 to 800 specimens g^{-1}) although the preservation is much better.

Zone DC-f (0.5–0 m) is characterized by the dominance of *L. machaerophorum* morphotypes whose relative abundances abruptly increase from 0.5 m upwards (normal length processes: 20%; long processes: 10%; short processes: 30%; bulbous processes: 1% at the very top). Conversely, relative abundances of *I. caspienense*, protoperidiniacean cysts and morphotypes of *S. cruciformis* noticeably decrease between 0.5 m and the topmost part of this zone, with respective values of 16% at 0.5 m to 8% at 0 m for *I. caspienense*, 68% to 23% for the protoperidiniacean cysts and 21% to 7% for the morphotypes of *S. cruciformis*. Cysts of *P. dalei* progressively disappear with values ranging from 16% at 0.5 m to 0% at the top. Dinoflagellate cyst preservation is very good throughout this zone but the concentration remains relatively low (200–8,000 cysts g^{-1}).

III.4. Discussion

III.4.1. Palaeoenvironmental reconstruction

For the past 2000 years, two contrasting environmental states can be distinguished, each with distinct extremes. Transiently highly saline (poly- to meta- / hypersaline) conditions are inferred by specific dinoflagellate cyst assemblages characterized by increasing / high abundances of *L. machaerophorum*. Coevally, gypsum starts to precipitate from the water column as soon as the salinity reaches 28 g kg^{-1} (Brodskaya, 1952; Bortnik and Chistyaeva, 1990). Since the motile stage of *L. machaerophorum* commonly blooms in late summer, persistently higher abundances of this species may imply sustained levels of enhanced evaporation. Conversely, periods of decreasing salinity (oligo- / mesosaline conditions: 0.5–25 g kg^{-1}) are inferred from dinoflagellate cyst assemblages characterized by decreasing frequencies of *L. machaerophorum* (and reduced processes: <5 µm) but increased abundances of other autotrophic (notably *I. caspiniense*) and heterotrophic (protoperidiniacean cysts) species. Higher abundances of freshwater algae (*Pediastrum*, *B. braunii*-type) imply river discharge and periods of freshening of the lake. Furthermore, due to its ecological preferences, *P. dalei* may serve as a proxy for cool spring surface-waters following cold winters. The dinoflagellate cyst record

can thus be used to infer surface-water variations in salinity, palaeoproductivity and potentially also temperature. Because these changes imply fluctuations in lake water level, coeval changes in sedimentation and environmental processes should have occurred. The palaeoenvionmental changes are discussed here in terms of contrasting environmental states, notably salinity and lake water levels (see Fig. 3.4).

Today, salt concentrations in the Western Basin have increased to 82 g kg^{-1} in surface-waters and 110 g kg^{-1} at depth (Friedrich and Oberhänsli, 2004). This is reflected in the topmost sediment of section CH2/1 by an abrupt increase in abundance of the autotrophic species *L. machaerophorum* (especially morphotypes with long, i.e. >15 µm and normal length, i.e. 5–15 µm, processes; Zone DC-f) within a trend strengthened at the very top. Based on this observation and the aforementioned ecological tolerances of the species, we confirm *L. machaerophorum* as a reliable environmental indicator indicating salinity increase in surface-water layers. It must be understood, however, that the motile stage of *L. machaerophorum* blooms mostly in late summer (Lewis and Hallett, 1997) and its cyst record therefore does not necessarily reflect conditions at other times of the year.

4.1.1. Zone DC-a (10.75–9.97 m: 100? BC–425 AD). This zone is interpreted as representing a period of low lake level due to evaporative drawdown, indicated by high levels of *L. machaerophorum* and deposition of gypsum (G_1). In the Aral Sea, gypsum precipitates out in the water column once salinity attains 28 g kg^{-1} (Brodskaya, 1952; Bortnik and Chistyaeva, 1990), which thus suggests that surface water salinity during Zone DC-a was above 28 g kg^{-1}. This is in agreement with the salinity tolerance of *L. machaerophorum*, a species grown in the laboratory in salinities up to 40 g kg^{-1} (Lewis and Hallett, 1997; Hallett, 1999) and whose modern distribution in surface sediments of the Gulf of Persia implies a tolerance to salinities exceeding 40 g kg^{-1} and indeed approaching 50 g kg^{-1} (Bradford and Wall, 1984). *L. machaerophorum* blooms in late summer, and high numbers indicate sustained periods of enhanced summer evaporation during Zone DC-a. At the same time, abundant fresh-water algae *B. braunii*-type and *Pediastrum* sp., and nutrient-dependent (protoperidiniacean) cysts, also characterise this zone and indicate freshwater inflow and increased palaeoproductivity. The source of the freshwater inflows remains debatable. These episodic freshwater influxes are possibly linked to phases of stronger discharges of the Syr Darya and Amu Darya rivers in late spring / early summer. They can also originate from local rivers episodically flushing into the bay (Fig. 3.1), such as the Irgiz River in the north (see Aleshinskaya et al., 1996). The seasonal contrast in sea-surface temperatures, when judging from significant numbers of cysts of the spring-blooming, cool-tolerant species *P. dalei*, was probably higher between 100? BC and 425 AD, with relatively cool spring surface-water temperatures following cold winters.

4.1.2. Zone DC-b (9.97–6.18 m: 425–920 AD). *I. caspienense* is a brackish species judging from its modern distribution in the Caspian Sea, although it overlaps ecologically with *L. machaerophorum*

in the lower range of the latter species' salinity tolerance (Marret et al., 2004). The dominance of *I. caspienense* in this zone and near absence of *L. machaerophorum* indicates that the surface water salinity was below 15 g kg^{-1} and probably around 10 g kg^{-1} (the approximate lower limit for *L. machaerophorum*). The presence of *P. dalei* and protoperidiniacean cysts is not inconsistent with this interpretation, as these species are present in the low-salinity Caspian Sea today (Marret et al., 2004). The reduction in salinity during Zone DC-b implies that the lake level had risen substantially (although we don't know if this was gradual or abrupt because of the coring break). Because of the low topography of the shorelines around the lake, even a slight rise in lake level will have a substantial effect on the position of the shoreline. It will have expanded outwards considerably in all directions, and will have moved substantially away from the coring site. This may explain why Zone DC-b has low representations of *B. braunii*-type and *Pediastrum* sp. – the river discharges supplying these allochthonous palynomorphs being further away.

4.1.3. Zone DC-c (6.18–4.64 m: 920–1230 AD). A relatively steady increase in *L. machaerophorum* and reciprocal decrease in the brackish species *I. caspienense* together evidences a progressive salinity increase in this zone, with precipitation of gypsum (G_2) near the top. A pronounced increase in dinoflagellate cyst concentration within this zone probably signifies increased productivity as a response to the rise in salinity. Judging from the presence of gypsum deposits and tolerance of *L. machaerophorum* to high salinities, it would seem that salinities rose above 28 g kg^{-1}. The increasing salinity throughout this zone suggests progressive lowering of the lake level.

4.1.4. Zone DC-d (4.64–2.62 m: 1230–1400 AD). This zone represents a progressive decline in salinity, as evidenced by a reduction in *L. machaerophorum* to near disappearance at the top of the zone. This was evidently caused by freshwater inflow into the lake, as indicated by abundant *B. braunii*-type. This zone is also characterized by a drastic change in sedimentation from the deposition of laminated sediments to silty clays (Fig. 3.2) rather poor in palynomorphs (Fig. 3.5). The coring site was clearly receiving significant river discharges because reworked cysts are also abundant. These reworked cysts attest to active erosion of Neogene and late Quaternary deposits during periods of elevated sheet-wash from shore, and account for the high sediment accumulation rates in this zone (16 mm yr^{-1}, see also Nourgaliev et al., 2003). Nutrient input at this time is reflected in the high levels of protoperidiniacean cysts. However, general productivity is likely to have been lower in this zone than in Zone DC-c because of the declining salinity. The low values of *I. caspienense* seem to be caused by reciprocally high values of protoperidiniacean cysts. The progressive decline in both *B. braunii*-type and reworked cysts probably relates to the expansion of the lake as it continued to fill, which will have caused rivers supplying freshwater to the lake to recede from the core site. Judging from low numbers of the cool-tolerant species *P. dalei*, spring surface-water temperatures were probably higher between 1230 AD and 1400 AD, implying relatively mild winters.

4.1.5. Zone DC-e (2.62–0.5 m: 1400–1800 AD). The lower part of this zone represents a continuance of reduced salinities established at the top of Zone DC-d, marked by low levels of *L. machaerophorum* and high levels of *I. caspienense*. Conditions were comparable to those in DC-b, with salinity probably around 10–15 g kg^{-1} or slightly less. The abrupt decline in protoperidiniacean cysts (causing a reciprocally abrupt increase in *I. caspienense*) might be explained in terms of a gradual lowering of salinity that abruptly exceeded the physiological limit of the protoperidiniaceans. Salinities were evidently increasing through the lower part of Zone DC-e (1500 AD and 1600–1650 AD), as evidenced by increased values of *L. machaerophorum* and declining values of *I. caspienense*. This seems to have culminated in the gypsum layer G_3 in the middle of the zone. The upper part of Zone DC-e is more difficult to reconstruct but salinities were certainly above 10 g kg^{-1}, judging from the persistence of *L. machaerophorum*, yet remained brackish given the high values of *I. caspienense*.

4.1.6. Zone DC-f (0.5–0 m: 1800–1980 AD). A return to progressively more saline conditions, as prevails today, is evidenced by an increase in *L. machaerophorum*, reduced levels of *I. caspienense*, and the formation of gypsum (G_4) within this zone. Also cooler spring surface-water temperatures following harsher winter conditions are reflected by higher abundances of cysts of *P. dalei* around 1900 AD.

III.4.2. Palaeoclimatic changes inferred from dinoflagellate cysts

Numerous previous studies indicate that climates of the Central Asian deserts and semi-deserts have experienced different changes from hyper-arid deserts to more humid semi-arid conditions at various temporal scales during the late Quaternary and Holocene (e.g. Tarasov et al., 1998; Velichko, 1989). During the past few thousand years these changes have resulted in multiple lake level changes (e.g. Létolle and Mainguet, 1993, Boomer et al., 2000; Boroffka et al., 2005). The present-day climate in western Central Asia is mainly controlled by the Westwind Drift carrying moist air to the mountain ranges which condenses as snow in the Pamir and Tien-Shan, the catchment areas of the two tributaries feeding the Aral Sea. Thus the meltwater discharged by Syr Darya and Amu Darya rivers largely controls the hydrological balance in the lake during late spring and early summer. In addition, local precipitation occurs during winter and early spring when depressions, developing over the Eastern Mediterranean, subsequently move along a northeast trajectory where they may even replenish moisture over the Caspian Sea (Lioubimsteva, 2002). This adds to the water balance in the Aral Sea. Hence the relative abundance of reworked dinoflagellate cysts is expected to increase during periods of elevated sheet-wash from shore caused by enhanced moisture derived from the Mediterranean Sea. A third factor of importance, though difficult to quantify is the seasonally changing evaporation rate probably due to short-term changes in solar insolation. During the past few thousand years these factors have exerted control on the water balance to varying degrees.

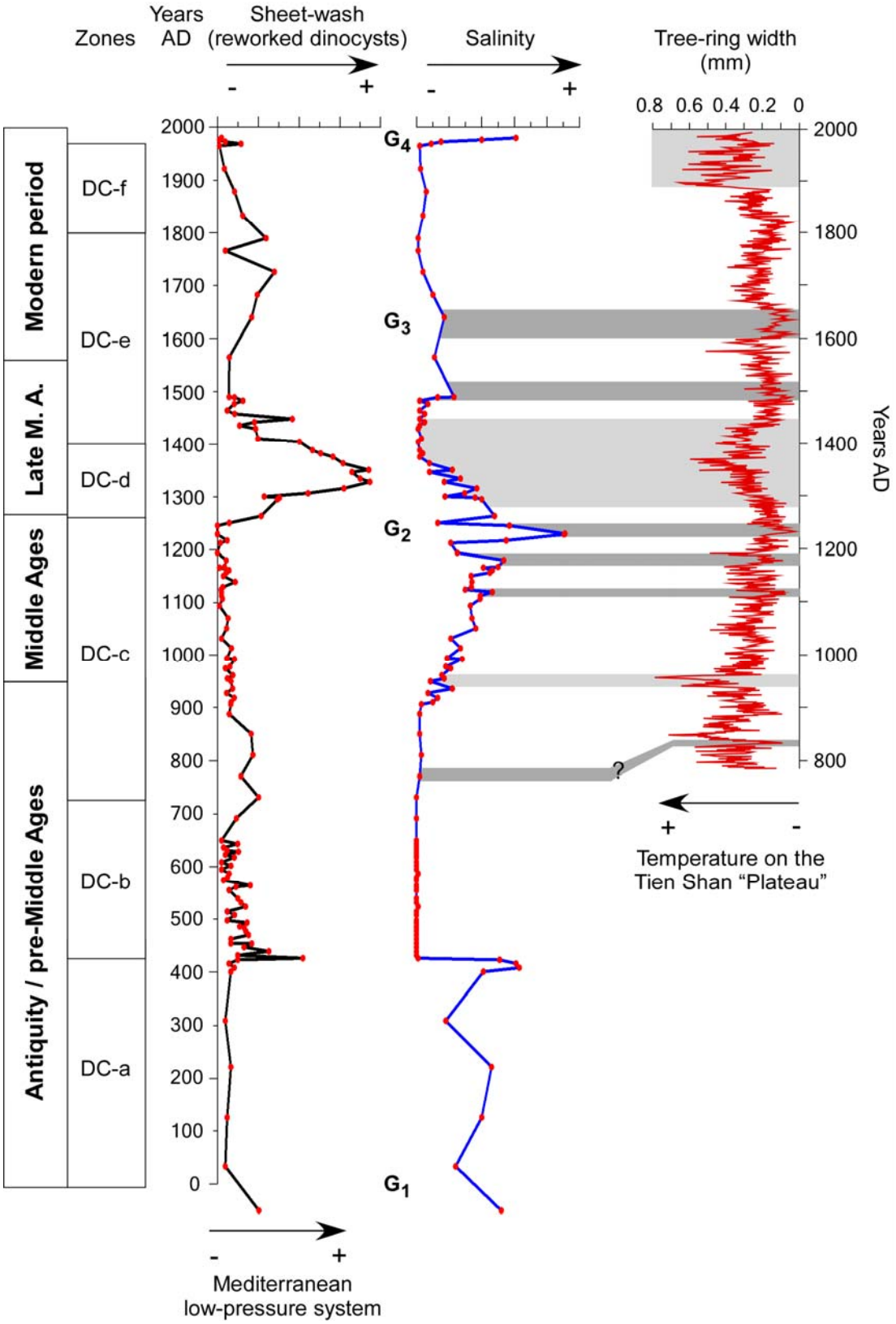

Figure 3.11: *Correlation of palaeoenvironmental changes during the last 2000 years as inferred from section CH2/1 with the tree-ring width record of Esper et al. (2002). The salinity reconstruction (blue curve) is estimated from the relative abundances of L. machaerophorum. Data are plotted according to the age model as detailed in Section 3.2.2 (Fig. 4). G_1 to G_4 refer to chemical precipitates of gypsum in section CH2/1 (see Section 3.2.1; Fig. 2).*

The dinoflagellate cyst record indicates prominent salinity increases during the intervals ca. 0–425 AD (or 100? BC–425 AD), 920–1230 AD, 1500 AD, 1600–1650 AD, 1800 AD and the modern increase (Fig. 3.11). The lowermost sequence (Zone DC-a, Unit 4), which represents the first few centuries AD, characterizes as a whole elevated salinity levels resulting in gypsum precipitation (G_1) during an important phase of lake level lowering (27–28 m.a.s.l.; see Nurtaev, 2004). During this time period, salinity increases mainly occurred at around 0 AD, 100–200 AD and 350–425 AD, probably resulting from considerably lowered meltwater run-off supplied by the rivers due to lowered late spring and early summer temperatures in the mountains of the high altitude catchment. This is contemporaneous with glacier expansion during 2100–1700 yr BP in the northern and western Tien Shan (Savoskul and Solomina, 1996) and in the Pamir (Zech et al., 2000). Coevally, at approximately 2000 yrs BP, a lake level recession is reported from Lake Van (Turkey) based on detailed palaeoclimatological studies (Landmann et al., 1996, Lemcke and Sturm, 1996) that demonstrate a period of decreasing humidity beginning at about 3500 and culminating at 2000 years BP. Similarly in Syria (Bryson, 1996) and Israel (Schilman et al., 2002), declining rainfall leading to dry events is also reported at around 2000 years BP. The decrease of rainfall is possibly related to a waning of the low-pressure system that developed over the Eastern Mediterranean and/or to a shift of the trajectories bringing moist air from the Eastern Mediterranean to the Middle East and Western Central Asia. In the Aral Sea hinterland, low levels of rainfall are inferred from low abundances of reworked dinocysts hence suggesting reduced on-land sheet-wash too.

The causes driving the progressive increase in salinity at ca. 920–1230 AD (Middle Age) may be climatically-controlled as well. The increase in salinity is accompanied by a progressive lake level fall of the Aral Sea to a large extent, as a pronounced regression was also recorded in Tschebas Bay (Wünnemann et al., submitted), and reflects long-term declining discharges from the Syr Darya and the Amu Darya rivers around 1200 AD. These results are fairly consistent with the tree-ring width records of Esper et al. (2002) (Fig. 3.11) and Mukhamedshin (1977), where several short-lasting events can be correlated with our salinity curve. These authors report a notable decrease in ring width from 800 AD to 1250 AD, corresponding to a colder phase in the Tien Shan and Pamir-Alay mountains, respectively, with lowered late spring and early summer temperatures. This is further supported by preliminary pollen analyses conducted on section CH2/1, which reflects cool and arid conditions in the Aral Sea Basin after 1000 AD. This aridification of the climate matches relatively well with variations observed in the western Tibetan Plateau by Bao et al. (2003). From air-temperature reconstructions, these authors report warming conditions during the intervals 800–1050 AD and 1250–1400 AD (Medieval Warm/Wet Period) with a short colder phase during ca. 1050–1250 AD and especially at around 1200 AD. The salinity increase intervening between 920 AD and 1230 AD in our record is accompanied by very low abundances of reworked dinoflagellate cysts (Fig. 3.11) suggesting again considerably reduced sheet-wash from the shore and thus lowered moisture derived

from the Eastern Mediterranean region during the late winter and early spring seasons. This is well-supported through palaeoenvironmental records from the Eastern Mediterranean Sea (Issar et al., 1990; Schilman et al., 2002) that document colder conditions resulting in a decrease of evaporation and reduced rainfall as inferred from $\delta^{18}O$ variations of pelagic foraminifera and carbonate cave deposits (Soreq cave, Israel).

A progressive decrease in salinity (oligo-/mesosaline conditions) and a return to higher lake levels characterize the period 1230–1450 AD. Coevally, tree-ring width conspicuously increased, growing at similar rates during ca. 1360–1370 AD to those observed for the last 100 years (Esper et al., 2002). This is further confirmed by Kotlyakov et al. (1991) who reported a warming phase between the 11th and 14th–15th centuries, based on tree-ring data from the Tien Shan. Increased growing rates thus characterize higher temperatures in the mountains that result in elevated meltwater discharges to the Aral Sea in late spring / early summer. Moreover, higher abundances of reworked dinoflagellate cysts of Neogene / late Quaternary ages reflect enhanced regional spring precipitation in Central Asia from 1230–1400 AD. They document the intensified erosion of shore sediments which occurred frequently during extreme sheet-wash events linked to intensified low pressure systems over the Eastern Mediterranean. The latter is confirmed by Schilman et al. (2002) who documented higher rainfall over Israel between 1250 AD and 1500 AD.

Similarly, the two slight increases in salinity as recorded at ca. 1500 AD and 1600–1650 AD from the dinoflagellate cysts are probably climatically driven as well. The interval from 1500–1650 AD includes the coldest decades according to the mean annual temperature reconstruction for the Northern Hemisphere (Bradley, 2000). New archaeological findings from the south Aral Sea (Boroffka et al., 2005, Shirinov et al., 2004) indicate that the lake level lowered to as much as 31 m a.s.l. at that time. A similar brief drying episode has been reported at about 1650 AD by Boomer et al. (2003) based on their studies on ostracods. Besides, these events are well-constrained with other records from Central Asia. Two successive decreases in tree-ring width are reported from Esper et al. (2002) between 1500 AD and 1600–1650 AD. These events match well with two salinity increases in the Aral Sea (Fig. 3.11) and reflect reduced meltwater inflow from the catchment area. This also closely matches a cooler phase from the Western Tibetan Plateau at ca. 1500–1550 AD and 1600–1650 AD when glaciers advanced on the southern Tibetan Plateau (Bao et al., 2003). We thus propose that this event widely expressed north of 35°N may correspond to a short-lived Little Ice Age signature in sediments from the Aral Sea.

After 1650 AD, salinity slightly fluctuated around lower levels (oligo-/mesosaline conditions) suggesting higher lake levels up to 1900 AD, with nevertheless a short-lasting salinity increase around 1800 AD. This is again consistent with the tree-ring record for this time window (Esper et al., 2002), where climatic conditions appear relatively favourable for growth, except around 1800 AD where a

decrease in the tree-ring width can be observed. Precipitation frequency, as inferred from the reworked dinoflagellate cysts, fluctuated slightly during this period, with probably higher rainfall at ca. 1650 and 1700 AD, but declined afterwards. Near to the top of section CH2/1, a strong environmental shift (Zone DC-f; Figs. 3.4 and 3.11) documents the onset of the modern lake level regression. Though this disaster is mostly due to the intensification of irrigation in the hinterland since the early 1960s, instrumental data already document a lake whose level was starting to lower in the late 1950s (Krivonogov, pers. comm., 2005).

III.4.3. Human influence on hydrography

Climate variability is probably the dominant factor controlling the hydrology in western Central Asia and thus the salinity in the Aral Sea, but one might expect human influence (irrigation activities) too also have exerted an important role in this densely settled region along the Silk Route during the past 2000 years. Since Early Antiquity (4^{th}–2^{nd} centuries BC) up to the pre-Islamic Middle Age (4th–6^{th} centuries AD), water from the Syr Darya and the Amu Darya rivers has been used on a large scale for irrigation, mostly in open canals (see Boroffka et al., 2005, in press). According to Létolle and Mainguet (1993), the hydraulic installations on the Amu Darya were completely destroyed after the invasion of Mongol warriors (the Huns Hephtalites) around 380–400 AD. Thus at that time the Aral Sea was reported to be cut-off from its main source of freshwater. Historical reports from Greek sources (Barthold, 1910) further indicate that the Amu Darya discharged into the Caspian Sea during this period. However, this event may not be at the origin of the lake regression observed at ca. 2000 years BP because a time lag of almost 400 years would be implied. Instead it may have only amplified the retreat of the water body witnessed by an aridification in Central Asia. Similar considerations may be regarded concerning the period 920–1230 AD (Zone DC-c), which records the Middle Age lake regression. Although irrigation gradually declined up to the 13^{th} century AD (Boroffka et al., 2005), historical reports document a total destruction of the hydraulic installations in the Khorezm region after Genghis-Khan's invasion documented at 1221 AD (Létolle and Mainguet, 1993). This catastrophic event led again to a severing of the Amu Darya from the Aral Sea, which was reported as discharging into the Caspian Sea at that time. Nonetheless, our dinoflagellate cyst record rather reflects a gradual regressive phase which would not match with a catastrophic event resulting from the destruction of dams in the Amu Darya delta. We thus propose that the progressive lake level lowering inferred for the period 920–1230 AD is again most probably climatically driven, but that human activities might have further strengthened the lake level fall.

III.4.4. Conclusions

This is the first ecostratigraphic study using dinoflagellate cysts from the late Quaternary of the Aral Sea and has led to an improved understanding of the mechanisms that control environmental changes in the Aral Sea during the Late Holocene. It has also helped to unravel the influence of climate and anthropogenic activities on the hydrographic development of the Aral Sea during the past 2000 years. The results suggest that the successive lake level fluctuations are indeed climatically triggered, and result from different factors controlling the water balance in Central Asia, notably the Westwind Drift controlling temperatures in the montane regions, and local to regional rainfall sourced by migrating moisture from the Eastern Mediterranean Sea. Other factors may have influenced climate conditions over the Aral Sea Basin, such as variable solar activity, as suggested by Crowley (2000) based on climate-modelled simulations over the Northern Hemisphere. Testing this proposal would require higher-resolution analyses than presently undertaken. However, the degree of lake-level lowering may have been amplified by humans responding to changing environmental conditions. Irrigation systems were probably extended during periods of more arid conditions. Documentary evidence shows the existence of irrigation activities already during Early Classical Antiquity (before 0 BC) (Boroffka et al., 2005), indicating that lake water levels strongly depended on climate conditions at that time too. As to changes during the early to middle Holocene, ongoing research aims to unravel the respective impacts of climate and tectonics on the hydrology of the Aral Sea ecosystem.

Acknowledgments

The CLIMAN project is funded by the INTAS organization of the European Union (Project N° Aral 00-1030) and the German Science Foundation (DFG Project 436 RUS 111/663 – OB 86/4). We are grateful for this support. We wish to thank especially Dr. François Demory for excellent support in the field. We acknowledge Dr. Gilles Escarguel, Dr. Jean-Jacques Cornée, Dr. Pierpaolo Zuddas and Samuel Mailliot (University Claude Bernard-Lyon 1) for valuable discussions and insights. The manuscript reviewers are also acknowledged for contributing to improve the manuscript.

References

Aksu, A.E., Yasar, D., Mudie, P.J., 1995a. Palaeoclimatic and paleooceanographic conditions leading to development of sapropel layer S1 in the Aegean Sea. Palaeogeography, Palaeoclimatology. Palaeoecology 116, 71–101.

Aksu, A.E., Yasar, D., Mudie, P.J., Gillespie, H., 1995b. Late glacial–Holocene paleoclimatic and palaeoceanographic evolution of the Aegean Sea: micropaleontological and stable isotope evidence. Marine Geology 123, 33–59.

Aleshinskaya, Z.G., Tarasov, P.E., Harrison, S.P., 1996. Aral Sea, Kazakhstan-Uzbekistan. Lake Status Records FSU and Mongolia, 108–114.

Baltes, N., 1971a. Tertiary plant microfossil assemblages from the Pannonian Depression (Rumania) and their paleoecology. Review of Palaeobotany and Palynology 11, 125–158.

Baltes, N., 1971b. Pliocene Dinoflagellata and Acritarcha in Romania. In: Farinacci, A. (Ed.), Proceedings, Second Planktonic Conference, Rome. Edizioni Tecnoscienza, Rome 1970 (1), 1–19.

Bao, Y., Bräuning, A., Yafeng, S., 2003. Late Holocene temperature fluctuations on the Tibetan Plateau. Quaternary Science Reviews 22, 2335–2344.

Barthold, W., 1910. Nachrichten über den Aral-See und den unteren Lauf des Amu-darja von den ältesten Zeiten bis zum XVII. Jahrhundert. Quellen und Forschungen zur Erd- und Kulturkunde 2. Leipzig: Otto Wigand m.b.H.

Batten, D.J., Grenfell, H.R., 1996. Green and blue-green algae. 7D – *Botryococcus*. In: Jansonius, J., McGregor, D.C. (Eds), Palynology: Principles and Applications, vol. 1. American Association of Stratigraphic Palynologists Foundation, Dallas, Texas, pp. 205–214.

Bold, H.C., Wynne, M.J., 1985. Introduction of the Algae, 2nd Edition, Prentice-Hall, Englewood Cliffs, NJ, 720 pp.

Boomer, I., Horne, D.J., Slipper, I., 2003. The use of ostracodes in palaeoenvironmental studies or what can you do with an ostracod shell? Palaeontological Society Papers 9, 153–180.

Boomer, I, Aladin, N., Plotnikov, I., Whatley, R., 2000. The palaeolimnology of the Aral Sea: a review. Quaternary Science Reviews 19, 1259–1278.

Boroffka, N.G.O., Oberhänsli H., Achatov, G.A., Aladin, N.V., Baipakov, K.M., Erzhanova, A., Hoernig, A., Krivonogov, S.K., Lobas, D.A., Savel'eva, T.V., Wuennemann, B., 2005. Human settlements on the northern shores of Lake Aral and water level changes. Mitigation and Adaptation Strategies for Global Change 10, 71–85.

Boroffka, N.G.O., Oberhänsli, H., Sorrel, P., Reinhardt, C., Wünnemann, B., Alimov, K., Baratov, S., Rakhimov, K., Saparov, N., Shirinov, T., Krivonogov, S.K. Archaeology and climate: Settlement and lake level changes at the Aral Sea. Geoarchaeology (in press).

Bortnik, V.N., Chistyaeva, S.P. (Eds), 1990. Hydrometeorology and hydrochemistry of the USSR seas. Vol. VII: The Aral Sea. Gidrometeoizdat, Leningrad, 196 pp. (in Russian).

Bradford, M.R., Wall, D.A., 1984. The distribution of Recent organic-walled dinoflagellate cysts in the Persian Gulf, Gulf of Oman, and northwestern Arabian Sea. Palaeontographica Abt. B 192, 16–84.

Bradley, R.S., 2000. 1000 years of climate change. Science 288, 1353–1354.

Brenner, W.W., 2001. Organic-walled microfossils from the central Baltic Sea, indicators of environmental change and base for ecostratigraphic correlation. Baltica 14, 40–51.

Brodskaya, I.G., 1952. Data and Processes on Sedimentary Deposits of the Aral Sea of the Aral Sea, tr. In-Ta Geol. Nauk, AN SSSR 115, 140 p. (in Russian).

Bryson, R.A., 1996. Proxy indications of Holocene winter rains in southwest Asia compared with simulated rainfall. In: Dalfes, H.N., Kukla, G., Weiss, H. (eds), Third Millenium BC; Climate Change and Old World Collapse. NATO ASI Series I, vol. 49. Springer Verlag, pp. 465–473.

Cleve, P.T., 1900. The plankton of the North Sea, the English Channel, and the Skagerrak in 1898. Kongliga Svenska Vetenskaps-akademiens Handlingar, 32 (8), 1–53.

Cour, P., 1974. Nouvelles techniques de détection des flux et de retombées polliniques: étude de la sédimentation des pollens et des spores à la surface du sol. Pollen et Spores 23 (2), 247–258.

Crowley, T.J., 2000. Causes of climate change over the past 1000 years. Science 289, 270–277.

Dale, B., 2001. The sedimentary record of dinoflagellate cysts: looking back into the future of phytoplankton blooms. Scientia Marina 65 (Suppl. 2), 257–272.

Dale, B., 1996. Dinoflagellate cyst ecology: modelling and geological applications. In: Jansonius, J., McGregor, D.C. (Eds), Palynology: Principles and Applications, vol. 3. American Association of Stratigraphic Palynologists Foundation, Dallas TX, pp. 1249–1275.

Dale, B., Gjellsa, A., 1993. Dinoflagellate cysts as paleoproductivity indicators: State of the art, potential, and limits. In: Zahn, R., Pedersen, T.F., Kaminski, M.A., Labeyrie, L. (Eds), Carbon Cycling in the Glacial Ocean:

Constrains on the Ocean's Role in Global Change: Quantitative Approaches in Paleooceanography. NATO ASI Series I, Global Environmental Change, Springer, Berlin, pp. 521–537.

Deflandre, G., Cookson, I.C., 1955. Fossil microplankton from Australian late Mesozoic and Tertiary sediments. Australian Journal of Marine and Freshwater Research 6, 242–313.

de Vernal, A., Henry, M., Matthiessen, J., Mudie, P.J., Rochon, A., Boessenkool, K.P., Eynaud, F., Grøsfjeld, K., Guiot, J., Hamel, D., Harland, R., Head, M.J., Kunz-Pirrung, M., Levac, E., Loucheur, V., Peyron, O., Pospelova, V., Radi, T., Turon, J-L., Voronina, E., 2001. Dinoflagellate cyst assemblages as tracers of sea-surface conditions in the northern North Atlantic, Arctic and sub-Arctic seas: the new 'n=677' data base and its application for quantitative palaeoceanographic reconstruction. Journal of Quaternary Sciences 16, 681–698.

Esper, J., Schweingruber, F.H., Winiger, M., 2002. 1300 years of climate history for Western Central Asia inferred from tree-rings. Holocene 12, 267–277.

Friedrich, J., Oberhänsli, H., 2004. Hydrochemical properties of the Aral Sea water in summer 2002. Journal of Marine Systems 47, 77–88.

Gundersen, N., 1988. En palynologisk undersøkelse av dinoflagellatcyster langs en synkende salinitetsgradient i recente sedimenter fra Østersjø-området. Cand. Scient. Dissertation, Geologisk Institutt, Universitetet i Oslo.

Hallett, R.I., 1999. Consequences of environmental change on the growth and morphology of *Lingulodinium polyedrum* (Dinophyceae) in culture. PhD Thesis, University of Westminster, London.

Harland, R., 1977. Recent and late Quaternary (Flandrian and Devensian) dinoflagellate cysts from marine continental shelf sediments around the British Isles. Palaeontographica Abt. B 164, 87–126.

Head, M.J., Seidenkrantz, M.-S., Janczyk-Kopikowa, Z., Marks, L., Gibbard, P.L. 2005. Last Interglacial (Eemian) hydrographic conditions in the southeastern Baltic Sea, NE Europe, based on dinoflagellate cysts. Quaternary International 130, 3–30.

Heim, C., 2005. Die Geochemische Zusammensetzung der Sedimente im Aralsee und Sedimentationsprozesse während der letzten 100 Jahre. Diploma thesis, Alfred-Wegener-Institut Bremerhaven.

Hensen, V., 1887. Über die Bestimmung des Planktons oder des im Meere treibenden Materials an Pflanzen und Thieren. Berichte der Kommission zur wissenschaftlichen Untersuchung der deutschen Meere in Kiel 5, 107.

Issar, A.S., Govrin, Y., Geyh, A. M., Wakshal, E., Wolf, M., 1990. Climate changes during the Upper Holocene in Israel. Israel Journal of Earth Sciences 40, 219–223.

Kloosterboer-van Hoeve, M.L., Steenbrink, J., Brinkhuis, H., 2001. A short-term cooling event, 4.205 million years ago, in the Ptolemais basin, northern Greece. Palaeogeography, Palaeoclimatology, Palaeoecology 173, 61–73.

Kokinos, J.P., Anderson, D.M., 1995. Morphological development of resting cysts in cultures of the marine dinoflagellate *Lingulodinium polyedrum* (= *L. machaerophorum*). Palynology 19, 143–166.

Kotlyakov, V.M., Serebryanny, R., Solomina, O.N., 1991. Climate change and glacier fluctuation during the last 1000 years in the southern Mountains of the USSR. Mountain Research and Development 11 (1), 1–12.

Kouli, K., Brinkhuis, H., Dale, B., 2001. *Spiniferites cruciformis*: a fresh water dinoflagellate cyst? Review of Palaeobotany and Palynology 133, 273–286.

Kunz-Pirrung M. 1998. Rekonstruktion der Oberflächenwassermassen der östlichen Laptevsee im Holozän anhand von aquatischen Palynomorphen. Berichte zur Polarforschung 281, 1–117.

Kunz-Pirrung M. 1999. Distribution of aquatic palynomorphs in surface sediments from the Laptev Sea, Eastern Arctic Ocean. In: Kassens, H., Bauch, H.A., Dmitrenko, I. et al. (eds.), Land–Ocean Systems in the Siberian Arctic: Dynamics and History. Springer-Verlag, Berlin, pp. 561–575.

Landmann, G., Reimer, A., Lemcke, G., Kempe, S., 1996. Dating Late Glacial abrupt climate changes in the 14,570-yr long continous varve record of Lake Van, Turkey. Palaeogeography, Palaeoclimatology, Palaeoecology 122, 107–118.

Leegaard, C., 1920. Microplankton from the Finnish waters during the Month of May 1912. Acta Societatis Scientiarum Fennicae 48, 1–44.

Lemcke, G., Sturm, M., 1996. ^{18}O and trace element measurements as proxy for the reconstruction of climate changes at Lake Van (Turkey). In: Dalfes, H.N., Kukla, G., Weiss, H. (eds), Third Millenium BC; Climate Change and Old World Collapse. NATO ASI Series I, vol. 49. Springer Verlag, pp. 653–678.

Létolle, R., Mainguet, M., 1993. Aral. Springer Verlag, Paris.

Lewis, J., Hallett, R., 1997. *Lingulodinium polyedrum* (*Gonyaulax polyedra)* a blooming dinoflagellate. Oceanography and Marine Biology: An Annual Review 35, 97–161.

Lioubimtseva, E., 2002. Arid environments. In: Shahgedanova, M. (Ed.), Physical Geography of Northern Eurasia. Oxford University Press, Oxford, 571 pp.

Maev, E. G., Karpychev, Yu, A., 1999. Radiocarbon dating of bottom sediments in the Aral Sea: Age deposits and sea level fluctuations. Water Resources 26/2, 187–194.

Marret, F., Leroy, S., Chalié, F., Gasse, F., 2004. New organic-walled dinoflagellate cysts from recent sediments of Central Asian seas. Review of Palaebotany and Palynology 129, 1–20.

Marret, F., Zonneveld, K.A.F., 2003. Atlas of modern organic-walled dinoflagellate cyst distribution. Review of Palaeobotany and Palynology 125, 1–200.

Matthiessen, J., Kunz-Pirrung, M., Mudie, P. J., 2000. Freshwater chlorophycean algae in recent marine sediments of the Beaufort, Laptev and Kara Seas (Arctic Ocean) as indicators of river runoff. International Journal of Earth Sciences 89, 470–485.

Meunier, A., 1910. Microplankton des Mers de Barents et de Kara. Charles Bulens, Imprimerie Scientifique, Bruxelles.

Mirabdullayev, I.M., Joldasova, I.M., Mustafaeva, Z.A., Kazakhbaev, S.K., Lyubimova, S.A., Tashmukhamedov, B.A., 2004. Succession of the ecosystems of the Aral Sea during its transition from oligosaline to polyhaline conditions. Journal of Marine Systems 47, 101–107.

Mudie, P.J., 1992. Circum-arctic Quaternary and Neogene marine palynofloras: paleoecology and statistical analysis. In: Head, M.J., Wrenn, J.H. (eds), Neogene and Quaternary dinoflagellate cysts and acritarchs. American Association of Stratigraphic Palynologists, Foundation, Dallas, TX, pp. 347–390.

Mudie, P.J., Aksu, A.E., Duman, M., 1998. Late Quaternary dinocysts from the Black, the Marmara and Aegean seas: variations in assemblages, morphology and paleosalinity. In: M. Smelror, M. (Ed.), Abstracts from the Sixth International Conference on Modern and Fossil Dinoflagellates Dino 6, Trondheim, June 1998. Norges teknisk-naturvitenskapelige universitet Vitenskapsmuseet, Rapport botanisk serie, 1998-1.

Mudie, P.J., Aksu, A.E., Yasar, D., 2001. Late Quaternary dinoflagellates cyst distribution. Review of Palaebotany and Palynology 125, 1–200.

Mudie, P.J., Rochon, A., Aksu, A.E., Gillespie, H., 2002. Dinoflagellate cysts, freshwater algae and fungal spores as salinity indicators in Late Quaternary cores from Marmara and Black seas. Marine Geology 190, 203–231.

Mukhamedshin, K.D., 1977. Tien Shan juniper forests and their economic significance (Archevniki Tian'-Shanya I ikh lesokhoziaistvennoye znacheniye). Ilim, Frunze.

Nehring, S., 1994. Spatial distribution of dinoflagellate resting cysts in Recent sediments of Kiel Bight, Germany (Baltic Sea). Ophelia 39: 137–158.

Nourgaliev, D.K., Heller, F., Borisov, A.S., Hajdas, I., Bonani, G., Iassonov, P.G., Oberhänsli, H., 2003. Very high resolution paleosecular variation record for the last 1200 years from the Aral Sea. Geophysical Research Letters 30 (17), 4-1–4-4.

Nurtaev, B., 2004. Aral Sea Basin evolution: Geodynamic aspect. In: Nihoul, J.C.J., Zavialov P.O., Micklin Ph.P. (Eds.), Dying and Dead Seas Climatic Anthropic Causes. Proceedings of the NATO Advanced Research Workshop, Liège, Belgium, 7–10 May, 2003. Nato Science Series: IV: Earth and Environmental Sciences 36, pp. 91–97. Berlin, Heidelberg, New York: Springer-Verlag.

Parra Barientos, O.O., 1979. Revision der Gattung *Pediastrum* Meyen (Chlorophyta). Bibliotheca Phycologia 48 (1-186), 1–55.

Popescu, S.-M., 2001. Végétation, climat et cyclostratigraphie en Paratéthys centrale au Miocène supérieur et au Pliocène inférieur d'après la palynologie. Thèse de doctorat, Université Claude Bernard-Lyon 1.

Popescu, S.-M. Upper Miocene and Lower Pliocene environments in the southwestern Black Sea region from high-resolution palynology of DSDP site 380A (Leg 42B). Palaeogeography, Palaeoclimatology, Palaeoecology, in press.

Reimer, P.J., Baillie, M.G.L., Bard, E., Bayliss, A., Beck, J.W., Bertrand, C.J.H., Blackwell, P.G., Buck, C.E., Burr, G.S., Cutler, K.B., Damon, P.E., Lawrence Edwards, R., Fairbanks, R.G., Friedrich, M., Guilderson, T.P., Hogg, A.G., Hughen, K.A., Kromer, B., McCormac, G., Manning, S., Bronk Ramsey, C., Reimer, R.W., Remmele, S., Southon, J.R., Stuiver, M., Talamo, S., Taylor, F.W., van der Plicht, J., Weiyhenmeyer, C.E., 2004. IntCal04 terrestrial radiocarbon age calibration, 0-26 cal. yr BP. Radiocarbon 46 (3), 1029–1058.

Rochon, A., de Vernal, A., Turon, J.-L., Matthiessen, J., Head, M.J., 1999. Distribution of recent dinoflagellate cysts in surface sediments from the North Atlantic Ocean and adjacent seas in relation to sea-surface parameters. American Association of Stratigraphic Palynologists, Contributions Series 35, 1–150.

Savoskul, O.S., Solomina, O.N., 1996. Lvariations in the frontal and inner ranges of the Tien Shan, central Asia. The Holocene 6 (1), 25–35.

Schilman, B., Ayalon, A., Bar-Matthews, M., Kagan, E.J., Almogi-Labin, A., 2002. Sea–land palaeoclimate correlation in the Eastern Mediterranean region during the Late Holocene. Israel Journal of Earth Sciences 51, 181–190.

Shirinov, T., Alimov, K., Baratov, S., Rakhimov, K., Saparov, N., Boroffka, N., Vjunnemann, B, Rajnkhardt, Khr., Sorrel, P. and Krivonogov, S., 2004. Polevye raboty po proektu INTAS Aral No. 00-130: "Klimaticheskie izmenenija v epochu golocena i razvitie poselenij cheloveka v bassejne Aral´skogo Morja" "Holocene climatic variability and evolution of human settlement in the Aral Sea basin (CLIMAN)". Arkheologicheskie issledovanija v Uzbekistane 2003 goda, 4, 197–205.

Tarasov, P.E., Webb III, T., Andreev, A.A., Afanas'eva, N.B., Berezina, N.A., Bezusko, L.G., Blyakharchuk, T.A., Bolikhovskaya, N.S., Cheddadi, R., Chernavskaya, M.M., Chernova, G.M., Dorofeyuk, N.I., Dirksen, V.G., Elina, G.A., Filimonova, L.V., Glebov, F.Z., Guiot, J., Gunova, V.S., Harrison, S.P., Jolly, D., Khomutova, V.I., Kvavadze, E.V., Osipova, I.M., Panova, N.K., Prentice, I.C., Saarse, L., Sevastyanov, D.V., Volkova, V.S., Zernitskaya, V.P., 1998. Present-day and mid-Holocene biomes reconstructed from pollen and plant macrofossil data from the former Soviet Union and Mongolia. Journal of Biogeography 25, 1029–1053.

Tchepaliga, A., 2004. Late Glacial great flood in the Black Sea and Caspian Sea. Geological Society of America Annual Meeting, Seattle, 2–5 November 2003; Abstract, session No 189.

Velichko, A.A., 1989. The relationship of the climatic changes in the high and low latitudes of the Earth during the Late Pleistocene and Holocene. In: Velichko, A.A. et al. (ed.)., Paleoclimates and Glaciation in the Pleistocene, Nauka Press, Moscow, 5–19.

Wall, D., Dale, B., 1966. "Living fossils" in Western Atlantic plankton. Nature, 211(5053), 1025–1026.

Wall, D., Dale, B., Harada, K., 1973. Description of new fossil dinoflagellates from the Late Quaternary of the Black Sea. Micropaleontology 19, 18–31.

Wall, D., Dale, B., 1974. Dinoflagellates in late Quaternary deep-water sediments of the Black Sea. In: Degens, R.T., Ross, D.A. (Eds), The Black Sea – Geology, Chemistry and Biology. Memoir, American Association of Petroleum Geologists 20, pp. 364–380.

Wünnemann, B., Riedel, F., Keyser, D., Reinhardt, C., Pint, A., Sorrel, P., Oberhänsli, H. The limnological development of the Aral Sea since the early Middle Ages inferred from sediments and aquatic organism. Quaternary Research, submitted.

Zavialov, P.O., Kostianoy, A.G., Emelianov, S.V., Ni, A.A., Ishniyazov, D., Khan, V.M., Kudyshkin, T.V., 2003. Hydrographic survey in the dying Aral Sea. Geophysical Research Letters 30 (13), 2.1–2.4.

Zavialov, P.O., 2005. Physical Oceanography of the Dying Aral Sea. Springer Verlag, Chichester, UK, 146 pp.

Zech, W., Glaser, B., Ni, A., Petrov, M., Lemzin, I., 2000. Soils as indicators of the Pleistocene and Holocene landcsape evolution in the Alay Range (Kyrghystan). Quaternary International 65/66, 161–169.

Zonneveld, K.A.F., Versteegh, G.J.M., de Lange, G.J., 2001. Palaeoproductivity and post-depositional aerobic matter decay reflected by dinoflagellate cyst assemblages of the Eastern Mediterranean S1 sapropel. Marine Geology 172, 181–195.

Chapter IV: Climate variability in the Aral Sea Basin (Central Asia) during the late Holocene based on vegetation changes

Philippe **Sorrel** [1,2], Speranta-Maria **Popescu** [1], Stefan **Klotz** [1,3], Jean-Pierre **Suc** [1], Hedi **Oberhänsli** [2]

(1) Laboratoire PaléoEnvironnements et PaléobioSphère (UMR 5125 CNRS), Université Claude Bernard – Lyon 1, 27–43, boulevard du 11 Novembre, F-69622 Villeurbanne Cedex, France ;
(2) GeoForschungsZentrum Potsdam, Telegraphenberg, D-14473 Potsdam, Germany;
(3) Institut für Geowissenschaften, Universität Tübingen, Sigwartstrasse 10, 72070 Tübingen, Germany.

Accepted with revision in *Quaternary Research*

Abstract

High-resolution pollen analyses (~50 years) from sediment cores retrieved at Chernyshov Bay in the NW Large Aral Sea record shifts in vegetational development from subdesertic to steppe vegetation in the Aral Sea Basin during the late Holocene. Using pollen data to quantify climatic parameters, we reconstruct and date for the first time significant changes in moisture conditions in Central Asia during the past 2000 years. Cold and arid conditions prevailed between ca. 0 and 400, 900 and 1150, 1500 and 1650 yr AD with the extension of xeric vegetation dominated by steppe elements. These intervals are characterized by low winter and summer mean temperatures and low mean annual precipitation (P_{mm} <250 mm/yr). Conversely, the most suitable climate conditions occurred between ca. 400 and 900, 1150 and 1450 yr AD, where steppe vegetation was enriched by plants requiring moister conditions (P_{mm} ~250–500 mm/yr) and some trees developed. Our results are fairly consistent with other late Holocene records from the Eastern Mediterranean region and the Middle East. It is showed that regional rainfall in Central Asia is predominantly controlled by the Eastern Mediterranean cyclonic system when the North Atlantic Oscillation (NAO) is in a negative phase.

Keywords: Pollen analysis; Vegetation; Climate; Aral Sea; Late Holocene; Central Asia, negative NAO.

IV.1. Introduction

Numerous biostratigraphic, geomorphological and archaeological proxy data document that climate of Central Asian deserts and semi-deserts experienced many changes at various time scales through the Late Pleistocene and Holocene (e.g. Velichko, 1989; Tarasov et al., 1998a; Boomer et al., 2000; Boroffka et al., 2005; Boroffka et al., in press). Climatic variations resulted in multiple shifts from hyper-arid to semi-arid deserts and even steppe vegetations with development of shrubs (Kremenetski and Tarasov, 1997; Kremenetski et al., 1997; Tarasov, 1992; Tarasov et al., 1997, 1998a). However, whereas environmental and climate changes are well-documented in southwestern Siberia and Kazakhstan during the Pleistocene and early Holocene (Kremenetski and Tarasov, 1997; Kremenetski et al., 1997; Tarasov et al., 1997), they are still scarse for the Aral Sea Basin (e.g. Rubanov et al, 1987; Boomer et al., 2000). Using pollen and tree macrofossil records, Tarasov et al. (1998a) reconstructed vegetation biomes at 6000 yr BP, and documented dry conditions similar to present-day ones around the Aral Sea. Distinct vegetation changes occurred in northeastern Kazakhstan (Kremenetski and Tarasov, 1997). From two peatlands and two lakes sections, they document a milder climate between 6000 and 4500 yr BP, followed by drier and more continental conditions during 4500–3600 yr BP, and a "less continental" climate during 3300–2800/2700 yr BP. Recently, Esper et al. (2002) published a high-resolution climate record from the Karakorum and Tien-Shan Mountains based on tree-ring width, documenting prominent temperature changes for the last 1200 years. They reported warm conditions during 800–1000 yr AD, 1300–1450 yr AD and during the past century. In contrast, lowered temperatures were inferred during 1000–1200 yr AD and during the "Little Ice Age" (1450–1900 yr AD).

In the Aral Sea area, high-resolution climatic studies have been recently undertaken in the frame of the project CLIMAN (Nourgaliev et al., 2003; Sorrel et al., 2006). In this study, we present a new pollen record covering the last 2000 years with a time resolution of ca. 50 years. Based on quantitative pollen analyses, we provide evidence for significant changes in moisture conditions and vegetation patterns in the Aral Sea Basin. We use pollen data to reconstruct past temperature and mean annual precipitation during the past 2000 years. Our objective is to identify climatically induced shifts in the terrestrial vegetation surrounding the lake and to compare them to other records from the Middle East and Central Asia. These data are then critically evaluated in order to provide initial assessment of late Holocene climatic changes in Central Asia.

Geological and climatic frame of the Aral Sea Basin

The Aral Sea, situated in Central Asia (Fig. 4.1), represents an ideal sedimentary archive for studying environmental and climate changes in the past. The present-day climate is marked by extreme continental conditions that are mediated by a complex topography around the Aral Sea.

Figure 4.1: *Location map of the Aral Sea and the study area (modified from Lioubimtseva et al., 2005).*

The Central Asian arid region (= Aral Sea Basin) comprises the Turan Lowland and the Kyzyl Kum, and is surrounded in the North by the southern margin of the Kazakh Hills (at ca. 48°N), the Middle Asian Mountains on its southern and southeastern edges (Pamir, Tien Shan), and the lower mountains of the Kopet Dagh (2000 m in altitude) in the SouthWest (Fig. 4.1). In the North, the Turan Lowland descends progressively northward and westward and opens towards the Caspian lowland (Lioubimtseva et al., 2005). In the Aral Sea Basin, ecosystems mostly represented by steppes (including shrubs) are the prevailing landscapes. Some isolated trees (poplar, tamarisk, elm, oak, etc.), which are typical for riparian ecosystems, are restricted to the banks of two major Central Asian rivers, the Syr Darya and the Amu Darya. Winters, dominated by the Siberian High Pressure Cell (Zavialov, 2005) are cold and dry. Severe frosts, with mean temperatures of -26°C and absolute minimum of -40°C are common (Lioubimtseva et al., 2005). In contrast, summers are hot, cloudless and dry. In

autumn, a rapid cooling of the land tends to stabilize the atmosphere, protracting the dry season. Therefore, rain is rare in the basin with maximum precipitation in winter and early spring (Lioubimtseva, 2002; Nezlin et al., 2005), whereas almost no rain occurs between May and October (e.g. Létolle and Mainguet, 1993; Zavialov, 2005). Overall, the characteristic number of rainy days is 30–45 per year (Bortnik and Chistyaeva, 1990), and precipitation over the Aral Sea tends to increase northwards (Zavialov, 2005).

IV.2. Material and methods

IV.2.1. Site, sediments and chronology

During a field campaign in the summer 2002, Piston cores CH1 (11.04 m) and CH2 (6.0 m) (45°58'528'' N, 59°14'459'' E; water depth 22 m) were retrieved with a Usinger piston corer (http://www.uvitec.ut) about one km off the shoreline at Chernyshov Bay (Fig. 4.1). We investigated the composite sediment core CH2/1 (Cores CH1 and CH2), whose total length is 10.79 m. The correlation between Cores CH1 and CH2 was performed by matching laminations, using photographs, physical properties and XRF scanning data (see Fig. 2.3). Detailed lithological description of section CH2/1 is given in Sorrel et al. (2006). A simplified lithological profile and the age model for section CH2/1 are presented in Figure 4.2.

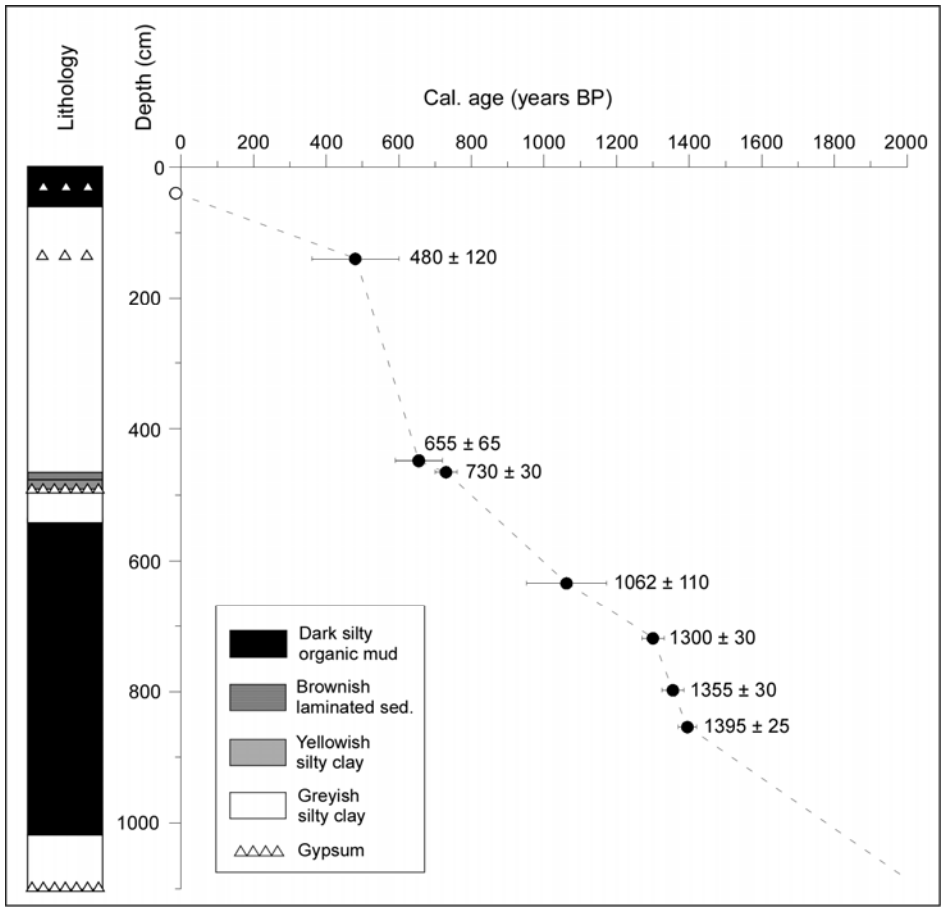

Figure 4.2: *Simplified lithological profile and age model for section CH2/1 based on AMS ^{14}C dating on the green alga Vaucheria sp. (full dots). Open dot: peak in ^{137}Cs [1963–1964 AD].*

In section CH2/1, reliable dating for the upper 5 m was obtained by correlation with the magnetic susceptibility record from parallel cores 7, 8 and 9 retrieved ca. 50 m apart from the studied cores (Nourgaliev et al., 2003). This correlation provides an age of 480±120 yr BP (cal. years) at 1.4 m depth and 655±65 yr BP at 4.48 m in section CH2/1 (Table 2). For the lower part of section CH2/1 [5–10.79 m], AMS radiocarbon ages were determined using the green alga *Vaucheria* sp. and $CaCO_3$ from mollusc shells, which were successively picked from the washed sediment sample and carefully cleaned from adhering particles. Algae were stored in distilled water within a glass vessel. For each sample, AMS ^{14}C dating was performed using between 0.2 and 1.0 mg of pure extracted carbon. Extrapolation of sedimentation rates below 8.3 m provides an age of ca. 2000 yr BP for the basement of section CH2/1. A sampling interval of 30 to 40 cm was selected, which provides a time resolution of ca. 50 years. The top of the core (uppermost 40 cm) has been dated as post-1963, as based on a peak in ^{137}Cs at 0.46 m reflecting the bomb period (ca. 1963–1964 AD) (Heim, 2005). Accordingly, dating on *Vaucheria* sp. at 0.55 m reveals an age of 101.9 ± 0.3 pMC (post-1950).

Sample name	Core depth (m)	Lab. no.	Age ^{14}C	Error bar	Calibrated age (yr BP)	Dated material
Aral 30 53-57cm	0,55	Poz-12281	101.9 pMC	0.3	modern	*Vaucheria* sp.
Nourgaliev *et al.* (2003)[1]	1,4			120	480	*Vaucheria* sp.
Nourgaliev *et al.* (2003)[2]	4,48			65	655	*Vaucheria* sp.
Aral 32 134.5-138.5cm	4,65	Poz-13511	815	30	730	TOC
Aral 27 209-212cm	6,34	Poz-12279	1160	110	1062	*Vaucheria* sp.
Aral 27 269-271cm	6,93	Poz-4762	1395	30	1300	*Vaucheria* sp.
Aral 28 40-45; 52-54cm	~7,73	Poz-9662	1480	30	1355	molluscs
Aral 28 112-114cm	8,285	Poz-4760	1515	25	1395	*Vaucheria* sp.

Table 2: *Radiocarbon dates for section CH2/1. AMS ^{14}C ages were measured at Poznań Radiocarbon Laboratory (Poland). Radiocarbon ages were then corrected to calibrated (cal) ages using the IntCal04 calibration curve (Reimer et al., 2004). They indicate values with 2 standard deviations (95% of confidence).*

IV.2.2. Sample processing

Pollen slide preparation followed the Cour's method (Cour, 1974). 35 sediment samples (15–25 g dry weight) were treated with cold HCl (35%) and cold HF (70%) to remove carbonates and silicates. Denser particles were separated from the organic residue using $ZnCl_2$ (density = 2.0). Residues were filtered through a 150-µm nylon sieve to eliminate the coarser particles including organic macroremains. Palynomorphs were further concentrated using a 10-µm nylon sieve after a brief sonication (about 30 s). The final residue was then homogenized, and mounted onto microscope slides with glycerol. A transmitting light microscop using ×400 and ×1000 magnifications was used for pollen identification. Pollen identification was performed using the pollen photograph bank and several atlases of the 'Laboratoire PaléoEnvironnements et PaléobioSphère' (Lyon) as well as its pollen database "Photopal" (http://medias.obs-mip.fr/photopal). Pollen grains are very well-preserved in late Holocene sediments from section CH2/1 and abundant in all samples. Pollen concentration was estimated using the Cour's method (Cour, 1974). Concentration in palynomorphs varies from <500 to >45,000 grains/g. Pollen zones were assessed using a canonical correspondence analysis performed on selected taxa representing variables. Pollen enumeration was conducted at the Laboratory

'PaléoEnvironnements et PaléobioSphère' and data are stored in the C.P.C. database (http://cpc.mediasfrance.org).

IV.2.3. Taxonomy and ecological grouping of pollen grains

Since pollen grains found in modern sediments transported either by air or by rivers reflect the local to regional vegetation, we used the botanical determination of pollens grains to reconstruct palaeovegetation in the Aral Sea Basin. A minimum of 100 pollen grains, excluding Amaranthaceae-Chenopodiaceae and *Artemisia*, which are usually over-represented in arid environments, and non-determinable (i.e. poorly preserved) pollen grains were counted in each sample. Generally more than 25 different taxa were found in each sample. 79 taxa have been identified whereas 17,356 pollen grains were enumerated. Two different diagrams have been assessed.

(A) A simplified detailed pollen diagram (Fig. 4.3) displays percentages of the most frequent taxa, which were calculated relative to the total pollen sum. Taxa are represented according to the following ecological groups (trees + shrubs; herbs): (1) mega-mesothermic (= subtropical) elements: *Engelhardia*, *Myrica*, Taxodiaceae (including *Taxodium*-type), plus *Nyssa*, *Mappianthus*, Euphorbiaceae (i.e. the other mega-mesothermic elements); (2) mesothermic (warm-temperate) elements: *Quercus*, *Alnus*, *Liquidambar*, *Juglans*, *Ulmus*, *Carpinus*, *Populus*, *Betula*, *Corylus*, plus *Buxus sempervirens* type, *Vitis*, *Juglans* cf. *cathayensis*, *Zelkova*, *Tilia*, *Taxus*, *Salix*, *Fagus*, *Platanus*, *Fraxinus*, *Acer*, *Carya*, *Pterocarya*, *Eucommia ulmoides* (i.e. the other mesothermic elements); (3) meso-microthermic (mid-altitude) elements: *Tsuga*, *Cathaya*; (4) microthermic (high-altitude) arboreal elements: *Abies*; (5) the other Pinaceae (mostly composed of *Pinus)*; (6) sclerophyllous elements: Cupressaceae, evergreen *Quercus*; (7) aquatic plants: *Sparganium* + *Typha*, *Potamogeton*, plus Myriophyllum, *Aristolochia*, *Alisma*, *Nymphea* (i.e. the other aquatic plants); (8) non-significant elements (because being cosmopolitan plants): Rosaceae, Ranunculaceae; (9) herbs: Amaranthaceae-Chenopodiaceae, Asteraceae Asteroidae, Poaceae, *Rumex*, *Polygonum*, Caryophyllaceae, *Phlomis*, Cyperaceae, plus Asteraceae Cichorioidae type, *Polygonum*, *Gallium*, Cannabaceae, Fabaceae, Plumbaginaceae, *Urtica*, Zygophyllaceae, Brassicaceae, *Helianthemum*, *Geraniaceae*, *Sambucus*, Papaveraceae, *Plantago*, Apiaceae, Ericaceae, Liliaceae, *Narcissus*, including some subdesertic elements such as *Calligonum*, *Nitraria*, *Ziziphus spina-christi* (i.e. the other herbs); (10) steppe elements: *Artemisia* and *Ephedra*.

(B) In order to simplify the pollen record, a composite diagram is presented in Figure 4.4, where the relative percentages of the ten relevant ecological groups are presented.

IV.2.4. Climate reconstruction

For the quantification of palaeoclimate signals recorded in plant assemblages, the "probability mutual climatic spheres" (PCS) method described in detail by Klotz and Pross (1999) and Klotz et al. (2003, 2004) was favoured over modern analogue methods (e.g., Guiot, 1987, 1990; Prentice et al., 1992, 1996; Peyron et al., 1998; Tarasov et al., 1998a, b; Klotz, 1999). Generally, modern analogue methods (MAM) are based primarily on comparing past pollen spectra with present-day analogues. In this study, the main restriction in applying this technique is the general poorness of the underlying available database of surface pollen spectra from the Aral Sea region (only 91 in Kazakhstan, Tarasov et al., 1998a) which may serve as modern analogues for reliable climate reconstructions. Besides, the usefulness of these methods is restricted when no present-day analogues exist for past pollen floras, as it is the case for the association Amaranthaceae–*Artemisia*–*Taxodium* found in this record. In addition, climate reconstructions with modern analogue methods may be significantly influenced by taphonomic effects when applied for instance on records from areas such as the Aral Sea Basin, which experiences numerous dust storms throughout the year (Seredkina, 1960; Létolle and Mainguet, 1993; Zavialov, 2005). Hence, the use of the PCS method is clearly more suitable than MAM for reconstructing climatic change in this study.

The PCS method is independent from relative proportions of plants, considering only their presence (at a minimum level of 0.5% abundance). Generally, "mutual climatic range" methods determine the climatic tolerance of past taxa by means of mutual present-day ranges of the climatic tolerances of the nearest living relatives (NLR) of the taxa represented in the past assemblages. The principle of the method was firstly applied on beetles to reconstruct palaeoclimate conditions during the last glacial period and the Holocene (e.g., Coope, 1977; Atkinson et al., 1986; 1987; Elias, 2000), and has subsequently been used for the climatic interpretation of Holocene plant taxa (Kershaw & Nix, 1988). It has been recognized a considerable advantage of this reconstruction method to be independent from the availability of modern analogues and from taphonomic influences (Mosbrugger and Utescher, 1997). Especially, the PCS method (Klotz et al., 2003; 2004) calculates probability intervals within the mutual climatic spheres by the use of a multitude of present-day floras. The 2-dimensional spheres representing the present-day climate requirements of the NLR are derived from the correlation between present-day climate data on a 0.5°×0.5° latitude/longitude grid (New et al., 1999) with potential distribution maps of more than 205 present-day plants occurring in Europe and adjacent Asia (Meusel and Jäger, 1992; Walter and Straka, 1970). Within the mutual 2-dimensional climatic sphere of a past flora, probability intervals are calculated for the individual climate parameters. For explanation, we refer to the mean annual temperatures (MAT) as an example. The range of MAT defined by the mutual climatic sphere of the past flora is compared to MAT ranges calculated for 9555 synthetically generated floras (Klotz, 1999; Klotz and Pross, 1999; Pross et al., 2000) composed exactly of those of the 205 plants at a given geographical co-ordinate whose potential

distribution areas covers that location. We then select synthetic floras which show a MAT range similar to the range of the past flora. It can be observed that the distribution of actual MAT values is restricted to a smaller interval when compared to the reconstructed mutual ranges of the selected synthetic floras. This interval of preference is then interpreted as the probability interval of MAT, from which we only used the upper and lower limits for graphical presentation. The quality of PCS has been tested on the basis of a multitude of present-day floras (Klotz et al., 2003; 2004) documenting the large agreement between reconstructed and actual grid climate values, with correlation coefficients and mean average error of 0.95 and 1.1°C for summer temperatures, 0.95 and 1.7°C for winter temperatures, 0.95 and 1.1°C for mean annual temperature and 0.86 and 100 mm for mean annual precipitation. Therefore, the PCS is considered to represent a very sensitive method for the interpretation of climate variability.

IV.3. Results

Five ecostratigraphic pollen zones have been distinguished based on major changes in pollen assemblages, labelled as P1 to P5 (Figs. 4.3 and 4.4).

Pollen zone P1 (10.75–9.97 m; ca. 0 – 400 yr AD)

This zone is characterized by a large supremacy of herbs (45–47.6%), mainly represented by Amaranthaceae-Chenopodiaceae (35–40%), and steppe elements (43–47%) with frequencies of *Artemisia* fluctuating between 42.7 and 46.8%. Among other herbaceous plants (Caryophyllaceae, Asteraceae Asteroidae, *Rumex*, Cyperaceae), Poaceae appear abundant with values increasing towards the top (2.5–5.8%). Conversely, arboreal taxa are extremely rare (mega-mesothermic elements: <2%, mesothermic elements: <5%), respectively mostly represented by Taxodiaceae (1.2% at 9.97 m), *Betula* (1.2% at 9.97 m) and few *Alnus* (<1%). Pollen grains of *Quercus*, *Carpinus*, *Populus*, *Corylus* and Cupressaceae are also present at low percentages, with values never exceeding 1%. *Pinus* is found at low abundances (<5%), as pollen of Rosaceae and aquatic plants (>1%). Total pollen concentration is relatively high in the lowermost part of this zone (16,600 grains/g at 10.75 m) but decrease upwards (<4,000 grains/g at 9.97 m) (Fig. 4.4).

Pollen zone P2 (9.97–6.13 m; ca. 400 – 900 yr AD)

It shows a conspicuous increase in percentages of arboreal taxa characterized by higher abundances of mega-mesothermic (Taxodiaceae: 13.3% at 7.33 m) and mesothermic (6.8% at 7.33 m) elements. Among other warm-temperate trees, *Betula*, *Alnus* and *Corylus* are most abundant (Figs. 4.3 & 4.4). Frequency of Cupressaceae also slightly increases (1.7% at 7.33 m), while values of *Pinus* become more important (mean: 6.2%; 11.7% at 6.53 m). This zone is also characterized by a drastic decrease in percentages of Amaranthaceae-Chenopodiaceae (9%–21%), and numbers of Poaceae also

slightly decrease. Relative abundances of *Artemisia* (steppe) remain stable at relative high levels, even showing higher values than in zone P1 (47%–65%).

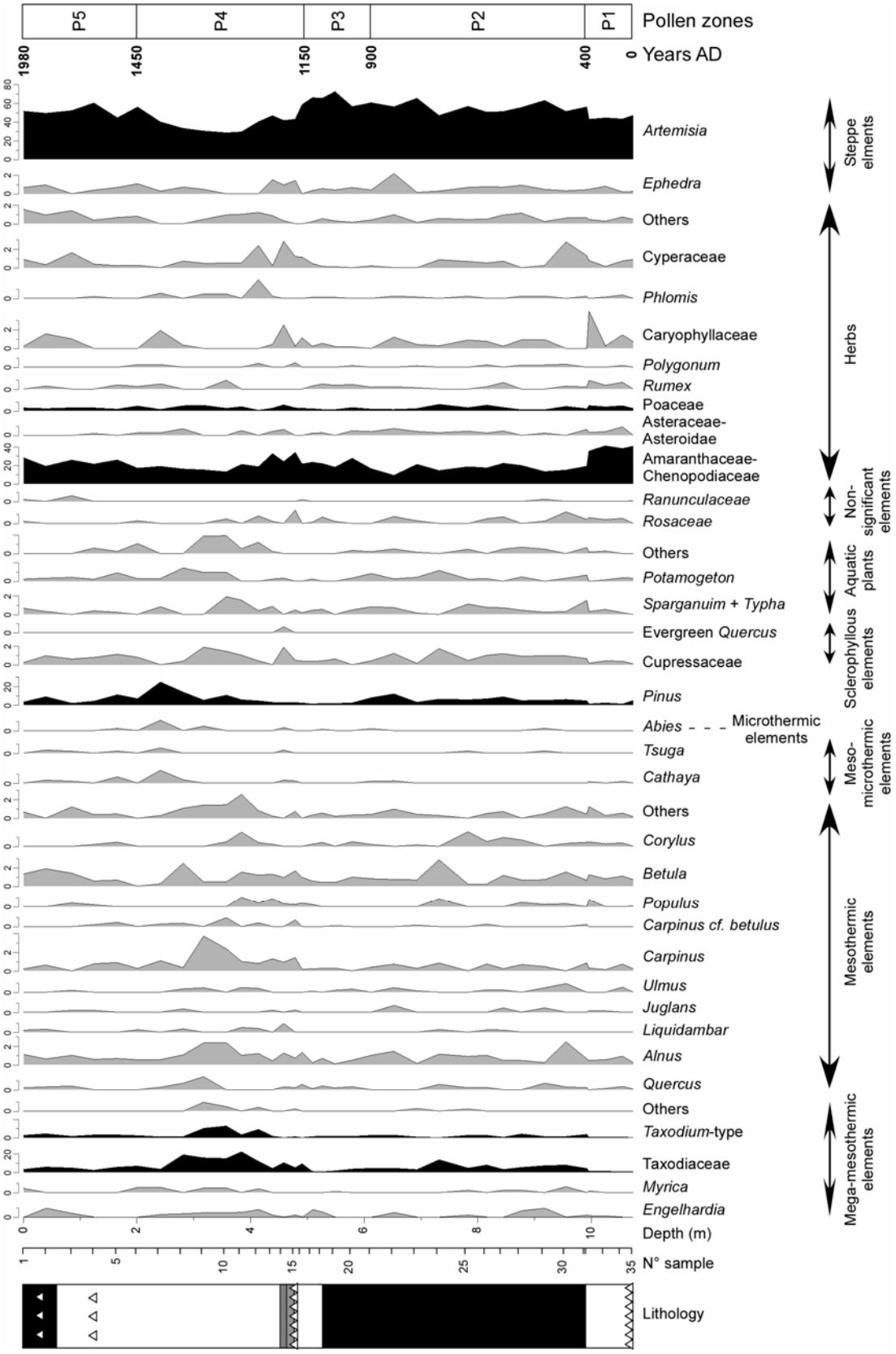

Figure 4.3: *Pollen simplified detailed diagramm for section CH2/1. Black-filled lines indicate percentage abundance and white-filled lines give ×10 exaggeration (i.e. per mill abundance). Pollen zones P1 to P5 are based on the present study. Lithology, see Fig. 2.*

Non-significant pollen grains are also present in low values (<1.5%) and abundance of aquatic plants slightly increases (0.6%–3%). Total pollen concentration is lower in this zone and fluctuates between 2,000 and 10,500 grains/g (Fig. 4.4).

Pollen zone P3 (6.13–4.92 m; ca. 900 – 1150 yr AD)

This zone is characterized by a general decrease in mega-mesothermic and mesothermic elements, with respective values of 2.8%–9% and 1.5%–3.4% (Fig. 4.4). Particularly, abundance of Taxodiaceae (mean: 3.1%) and *Taxodium*-type (0%–1.6%) shows pronounced lower values compared to the previous zone. Among the mesothermic elements, *Alnus*, *Betula* and to a lesser extent *Quercus* and *Carpinus* are the most represented taxa, with values rarely exceeding 1%. Though frequencies of herbs (Amaranthaceae-Chenopodiaceae, Asteraceae Asteroidae, *Rumex*, *Phlomis*, Cyperaceae) remain stable compared to in zone P2 (19.5%–32%) with a slight decrease in Poaceae (1.5%–3.6%), abundance of steppe elements conspicuously increases, through elevated frequency of *Artemisia* (56%–72%). Percentages of Cupressaceae, non-significant elements and aquatic plants are again relatively low (<2%), while *Pinus* frequency clearly decreases (mean: 2.7%). Total pollen concentration increases towards the top of this zone, with a maximum value of 40,000 grains/g at 5.1 m (Fig. 4.4).

Pollen zone P4 (4.92–2.02 m; ca. 1150 – 1450 yr AD)

Following the increase in steppe elements in zone P3, this zone emphasizes a pronounced increase in percentages of trees and notably of mega-mesothermic elements with a maximum of 28.3% at 3.58 m (Figs. 4.3 & 4.4). Noticeably relative abundances of Taxodiaceae fluctuate between 5% in the lowermost part of the zone (4.8 m) up to 21.7% at 3.85 m, while maximal values of *Taxodium*-type (12.23%) are recorded at 3.58 m. Pollen of *Engelhardia* and *Myrica* is also found but in low numbers (<1%), while rare specimens of *Nyssa* and *Mappianthus* have been recorded too. Mesothermic elements are common (3.5%–9.8%) and mostly represented, among other warm-temperate taxa, by *Carpinus* (3.7% at 3.18 m), *Alnus* (2.35% at 3.58 m), *Quercus* (1.4% at 3.18 m), *Betula* (1.15% at 3.85 m) and *Corylus* (1.5% at 3.85 m). *Populus* (≤1%) and higher frequency of *Liquidambar* (<1%) also occurred in this zone. *Pinus* becomes more abundant upwards, with a maximum of 24.3% at 2.42 m, while few pollen grains of *Tsuga* and *Abies* have been found as well. Though frequency of Poaceae noticeably increases (6.5% at 4.59 m; 6% at 3.18 m; 5.6% at 2.82 m) as do values of Cyperaceae (0.2%–2.8%), percentages of *Artemisia* conspicuously drop with a minimum of 28.3% at 3.58 m, and values fluctuating around 40% throughout the zone. Abundances of Amaranthaceae-Chenopodiaceae are relatively similar as in zones P2 and P3 (14.8–32%). Aquatic plants increase noticeably (4.7% at 3.58 m), as do Cupressaceae (1.9% at 4.59 m). Total pollen concentration decreases in this zone from 45,000 grains/g at 4.59 m to less than 500 grains/g at 2.42 m (Fig. 4.4).

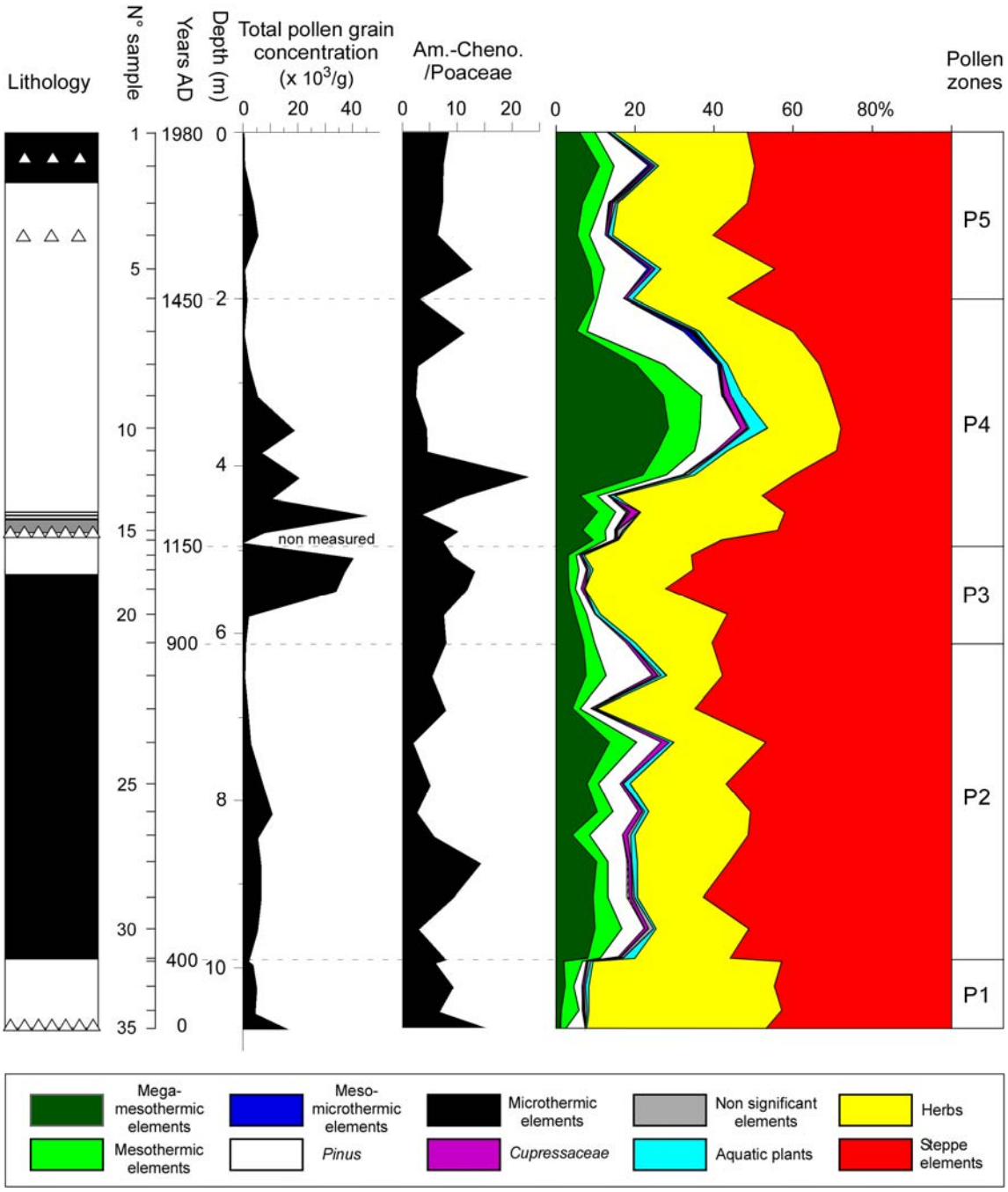

Figure 4.4: *Pollen synthetic diagram for section CH2/1. Grouping was performed regarding the ecology of the plants (see text for explanation). Concentrations (per gram of dry sediment) are relative to the total pollen sum. Each sample represents a 30 to 40 cm interval and is plotted by its mean depth (see text for details). The ratio Amaranthaceae-Chenopodiaceae / Poaceae is regarded as representing a semi-quantitative index of aridity. Lithology, see Fig. 2.*

Pollen zone P5 (2.02–0.00 m; ca. 1450 – 1980 yr AD)

It is characterized by the transition to present-day vegetation types, with an abrupt decrease in percentages of mega-mesothermic elements (5.15%–10.6%) and to a lesser extent of warm temperate trees (1%–4.8%) correlatively with an increase in herbs (23.8%–33.6%) and steppe (45% to ca. 52% at the top) frequency (Figs. 4.3 & 4.4). Mega-mesothermic elements are mainly represented by

Taxodiaceae (including *Taxodium*-type) that nonetheless never exceed 10%, while other taxa from this group become scarce. Among the mesothermic elements, only abundance of *Betula* regularly exceeds 1%, when *Quercus*, *Alnus*, *Liquidambar*, *Populus* and *Corylus* mostly run below 1%. Percentages of Cupressaceae slightly decrease (0.2–1.1%), as does *Pinus* from 10.8% at 1.66 m to 3% at the top. *Tsuga*, *Abies* and non-significant elements still occur, but at very low numbers (<1%). Although Amaranthaceae-Chenopodiaceae yield a pronounced increase in this zone (16.7%–27.7%), the frequency of Poaceae conversely decreases (2%–5.3%). Total pollen concentration is relatively low in this zone (<500–5,550 grains/g) (Fig. 4.4).

IV.4. Vegetation patterns derived from the pollen record

Herbs, predominant in all samples (Fig. 4.4), are characterized by an overwhelming presence of *Artemisia* that accounts for 28%–72% of the pollen sum, and pollen of Amaranthaceae-Chenopodiaceae (20–25%). Poaceae (mean: 3.5%) is also common. Studies of pollen composition in aerosols indicate that both *Artemisia* and Amaranthaceae-Chenopodiaceae are high pollen producers (Van Campo et al., 1996; Cour et al., 1999), whereas Poaceae are rare in arid regions (Cour and Duzer, 1978; Van Campo et al., 1996). At present in Central Asia, *Artemisia* and Amaranthaceae-Chenopodiaceae are characteristic elements of steppe, semi-desert and desert environments (Tarasov et al., 1998a, 1998b). Since Amaranthaceae-Chenopodiaceae are commonly present under saline and desert conditions but can be easily replaced, even during periods of minor elevation in precipitation, a slight increase in abundance can be interpreted as an increase in salinity and/or aridification (El Moslimany, 1990).

Pollen data suggest that open vegetation types with typical steppe elements (shrubs, herbs) were always predominant in the Aral Sea Basin during the last 2000 years. This implies that xeric conditions prevailed in the region, interrupted by periods of slightly enhanced moisture as reflected by slightly increased values of Poaceae. Based on the above ecological significance of Amaranthaceae-Chenopodiaceae (indicative of dry conditions) and Poaceae which abundance generally increases with rain, we use the ratio Amaranthaceae-Chenopodiaceae / Poaceae as a semi-quantitative index of aridity (Fig. 4.4). In this diagram, high values of the ratio (>10) are considered indicative of arid conditions that favour semi-desert–steppe vegetation, whereas low values (<10) reflect periods of slightly elevated moisture conditions and the development of few trees in a less arid steppe. This is concurrent with abundance of aquatic plants and Cyperaceae which reflect some extension in aquatic environment (Fig. 4.3). Therefore, correspondence between low ratio values, sedimentological data and changes in lake water levels (Sorrel et al., 2006) validate the use of the ratio as a proxy for relative moisture availability in the Aral Sea Basin.

Halophytes (Amaranthaceae-Chenopodiaceae, *Ephedra*, partly *Artemisia*) probably contribute to the predominant vegetation along the Aral Sea shoreline. However, the presence of aquatic plants is

also common in the pollen flora. In general, frequency of aquatic plants is almost parallel to that of Poaceae (Fig. 4.3). Increasing frequency of these taxa may be thus representative of some extension of local marshes accompanied by some development of herbs requiring less dry conditions, reflecting a slight increase in humidity.

Trees are a minor component of the pollen flora, averaging 20% on the whole downcore, with however a maximum value of 28% in zone P4. Each arboreal group is indicative of specific environmental conditions, permitting to trace the probable origin of each taxon according to its ecology and present-day distribution. Probably, *Pinus* was not an eminent component of the regional vegetation; its frequency, even being modest, may be caused by its prolific production and overabundance in air- and water-transport. Warm-temperate elements (2%–10%), also common in the pollen record, comprise some elements today restricted to the Middle East, such as *Liquidambar* and *Pterocarya*. The presence of these mesothermic elements may reflect the past development of some riparian vegetation in the Aral Sea Basin. More surprisingly, in a region where so dry climate conditions predominated judging from the overwhelming dominance of herbs in the pollen record, some mega-mesothermic elements indicative of relatively warmer and wetter environments have been found in every sample analysed. These elements are mostly represented by Taxodiaceae (including the *Taxodium*-type pollen, a swamp element) and to a lesser extent by *Engelhardia* and *Myrica*. Considering the regional near sub-arid conditions in the basin during the last 2000 years, the presence of these relictuous elements in the Aral Sea sediments would require comment. Similarly, the presence of *Cathaya* (a past conifer restricted today in a few mid-altitude environments of the southwestern subtropical China) among the mid-altitude elements would be unexpected in such conditions.

Because the Aral Sea is surrounded by older deposits mostly of Paleogene and Neogene age, we might expect increased reworking of older material from shore during periods of sheet-wash erosion, as it is the case for dinoflagellate cysts (see Fig. 4.6). However, from several samples of Miocene marls collected nearby the Chernyshov Bay, no pollen grain of *Taxodium*–type, Taxodiaceae, *Cathaya*, *Engelhardia*, *Myrica* was found. On the contrary, in section CH2/1, most of these pollen grains are found well-preserved, rarely broken or damaged, and exhibit all the criteria characteristic of fresh pollens. For further reliability, we carefully examined them under fluorescence light, a method which is currently used by palynologists to distinguish fresh from reworked specimens. Results showed that the pollen grains of *Cathaya, Taxodium*-type and other relictuous taxa display whitish to yellow tints that are usually characteristic of non-reworked pollen grains (Sorrel et al., in progress). Similar observations raised from tests conducted on *Artemisia* and pollen grains of Amaranthaceae-Chenopodiaceae. Hence, the presence of mesothermic and mega-mesothermic relictuous taxa in sediments from Chernyshov Bay is probably linked with mid- to long-distance wind transport, respectively. The unquestionable relevance of these findings will be discussed in a forthcoming paper (Sorrel et al., in progress). Nevertheless, for this paper, since (1) the Taxodiaceae have not been

considered for the palaeoclimate reconstructions and (2) other arboreal taxa (*Alnus*, *Ulmus*) document the existence of a riparian association in the Aral Sea Basin, this discussion is not crucial at that stage.

IV.5. Climate reconstruction

The composite pollen diagram (Fig. 4.4) suggests that some limited but significant changes in the vegetation pattern occurred in the Aral Sea Basin during the last 2000 years. Changes in the pollen flora document switches between sub-desertic conditions (steppe almost constituted of *Artemisia*) and less dry environments (steppe enriched in Poaceae) coeval to the installation of some riparian trees. Since the expansion of open vegetation and the development of trees are controlled by climate conditions, we used the pollen data to reconstruct climate variability in terms of different temperature parameters and mean annual precipitation during the last 2000 years (Fig. 4.5). For the climate reconstruction, all taxa recorded in samples from section CH2/1 have been included with the exception of Taxodiaceae. Indeed, *Taxodium* is naturally found today only in very restricted regions of south-eastern Asia, making the derived climatic sphere (e.g., coldest and warmest spheres of the species and their relationship) based on its geographical distribution very approximate. This is in contrast to the climate spheres of the other azonal vegetation elements used in the reconstruction whose present-day distributions are well known and which are, therefore, of higher resolution.

Because the source of some pollen grains may be distant from the central depression of the basin, this quantitative reconstruction of climatic parameters gives a regional widespread picture of the changes in moisture conditions rather than a local signal restricted to the Aral Sea and its nearest adjacent areas. To further constrain our climatic reconstruction, we compared the reconstructed values to modern instrumental data from Central Asia along the latitudinal gradient [40°75'–50°25'], across the Aral Sea Basin (Fig. 4.5).

Pollen zone P1 (10.75–9.97 m; ca. 0 – 400 yr AD): basal arid interval

High values of the ratio Amaranthaceae-Chenopodiaceae/Poaceae concurrently with high frequency of steppe elements *Artemisia* and Amaranthaceae-Chenopodiaceae indicate that prevailing climate from ca. 0 to 400 yr AD was colder and more arid than today, with mean annual temperatures of 4°–6°C, temperatures for the coldest month averaging –6°C and mean annual precipitation never exceeding 300 mm/yr. The general feature of such climatic conditions is supported by sedimentological data and precipitation of gypsum interbedded with fine clays in the lowermost part of this zone. The transition between pollen zones P1 and P2 is characterized by a probably very short coring gap.

Figure 4.5: *Reconstructed climate parameters: mean annual temperature (MAT in °C), mean temperature of the coldest month (MTC in °C), mean temperature for the warmest month (MTW in °C) and for mean annual precipitation (MAP in mm/yr) for section CH2/1 during the last 2000 years (lower diagram). Taxodiaceae and Taxodium-type have not been included for climate quantification (see text for detail). The upper figure represents instrumental data for present-day (i) different temperature parameters, and (ii) mean annual precipitation in Central Asia. Data have been plotted along the latitudinal gradient [40°75'–50°25'] (y). Data were extracted from New et al. (1999).*

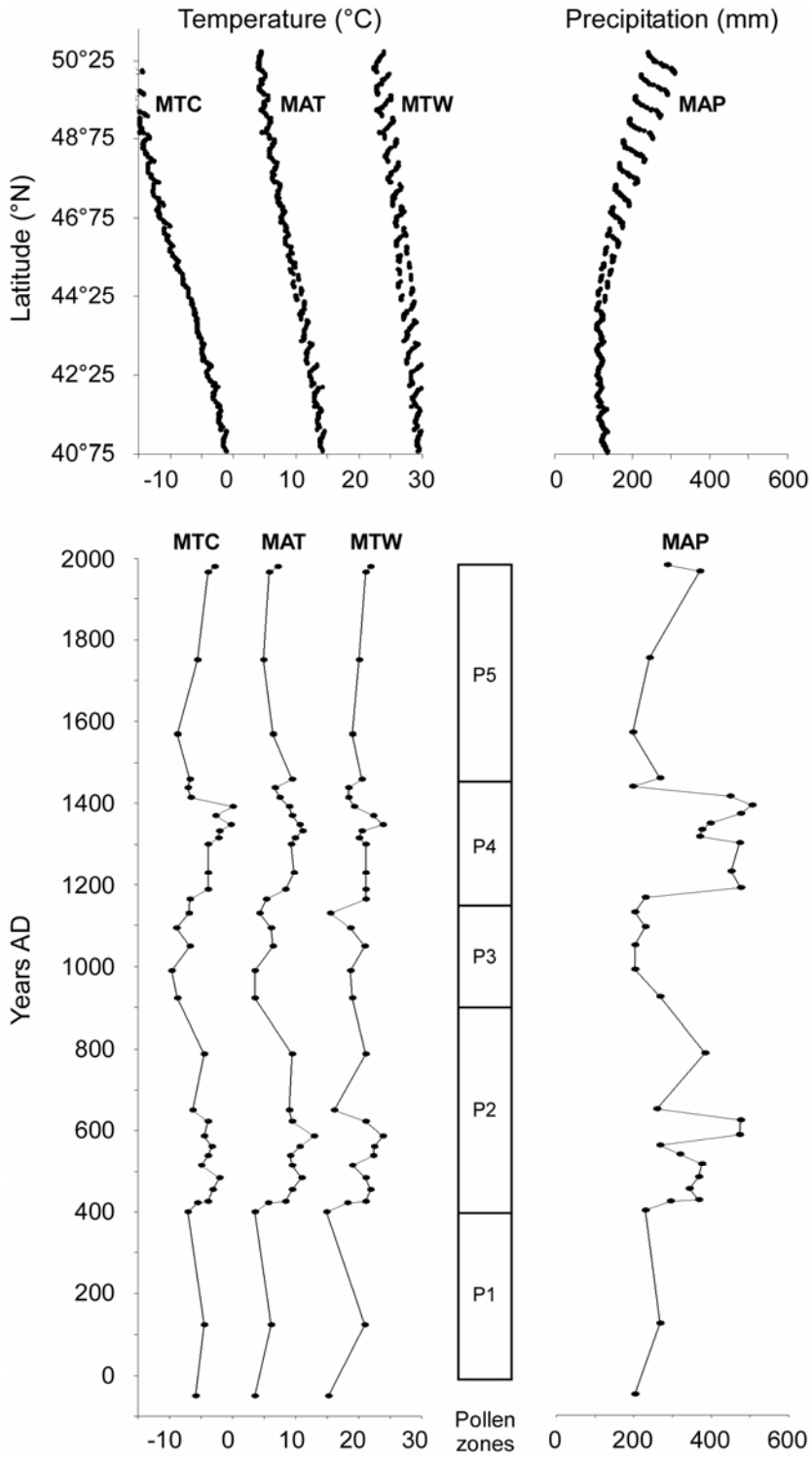

Pollen zone P2 (9.97–6.13 m; ca. 400 – 900 yr AD): increasing humidity

Decreasing xeric conditions are inferred from low values of the ratio Amaranthaceae-Chenopodiaceae/Poaceae (<10) between ca. 400 and 900 yr AD. Coevally, an increase in the abundance of warm-temperate elements and aquatic plants suggests that the climate became moderately wetter and potentially warmer. Reconstructed climate conditions indeed document that mean annual precipitation fluctuated between 270 and 475 mm/yr, whereas temperatures of the warmest month averaged 21°C (coldest month: -5°C) and mean annual temperatures 9°C. Increase in

moisture conditions are concurrent with the evidence of lake-level rise, inferred from dinoflagellate cyst assemblages (Sorrel et al., 2006), and may have favoured the expansion of some riparian trees.

Pollen zone P3 (6.13–4.92 m; ca. 900 – 1150 yr AD): strong aridification

This zone documents a return to strong arid conditions, as reflected by the progressive decrease in warm-temperate trees and the expansion of steppe elements *Artemisia* and Amaranthaceae-Chenopodiaceae. This is concurrent with high values of the aridity index (>10) and declined rainfall (200–230 mm/yr). Climate reconstruction document lower temperatures during this interval (coldest month: -7°–-10°C; warmest month: 15°–21°C; mean annual temperature: 4°–6°C). Further evidence for a long-term aridification is provided by a gypsum layer at 4.86 m (Fig. 4.4).

Pollen zone P4 (4.92–2.02 m; ca. 1150 – 1450 yr AD): increasing humidity

Increasing moisture conditions are inferred from a drop in the abundance of both steppe herbs and shrubs coincident with higher percentages of Poaceae and trees. Based on the ratio Amaranthaceae-Chenopodiaceae/Poaceae (<10), prevailing climate conditions were noticeably wetter than at present. This is concurrent with enhanced precipitation (370–505 mm/yr). Reconstructed temperatures for this interval were higher (mean annual: 7°–11°C; coldest month: -4°C). Increasing moisture conditions are consistent with rising lake levels and important freshwater discharges in the Aral Sea, as indicated in the dinoflagellate cyst assemblages (Sorrel et al., 2006). Higher-water availability between ca. 1150 and 1450 yr AD probably favoured the expansion of trees onshore, with a possible development of a riparian association (Sorrel et al., in progress) comprising warm-temperate trees (*Ulmus*, *Alnus*, *Populus*, *Corylus*) and maybe few mega-mesothermic elements (*Taxodium*-type, *Engelhardia*). The last sample records the onset of more arid conditions resulting in lower precipitation rates (<200 mm/yr).

Pollen zone P5 (2.02–0.00 m; ca. 1450–1980 yr AD): brief aridification followed by present-day climate conditions

A third arid interval is recorded during ca. 1450–1550 yr AD, as reflected by increasing abundance of steppe element *Artemisia* and slightly higher values of the ratio Amaranthaceae-Chenopodiaceae/Poaceae. This short phase is characterized by low precipitation rates (200–270 mm/yr) but more contrasting temperatures. Whereas both mean annual values (6°–9°C) and temperatures for the warmest month (18.9°–20.5°C) suggest warmer conditions in this interval, mean values for the coldest month decrease from -7°C around 1450 yr AD to -9°C at 1550 yr AD. This interpretation is confirmed by sedimentological data, with precipitation of gypsum crystals in clay sediments around 1500 AD. Reconstructed climatic parameters from the pollen content of surface sediments (1550–1980 yr AD) indicate contrasting precipitation rates (240–370 m/yr) and a slight warming trend (coldest month: -6°–-3°C; warmest month: 20°–22°C; mean annual temperature: 7°C).

Observations of present-day landscapes along the northern shore of the Aral Sea corroborate pollen evidence of enhanced aridity and higher temperatures in recent decades. The reconstructed climate parameters in the uppermost sample (i.e. 1980 AD) are in accordance with present-day instrumental data from Central Asia (Fig. 4.5), where mean annual temperature and precipitation respectively decrease / increase from 14°C / 110 mm at 40°75'N to 4°C / 310 mm at 50°25'N, validating the ranges of values obtained in our climate quantification. However, whether reconstructed temperature for the coldest month (-3°C) fairly overlaps instrumental values (-1°–-16°C), the estimated value for the warmest month (22°C) appears slightly lower than the instrumental ones (22°–30°C). An explanation for this could be the rapid warming trend observed during the past 20 years, which is not documented in our pollen record.

IV.6. Discussion and conclusions

Today, the climate in the deserts of Central Asia is mostly controlled by the shifts of the westerly cyclonic circulation and depends on the position of the Siberian High during winter and spring (Zavialov, 2005). In addition, local precipitation occurs during winter and early spring when depressions, developing over the Eastern Mediterranean, subsequently move along a northeast trajectory where they may even replenish moisture over the Caspian Sea (Aizen et al., 2001; Létolle and Mainguet, 1993; Lioubimtseva, 2002; Roberts and Wright, 1993). Therefore, we may expect elevated precipitation in Central Asia when moisture-transporting storms are stronger in the Eastern Mediterranean region and if so, we should find similar pattern of humidity between areas influenced by eastward moving storms (Israel, Turkey, Iran) and the Aral Sea Basin during the last 2000 years. Detailed palaeoclimatological studies based on $\delta^{18}O$ measurements from carbonate deposits of the Soreq Cave (Israel) (Schilman et al., 2002) provide a reliable record for comparison with the pollen-derived climate reconstruction presented here (Fig. 4.6). In addition, we present the relative abundance of reworked dinoflagellate cysts (Sorrel et al., 2006), which is expected to increase during periods of elevated sheet-wash from shore caused by enhanced rainfall.

When a cold and arid period (mean annual rainfall <300 mm) has been inferred from the pollen flora during 0–400 yr AD, Schilman et al. (2002) document declining rainfall leading to dry events in Israel around 0 yr AD. A similar phenomenon was reported in Syria, with reduced winter / spring rains (Bryson, 1996). Coevally, a decrease in lake level is reported from Lake Van in Turkey, evidencing a period of decreasing humidity between ca. -1500 and 0 yr AD (Landmann et al., 1996, Lemcke and Sturm, 1996). The decrease of rainfall is possibly related to a change in the mode of the North Atlantic Oscillation (NAO) that reduced cyclonic activity over the Eastern Mediterranean, being high during a negative NAO mode (Hurrell, 1995; Hurrell et al., 2003). This is in accordance with Aizen et al. (2001) who found that the NAO has a statistically significant inverse relationship with moisture availability over mid-latitudes of continental Asia. Based on correlation analyses between atmospheric

circulation patterns and regional precipitation, they reported that a negative (positive) difference in anomalies of sea-level pressure between the Azores and the Iceland is favourable (unfavourable) for precipitation development over the middle plains of Asia.

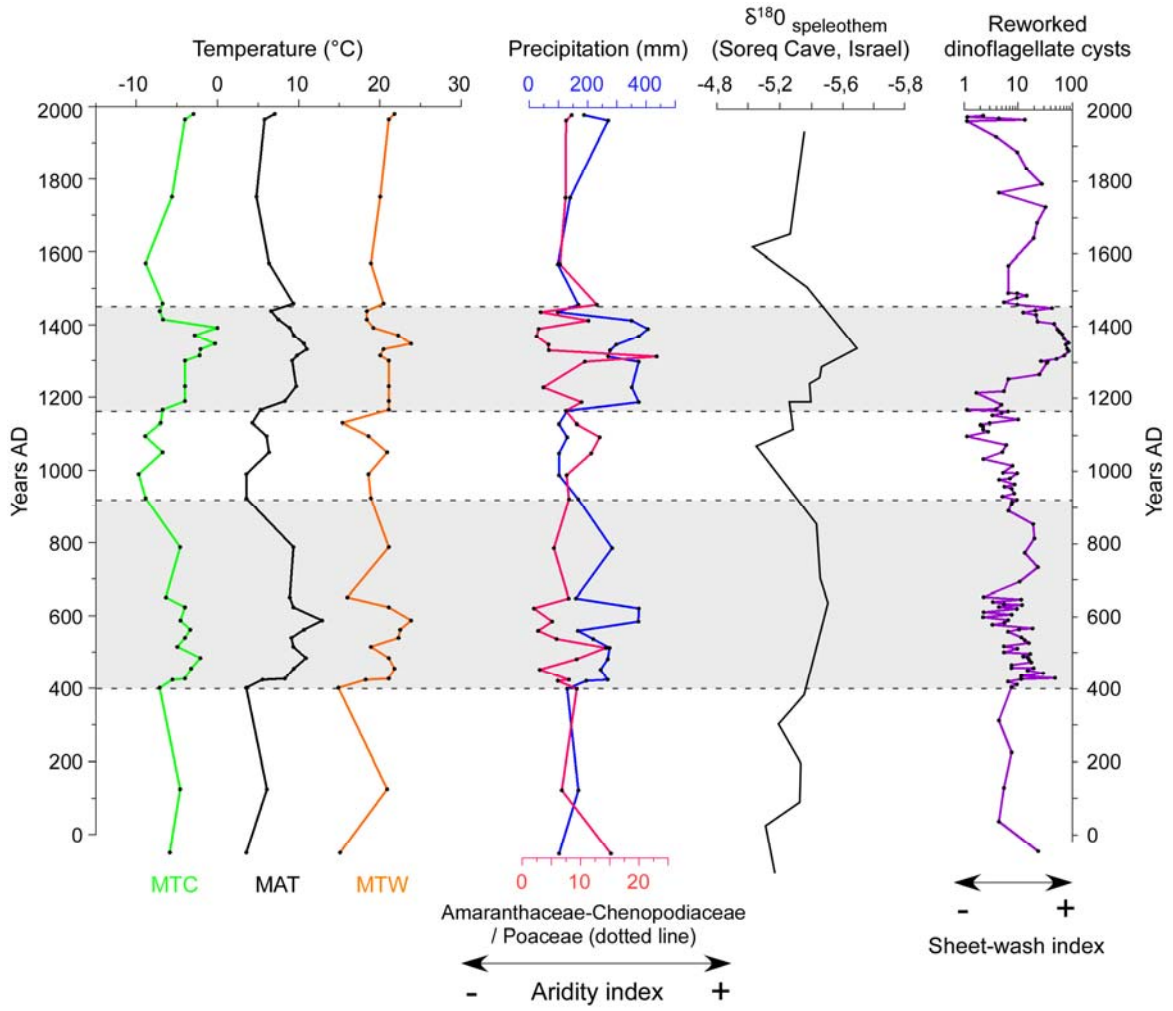

Figure 4.6: *Comparison between reconstructed climate parameters (temperature, precipitation) from section CH2/1, the $\delta^{18}O$ record from carbonate deposits in the Soreq Cave (Israel, Schilman et al., 2002) and the sheet-wash index derived from the relative abundance of reworked dinoflagellates cysts at Chernyshov Bay (Sorrel et al., 2006). Grey shadings represent periods with increased temperature and rainfall in the Aral Sea Basin when moisture-transporting storms are stronger from the Mediterranean Sea.*

Following this aridification, the time-interval ca. 400–900 yr AD is characterized by some warmer and wetter climate conditions in the Aral Sea Basin, which favoured the development of some arboreal vegetation in the less dry edaphic areas. This is supported by a conspicuous decrease in the $\delta^{18}O$ of carbonate deposits from the Soreq Cave (Schilman et al., 2002; Fig. 4.6), which infers elevated precipitation rates in Israel during 400–900 yr AD linked to stronger storms over the Eastern Mediterranean. Other evidences document a period of maximum precipitation around 700 yr AD, as inferred from land records including tree assemblages (Lipschitz et al., 1981), high-stand levels of the Dead Sea (Frumkin et al., 1991) and carbonate cave deposits in Israel (Bar-Matthews et al., 1998). The

period 900–1150 yr AD is characterized by a return to colder and more arid conditions in the Aral Sea Basin concurrently with declining rainfall (<270 mm/yr) and low mean annual temperatures, suggesting hence lowered moisture derived from the Eastern Mediterranean in winter and early spring during a possible positive phase of the NAO. This is in accordance with other palaeoenvironmental records from the Eastern Mediterranean which document colder conditions and reduced precipitation between 850 and 1200 yr AD (Issar et al., 1991; Schilman et al., 2002). After 1150 yr AD, elevated moisture conditions during a warmer period are inferred, with precipitation rates frequently beyond 400 mm/yr and enhanced sheet-wash from shore as reflected by higher abundance of reworked dinoflagellate cysts. A similar pattern is inferred from lowered $\delta^{18}O$ values in speleothems from the Soreq Cave between 1200 and 1500 yr AD (Fig. 4.6), suggesting higher rainfall over the Eastern Mediterranean region during the Medieval Warm Period. This event also corresponds to high-stand levels of the Dead Sea (Issar et al., 1991) and the Sea of Galilee (Frumkin et al., 1991).

A brief aridification occurred again during 1450–1550 yr AD. This short-term change towards colder/drier conditions probably coincide with the Little Ice Age which signature has been previously recorded in $\delta^{18}O$ values from the foraminiferan *G. ruber* in the Eastern Mediterranean Sea (Schilman et al., 2001) and in carbonate deposits from Israel (Bar-Matthews et al., 1998; Schilman et al., 2002). From 1550 yr AD upwards, increased temperatures document a progressive warming. For the last 2000 years, no human activity exerting control on vegetation change has been detected from the pollen record of Chernyshov Bay.

Despite a time-resolution of ca. 50 years, the climate reconstruction provides compelling evidence that centennial scale events are recorded for the last 2000 years (Fig. 4.6). In the Aral Sea Basin, climate conditions may fluctuate with a periodicity of ~400 year, with intervals of relatively elevated moisture conditions alternating with more arid phases. Since our data match fairly well with the Soreq cave record from Israel (Schilman et al., 2002), we thus conclude that the precipitation pattern in the Aral Sea Basin is directly linked to atmospheric changes in the Eastern Mediterranean region modulating moisture distribution towards the Middle East and Western Central Asia. This link may document a teleconnection to the NAO during negative phases. Modelling of Holocene climatic scenarios would improve our understanding of atmosphere–biosphere interactions in this vast arid region, and identify important thresholds between climate changes and landscape responses.

Acknowledgments

The CLIMAN project was funded by INTAS (European Union) (Project N° Aral 00-1030), the German Science Foundation (DFG Project 436 RUS 111/663 – OB 86/4) and NATO CLG Ref. 980445. We are grateful for this support. We wish to thank especially Dr. François Demory for excellent support in the field.

References

Aizen, E.M., Aizen, V.B., Melack, J.M., Nakamura, T., Ohta, T., 2001. Precipitation and atmospheric circulation patterns at mid-latitudes of Asia. International Journal of Climatology 21, 535–556.

Atkinson, T.C., Briffa, K.R., Coope, G.R., Joachim, M.J., Perzy, D.W., 1986. Climatic calibration of Coleopteran data. In: Berglund B.E. (Ed.), Handbook of Holocene Palaeoecology and Palaeohydrology. John Wiley and Sons, Chichester, pp 851–858.

Atkinson, T.C., Briffa, K.R., Coope, G.R., 1987. Seasonal temperatures in Britain during the past 22,000 years, reconstructed using beetle remains. Nature 325, 587–592.

Bar-Matthews, M., Ayalon, A., Kaufmann, A., 1998. Middle to late Holocene (6500 years period) palaeoclimate in the eastern Mediterranean region from stable isotopic composition of speleothems from Soreq Cave, Israel. In: Issar, A.S., Brown, N. (Eds.), Water, Environment and Society in Time of Climate Change. Kluwer Academic Publishers, pp. 203–214.

Boomer, I, Aladin, N., Plotnikov, I., Whatley, R., 2000. The palaeolimnology of the Aral Sea: a review. Quaternary Science Reviews 19, 1259–1278.

Boroffka, N.G.O., Oberhänsli H., Achatov, G.A., Aladin, N.V., Baipakov, K.M., Erzhanova, A., Hoernig, A., Krivonogov, S.K., Lobas, D.A., Savel'eva, T.V., Wuennemann, B., 2005. Human settlements on the northern shores of Lake Aral and water level changes. Mitigation and Adaptation Strategies for Global Change 10, 71–85.

Boroffka, N.G.O., Oberhänsli, H., Sorrel, P., Reinhardt, C., Wünnemann, B., Alimov, K., Baratov, S., Rakhimov, K., Saparov, N., Shirinov, T., Krivonogov, S.K. Archaeology and climate: Settlement and lake level changes at the Aral Sea. Geoarchaeology (in press).

Bortnik, V.N., Chistyaeva, S.P., (Eds.), 1990. Hydrometeorology and hydrochemistry of the USSR Seas. Vol. VII: The Aral Sea. Gidrometeoizdat, Leningrad, 196 pp. (in Russian)

Bryson, R.A., 1996. Proxy indications of Holocene winter rains in southwest Asia compared with simulated rainfall. In: Dalfes, H.N., Kukla, G., Weiss, H. (Eds.), Third Millenium BC; Climate Change and Old World Collapse. NATO ASI Series I, vol. 49. Springer Verlag, pp. 465–473.

Cour, P., 1974. Nouvelles techniques de détection des flux et de retombées polliniques: étude de la sédimentation des pollens et des spores à la surface du sol. Pollen et Spores 23 (2), 247–258.

Cour, P., Duzer, D., 1978. La signification climatique, édaphique et sédimentologique des rapports entre taxons en analyse pollinique. Annales des Mines de Belgique 7/8, 155–164.

Cour, P., Zheng, Z., Duzer, D., Calleja, M., Yao, Z., 1999. Vegetational and climatic significance of modern pollen rain in northwestern Tibet. Review of Palaeobotany and Palynology 104, 183–204.

Elias, S.A., 2000. Late Pleistocene Climates of Beringia, Based on Analysis of Fossil Beetles. Quaternary Research 53, 229–235.

El Moslimany, A.P., 1990. Ecological significance of common non-arboreal pollen: examples from drylands of the Middle East. Review of Palaeobotany and Palynology 76 (2–4), 343–350.

Esper, J., Schweingruber, F.H., Winiger, M., 2002. 1300 years of climate history for Western Central Asia inferred from tree-rings. Holocene 12, 267–277.

Frumkin, A., Magaritz, M., Carmi, I., Zak, I., 1991. The Holocene climatic record of the salt caves of Mount Sedom, Israel. Holocene 1, 191–200.

Guiot, J., 1987. Late Quaternary climatic change in France estimated from multivariate pollen time series. Quaternary Research 28, 100–118.

Guiot, J., 1990. Methodology of the last climatic cycle reconstruction in France from pollen data. Palaeogeography, Palaeoclimatology, Palaeoecology 80, 49–69.

Heim, C., 2005. Die Geochemische Zusammensetzung der Sedimente im Aralsee und Sedimentationsprozesse während der letzten 100 Jahre. Diploma thesis, Alfred-Wegener-Institut Bremerhaven.

Hurrell, J., 1995. Decadal trends in the North Atlantic Oscillation–regional temperatures and precipitation. Science 269,

Hurrell, J., Kushnir, Y., Ottersen, G., Visbeck, M., 2003. An overview of the North Atlantic Oscillation. In: Hurrell, J., Kushnir, Y., Ottersen, G., Visbeck, M. (Eds.), The North Atlantic Oscillation: Climatic Significance and Environmental Impact. AGU, Washington, pp. 1–35.

Issar, A.S., Govrin, Y., Geyh, A. M., Wakshal, E., Wolf, M., 1991. Climate changes during the Upper Holocene in Israel. Israelian Journal Earth Sciences 40, 219–223.

Kershaw, A.P., Nix, H.A., 1988. Quantitative paleoclimatic estimates from pollen data using bioclimatic profiles of extant taxa. Journal of Biogeography 15, 589–602.

Klotz, S., 1999. Neue Methoden der Klimarekonstruktion - angewendet auf quartäre Pollensequenzen der französischen Alpen. Tübinger Mikropaläontologische Mitteilungen, 21, Tübingen.

Klotz, S., Pross, J., 1999. Pollen-based reconstructions in the European Pleistocene: The modified indicator species approach as a tool for quantitative analysis. Acta Palaeobotanica, Supplementum, 2, 481–486.

Klotz, S., Guiot, J., Mosbrugger, V., 2003. Continental European Eemian and early Würmian climate evolution: comparing signals using different quantitative reconstruction approaches based on pollen. Global and Planetary Change, 36, 277–294.

Klotz, S., Müller, U., Mosbrugger, V., Beaulieu, J.L. de, Reille, M., 2004. Eemian to early Würmian climate dynamics: history and pattern of changes in Central Europe. Palaeogeography, Palaeoclimatology, Palaeoecology, 211, 107–126.

Kremenetski, C.-V., Tarasov, P.E., 1997. Postglacial development of Kazakhstan pine forests. Géographie Physique et Quaternaire 51 (3), 391–404.

Kremenetski, C.-V., Tarasov, P.E., Cherkinsky, A.E., 1997. The latest Pleistocene in Southwestern Siberia and Kazakhstan. Quaternary International 41/42, 125–134.

Landmann, G., Reimer, A., Lemcke, G., Kempe, S., 1996. Dating Late Glacial abrupt climate changes in the 14,570-yr long continous varve record of Lake Van, Turkey. Palaeogeography, Palaeoclimatology, Palaeoecology 122, 107–118.

Lemcke, G., Sturm, M., 1996. ^{18}O and trace element measurements as proxy for the reconstruction of climate changes at Lake Van (Turkey). In: Dalfes, H.N., Kukla, G., Weiss, H. (Eds.), Third Millenium BC; Climate Change and Old World Collapse. NATO ASI Series I, vol. 49. Springer Verlag, pp. 653–678.

Létolle, R., Mainguet, M., 1993. Aral. Springer Verlag, Paris, 358 pp.

Lipschitz, N., Lev-Yadun, S., Waisel, Y., 1981. Dendroarchaeological investigations sin Israel (Asada). Israel Exploration Journal 31, 230–234.

Lioubimtseva, E., 2002. Arid environments. In: Shahgedanova, M. (Ed.), Physical Geography of Northern Eurasia. Oxford University Press, Oxford 571 pp.

Lioubimtseva, E., Cole, R., Adams, J.M., Kapustin, G., 2005. Impacts of climate and land-cover changes in arid lands of Central Asia. Journal of Arid Environments 62, 285–308.

Meusel, H., Jäger, E.J. (Eds.), 1992. Vergleichende Chorologie der zentraleuropäischen Flora. Fischer, Jena.

Mosbrugger, V., Utescher, T., 1997. The coexistence approach – a method for quantitative reconstructions of Tertiary terrestrial palaeoclimate data using plant fossils. Palaeogeography, Palaeoclimatology, Palaeoecology 134, 61–6.

New, M., Hulme, M., Jones, P., 1999. Representing twentieth century space-time climate variability. I: Development of a 1961-1990 mean monthly terrestrial climatology. Journal of Climate 12, 829–856.

Nezlin, N.P., Kostianoy, A.G., Li, B.-L., 2005. Inter-annual variability and interaction of remote-sensed vegetation index and atmospheric precipitation in the Aral Sea region. Journal of Arid Environments 62, 677–700.

Nourgaliev, D.K., Heller, F., Borisov, A.S., Hajdas, I., Bonani, G., Iassonov, P.G., Oberhänsli, H., 2003. Very high resolution paleosecular variation record for the last 1200 years from the Aral Sea. Geophysical Research Letters 30 (17), 4-1–4-4.

Peyron, O., Guiot, J., Cheddadi, R., Tarasov, P., Reille, M., de Beaulieu, J.L., Bottema, S., Andreu, V., 1998. Climate reconstruction in Europe for 18 000 yr B.P. from pollen data. Quaternary Research 49, 183–196.

Prentice, I.C., Cramer, W., Harrison, S.P., Leemans, R., Monserud, R.A., Solomon, A.M., 1992. A global biome model based on plant physiology and dominance, soil properties and climate. Journal of Biogeography 19, 117–134.

Prentice, I.C., Guiot, J., Huntley, B., Jolly, D., Cheddadi, R., 1996. Reconstructing biomes from palaeoecological data: a general method and its application to European pollen data at 0 and 6 ka. Climate Dynamics 12, 185–194.

Pross, J., Klotz, S., 2002. Palaeotemperature calculations from the Praetiglian/Tiglian (Plio-Pleistocene) pollen record of Lieth, northern Germany: Implications for the climatic evolution of NW Europe. Global and Planetary Change 34, 253–267.

Reimer, P.J., Baillie, M.G.L., Bard, E., Bayliss, A., Beck, J.W., Bertrand, C.J.H., Blackwell, P.G., Buck, C.E., Burr, G.S., Cutler, K.B., Damon, P.E., Lawrence Edwards, R., Fairbanks, R.G., Friedrich, M., Guilderson, T.P., Hogg, A.G., Hughen, K.A., Kromer, B., McCormac, G., Manning, S., Bronk Ramsey, C., Reimer, R.W., Remmele, S., Southon, J.R., Stuiver, M., Talamo, S., Taylor, F.W., van der Plicht, J., Weiyhenmeyer, C.E., 2004. IntCal04 terrestrial radiocarbon age calibration, 0-26 cal. yr BP. Radiocarbon 46 (3), 1029–1058.

Roberts, N., Wright, H.E., 1993. Vegetational, lake-level, and climatic history of the Near East and Southwest Asia. In: Wright, H.E. (Ed.), Global Climates since the Last Glacial Maximum. University of Minnesota Press, pp. 194–220.

Rubanov, I.V., Ischniyanov, D.P., Baskakova, M.A., 1987. Geology of the Aral Sea. Tashkent, 248 pp. (in Russian).

Schilman, B., Bar-Matthews, M., Almogi-Labin, A., Luz, B., 2001. Global climate instability reflected by Eastern Mediterranean marine records during the Late Holocene. Palaeogeography, Palaeoclimatology, Palaeoecology 176, 157–176.

Schilman, B., Ayalon, A., Bar-Matthews, M., Kagan, E.J., Almogi-Labin, A., 2002. Sea–land palaeoclimate correlation in the Eastern Mediterranean region during the Late Holocene. Israel Journal of Earth Sciences 51, 181–190.

Sorrel, P., Popescu, S.-M., Head, M.J., Suc, J.P., Klotz, S., Oberhänsli, H., 2006. Hydrographic development of the Aral Sea during the last 2000 years based on a quantitative analysis of dinoflagellate cysts. Palaeogeography, Palaeoclimatology, Palaeoecology 234 (2–4), 304–327.

Tarasov, P.E., 1992. Holocene palaeogeography of the steppe zone of Northern and Central Kazakhstan. Thesis, Moscow University, 213 pp.

Tarasov, P.E., Jolly, D., Kaplan, J.O., 1997. A continuous Late Glacial and Holocene record of vegetation changes in Kazakhstan. Palaeogeography, Palaeoclimatology, Palaeoecology 136, 281–292.

Tarasov, P.E., Webb III, T., Andreev, A.A., Afanas'eva, N.B., Berezina, N.A., Bezusko, L.G., Blyakharchuk, T.A., Bolikhovskaya, N.S., Cheddadi, R., Chernavskaya, M.M., Chernova, G.M., Dorofeyuk, N.I., Dirksen, V.G., Elina, G.A., Filimonova, L.V., Glebov, F.Z., Guiot, J., Gunova, V.S., Harrison, S.P., Jolly, D., Khomutova, V.I., Kvavadze, E.V., Osipova, I.M., Panova, N.K., Prentice, I.C., Saarse, L., Sevastyanov, D.V., Volkova, V.S., Zernitskaya, V.P., 1998a. Present-day and mid-Holocene biomes reconstructed from pollen and plant macrofossil data from the former Soviet Union and Mongolia. Journal of Biogeography 25, 1029–1053.

Tarasov, P.E., Cheddadi, R., Guiot, J., Bottema, S., Peyron, O., Belmonte, J., Ruiz-Sanchez, V., Saadi, F.A., Brewer, S., 1998b. A method to determine warm and cool steppe biomes from pollen data; application to the Mediterranean and Kazakhstan regions. Journal of Quaternary Sciences 13, 335–344.

Van Campo, E., Cour, P., Sixuan, H., 1996. Holocene environmental changes in Bangong Co Basin (Western Tibet). Part 2: The pollen record. Palaeogeography, Palaeoclimatology, Palaeoecology 120, 49–63.

Velichko, A.A., 1989. The relationship of the climatic changes in the high and low latitudes of the Earth during the Late Pleistocene and Holocene. In: Velichko, A.A. et al. (ed.)., Paleoclimates and Glaciation in the Pleistocene, Nauka Press, Moscow, 5–19.

Walter, H., Straka, H., 1970. Arealkunde. Floristisch-historische Geobotanik. Ulmer, Stuttgart.

Zavialov, P.O., 2005. Physical oceanography of the dying Aral Sea. Springer Verlag, published in association with Praxis Publishing, Chichester, UK, 146 pp.

Chapter V: Control of wind dynamics in the Aral Sea Basin during the late Holocene

Philippe **Sorrel** [1,2]*, Hedi **Oberhänsli** [1], Nikolaus **Boroffka** [1], Danis **Nourgaliev** [3], Peter **Dulski** [1], Ursula **Röhl** [4]

(1) Sektion 3.3, GeoForschungsZentrum, Telegraphenberg, D-14473 Potsdam, Germany;
(2) University Potsdam, Karl-Liebknecht-Strasse, D14479 Potsdam, Germany;
(3) Faculty of Geology, Kazan State University, Kazan, Russia;
(4) DFG Research Center for Ocean Margins (RCOM), Bremen University, Leobener Strasse, 28359 Bremen, Germany

Accepted with revision in *Quaternary Research*

Abstract

Changing content of detrital input in laminated sediments traced by XRF scanning and microfacies analyses (1 cm-resolution) document prominent changes in wind strength and frequency in Western Central Asia. A core retrieved from the NW Large Aral Sea allows a continuous reconstruction of wind dynamics in western Central Asia for the past 1500 years. During 450–700 AD, 1210–1265 AD, 1350–1750 AD and 1800–1975 AD detrital inputs (Titanium) are high, documenting an enhanced spring atmospheric circulation associated with an increase in intensity of the Siberian High pressure system over Central Asia. In contrast, lower Titanium content during 1750–1800 AD and 1980–1985 AD reflect a diminished influence of the Siberian High during springs with a reduced atmospheric circulation, whereas a moderate spring circulation characterizes the time period 700–1150 AD. Unprecedented weakened atmospheric circulation over Western Central Asia are inferred during ca. 1180–1210 AD and 1265–1310 AD, with a considerable decrease in dust storm frequency, sedimentation rates, lamination thickness and detrital inputs (screened at 40 μm-resolution). Our results are fairly consistent with changes in the intensity of the Siberian High during the past 1400 years as reported in the GISP2 Ice Core from Greenland.

Keywords: Chemical composition; laminated sediments; wind dynamics; Siberian High; Aral Sea; late Holocene.

V.1. Introduction

Despite a growing understanding of the regional impacts of global climate change during the last few thousand years (Bond et al., 2001; Bradley, 2000, 2003; Briffa, 2000; Cook et al., 2004; Crowley, 2000; Mann and Jones, 2003; Moberg, 2005), little attention has been granted to the Aral Sea basin. Since Western Central Asia is situated at a confluence where different climate dynamics control the hydrology and environmental conditions (Khan et al., 2004; Small et al., 2001; Sorrel et al., 2006), the Aral Sea is an important archive for studying possible feedbacks between relevant climate features and their driving forces. Today the moisture distribution is controlled by the North Atlantic Oscillation (NAO) when the system is in a negative phase (Aizen et al., 2001), whereas draughts are possibly controlled by ENSO as proposed by Barlow et al. (2002), Khan et al. (2004) and Nezlin et al. (2005). Precipitation, which essentially occur during winter and early spring in the deserts of Central Asia (Lioubimtseva et al., 2005; Nezlin et al., 2005), are associated with moisture originating from the Eastern Mediterranean and are migrating along a northeast trajectory to western Central Asia (Aizen et al., 2001; Lioubimtseva, 2002; Roberts and Wright, 1993; Sorrel et al., this issue). In late spring and summer, precipitation is significantly reduced and heating of the desert lowlands in the Aral Sea Basin causes local- to regional advection responsible for numerous violent cyclones (>100 dust storms per year; Seredkina, 1960) especially in areas adjacent to the northern shore of the Aral Sea (Zavialov, 2005). The dust storms are particularly favoured by northern, north-western and preferentially north-eastern winds (Romanov, 1961; Fig. 5.1) and represent the dominant mode of transport of detrital particles (Létolle and Mainguet, 1993; Orlovsky et al., 2005). Studies on dust storms in Central Asia have been mostly undertaken since the 1960s (Middleton, 1986; Romanov, 1961; Romanov, 1986; Seredkina, 1960; Zolotokrylin, 1996). Recently, Orlovsky and Orlovsky (2002) provided general characteristics on frequency, distribution and seasonality of dust storms in Central Asia, with a specific concern on the dust storms originating around the Aral Sea. Analyses of longer-term changes in zonal and meridional atmospheric circulation patters in middle Asia have been documented by Subbotina (1995). However, most of these pioneer studies were limited to short periods of observations based on instrumental data of various sources, so that dust storm distribution and investigations on climate forcing mechanisms in the past are still insufficiently explored.

The principal obstacle for investigating late Holocene climate archives in western Central Asia is the lack of well-dated high resolution sedimentary archives. Clastic material of lake sediments forming in arid and semi-arid environments reliably records changes of past atmospheric dynamics. In this study, we present high resolution Ti and Ca XRF-scanning data and microfacies observations from laminated sediments at Chernyshov Bay (Fig. 5.1) and extent knowledge of atmospheric circulation over Western Central Asia to 1500 years ago. The data reflect the variability of clastic input and shed lights on changes in aeolian dynamics during the past 1500 years in connection with the main pattern

of spring atmospheric circulation regulating climate variability in the Northern Hemisphere, i.e., the Siberian High pressure system.

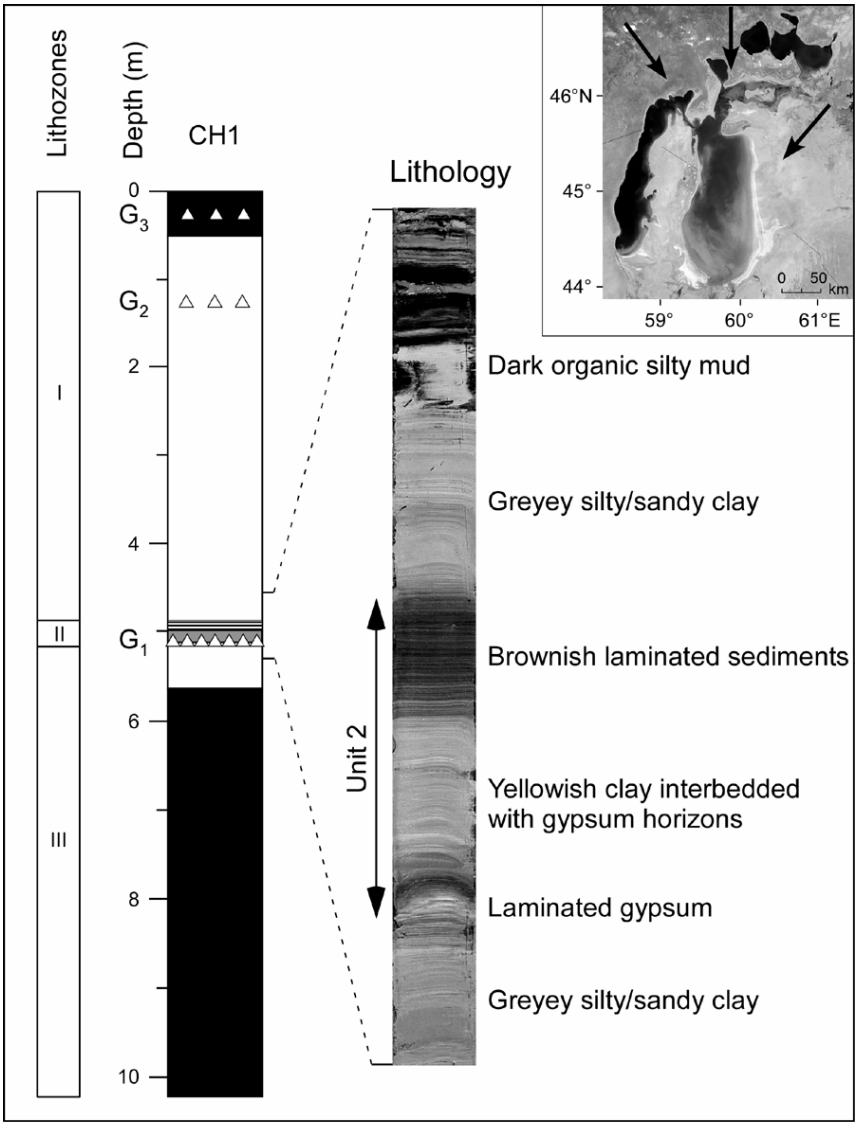

Figure 5.1: *Location map of the study area (black arrows represent the dominant wind directions during the winter–early spring season) and simplified stratigraphic log of Core CH1 (10.20 m) with lithology of Lithozone II. Lithozones I–III and gypsum horizons G_1–G_3 are described in the text.*

V.2. Material and methods

V.2.1. Coring locations

In August 2002, two piston cores (Cores CH1 and CH2 with respective total lengths of 10.20 m and 6.2 m) were retrieved with a Usinger piston corer (http://www.uvitec.ut) at Chernyshov Bay in the NW Large Aral Sea (Fig. 5.1). These cores were collected 1 km off the shoreline (45°58'528'' N, 59°14'459'' E) at a water depth of 22 m. Core CH1 consists of sections 21, 22, 23, 27 and 28, whereas Core CH2 consists of sections 30, 31 and 32. The coring sites CH1 and CH2 were separated by a few

meters. Correlation between Cores CH1 and CH2 were performed by matching laminations using photographs, physical properties (bulk sediment density, magnetic susceptibility) and XRF scanning data (see Fig. 2.3).

V.2.2. Thin sections

For microfacies analyses and micro XRF-scanning, we prepared a continuous series of 10 cm-long sediment samples from the interval 4.28–4-98 m in Core CH2, corresponding to the interval 4.58–5.28 m in Core CH1 (i.e. Lithozone II plus 0.31 m in Lithozone I and 0.13 m in Lithozone III). The samples were freeze-dried and soaked with a transparent epoxy resin (Araldite® 2020; Vantico, Basel, Switzerland) and subsequently polished. An overlap of 4 cm between each thin section provided a detailed correlation at a scale of single laminations confirming the macroscopic correlation. Overall, 13 thin sections were analysed under parallel and polarized light with a microscope (Carl Zeiss Axiophot; Carl Zeiss, Germany). Magnifications used were 25x (overview) and 100x (measurement of lamination thickness and microfacies description). Thin sections photographs were performed using a digital camera (Carl Zeiss Axiocam) and the software Carl Zeiss Axiovision 2·0. From thin sections we determined semi-quantitatively changes in grain size, thickness of lamination, abundance of selected diatom species and searched for possible micro-disturbances in sedimentation.

V.2.3. X-Ray Fluorescence (XRF) scanning, magnetic susceptibility measurements and X-Ray Diffraction (XRD)

Titanium and calcium contents of the whole core were measured at Bremen University with a profiling X-ray fluorescence scanner (XRF) core scanner (Jansen et al., 1998; Röhl and Abrams, 2000) at scanning steps of 1 cm using standard parameters (20 kV, 0.087 mA; 30 s detector accumulation time). When necessary, the measuring strategy was adjusted to avoid gaps. At GFZ Potsdam we measured the interval 4.58–5.28 m for elements Al, Ca and Ti at a 40 µm-resolution. The profiling was performed with a micro X-ray fluorescence scanner (EAGLE III XL; Röntgenanalytik Meßtechnik GmbH) at 40 kV, 0.25 mA, 10 s detector accumulation time. For the scans we used the Araldite®-impregnated polished slabs, prepared for thin sections. Scans of pure Araldite resin (without sediment) indicated zero counts for investigated elements, proving that the resin does not influence the results.

Magnetic susceptibility was measured directly after core opening on the surface of split core halves with a Bartington MS2E sensor (GFZ Potsdam) at a resolution of 1 to 2 mm. For salt mineral identification we performed XRD analyses on selected samples from Core CH1 using a Siemens D 5005 diffractometer at the University Potsdam, and used the program MacDiff 4·2·5 (Petschick, 2000) for mineral identification.

V.2.4. Lithology

Sediments retrieved from Chernyshov Bay (Fig. 5.1) consist of greenish to greyish silty clays and dark water-saturated organic muds with sporadically-intercalated more sandy material. The sediments, which are finely laminated, comprise material of variable origin (terrigenous, biogenic and chemogenic) and size (from clay and fine silt to fine sand and mollusc shell fragments). Chemical precipitates, such as gypsum, occur as dispersed microcrystals in the sediment (G_2; G_3; Fig. 5.1) and discrete layers (G_1). Neither erosive discontinuity, nor features of bottom traction are observed in the core. The laminated character of Core CH1 indicates probable settling of various autochthonous and allochthonous particles from the water column during seasonally varying hydrographic conditions. Three lithological units are recognized.

Between 0.0 and 4.88 m (lithozone I), the sediment is mostly composed of a greyey silty to sandy clay intercalated with organic mud horizons whereas the uppermost part (0.0–0.5 m) consists entirely of a dark, organic, finely laminated mud.

Lithozone II (4.89–5.15 m) is characterized by a horizon of laminated gypsum at its base (G_2: 1-cm thick) overlain by a 1-cm thick horizon consisting of brownish thinly-laminated sediments. This latter horizon is overlain by a 12.5-cm thick interval of yellowish thinly-laminated sediments which in turn are progressively replaced by brownish thinly-laminated sediments (11.5-cm thick interval).

Between 5.15 and 10.20 m depth (Lithozone III), the sediments consist of a dark silty to sandy organic mud, often water-saturated and very rich in organic matter including allochthonous aquatic plant remains. The plant remains occur both as a dispersed phase in the matrix and as partly decayed fragments that constitute organic horizons. These sediments are characteristic of dysoxic to anoxic bottom-water conditions.

No turbiditic sediments have been recognized. The hydrochemical conditions at Chernyshov Bay today are very pronounced. In 2002 a strong pycnocline has developed that maintains and stabilises an underlying anoxic deep-water body (Friedrich and Oberhänsli, 2004) that in turn influences sedimentation and prevents bioturbation. Hence, sediments from Chernyshov Bay show mostly well-preserved laminations.

V.2.5. Chronology

In Core CH1 (see Table 1), AMS radiocarbon ages were determined using the green alga *Vaucheria* sp. and $CaCO_3$ from mollusc shells, which were successively picked from the washed sediment sample and carefully cleaned from adhering particles. Algae were stored in distilled water within a glass vessel. For each sample, AMS ^{14}C dating was performed using between 0.2 and 1.0 mg of pure extracted carbon. AMS ^{14}C ages were measured at Poznań Radiocarbon Laboratory (Poland). Radiocarbon ages were corrected to calibrated (cal) ages using the IntCal04 calibration curve (Reimer et al., 2004). An age model for Core CH1 based on AMS radiocarbon dating is proposed in Fig. 5.2.

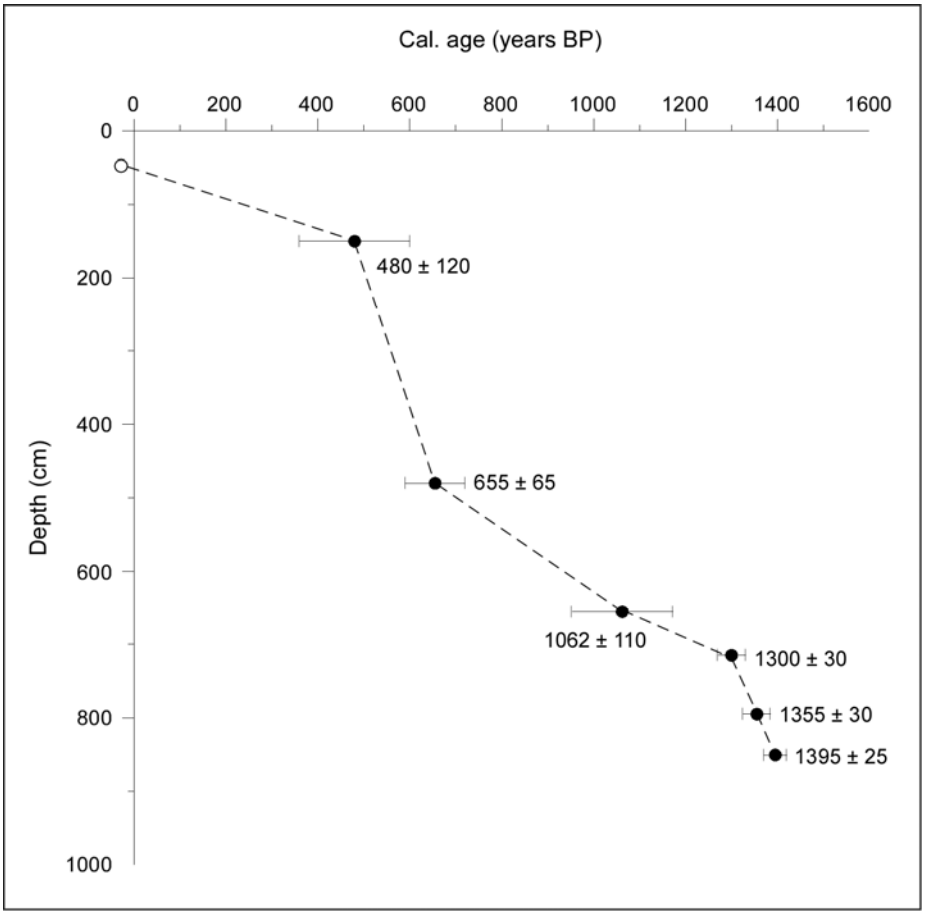

Figure 5.2: *Age-depth relation for Core CH1 based on six ^{14}C AMS dates. ^{14}C ages are shown in calendar years.*

Reliable dating for the upper 5 m of core CH1 was obtained by correlation with the magnetic susceptibility record from parallel cores 7, 8 and 9 retrieved ca. 50 m apart from the studied cores (Nourgaliev et al., 2003). AMS ^{14}C dating on cores 7, 8 and 9 was performed on the green alga *Vaucheria* sp. This correlation gives an age of 480±120 yr BP (cal. years) at 1.5 m depth for Core CH1. In addition, the time interval represented by Lithozone II is temporally constrained between 655±55 cal. yr BP at 4.8 m depth and ca. 770 yr BP at 5.15 m for the laminated gypsum (Sorrel et al., 2006). These results imply high mean sedimentation rates during the deposition of Lithozone I (3 cm yr^{-1} between 1.5 and 4.8 m) but conversely very low sedimentation rates for Lithozone II (~0.2 cm yr^{-1}). Supplementary ^{14}C dating performed on *Vaucheria* sp. provides an age of 1062±110 cal. yr BP at 6.55 m, 1300±30 cal. yr BP at 7.15 m and of 1395±25 cal. yr BP at 8.50 m, while ^{14}C dating from mollusc shells indicates an age of 1355±30 cal. yr BP at 7.95 m (see Table 1), implying relatively high mean sedimentation rates for Unit 3 (~1.5 cm yr^{-1} between 7.19 and 10.19 m). Moreover, based on a peak in ^{137}Cs at 0.39 m reflecting the climax of the bomb period (ca. 1963–1964 AD) (Heim, 2005), the top of Core CH1 has been dated as post-1950. This is in accordance with ^{210}Pb values measured both in the topmost part of Core CH1 (Austin et al., accepted) and in the Gravity Core Aral IX overlapping the first 0.5 m of Core CH1 (Heim, 2005). This is also concurrent with ^{14}C dating

obtained on *Vaucheria* sp. that reveals an age of 108.6±0.3 pMC at 0.56 m (thus confirming a post-1950 age). Due to a lack of dating of living algae samples from the near-shore, no reservoir correction can be applied yet. This is work in progress.

V.3. Results

V.3.1. Physical and geochemical variability in Core CH1 (Fig. 5.3)

Among seven elements analysed downcore using XRF scanning only counts of Calcium and Titanium were selected in this chapter since the distribution of these two elements enables to highlight prominent changes in sediment composition and properties. Others elements like K and Fe displayed either similar curves to Ti or were mostly close to or below the nominal sensitivity of the instrument (average response for Mn: 119 cps; Cu: 24 cps; Sr: 69 cps). Calcium show the clearest signal with highest values between 7.57–8.27 m, 5.14–5.15 m, 1.45–1.54 m and 0.00–0.25 m, where precipitates of gypsum are commonly found in the sediment (G_1–G_3; Fig. 5.1). Because higher values of calcium also match with phases of salinity increase as reflected by dinoflagellate cyst assemblages (Sorrel et al., 2006), we regard calcium as a proxy reflecting changes in chemical water properties linked to reduced/enhanced evaporation in the surface waters.

To show variability in the composition of detrital input at Chernyshov Bay, we chose titanium since it is clearly of terrigenous origin in the sediment fraction and influenced neither by productivity changes nor by early diagenetic processes. Relative abundance of Ti downcore further matches well with changes in the magnetic terrigenous input as reflected by the magnetic susceptibility curve. However, occasional mismatches between magnetic susceptibility measurements and relative abundance of Ti content occur, probably related to selective dissolution of magnetic Fe-oxides as they are redox-sensitive (e.g. Demory et al., 2005). Nevertheless, both curves display similar features, i.e., high relative content in Titanium corresponding to high magnetic susceptibility values. The lowest Ti and magnetic susceptibility values occur between 7.57–8.27 m, 5.14–5.15 m, 4.89–4.99 m and 0–0.25 m representing the gypsum-rich levels.

V.3.2. Close-up interval 4.58–5.28 m

In order to gain a better understanding of the sub-millimetre geochemical variability of individual laminae and to decipher the sedimentation process dynamics, we combine here a microfacies analysis at very high-resolution with XRF scanning for the interval 4.58–5.28 m. The studied time interval (1150–1400 AD) corresponds to the lowermost part of Lithozone I, the entire Lithozone II and the uppermost section of Lithozone III. At the macroscopic scale, Lithozone II appears rather different to the adjacent Lithozones I and III, reflecting thus major change in depositional processes.

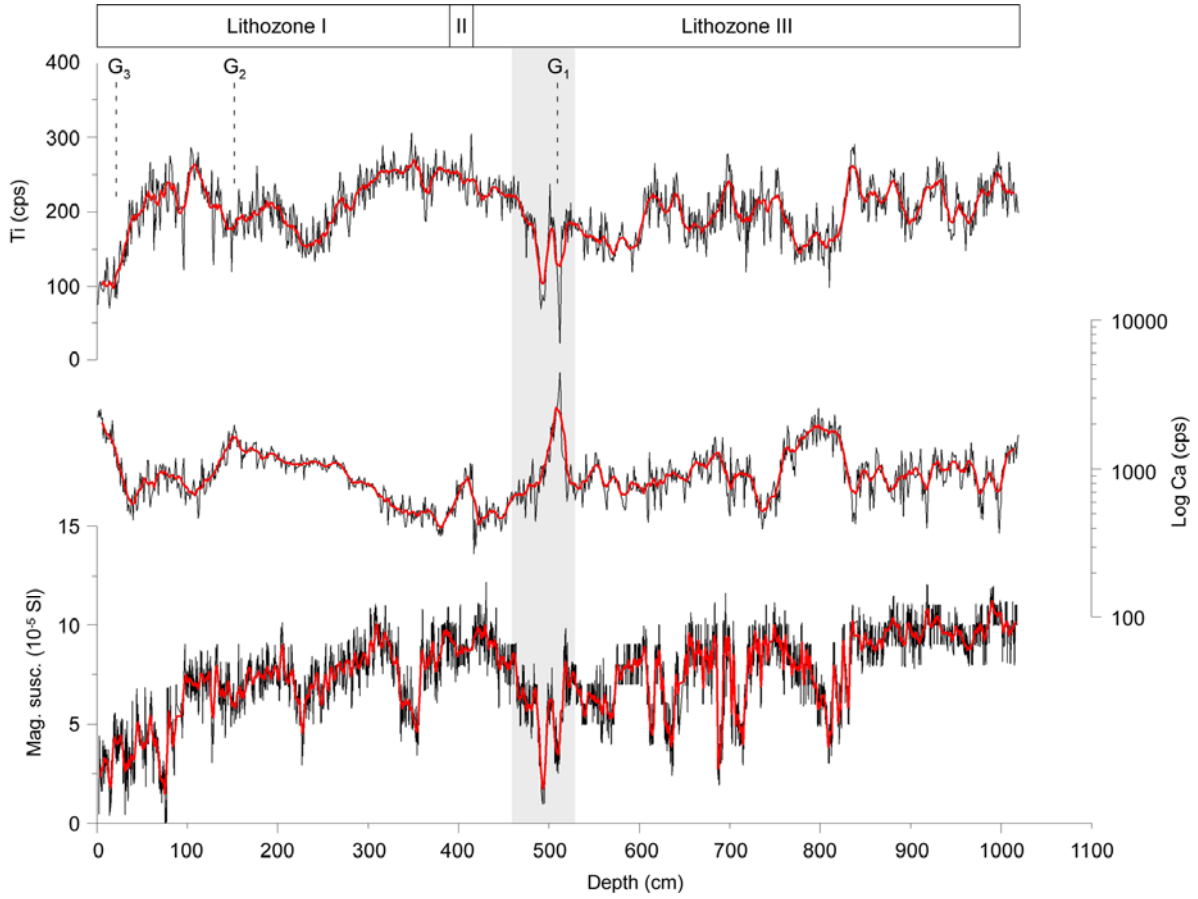

Figure 5.3: *Stacked magnetic susceptibility (Mag. susc.) and X-Ray fluorescence (XRF) data for calcium and titanium in Core CH1. Black thin lines represent original data; red thick lines are smoothed curves using a 21-point and 11-point running average for magnetic susceptibility and XRF data, respectively. The light-grey shaded area refers to the close-up interval discussed in Chapter V.3.2.*

At the microscopic scale, these discrepancies are mostly related to changes in detrital inputs implying changing dilution rates of biogenic material. In total, 1105 layers have been identified within the studied interval 4.58–5.28m, 274 of them probably being of organic origin. The thickness of these layers ranges from ca. 0.025 to 20 mm. In the studied interval, three distinct microfacies (Fig. 5.4) are distinguished: (A) detrital-dominated sequence, (B) organic-dominated sequence, (C) authigenic chemical precipitates.

(A) Detrital-dominated sequences (4.58–4.89 m; 5.00–5.13 m; 5.15–5.28 m)

Detrital-dominated sequences consist of graded, non-graded and transitional discrete detrital layers without primary textural organization, alternating with "organic-like" laminae. Detrital layers (Fig. 5.4.5) are composed of biogenic clasts (ostracods, diatoms, foraminiferans, molluscan shells) and detrital grains with grain sizes ranging from clay sized to medium-sized [4–30µm] and coarse silt particles [ca. 30–63µm]. Isolated sand grains (up to ca. 170x100 µm) were observed in a few cases. Prevailing mineral phases are allochtonous carbonates from the surrounding Palaeogene marls (Bolle and Adatte, 2001), sub-angular to angular xenomorphous quartz, feldspars, rounded glauconite grains,

amorphous pyrite, gypsum crystals (5.15–5.18 m) and clay minerals. Detrital layers usually contain mixed species diatom assemblages (*Actinocyclus* spp., *Cyclothella* spp., *Fragilaria* spp., *Navicula* spp., *Gyrosigma* spp., *Aulacoseira* spp., *Nitzschia* spp., *Amphora* spp., *Cocconeis* spp.) however commonly dominated by the large centric diatom (> 50 µm) *Actinocyclus* spp. randomly distributed throughout the layer. Clay-sized barren laminae were observed in a few cases. The thickness of detrital layers varies from 0.025 to 20 mm, but most of them are >0.2 mm-thick. "Organic-like" laminae (see Fig. 5.4.6) occur more seldom. They are commonly matrix-supported with a dominance of clay-sized detrital particles and medium silt-sized [ca. 4–25µm] detrital particles. "Organic-like" laminae are characterized by higher contents in black organic matter and usually by higher abundance in diatoms, notably *Actinocyclus* spp. and *Navicula* spp. This would suggest a less detritally diluted and quieter deposition mode than during the deposition of detrital layers in Chernyshov Bay.

(B) Organic-dominated sequences (4.89–5.00 m; 5.13–5.14)

Organic-dominated sequences (Fig. 5.4.1) are characterized by a regular alternance of diatomaceous organic mud laminae and detrital laminae with no obvious primary textural organization. Detrital laminae are composed of detrital grains with grain sizes ranging from clay sized to angular medium-sized [4–30µm] and coarse silt particles [ca. 30–63µm]. Isolated sand grains (up to ca. 100x100 µm) were observed in a few cases scattered in the detrital laminae. Prevailing mineral phases are allochtonous biogenic carbonates (mostly remains of coccoliths) with subordinate xenomorphous quartz, feldspars and clay minerals. The detrital laminae usually contain scarce mixed diatom assemblages (most present are *Actinocyclus* spp.: 4.88–4.97 m and *Navicula* spp.: 4.97–5.00 m; 5.11–5.12 m) but sometimes are even barren in diatoms (Fig. 5.4.1). The thickness of detrital laminae varies from 0.025 to 2.65 mm, but the majority of them are >0.1 mm (averaged thickness: ca. 0.3 mm). Diatomaceous organic mud laminae commonly consist of a mixture of organics and fine- to medium sized [4–30µm] detrital grains forming the matrix but also often occur matrix-free as well, and only diatom-supported (e.g. diatom ooze). Diatom ooze laminae are typically near-monospecific oozes of *Actinocyclus* spp. (Fig. 5.4.2). The thickness of diatomaceous mud laminae varies from 0.05 to 0.5 mm (averaged thickness: ca. 0.15 mm). As to the regularity in the alternance of the couplets "diatomaceous mud laminae–detrital laminae" (but triplets are also occasionally observed based on the presence of an additional distinct detrital lamina), we regard these couplets as probable seasonal deposits, that we describe as "varve-like" sediments. XRD analyses conducted at 5.02 m and 5.07 m revealed the presence of halite (2θ= 31.718°; 45.487°) in sediments, which matches well with highly saline conditions as reflected by dinoflagellate cyst assemblages (Sorrel et al., 2006).

Figure 5.4: *Thin-section images (crossed polarized light) of the three microfacies types identified: (1–2) organic-dominated ('varved-like') sequence (32W3; 4.89–5.00 m; microfacies 'B'); (3–4) authigenic chemical precipitates (32W5; 5.14–5.15 m; microfacies 'C'); (5–6) detrital-dominated sequence (32W18; 4.58–4.89 m; microfacies 'A').*

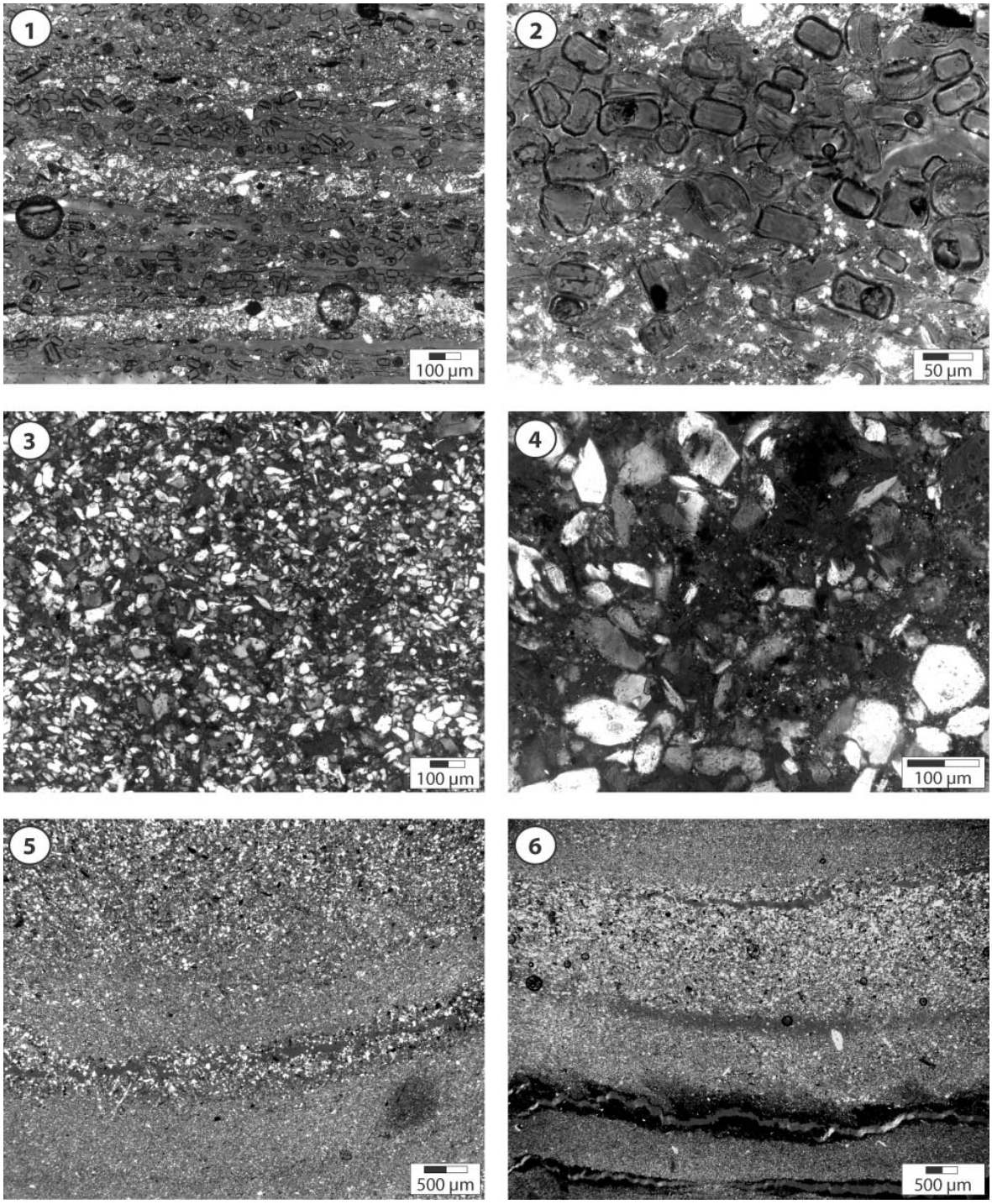

(C) Authigenic chemical precipitates (5.14–5.15 m)

Authigenic chemical precipitates consist of isomorphic crystals of gypsum (Fig. 5.4.3–5.4.4) with grain size ranging from 20x25 µm up to ca. 50x65 µm. Authigenic deposits are generally deprived of any matrix; however they were occasionally observed slightly matrix-supported as well, with clay-sized detrital grains forming the matrix. Authigenic gypsum precipitates are usually barren in diatoms. Its presence in significant abundance has been further confirmed by XRD analysis performed at 5.15m, displaying typical peaks at 2θ= 11.705°, 20.802° and 29.193°.

Ultra high-resolution XRF scanning and microfacies analysis (Fig. 5.5)

As inferred from Fig. 5.3, Titanium is regarded as a reliable proxy for tracing changes in detrital terrigenous inputs at Chernyshov Bay. In the studied close-up interval (Fig. 5.5), the Aluminium curve displays mirrored variations with Ti suggesting that this element is similarly of terrigenous origin (mainly in the clay fraction), neither influenced by productivity changes nor by early diagenetic processes. In general, the thickness of the laminations follows the same trend as the Al and Ti distribution through the interval, i.e., the thicker the lamination, the higher Al and Ti count rates. This is especially obvious between 1180 and 1360 AD (e.g. 4.74–5.15m), but less pronounced in the uppermost part of the interval (4.58–4.68m). Conversely, the thinnest laminations correlating with the lowest Al and Ti values occur within the intervals 4.89–5.00 m and 5.13–5.14 m. In order to get a better understanding of the composition of laminae, i.e., the relation between biogenic and mineralogical grains, we added on Fig. 5.5 the relative abundance of *Actinocyclus* spp. as well as a grain size index corresponding to the averaged grain size measured on detrital particles, for each lamination identified. In general, both curves show a remarkable anti-correlation, especially between 4.58–4.68 m (microfacies A) and 4.74–5.15 m, where increased content in *Actinocyclus* spp. correlate with smaller grain size. Moreover, plots of relative abundance of *Actinocyclus* spp. and lamination thickness yield conspicuous anti-correlated features through this interval, with lower content in *Actinocyclus* spp. corresponding to thicker laminations (4.58–4.68 m; 5.00–5.13 m; 5.15–5.28 m). The opposite pattern is particularly obvious in the upper part of Lithozone II (4.89–5.00 m; microfacies B). Though no straightforward correlation is obvious between the grain size and the lamination thickness, they both show similar features in general, with the same trend.

V.4. Interpretation and discussion

V.4.1. Reconstruction of environmental dynamics during 1150–1400 AD

To infer the signals contained in the inorganic phases of the sediments, the pathway of the elements Al and Ti must be assessed. Ti, which is commonly concentrated in heavy minerals, is preferentially enriched in iron-titanium oxides concentrated in the clay and silt fractions. Because plots of Ti and Al show a very good correlation in the interval 4.58–5.28 m (Fig. 5.5), we propose that both elements are of similar origin (although Al is preferentially enriched in the clay fraction) and thus reflect changes in detrital input. At Chernyshov Bay, the fluvial discharges from the Syr Darya and Amu Darya Rivers are remote from the coring location (Fig. 1.1) and may, therefore, unlikely deliver detrital Ti-bearing particles to the coring site. Similarly, the riverine discharge from small ephemeral rivers eroding the adjacent hilly outcrops consisting of early and late Tertiary marls can hardly account for the high Ti content recorded in Core CH1. Hence we postulate that water- transported suspended particles are less important contributors to terrigenous particles at Chernyshov Bay. Instead, due to the

position of the Aral Sea in a basin characterized by semi-desert to desert conditions, aeolian remobilization of weathered sediment particles by dominant NE winds is the crucial process of reworking as earlier proposed by Mainguet et al. (2002) and Singer et al. (2003). Extreme heating of the dark desert areas of Central Asia (Kyzyl Kum = black desert) favours the formation of dust storms during the summer season (Orlovsky et al., 2005). During spring, regional pressure distribution in combination with raising temperatures over the continent cause the evaporation of the weak seasonal precipitation and the drying of the upper silty and sandy surface beds, both favourable conditions for the formation of dust storms during springtime too (Orlovsky and Orlovsky, 2002). In the Aral Sea basin, a maximum frequency of dust events has been indeed registered during spring in the plain areas including the Ustjurt Plateau and Central Karakum Deserts (> 100 dust storms per year), and in the middle part of the Amu Darya River (Orlovsky et al., 2005). Hence, aeolian transport of particles is by far the dominant process for removal of detrital particles in the northwestern part of the Aral Sea, and can thus realistically account for the high sedimentation rates recorded in Core CH1. We then propose that variations in Al and Ti are mainly the result of changes in the intensity of wind energy.

Moreover, because both geochemical proxies and lamination thickness are positively correlated (i.e. a high content in detrital elements corresponds to thicker laminations suggesting a genetic relationship for these components), we use the lamination thickness as a reliable indicator of wind dynamics. The most conspicuous changes in frequencies of *Actinocyclus* spp. inversely mirror variations in lamination thickness (Fig. 5.5). This would suggest that the abundance of *Actinocyclus* spp. in the sediment is rather linked to sedimentation processes than to productivity in surface waters, reflecting the intensity of dilution as to the deposition of particles on the lake bottom. As a result, the more (less) frequent dust storms, the denser (weaker) detrital particle rain in the water column, and the higher (weaker) dilution of biogenic particles in laminations. A similar phenomenon can be observed from other diatom species (*Navicula* sp. for instance) whose abundance in sediment inversely matches changes in lamination thickness (not shown here). This implies that some of the biogenic grains found at the coring location are not *in-situ* but may originate from the remobilization of sub-contemporaneous near-shore sediments. In addition, the grain size can serve as a further proxy for characterizing wind dynamics, i.e., the stronger the storms, the coarser the detrital grains brought into the system (Fig. 5.5).

Using geochemical and sedimentological proxies at high resolution, the following picture of wind dynamic evolution can be drawn for the interval 4.58–5.28 m covering the time interval ca. 1150–1400 AD.

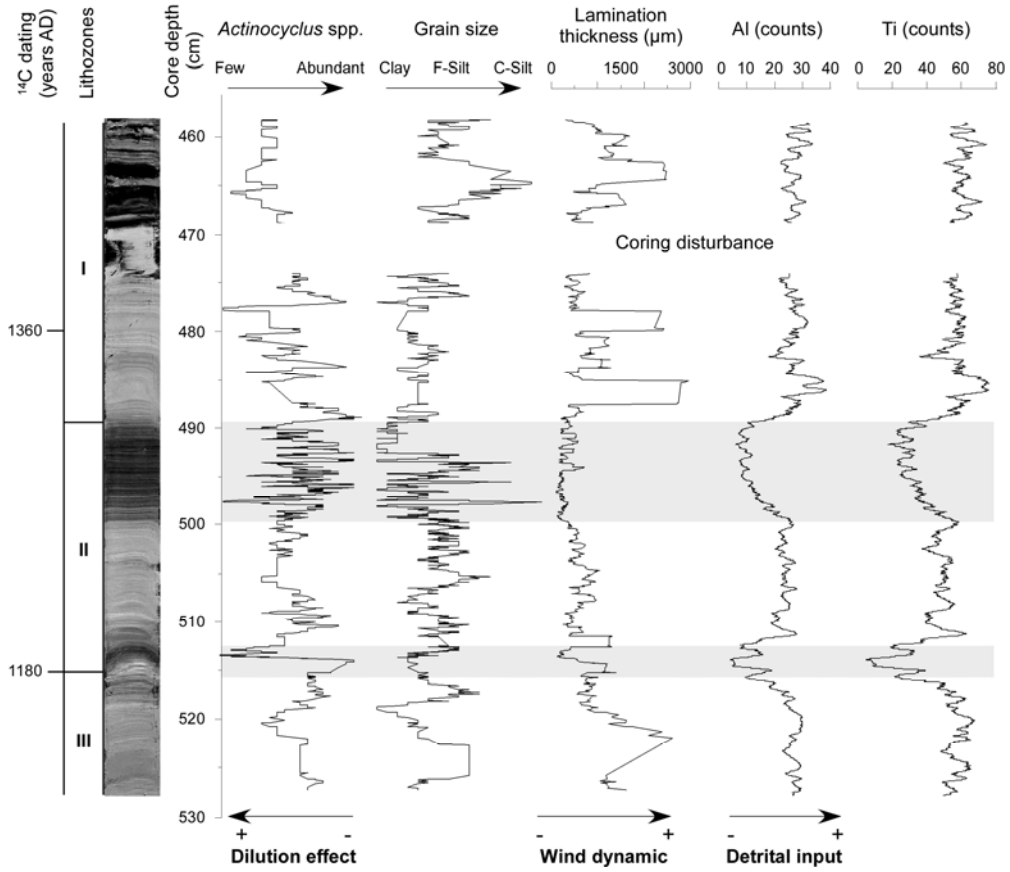

Figure 5.5: *High-resolution XRF (Al, Ti: 40 µm) and microfacies (relative abundance of Actinocyclus spp., grain size and lamination thickness) palaeoclimatic proxy data for the close-up interval [4.58 m–5.28 m; ca. 1150–1400 AD]. Plotted data are smoothed curves using a 9-point and 101-point running average for microfacies and XRF data, respectively. Shaded area corresponds to time periods characterized by a considerable decrease in dust storm frequency in the Aral Sea Basin.*

High content in Al and Ti, thick laminations and low abundance of *Actinocyclus* spp. suggest elevated aeolian detrital inputs in Chernyshov Bay in the uppermost part of Lithozone III (ca. 1150–1180 AD), linked with prominent dust storms and strong wind dynamics (microfacies B). The lithological transition II/III is characterized by a drastic waning of wind dynamics. Minimal values of Ti and Al in the gypsum layer (microfacies C) at ca. 1180 AD document decreasing detrital inputs at that time, during a pronounced salinity increase in the Aral Sea linked to reduced meltwater discharges (Sorrel et al., 2006). Subsequently, on the basis of higher values of detrital inputs (Ti, Al), thicker laminations containing coarser grains and an enhanced dilution of *Actinocyclus* spp. in the sediments, stronger and more frequent dust storms are inferred in the lower part of Lithozone II (5.13–5.00 m; ca. 1210–1265 AD). Wind dynamics, however, rapidly weakened upwards (5.00–4.89 m; ca. 1265–1310 AD), as reflected by drastically lower detrital inputs (Ti, Al), thin "varve-like" brownish sediments containing oozes with abundant *Actinocyclus* spp. (microfacies A) and low sedimentation rates (<0.2 cm yr^{-1}). Between ca. 1360 and ca. 1400 AD prominent and frequent dust storms responsible for high sedimentation rates in Lithozone I (~0.8 cm yr^{-1}; microfacies B) are implied, through elevated values of Al and Ti, frequent occurrences of thicker laminations and an enhanced dilution of diatoms.

V.4.2. Control of wind dynamics in the Aral Sea

Wind dynamics regulating the strength of dust storms, and thus the detrital eolian input into the Aral Sea, is an important factor in the Central Asian climate system. Maximum frequency of dust storms and high wind speeds occur during the spring months (Létolle and Mainguet, 1993), favoured by an increase in intensity of the general circulation due to the seasonal warming, more energetic cyclone activity and cold-wave intrusions (Orlovsky et al., 2005). Hence, because changes in spring wind dynamics are the result of changes in the atmospheric circulation on a broad-scale associated with seasonal shifts in temperature and pressure gradients, it is crucial to examine connections with other climate dynamics.

In western Central Asia the seasonal wind field is controlled by the following feature and process, (i) the Siberian High (SH) feature and (ii) the Tibetan Plateau thermal forcing. The Siberian High anticyclonic feature is broadly recognized as the dominant mode of winter / spring climate over Eurasia (Sahsamanoglou et al., 1991; Savelieva et al., 1991). Its intensity and geographical position strongly control precipitation and atmospheric circulation patterns (meridional or zonal) at mid-latitudes of Asia (Aizen et al., 2001) though its influence on snow-cover extent is questionable (Clark et al., 1999). During spring, the Aral Sea Basin in western Central Asia is influenced by the western periphery of the SH and experiences air mass intrusions from the north, northeast and northwest (Orlovsky et al., 2005; Zavialov, 2005). A recent study by Meeker and Mayewski (2002) based on instrumental data shows that maxima in non-seasalt potassium (nssK) deposition in Greenland correlate to a spring strengthening of the SH pressure system which obviously has an impact on the wind pattern in W Central Asia. This proxy has been also used by Rohling et al. (2002) for examining the influence of winter/spring intensity of the SH on Aegean sea-surface temperatures. Therefore, in W Central Asia, time periods characterized by increased (reduced) content in detrital input (Ti) corresponds to stronger (weaker) and more westward (eastward) SH during enhanced (reduced) spring meridional (zonal; Clark et al., 1999) atmospheric circulation. The organization of the major long-wave pattern, when a meridional circulation mode prevails, results in increasing frequency of the synoptic processes with large-amplitude stationary waves, low pressure systems with small barometric gradients (Subbotina, 1995). It has to be kept in mind, however, that years with prolonged ice-cover extent in the Aral Sea Basin (April–May) may considerably reduce the aeolian remobilization of sediment particles and occurrence of spring dust storms, independently of the strength and position of the Siberian High (Clark et al., 1999).

On the other hand, the feedback of the Tibetan Plateau heating which leads to dry and hot conditions to the west is crucial for the summer circulation in the Aral Sea Basin (Duan and Wu, 2005). According to these authors a divergence/convergence develops in the lower/upper layers, a

circulation embedded in the large-scale circulation pattern forced by the Eurasian continental heating with prevailing E-NE winds at the surface, resulting in multiple summer dust storm events in the Aral Sea Basin. However, since the maximum frequency of dust storms occur during the spring months we rather focus here on the spring mechanisms regulating changes in wind dynamics in W Central Asia, i.e., the SH.

For the past 1400 years, Meeker and Mayewski (2002) documented prominent variations in strength of the Siberian High associated with changing modes of atmospheric circulation over Eurasia, based on glaciochemical series from the GISP2 Ice Core (O'Brien et al., 1995; Mayewski et al., 1994). Here, we examine the general state of the atmosphere in W Central Asia for the past 1500 years based on changing deposition of Ti representing aeolian detrital inputs in Core CH1 correlated with the SH record of Meeker and Mayewski (2002) (Fig. 5.6). Our site location, in the continental interior of Asia, may even represent a more suitable area for characterizing changes in circulation pattern in W Central Asia, compared to what is recorded in Greenland after transport in the atmosphere far to the East.

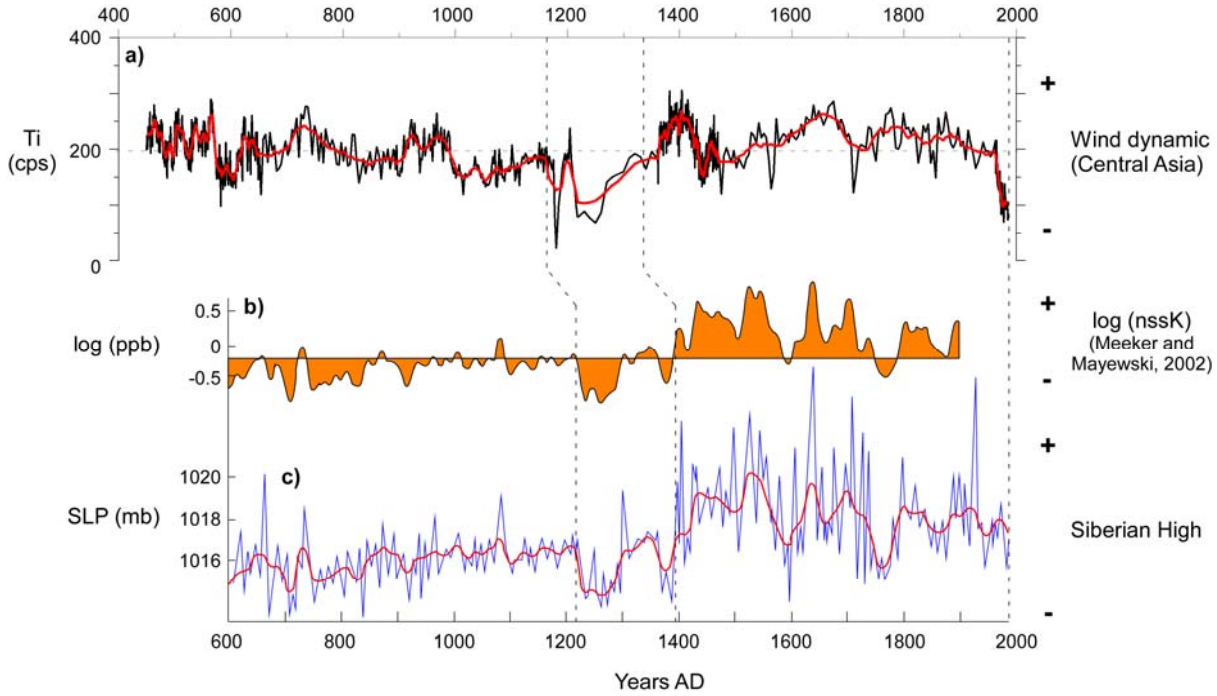

Figure 5.6: *Comparison between the bulk Titanium record of Core CH1 from the Large Aral Sea (a), the non-seasalt Potassium (nssK) (b) and the Siberian High (c) records of Meeker and Mayewski (2002). Red thick lines represent smoothed curves using a 11–year and 20–year running average for Titanium and nssK–Siberian High records, respectively.*

Based on low content of Ti and nssK in Cores CH1 and GISP2 (Fig. 5.6), respectively, relatively weak spring (i.e. March-April-May or MAM) SH characterize the period 700–1150 AD, with the prevalence of a more zonal circulation. Prior to 700 AD (600–700 AD), intensity of the SH fluctuate with more contrasts, in a trend of a more pronounced atmospheric circulation. This period follows a phase of stronger SH from 450–600 AD as reflected by increased deposition of Ti in the Aral Sea.

The Medieval Warm Period (MWP) and Little Ice Age (LIA) provide the most suitable recent analogues for naturally warmer and colder than present climate (Crowley, 2000; Bradley, 2003). During the late MWP (1200–1400 AD), aeolian detrital markers in Core CH1 exhibit two abrupt shifts assignable to a pronounced modification of atmospheric circulation in W Central Asia. Significant weaker SH are inferred between ca. 1180–1210 AD and ca. 1265–1310 AD from minimal deposition of Ti (see also Fig. 5.5) suggesting the onset of prevailing zonal circulation, whereas intermediate periods (ca. 1210–1265 AD; ca. 1310–1400 AD) are indicative of moderately stronger SH, with a more meridional MAM circulation. Similar features are observed in nssK concentrations from Greenland (Meeker and Mayewski, 2002), although the timing of these events slightly differs (Fig. 5.6). A possible explanation for these discrepancies can be the error bars assignable to dating for both age models. In the GISP2 Ice Core, the current estimated age error is 2% for the time span 0–11,640 yr BP, which corresponds to about 40 years (Alley et al., 1993; Meese et al., 1994). In our age model, age uncertainty as discussed in Chapter 2.5 indicates possible error ranges of ca. ±30 years between 1200 and 1400 yr AD.

At the transition from MWP to LIA, the dominant mode of atmospheric circulation changed, coinciding with a transition from a period of relatively weak MAM SH to one in which the MAM circulation greatly intensified throughout the LIA (Meeker and Mayewski, 2002). This change in pressure distribution in Asia explains the increasing concentration of nssK in the GISP2 Ice Core between 1400 AD to about 1750 AD. We would thus expect to show an imprint of this atmospheric change on the wind dynamics in W Central Asia. Comparing the dust flow pattern from Core CH1 (Ti) with concentrations of nssK (Fig. 5.6), we observe that in the Aral Sea the dust input was increasing at ca. 1350 AD and remained high until about 1750 AD, indicating the prevalence of a more meridional atmospheric circulation in Central Asia. Subsequently, a prominent coeval decrease in Ti and nssK contents documents weaker MAM SH between 1750 and 1800 AD. In contrast, the period 1800–1980 AD records intensified MAM SH in W Central Asia, as reflected by elevated input of aolian particles in the Aral Sea and relatively high concentrations of nssK in Greenland. In most recent sediments, a significant decrease in the frequency of dust storms occurs after 1980 AD. This phenomenon has been recorded in other studies (Chub, 1998; Galaeva, 1998; Usmanov, 1998; Meeker and Mayewski, 2002), associated with prominent change in the atmospheric circulation pattern towards a weakening of the SH and a more zonal flow over East Asia (Savelieva et al., 1991; Clark et al., 1999; Panagiotopoulos et al., 2005). The decrease in the intensity of the SH may be linked with the global warming of the atmosphere, and is expected to amplify by the forthcoming years (Druyan & Rind, 1991).

V.5. Conclusions

Based on very high-resolution microfacies and inorganic geochemical analyses, we report prominent changes in wind dynamics in the Aral Sea Basin during the past 1500 years, associated with the atmospheric circulation system over western Central Asia. Changes in wind dynamics appear to be anchored and controlled by the intensity of the Siberian High pressure system during springs. Based on high relative content of Titanium in Core CH1, more intense meridional atmospheric circulation associated with stronger SH prevailed during 450–700 AD, ca. 1210–1265 AD, ca. 1350–1750 AD and 1800–1975 AD. In contrast, lower Ti content during ca. 1180–1210 AD, ca. 1265–1310 AD, 1750–1800 AD and after 1980 AD document weaker spring SH with a reduced and more zonal atmospheric circulation. Other climate forcing may play a significant role in the regulation of seasonal temperature and pressure gradients determining the intensity and the frequency of dust storms in Central Asia. Recent studies based on instrumental data (air temperature) and modelling demonstrated a possible influence of the El Nino Southern Oscillation (ENSO) in Western Central Asia (Gruza et al., 1999; Barlow et al., 2002; Khan et al., 2004). A possible influence of the southwest Indian monsoon on the regulation of wind dynamics in the Aral Sea Basin has been also suggested by several authors (e.g. Létolle and Mainguet, 1993) but in fact scarcely explored. Further investigations may show whether the Aral Sea sediments also hold information on past changes of the Tibetan thermal forcing which today plays an important role on ocean–atmosphere–land interactions during the summer season.

Acknowledgments

The CLIMAN project was funded by INTAS (European Union) (Project N° Aral 00-1030) and the German Science Foundation (DFG Project 436 RUS 111/663 – OB 86/4). We are indebted to them for this support. We are grateful to Prof. Dr. Tomasz Goslar (Poznań Radiocarbon Laboratory, Poland) for providing high-quality AMS ^{14}C dating. We also thank Dr. François Demory for excellent support in the field and Hans von Suchodoletz for his help during XRD measurements.

References

Aizen, E.M., Aizen, V.B., Melack, J.M., Nakamura, T., Ohta, T., 2001. Precipitation and atmospheric circulation patterns at mid-latitudes of Asia. International Journal of Climatology 21, 535–556.

Alley, R.B., Meese, D.A., Shuman, C.A., Gow, A.J., Taylor, K.C., Grootes, P.M., White, J.W.C., Ram, M., Waddington, E.D., Mayewski, P.A., Zielinski, G.A., 1993. Abrupt incease in Greenland snow accumulation at the end of the Younger Dryas event. Nature 362, 527–529.

Barlow, M.H., Cullen, B., Lyon, 2002. Drought in Central and southwest Asia: La Niña, the warm pool and the Indian precipitation. Journal of climate 15 (7), 697–700.

Bolle, M.P., Adatte, T., 2001. Palaeocene–early Eocene climatic evolution in the Tethyan realm: clay mineral evidence. Clay minerals 36 (2), 249–261.

Bond, G., Kromer, B., Beer, J., Muscheler, R., Evans, M.N., Showers, W., Hoffmann, S., Lotti-Bond, R., Hajdas, I., Bonani, G., 2001. Persistent solar influence on North Atlantic climate during the Holocene. Science 294, 2130–2136.

Bradley, R.S., 2000. 1000 years of climate change. Science 288, 1353–1354.

Bradley, R.S., 2003. Climate of the last Millenium. Holocene Working Group Workshop, Bjerknes Centre for Climate Research, August 2003.

Briffa, K.R., 2000. Annual climate variability in the Holocene: interpreting the message of ancient trees. Quaternary Science Reviews 19, 87–105.

Chub, V.E., 1998. Estimation of aerosol influence on climatic characteristics of the Aral Sea basin (Otzenka vliyaniya aerozolei na klimaticheskie kharakteristiki baseina Aral'skogo moray). Problems of Desert Development 3–4, 50–55 (in Russian).

Clark, M.P., Serreze, M.C., Robinson, D.A., 1999. Atmospheric controls on Eurasian snow extent. International Journal of Climatology 19, 27–40.

Cook, E.R., Esper, J., D'Arrigo, R.D., 2004. Extra-tropical Northern Hemisphere land temperature variability over the past 1000 years. Quaternary Science Reviews 23, 2063–2074.

Crowley, T.J., 2000. Causes of climate change over the past 1000 years. Science 289, 270–277.

Demory, F., Oberhänsli, H., Nowaczyk, N.R., Gottschalk, M., Wirth, R., Naumann, R., 2005. Detrital input and early diagenesis in sediments from Lake Baikal revealed by rock magnetism. Global and Planetary Change 46, 145–166.

Druyan, L.M., Rind, D., 1991. Implications of climate change on a regional scale. In: Graber, M., Cohen, A., Magaritz, M., (Eds.), Proceedings of the international workshop on regional implications of future climate change, Sep. 1993, 311 pp, pp. 75–78.

Duan, A.M., Wu, G.X., 2005. Role of the Tibetan Plateau thermal forcing in the summer climate patterns over subtropical Asia. Climate Dynamics 24, 793–807.

Friedrich, J., Oberhänsli, H., 2004. Hydrochemical properties of the Aral Sea water in summer 2002. Journal of Marine Systems 47, 77–88.

Galaeva, O.S., 1998. On the monitoring of carrying out of sandy salty aerosol from drained part of bottom of the Aral Sea (K monitoringu vinosa peschanih I solevih aerosolei s visohshego dna Aral'skogo moray). Problems of Desert Development 3–4, 17–21 (in Russian).

Gruza, G.V., Ran'kova, E.Ya, Kleschenko, L.K., Aristova, L.N., 1999. Relationship between climatic anomalies on territory of Russia and phenomena El Nino-South Oscillation. Meteorology and Hydrology 5, 32–51 (in Russian).

Heim, C., 2005. Die Geochemische Zusammensetzung der Sedimente im Aralsee und Sedimentationsprozesse während der letzten 100 Jahre. Diploma thesis, Alfred-Wegener-Institut für Polar- und Meeresforschung, Bremerhaven, 89 pp.

Jansen, J.H.F., van der Gaast, S.J., Koster, B., Vaars, A., 1998. CORTEX, a shipboard XRF–scanner for element analyses in split sediment cores. Marine Geology 151, 143–153.

Khan, V.M., Vilfand, R.M., Zavialov, P., 2004. Long-term variability of air temperature in the Aral sea region. Journal of Marine Systems 47, 25–33.

Létolle, R., Mainguet, M., 1993. Aral. Springer Verlag, Paris, 358 pp.

Lioubimtseva, E., 2002. Arid environments. In: Shahgedanova, M. (Ed.), Physical Geography of Northern Eurasia. Oxford University Press, Oxford 571 pp.

Lioubimtseva, E., Cole, R., Adams, J.M., Kapustin, G., 2005. Impacts of climate and land-cover changes in arid lands of Central Asia. Journal of Arid Environments 62, 285–308.

Mainguet, M., Létolle, R., Dumay, F., 2002. Le système régional d'action éolienne (SRAE) du bassin de l'Aral (Kazakhstan, Ouzbékistan et Turkménistan). C.R. Geosciences 334, 475–480.

Mann, M.E., Jones, P.D., 2003. Global surface temperatures over the past two millennia. Geophysical Research Letters 30 (15), 1820, doi: 10.1029/2003GL017814, 2003.

Mayewski, P.A., Meeker, L.D., Whitlow, S., Twickler, M.S., Morrison M.C., Bloomfield, P., Bond, G.C., Alley, R.B., Gow, A.J., Grootes, P.M., Meese, D.A., Ram, M., Taylor, K.C., Wumkes, W., 1994. Changes in atmospheric circulation and ocean ice cover over the North Atlantic during the last 41,000 years. Science 261, 195–197.

Meeker, L.D., Mayewski, P.A., 2002. A 1400-year high-resolution record of atmospheric circulation over the North Atlantic and Asia. The Holocene 12 (3), 257–266.

Meese, P.M., Alley, R.B., Gow, A.J., Grootes, P., Mayewski, P.A., Ram, D.A., Taylor, K.C., Waddington, E.D., Zielinski, G., 1994. Preliminary depth-age scale of the GISP2 ice core. U.S. Army Cold Regions Research Laboratory Publication SR94–01, Hanover, NH.

Middleton, N.J., 1986. Geography of dust storms in South-West Asia. Journal of Climatology 6, 183–196.

Moberg, A., Sonechkin, D.M., Holmgren, K., Datsenko, N.M., Karlén, W., 2005. Highly variable northern temperatures reconstructed from low- and high-resolution proxy data. Nature 433, 613–617.

Nezlin, N.P., Kostianoy, A.G., Li, B.-L., 2005. Inter-annual variability and interaction of remote-sensed vegetation index and atmospheric precipitation in the Aral Sea region. Journal of Arid Environments 62, 677–700.

Nourgaliev, D.K., Heller, F., Borisov, A.S., Hajdas, I., Bonani, G., Iassonov, P.G., Oberhänsli, H., 2003. Very high resolution paleosecular variation record for the last 1200 years from the Aral Sea. Geophysical Research Letters 30 (17), 4-1–4-4.

O'Brien, S.R., Mayewski, P.A., Meeker, L.D., Meese, D.A., Twickler, M.S., Whitlow, S.I., 1995. Complexity of Holocene climate as reconstructed from a Greenland ice core. Science 270, 1962–1964.

Orlovsky, L., Orlovsky, N., 2002. White sand storms in Central Asia. In: Yang Youlin, Squires, V., Lu Qi (Eds.), Global Alarm: Dust and sand storms from the World's Drylands. UNCCD, Bangkok, pp. 169–201.

Orlovsky, L., Orlovsky, N., Durdyev, A., 2005. Dust storms in Turkmenistan. Journal of Arid Environments 60, 83–97.

Panagiotopoulos, F., Shahgedanova, M., Hannachi, A., Stephenson, D.B., 2005. Observed trends and teleconnections of the Siberian High: a recently declining center of action. Journal of climate 18, 1411–1422.

Petschick, R., 2000. MacDiff 4.2.5 Bedienungsanleitung (http://servemac.geologie.uni-frankfurt.de/Rainer/html)

Reimer, P.J., Baillie, M.G.L., Bard, E., Bayliss, A., Beck, J.W., Bertrand, C.J.H., Blackwell, P.G., Buck, C.E., Burr, G.S., Cutler, K.B., Damon, P.E., Lawrence Edwards, R., Fairbanks, R.G., Friedrich, M., Guilderson, T.P., Hogg, A.G., Hughen, K.A., Kromer, B., McCormac, G., Manning, S., Bronk Ramsey, C., Reimer, R.W., Remmele, S., Southon, J.R., Stuiver, M., Talamo, S., Taylor, F.W., van der Plicht, J., Weiyhenmeyer, C.E., 2004. IntCal04 terrestrial radiocarbon age calibration, 0-26 cal. yr BP. Radiocarbon 46 (3), 1029–1058.

Roberts, N., Wright, H.E., 1993. Vegetational, lake-level, and climatic history of the Near East and Southwest Asia. In: Wright, H.E. (Ed.), Global Climates since the Last Glacial Maximum. University of Minnesota Press, pp. 194–220.

Röhl, U., Abrams, L.J., 2000. High-resolution, downhole and non-destructive core measurements from Sites 999 and 1001 in the Carribean Sea: Application to the Late Paleocene Thermal Maximum. Proceedings of the Ocean Drilling Program (ODP) Scientific Results, 165, 191–204, College Station, TX (Ocean Drilling Programm).

Rohling, E.J., Mayewski, P.A., Abu-Zied, R.H., Casford, J.S.L., Hayes, A., 2002. Holocene atmosphere–ocean interactions: records from Greenland and the Aegean Sea. Climate dynamics 18, 578–593.

Romanov, N.N., 1961. Dust storms in Central Asia (Pyl'nye buri Srednei Asii). Samarkand University, Tashkent, 198 pp. (in Russian).

Romanov, N.N., 1986. Forecast of dust storms and advective dust haze. Instruction in short-term weather forecasts. Central Asia, Gidrometeoizdat Leningrad 2 (3), 210–216 (in Russian).

Sahsamanoglou, H.S., Makrogiannis, T.J., Kallimopoulos, P.P., 1991. 'Some aspects of the basic characteristics of the Siberian anticyclone'. International Journal of Climatology 11, 827–839.

Savelieva, N.I., Semiletov, I.P., Vasilevskaya, L.N., Pugach, S.P., 1991. A climate shift in seasonal values of meteorogical and hydrological parameters for Northeastern Asia. Progress in Oceanography 47, 279–297.

Seredkina, E.A., 1960. Dust storms in Kazakhstan (Pyl'nie buri v Kazakhstane). Proceedings of KazNIGMI 15, 54–59 (in Russian).

Singer, A., Zobeck, T., Poberezsky, L., Argaman, E, 2003. The PM_{10} and $PM_{2.5}$ dust genereation potential of soils/sediments in the Southern Aral Sea Basin, Uzbekistan. J. Arid Environm. 54, 705–728. Doi:10.1006/jare.2002.1084

Small, E.E., Giorgi, F.G., Sloan, L.S., Hostetler, S., 2001. The effects of dessication and climatic change on the hydrology of the Aral Sea. Journal of climate 14, 300–322.

Sorrel, P., Popescu, S.-M., Head, M.J., Suc, J.P., Klotz, S., Oberhänsli, H. Hydrographic development of the Aral Sea during the last 2000 years based on a quantitative analysis of dinoflagellate cysts. Palaeogeography, Palaeoclimatology, Palaeoecology 234 (2–4), 304–327.

Subbotina, O.I., 1995. Atmospheric circulation. In: Change of Climate in Middle Asia, Muminova FA, Inagamova SI (Eds.), SARNIIGMI Publishing: Tashkent, 8–34 (in Russian).

Usmanov, V.O., 1968. Estimation of the influence of dusty salt transfer on the productivity of agricultural crops in the Priaral region (Otzenka vliyaniya sole-pyleperenosa na productivnost' sel'skohozyaistvennih kultur v Priaral'skom regione). Problems of Desert Development 3–4, 147–151 (in Russian).

Zavialov, P.O., 2005. Physical oceanography of the dying Aral Sea. Springer Verlag, published in association with Praxis Publishing, Chichester, UK, 146 pp.

Zolotokrylin, A.N., 1996. Dust storms in Turanian Lowland. Proceedings of Russian Academy of Sciences, Geographic Series 6, 48–54 (in Russian).

Chapter VI: Synthesis

This thesis, embedded in the international INTAS/DFG CLIMAN project (http://climan.gfz-potsdam.de), presents high-resolution palaeoclimate studies in the Aral Sea Basin during the past 2000 years. Palynological and sedimentological proxies have been explored to (i) reconstruct late Holocene environments and climate change in the Aral Sea, and (ii) compare our results with other climatic records to better understand which mechanisms govern climate change in western Central Asia.

In this chapter, we firstly aim to discuss to which extent human activities might have exerted an influence on the Aral Sea's water balance. This section is discussed on the basis of a fourth paper: "*Archaeology and Climate: Settlement and lake level change at the Aral Sea"* by Boroffka *et al.* (Geoarchaeology in press), based on new archaeological findings combined with relative abundance of Ca in Core CH1, reflecting to a great extent the evaporation balance.

In the second part of this chapter, we discuss what kind of forcing is basically controlling climatic change during the past 2000 years. We ultimately aim to distinguish between all the active climatic systems (i.e., internal forcing) which control climate variability in western Central Asia, and to discuss to which extent external forcings impact on our system.

VI.1. Human influence on the hydrological balance (Boroffka *et al.*, in press)

The Aral Sea region is an excellent location for tracing human reactions to past climate change. In this climatically sensitive area, alternating between semi-arid and arid conditions, human influence can be traced back to the first millennium B.C (Boroffka et al., 2005). The Aral Sea Basin with extended arid semi-deserts and deserts has potential agricultural plains along the two major inflows (Amu Darya and Syr Darya), which were actively cultivated far back in historical time. The modern regression, starting 1960, has received much attention since the political opening of the former Soviet Union (e.g. Aral´skij krizis, 1991; Létolle and Mainguet, 1996; Micklin and Williams, 1996). While older lake level oscillations and human reactions to environmental change have hardly been studied, the latter is clearly triggered by

man, and its effects on the environment and the life of local populations have became a subject of discussion far beyond the scientific community (Létolle and Mainguet, 1993).

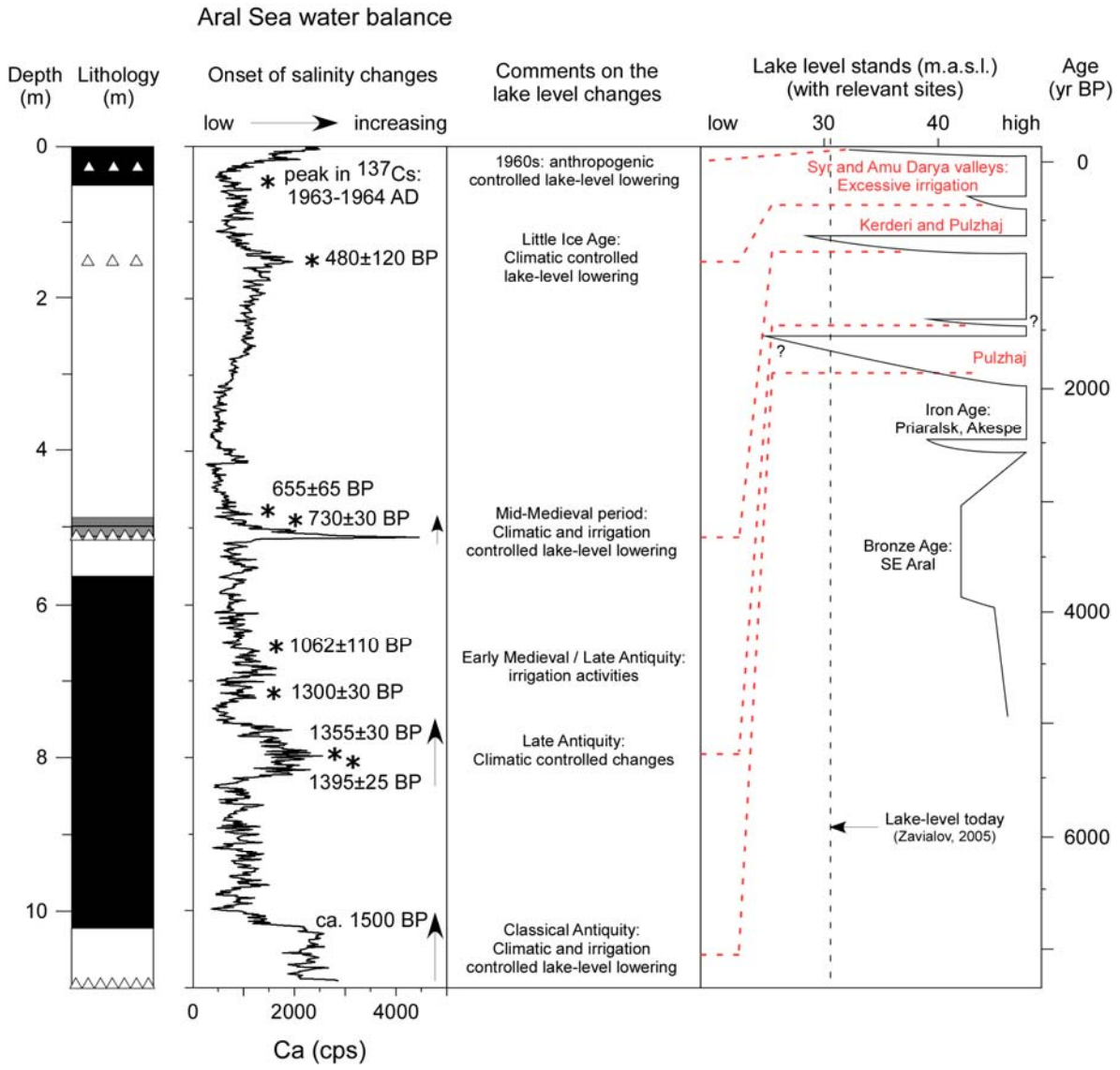

Figure 6.1: *Salinity changes and lake water level of the Aral Sea as controlled by river inflow and seasonal evaporation. The water balance is inferred from the relative abundance of the element Ca (counts reflect relative abundance) scanned at 1 cm-resolution with an XRF logger in Core CH1. Ca mainly traces the abundance of gypsum, which records the onset of salinisation. Major fluctuations in Ca abundance are assigned to climatically and, to some extent, anthropogenically-driven lake level changes. Important archaeological sites are assigned to specific lake level changes.*

Newly discovered archaeological sites from both northern and southern shores of the Aral Sea allow to reconstruct the history of human settlement in the past which, when available, were compared to lake level stands as recorded in palaeoshorelines and terraces (Fig. 6.1; Boroffka et al., 2005). Archaeological findings are integrated with the Aral Sea's water balance as reconstructed from the relative Ca content in Core CH1, a proxy for gypsum

deposition, to evaluate the human influence on the hydrological balance during the past 2000 years. Four levels of gypsum-rich mud, forming distinct bright beds or dark clayey muds with abundant idiomorphic gypsum crystals (Fig. 6.1) are described in Core CH1 (see also Chapter V.2.4). As gypsum ($CaSO_4 \cdot 2H_2O$) starts to precipitate when salinity exceeds 26–28 ppt (Bortnik and Chistayeva, 1990), it becomes a typical indicator for salinisation and we use the element scans of Ca to keep track of its abundance. Hence, relative abundance of this element is used to estimate beginning changes in the river inflow, which control together with the annual evaporation/precipitation budget, the chemical water balance and at longer time range the Aral Sea's lake level.

For late Classical Antiquity (ca. 1600-1500 yrs BP) a new site, Pulzhaj, was discovered at an elevation of 53 m a.s.l. to the southwest of the Aral Sea, at the foot of the Ustjurt Plateau (Fig. 1.1). Several coins were found, as well as large quantities of high quality ceramics, including original imports from China, Iran and Saraj or Sarajchik (capital of the Golden Horde near the mouth of the Wolga River), and are dated to the 4^{th} – 5^{th} and 13^{th} – early 14^{th} centuries AD. Hence this site can reliably witness for two successive regressions of the Aral Sea. The first regression is indicated by high Ca contents and the occurence of gypsum in sediments from Chernyshov Bay deposited between ca. 2000 and 1600 yr BP (0–400 AD) (Fig. 6.1). This event might be coeval to the deposition of mirabilite in the western basin (Maev and Karpychev, 1999), probably configurated as a series of shallow hypersaline lakes (Aleshinskaya et al., 1996), during a prolonged period of cold and dry conditions in the Aral Sea region (see Chapter V.6). As a salinity of 150 ppt is required for the precipitation of mirabilite (Létolle et al., 2005) a lake level of 23 m.a.s.l. would be inferred, making this regression more severe than the current one. The extensive irrigation systems initiated by the Persians in the 7^{th}–5^{th} centuries BC along the Amu Darya and the Syr Darya (Tolstov, 1962), at least partly, date to this period and culminated around 300–400 AD. Reports from Greek sources (Barthold, 1910), although not very accurate by modern standards, indicate that the Amu Darya was flowing to the west, through the Uzboj channel, into the Caspian Sea, so that a regression, possibly intensified by human activities seems evident (see Chapter III.4.2). After 300–400 AD, archaeological surveys document that the area southwest of the Aral Sea dried up completely and that the river diversion towards the Caspian Sea via the Uzboj has been stopped (Barthold, 1910). This may coincide with the destruction of hydraulic facilities in the Korezm region by Mongol warriors (the Huns Hephtalites) around 380–400 AD (Létolle and Mainguet, 1993), which may have resulted in diverting waters from the Amu

Darya back to their natural course and discharge into the Aral Sea. For the low level stand dated at about 550–600 cal. yr AD, however, no time equivalent archaeologic event has been reported yet, suggesting that this moderate regression is likely to be due to climate change.

The Early Medieval / Late Antiquity (7^{th}–10^{th} centuries AD) lake-level lowering, though moderate, is probably man made as no climate change is recorded in the region. In contrary, this is a period of increased temperature favourable for the growth of juniper in the Tien Shan (Esper et al., 2002a), especially between 800 and 1000 AD. Higher Ca content in Core CH1 is therefore likely to reflect a further episode of irrigation. Although irrigation systems were not as extensive as those previously (Boroffka et al., 2005), historical reports document by the 9^{th}–10^{th} centuries AD that the Korezm Basin and the area southwest from the Aral Sea was again exploited (Tsvetsinskaya et al., 2002).

From dinoflagellate cyst assemblages, increased salinities are reported from ca. 900 AD (see Chapter III) and prelude the occurrence of a major regression during the 13^{th}-14^{th} centuries AD, as documented by the gypsum layer from 4.96–5.05 m (Fig. 6.1). At Pulzhaj, the atypical stone foundations of houses, indicating prosperity, are dated to the 13^{th} – early 14^{th} centuries AD. Some time after the early 14^{th} century AD lower site was abandoned because of flooding and has been drowned in a newly formed bay of the Aral Sea. Other new archaeological sites from the Middle Age have been identified both in the north and in the south of the Aral Sea (Boroffka *et al.*, 2005). The sites in the north yielded imitations of Chinese porcellain and high quality glazed pottery, evidencing connections to long distance trade routes known collectively as the northern Silk Route. Further to the south, in the northern part of the Great Aral Sea, a *mazar* (islamic holy grave site) has been identified next to a settlement, named Kerderi, at an altitude of 32 m a.s.l. Both could be dated to the 13^{th} – 14^{th} centuries AD (Boroffka *et al.*, 2005). While the *mazar* lies on an artificial mound and is exposed today at least during the summer season, the adjacent settlement is still mostly submerged, indicating that the water level must have been clearly below 31 m a.s.l. during the Middle Age. This regression has been already described previously though considerably underestimated, when the lake level had been located around 44/45 m a.s.l. (Aladin and Plotnikov, 1995; Boomer et al., 2000). According to ancient documents (Barthold, 1910), the Amu Darya discharged into the Aral Sea until the devastating Mongol invasion in 1221, when reported that Genghis Khan's army destroyed hydraulic installations along the Amu Darya. Though, from historical earthquake, records a major event has been reported for 1221 in

western Central Asia. Hence, we can not exclude yet that river bed geometry in the flat delta area has been drastically modified by tectonical offsets, leading to deviations in flow direction. Shortly later, irrigation systems and large dams were reconstructed. However, the beginning of the 13th century AD is marked by pronounced lowered temperature in the Tien Shan (Esper et al., 2002a) which may have considerably reduce the contribution of meltwater to the flow of the tributaries during the melt season (Chapter III). As fluvial input account for 80% of the hydrological input into the Aral Sea, such a reduction in water inflow may have been drastic for lake levels and thus lead to a severe regression. Therefore it is more likely that climatic change rather than anthropogenic activity is responsible for the onset of this regression, even if human activities might have amplified to some extent the lake-level fall. Shortly later lake level may still be low, given that Hamdallah Kazwînî in 1339 AD mentions that the Aral Sea is a salt lake. Shallow basins may have disappeared completely, since the merchant Bedr-ad-dîn al-Khowârizmi does not refer to any lake at all, although he does describe the lower Syr Darya (Barthold, 1910; Létolle and Mainguet, 1996).

The following regression, possibly a time equivalent to the Little Ice Age, is clearly documented after 480 ± 120 cal yrs BP in Core CH1 by gypsum-rich silty clays and higher abundance in Ca (Fig. 6.1). It is only at 1573 AD according to a report by Khan Abulghazi (Barthold, 1910) that the Amu Darya changed its course and discharged again into the Aral Sea. Further support for a second regression during the Little Ice Age comes from drowned Saxaul stands, which had been dated to 287 ± 5 ^{14}C yrs BP (307 cal. yrs BP) (Boomer et al., 2000, p. 1266). Similar stands, yet undated, were also observed near the present shoreline at the southern edge of the western basin (44º20'42"N; 58º16'56"E), a region just fallen dry during the last CLIMAN expedition in late summer 2003. Both regressions correspond to reduced temperature in the Tien Shan mountains (Esper et al., 2002a), resulting in lowered meltwater discharges into the Aral Sea during spring. Thus, as for the lake-level lowstand recorded during the 13th – 14th centuries AD, these regressions are most probably climatically-driven through the onset of colder and drier conditions in the region. No significant human activity, which could have added to the negative water balance, is known for this time period.

We show that Aral Sea is indeed an excellent area for studying interactions between human activity and water level changes. However, most shifts in human adaptation strategies, which can be dated by archaeological material, have to be explained to a great part by climate changes. Before 1850 AD, the lake level had reached again about 55 m.a.s.l., which is

probably the highest Aral Sea's level during the Holocene and probably as far back as to the Palaeolithic Age as no archaeological remains were found between 35,000 and 7,000 yrs BP. Until 1960 AD, the lake level had decreased only slightly and it fluctuated around 53 m.a.s.l. (Létolle and Mainguet, 1996). As meteorological data show a steady increase of annual temperatures over the region during the 20th century (Lioubimtseva et al., 2005), it implies that without extensive irrigation activities, lake levels would not have been subjected to the regression witnessed today. A readjustment of the present low water level to present-day climatic conditions is, therefore, basically possible within less than few decades once irrigation will be considerably reduced.

VI.2. Natural forcing factors

VI.2.1. Climate dynamics (internal forcing mechanisms)

The climatology in western Central Asia can be defined by all the interactions between the active systems (Eastern Mediterranean Low, Siberian High, NAO, etc) that control the seasonal variability of climate conditions and its amplitude (Fig. 6.2).

Such interactions between active systems have a primary impact on the hydrological balance of the Aral Sea. Due to the strong dependence of the Aral Sea to hydrological inputs from its tributaries, the regressions and associated salinity increases recorded at Chernyshov Bay are ultimately linked to fluctuations in meltwater discharges during spring (Chapter III). The amplitude of the contribution in glacial meltwater inputs into the Aral Sea is thus largely controlled by temperature variations in the Tien Shan and Pamir Mountains where melting glaciers and snowfields feed the Amu Darya and the Syr Darya rivers. One source of moisture for the Aral Sea region is the Eastern Mediterranean cyclonic system where depressions occur and migrate across the Middle East and Central Asia during late winter and early spring (Chapter IV). As the Eastern Mediterranean region is strongly influenced by the polarity of the NAO during winter, the modulation of pressure distribution in the Atlantic Ocean is believed to have a significant impact on the humidity provided to Central Asia. However, when trying to ascertain a connection with the NAO, it is necessary to examine and quantify the genuine role of the westerly Jet Stream (WJS) which is another source of moisture in western Central Asia.

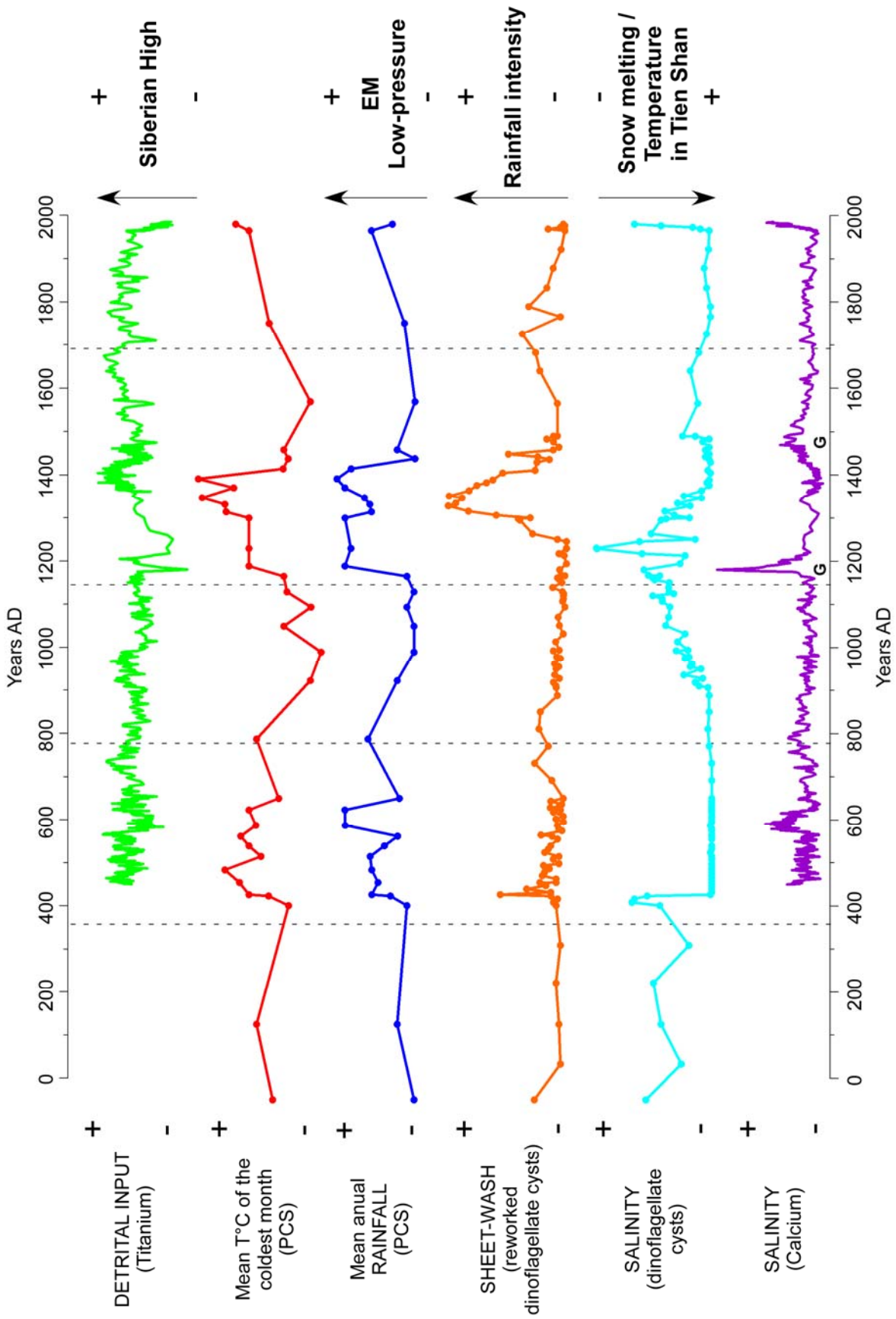

Figure 6.2: *Past environmental and climate variability in the Aral Sea Basin during the last 2000 years (internal forcing) based on the results developed in Chapters III, IV and V.*

By now, the lack of proxy data that would allow establishing relationships between the WJS and humidity in western Central Asia confines such connection to speculations. Forthcoming analyses would thus consist in extracting new cores from other lakes in the high catchment area (Tien Shan, Pamir Mountain ranges), where the humidity carried by the WJS precipitates as snow during winter.

This study, based on a multi-proxy approach, has also shown that besides a primary influence on hydrological changes during the past 2000 years, interactions between all active systems also control the wind dynamics within Central Asia. During spring, the Aral Sea Basin is influenced by the western periphery of the Siberian High (SH) and experiences air mass intrusions from the north, northeast and northwest (Orlovsky et al., 2005; Zavialov, 2005). We have demonstrated that the growing number of dust storms that occur when the continent is heating was primarily controlled by the SH (Chapter V; Fig. 6.2), whose intensity determine the temperature gradients over western and Central Asia (Panagiotopoulos et al., 2005). However, the prevalence of a northwesterly flow, the associated anticyclonic vorticity advection and the persistence of low temperatures during winter generally favours the development of the SH (Clark et al., 1999). These retroactive interactions thus imply a feedback mechanism between the severity of winters and the development of the SH, which ultimately has an impact on the frequency of dust storms and the intensity of detrital inputs in the Aral Sea Basin. Indeed, the dust load transported by winds depends on (i) the ease for storms to remobilize weathered sediment particles when the catchment is covered by snow and thus, the amplitude and the duration of snow-cover signals, and (ii) the duration of the frozen period which may prevent sediment particles to enter the water body.

Besides, the Siberian High itself may have an influence on the moisture transported from the Eastern Mediterranean region to western Central Asia during late winter and early spring. As reported by Panagiotopoulos et al. (2005), a stronger SH contributes to enhance cyclogenesis in the Mediterranean region (Fig. 1.3b). To some extent, this matches well with our results (Fig. 6.2), indicating that the increase in precipitation recorded during 400–700 AD and 1300–1400 AD are coeval with a stronger SH. This is, however, not the case for the period 1150–1300 AD, where the intensity of the SH was extremely low concurring with higher mean annual temperatures in the region (Fig. 6.2). Conversely, the low temperatures during 1500–1980 AD may stem from persistent intensified SH during springs (Meeker and Mayewski, 2002) that would be associated to prolonged freezing conditions (see Fig. 1.4f), thus delaying the onset of warming in western Central Asia.

VI.2.2. External forcing

Altough interactions between different climate systems primarily control environmental changes and determine climate conditions in western Central Asia at the short time run, we would expect external forcing mechanisms to have an influence, even weak, on climate and environmental change in this region. This chapter aims to investigate such relationships and to ultimately unravel the respective role and scope of both internal (climate dynamics) and external forcing mechanisms.

Within the Aral Sea proper, the temporal changes of the water body volume are determined to a great part by the water budget components (i.e., evaporation, precipitation, river discharges and groundwater inflow), which are on their part subject to change as a function of the lake volume, thus constituting feedbacks (Zavialov, 2005). This primarily points to the role of the evaporation rates (averaging 100 cm/year with maximum values observed in August which exceed those of February by a factor of 10) which depend on the temperature, the air humidity and salinity properties of the lake (Zavialov, 2005). Hence evaporation rates are likely to have been modulated during periods of dessication of the Aral Sea, and might be regarded to some extent as a good indicator of solar insolation changes in the past. Though evaporation rates or even sea-surface temperature are difficult yet to quantify as we do not have suitable proxies for tracing these components, we can nevertheless use the salinity record based on dinoflagellate cyst assemblages to evaluate to some extent the impact of solar activity on the Aral Sea's hydrological balance during the late Holocene.

The comparison between our record of salinity change and different reconstructions of solar activity show a moderate correlation over the past millennium (Fig. 6.3). Overall, it can be observed that the periods of increased / high salinity as during 1000–1300 AD, 1450–1550 and 1600–1700 AD coincide closely with periods of increased solar activity. However, no correlation is obvious during the intervening periods 1300–1450 AD and 1700–2000 AD when salinity levels are low and do not seem to be influenced by variations in solar activity. Hence the correspondence between the salinity record and the ^{10}Be and $\delta^{14}C$ solar intensity proxies is clearly more pronounced during periods of drastic salinity increase than during phases where salinity is low. This suggests non-linear relationships in which hydrological changes are more responsive to variation in solar activity (i.e. external forcing) when lake levels are low, indicating that an increase in the net radiative forcing may have amplify the lake shrinking during 1000–1300 AD and 1450–1700 AD. This agrees to some extent with results of Shermatov et al. (2004) based on an analysis of water resource variability in the

Aral Sea Basin who reported that maxima in solar activity coincided with low lake-levels during the past ca. 200 years.

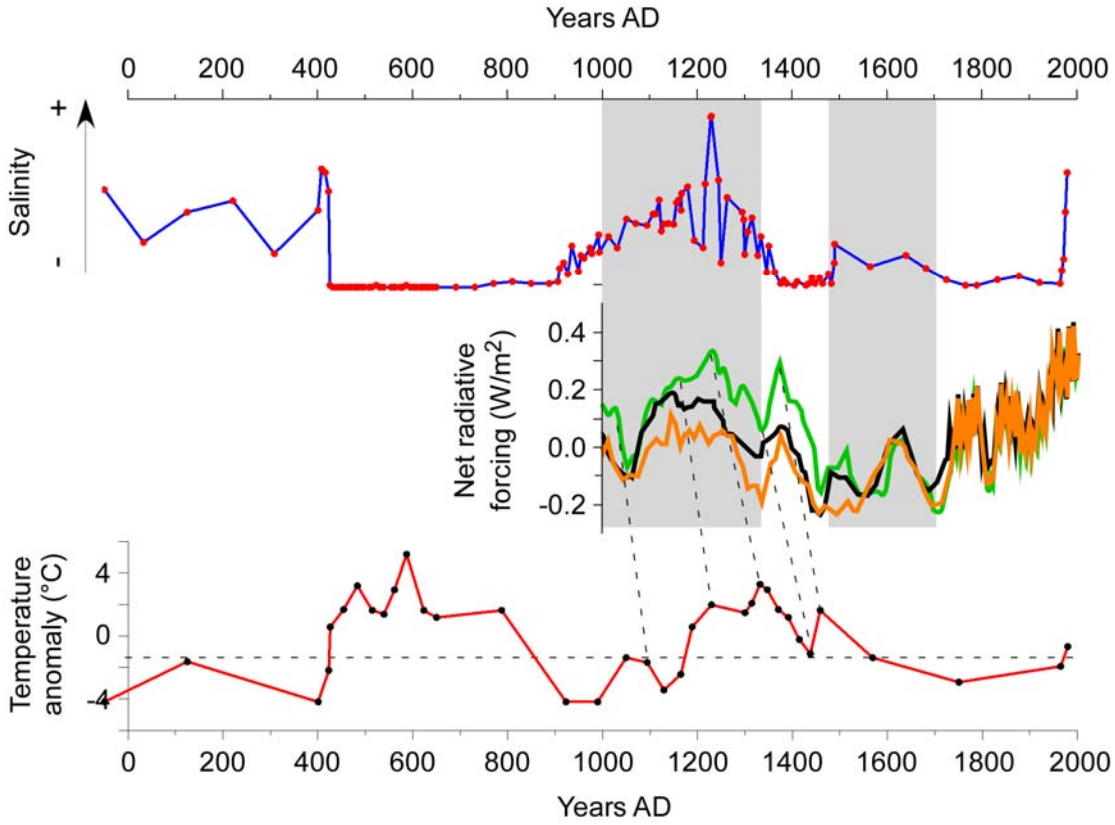

Figure 6.3: *Comparison of salinity change (blue curve) in the Aral Sea and temperature deviations (T°C, red curve) in the Aral Sea Basin with different reconstructions of solar activity during the past 1000 years. The three different reconstructions of solar activity are based on ^{10}Be measurements (Bard et al., 1997) (black), ^{14}C residuals (Stuiver and Braziunas, 1993) (orange) and calculated ^{14}C change based on ^{10}Be variations (Bard et al., 2000) (green) (modified after Crowley (2000). Shadings represent correlation between the salinity record and solar activity during 1000–1300 AD, 1450–1550 and 1600–1700 AD. Dashed lines represent correlation lines between temperature deviations in the Aral Sea Basin and the solar activity.*

In other words, though climate dynamics primarily controlled salinity and lake level changes through variation in meltwater discharges, it is likely that solar activity played a significant role on the Aral Sea's hydrological balance during periods of regressions over the past millennium. In contrast, during periods of higher lake levels, the hydrological balance of the lake was probably mostly determined by interactions and feedbacks between all active systems, whereas the impact of variations in solar activity was considerably weakened. Therefore, during intervals with higher precipitation averages, a coeval increase in air humidity would have lowered evaporation rates even when temperature is high, as during 1300–1400 AD. On the basis of the correlation drawn for the time interval 1000–2000 AD, the prolonged regression recorded during ca. 0–400 AD suggests that the intensity of the

radiative forcing might have been higher at that time, judging from the salinity increase inferred by dinoflagellate cyst assemblages and archaeological findings. This is concurrent with the reconstruction of Solanki et al. (2004) based on sunspot numbers, who reported high levels of solar activity around 0 AD.

In order to examinate how much external forcing is possible on terrestrial environmental change and climate variability we compare temperature deviations from mean annual values in the Aral Sea Basin (performed using the "probability mutual climatic spheres" method, Chapter IV) with variations in solar activity during the past 1000 years (Fig. 6.3). Although correlation is impossible between 1550 and 2000 AD due to the low-resolution of our reconstruction within this time interval, there is a rather good-match of long-term temperature variability in western Central Asia and the ^{10}Be and $\delta^{14}C$ solar intensity proxies during 1000–1500 AD. However, this correlation is not unequivocal and it is obvious that offsets of about 80 to 100 years are implied between the solar activity record and our temperature deviation curve, which are difficult to undertand yet. Nonetheless, it is likely that variation in solar activity act as a primary forcing mechanism of centennial temperature variability in western Central Asia at the beginning of the past millenium. We might expect this link to be more pronounced during summer when the radiative forcing is considerably enhanced in Central Asia (Fig. 1.4d) and result in a significant rise of air temperature (up to 52°C during July in the eastern Kara Kum (Lioubimtseva et al., 2005)).

Chapter VII: Concluding remarks

Given the long and high-quality coring from the Aral Sea, this thesis, based on a multidisciplinary approach, provides for the first time the chance to document facts on past environmental and climate variability in western Central Asia during the late Holocene, at a high time-resolution. Though human activities (irrigation, military conflicts) are likely to have moderately influenced the hydrology in this region, environmental change is ultimately linked to climate variability which is predominantly controlled by interaction between different climate mechanisms. The Siberian High is the dominant spring feature controlling temperature gradients and wind dynamics in western Central Asia, thus influencing the intensity of detrital input blown by the storms. Besides, the Aral Sea Basin's hydrological budget is basically regulated by the Westerlies and the Eastern Mediterranean cyclonic system. While the latter provides the moisture which falls as rain over Central Asia during late winter and early spring, the Westerlies are the main source of humidity to the montane regions (Tien Shan and Pamir) where melting glaciers and snowfields feed the Amu Darya and the Syr Darya rivers during the late spring and early summer season. In turn, the amplitude of the contribution in glacial meltwater inputs into the Aral Sea is largely controlled by temperature contrasts between the seasons in these montane regions, and has thus a primary impact on the Aral Sea's lake levels.

In addition, it is likely that external forcing has a significant imprint on environmental and climatic changes in this vast arid area. The solar activity's increase during the Middle Age is likely to have driven elevated annual temperatures over Central Asia, thus casting new perspectives for future work. Moreover, compelling evidence shows that non-linear relationships exist between salinity levels and variation in solar activity when the hydrological balance is negative. Hence, a higher radiative forcing may have strengthened Aral Sea's regressions in the past. A corollary pertinent to present-day concerns is that increased solar activity would amplify the modern regression, even if the lake level at the time of writing (30.24 m.a.s.l.; Zavialov, personal communication) has not reached yet the level of the Middle Age.

Outlook

This work provides ground truth data for modelling studies, which are required to broaden our understanding of the interactions which regulate the climatology of Central Asia.

Nonetheless, throughout this thesis, only a restricted number of these interactions have been evaluated, and the genuine role of dominant modes of climate variability such as the ENSO, the NAO or the AO is still confined to speculations. In order to improve the assessment of their respective impact on climate variability in Central Asia, further climate proxy data are required. Forthcoming analyses would consist in extracting new cores from different lakes in the montane regions with the aim to quantify the impact of the Westerlies transporting humidity through Eurasia on their hydrological balance. Future work would also deal with investigating the impact of the SW Indian summer monsoon over this region, even if its influence in the Aral Sea Basin is probably considerably weakened due to surrounding blocking mountain ranges (Létolle & Mainguet, 1993).

Finally, it would be essential to extend the existing station data network and reanalyses of climate state variables in western Central Asia further back in time, which would allow to propose quantified spatial climate-field reconstructions for this region (Fig. 7.1). This would then offer the perspective to detect the main seasonal patterns of atmospheric variability over the region, to define climate regimes, and to identify other teleconnections with remote climate modes.

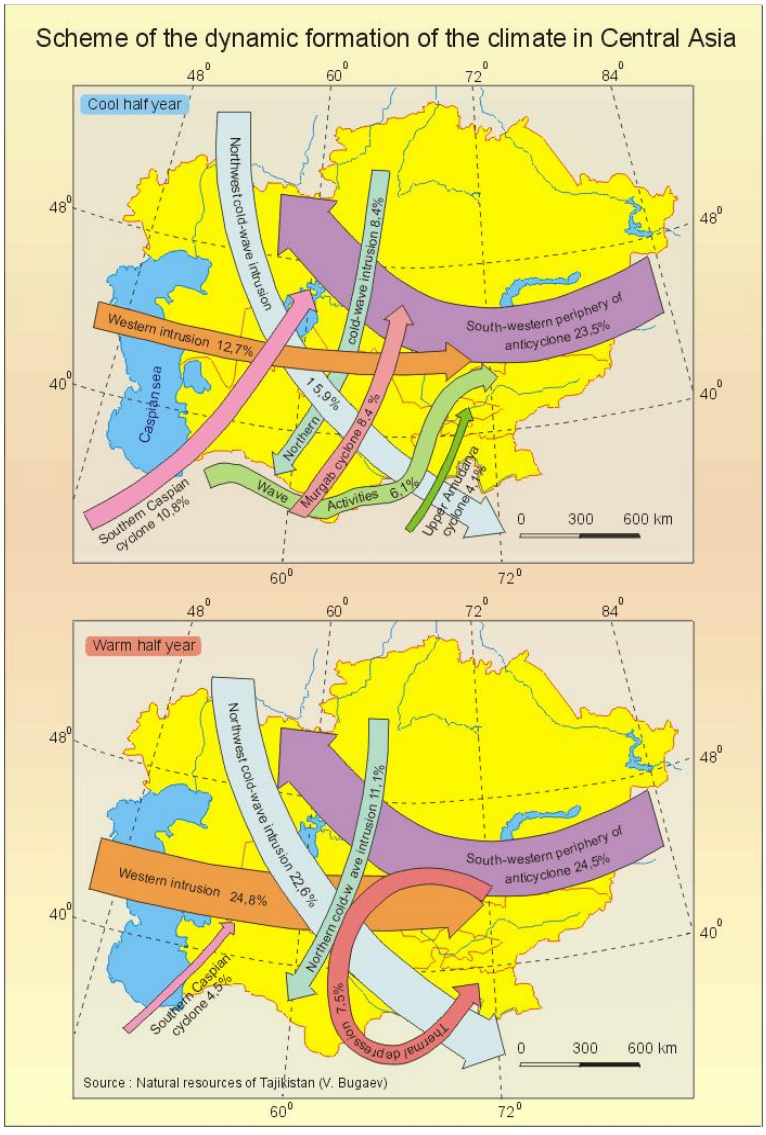

Fig. 7.1: *Present-day atmospheric dynamics of different meteorological systems for winter and summer times in Central Asia (Kyrghysian Meteorological Station), though the influencing factors are not well understood yet.*

References (not cited elsewhere)

Agrawala, S., Barlow, M., Cullen, H., Lyon, B., 2001. The drought and humanitarian crisis in Central and Southwest Asia: a climate perspective. IRI Special Report 01.11, 2001. International Research Institute for Climate Prediction, USA, 24 pp.

Aladin, N.V., Plotnikov, I.S., 1995. Izmenenie urovinia Aral'skogo morja: Paleolimnologicheskie I arkheologicheskie dokazatel'stva. In: Biologicheskie I prirodovedcheskie problemy Aral'skogo moria I Priaral'ia, part 1 (pp. 17–46). Trudy Zoologicheskogo institute RAN 262. Sankt-Peterburg, Nauka.

Aleshinskaya, Z.G., 1991. Diatom and palynological characteristics of bottom sediments. In: Sevastyanov, D.V. (Ed.), History of lakes Sevan, Issyk-Kul, Balkhash, Zaisan and Aral, Russian Academy of Sciences, Leningrad, pp. 245–253. (in russian).

Alpert, P., Reisin, T., 1986. An early winter polar air mass penetration to the eastern Mediterranean. Monthly Weather Review 114, 1411–1418.

Alpert, P., Neeman, B.U., Shay-El, Y., 1990a. Intermonthly variability of cyclone tracks in the Mediterranean. Journal of Climate 3, 1474–1478.

Appenzeller, C., Stocker, T.F., Anklin, M., 1998. North Atlantic Oscillation dynamics in Greenland ice cores. Science 282, 446–449.

Appleby, P.G., 1997. Sediment records of fall-out radionuclids and their application to studies of sediment-water interactions. Water, Air and Soil Pollution 99, pp. 573–586.

Aral'skij krizis, 1991. Aral'skij krizis (Istoriki-geograficheskaia retrospektiva). Moskva, Nauka.

Bard, E., Raisbeck, G.M., Yiou, F., Jouzel, J., 1997. Solar modulation of cosmogenic nuclide production over the last millennium: comparison between ^{14}C and ^{10}Be records. Earth and Planetary Science Letters 150, 435–462.

Bard, E., Raisbeck, G.M., Yiou, F., Jouzel, J., 2000. Solar irradiance during the last 1200 years based on cosmogenic nuclides. Tellus B 52, 985–993.

Ben-Gai, T., Bitan, A., Manes, A., Alpert, P., Kushnir, Y., 2001. Temperature and surface pressure anomalies in Israel and the North Atlantic Oscillation. Theoretical and Applied Climatology 69, 171–177.

Berner, R.A., 1980. Early diagenesis – a theoretical approach. Princeton University Press, Oxford, 241 pp.

Bodwaker, S.V., 1996. Nondestructive characterization of core porosity and lithology using Gamma-rays. Unpublished PhD dissertation, University of Texas, Austin, 246 pp.

Briffa, K.R., Osborn, T.J., Schweingruber, F.H., Harris, I.C., Jones, P.D., Shiyatov, S.G., Vaganov, E.A., 2001. Low-frequency temperature variations from a northern tree-ring density network. Journal of Geophysical Research 106, 2929–2941.

Briffa, K.R., Osborn, T.J., Schweingruber, F.H., Jones, P.D., Shiyatov, S.G., Vaganov, E.A., 2002. Tree-ring width and density data around the Northern Hemisphere: Part 2, spatio temporal variability and associated climate patterns. The Holocene 12 (6), 759–789.

Brooks, J., Shaw, G., 1968. Chemical nature of the exine of pollen walls and a new function for carotenoids in nature. In: Muir, M.D., Sarjeant, W.A.S., (Eds.), 1977. Palynology Part I: Spores and pollen. Dowden, Hutchinson & Ross, Inc, United Kingdom, 383 pp.

Buckland, P.C., Amorosi, T., Barlow, L.K., Dugmore, A.J., Mayewski, P.A., McGovern, T.H., Ogilvie, A.E.J., Sadler, J.P., Skidmore, P., 1995. Bioarchaeological evidence and climatological evidence for the fate of Norse farmers in medieval Greenland. Antiquity 70, 88–96.

Büntgen, U., Esper, J., Frank, D.C., Nicolussi, K., Schmidhalter, M., 2005. A 1052-year tree-ring proxy for Alpine summer temperatures. Climate dynamics 25, 141–153.

Casty, C., Wanner, H., Luterbacher, J., Esper, J., Böhm, R., 2005a. Temperature and precipitation variability in the European Alps since 1500. International Journal of Climatology 25, 1855–1880.

Casty, C., Handorf, D., Raible, C.C., González-Rouco, F.J., Weishemer, A., Xoplaki, E., Luterbacher, J., Dethloff, K., Wanner, H., 2005b. Recurrent climate winter regimes in reconstructed and modelled 500h Pa geopotential height fields over the North Atlantic / European sector 1659–1990. Climate Dynamics 24, 809–822.

Casty, C., Handorf, D., Sempf, M., 2005c. Combined climate winter regimes over the North Atlantic / European sector 1766–2000. Geophysical Research Letters 32, LI13801, DOI, 10.129/2005GL022431.

Chang, J.-H., 1972. *Atmospheric Circulation Systems and Climate.* Oriental Publishing, 326 pp.

Cohen, J., Entekhabi, D., 1999. Eurasian snow cover variability and Northern Hemisphere climate predictability. Geophysical Research Letters 26, 345–348.

Crowley, T.J., Lowery, T., 2000. How warm was the Medieval Warm Period? Ambio 29, 51–54.

Cullen, H.M., de Menocal, P., 2000. North Atlantic influence on Tigris–Euphrates streamflow. International Journal of Climatology 20, 853–863.

Cullen, H.M., Kaplan, A., Arkin, P.A., de Menocal, P.B., 2002. Impact of the North Atlantic Oscillation on Middle Eastern climate and streamflow. Climatic Change 55, 315–338.
Dale, B., Dale, A., 2002. Environmental applications on dinoflagellate cysts and acritarchs. In: Haslett, S.K. (Eds.), Quaternary Environmental Micropalaeontology. Arnold, London, UK, pp. 207–240.
de Menocal, P.B., 2001. Cultural responses to climate change during the late Holocene. Science 292, 667–673.
Diaz, H.F., Hoerling,M.P., Eischeid, J.K., 2001. ENSO variability, teleconnections and climate change. International Journal of Climatology 21, 1845–1862.
Erdtmann, G., 1966. Pollen morphology and plant taxonomy. Angiosperms: an introduction to palynology. Almqvist and Viksell, 12, 539 pp.
Eshel, G., Farrell, C.M., Farrell, B.F., 2000. 'Forecasting Eastern Mediterranean droughts'. Monthly Weather Review 128, 3618–3630.
Eshel, G., Farrell, B.F., 2001. Thermodynamics of Eastern Mediterranean rainfall variability. Journal of the Atmospheric Sciences 58, 87–92.Ben-Gai, T., Bitan, A., Manes, A., Alpert, P., Kushnir, Y., 2001. Temperature and surface pressure anomalies in Israel and the North Atlantic Oscillation. Theoretical Applied Climatology 69, 171–177.
Eshel, G., 2002. Mediterranean climates. Israel Journal of Earth Sciences 51, 157–168.
Esper, J., 2000. Long-term tree-ring variations in *Juniperus* at the upper timber-line in the Karakorum (Pakistan). The Holocene 10 (2), 253–260.
Esper, J., Cook, E.R., Schweingruber, F.H., 2002a. Low-frequency signals in long tree-ring chronologies for reconstructing past temperature variability. Science 295, 2250–2253.
Esper, J., Schweingruber, F.H., Winiger, M., 2002b. 1300 years of climate history for Western Central Asia inferred from tree-rings. Holocene 12, 267–277.
Esper, J., Shiyatov, S.G., Mazepa, V.S., Wilson, R.J.S., Graybill, D.A., Funkhouser, G., 2003. Temperature-sensitive Tien Shan tree ring chronologies show multi-centennial growth trends. Climate Dynamics 21, 699–706.
Fensome, R.A., Taylor, F.J.R., Norris, G., Sarjeant, W.A.S., Wharton, D.I, Williams, G.L., 1993. A Classification of Living and Fossil Dinoflagellates. American Museum of Natural History, Micropaleontology, Special Publication Number 7, 351 pp.
Ferronskii, V.I., Polyakov, V.A., Brezgunov, V.S., Vlasova, L.S., Karpychev, Y.A., Bobkov, A.F., Romaniovskii, V.V., Johnson, T., Ricketts, D., Rasmussen, K., 2003. Variations in the hydrological regime of Kara-Bogaz-Gol Gulf, the lake Issyk-Kul and the Aral Sea assessed based on data of bottom sediment studies. Water resources and the regime of water regimes 30 (3), 252–259.
Folland, C.K., Karl, T.R., Christy, J.R., Clarke, R.A., Gruza, G.V., Jouzel, J., Man, M.E., Oerlemans, J., Salinger, M.J., Wang, S.-W., 2001. Observed climate variability and change. In: Houghton et al., (Eds.), Climate change 2001: the scientific basis. Cambridge University Press, New York, pp. 99–181.
Gillett, N.P., Zwiers, F.W., Weaver, A.J., Scott, P.A., 2003. Detection of human influence on sea-level pressure. Nature 422, 292–294.
Hansen, J.I., Fung, A., Lacis, D., Rind, S., Lebedeff, R., Ruedy, B., Russell, G., 1988. Global climate change as forecast by Goddard Institute for Space Studies three-dimensional model. Journal of Geophysical Research 93, 9341–9364.
Hantemirov, R.M., Shiyatov, S.G., 2002. A continuous multimillennial ring-width chronology in Yamal, northwestern Siberia. The Holocene 12 (6), 717–726.
Haug, G.H., Günther, D., Peterson, L.C., Sigman, D.M., Hughen, K.A., Aeschlimann, B., 2003. Climate and the collapse of Maya civilization. Science 299, 1731–1735.
Head, M.J., 1996. Modern dinoflagellates cysts and their biological affinities. In: Jansonius, J., Mc Gregor, D.C. (Eds.), Palynology: Principles and applications, volume 3. American Association of Stratigraphic Palynologists Foundation, Dallas, TX, pp. 1197–1248.
Hurrell, J.W., 1996. Influence of variations in extratropical wintertime teleconnections on Northern Hemisphere temperature. Geophysical Research Letters 23 (6), 665–668.
Hurrell, J.W., van Loon, H., 1997. Decadal variations in climate associated with the North Atlantic Oscillation. Climate Change 36, 301–326.
Hurrell, J.W., Kushnir, Y., Visbeck, M., 2001. The North Atlantic Oscillation. Science 291, 603–605.
Jacobeit, J., Wanner, H., Luterbacher, J., Beck, C., Philipp, A., Sturm, K., 2003. Atmospheric circulation variability in the North-Atlantic-European area since the mid-seventeenth century. Climate Dynamics 20, 341–352.
Jarsjö, J., Destouni, G., 2004. Groundwater discharge into the Aral Sea after 1960. Journal of marine systems 47 1/4, 109–120.
Jenkins, R., 1999. X-Ray fluorescence spectrometry (2nd edition). Wiley, New-York, 232 pp.

Jones, P.D., Briffa, K.R., Barnett, P., Tett, S.F.B., 1998. High-resolution palaeoclimatic records for the last millennium: Interpretation, integration and comparison with General Circulation Model control-run temperatures. The Holocene 8, 455–471.

Jones, P.D., Osborn, T.J., Briffa, K.B., 2001. The evolution of climate over the last millennium. Science 292, 662–667.

Kadioğlu, M., Tulunay, Y., Borhan,Y., 1999. Variability of Turkish precipitation compared to El Niño events. Geophysical Research Letters 26, 1597–1600.

Kahana, R., Ziv, B., Enzel, Y., Dayan, U., 2002. Synoptic climatology of major floods in the Negev desert, Israel. International Journal of Climatology 22, 867–882.

Kahya, E., Karabörk, M.C., 2001. The analysis of El Niño and La Niña signals in streamflows of Turkey. International Journal of Climatology 21, 1231–1250.

Kallos, G., Metaxas, A., 1980. Synoptic processes for the formation of Cyprus lows. Rivista di Meteorologia Aeronautica 40 (2–3), 121–138.

Kalnay, E., Kana Mitsu, M., Kistler, R., et al., 1996. The NCEP/NCAR 40-year reanalysis project. Bulletin of the American Meteorological Society 77 (3), 437–471.

Karaca, M., Deniz, A., Tayanç, M., 2000. Cyclone track variability over Turkey in association with regional climate. International Journal of Climatology 20, 1225–1236.

Katsoulis, B.D., 1980. Climatic and synoptic considerations of the Mediterranean depressions developing and passing over or near the Balkan Peninsula. In: Proceedings of the 1st Hellenic–British Climatological Congress. Hellenic Meteorological Society, Athens, pp. 73–84.

Kelts, K., 1978. Geological and sedimentary evolution of lakes Zürich and Zug, Switzerland. PhD thesis, Eidgenössischen Technischen Hochschule Zürich, Zürich (Switzerland), 250 pp.

Kiladis, G.N., Diaz, H.F., 1989. Global climate anomalies associated with extremes in the Southern Oscillation. Journal of Climate 2, 1069–1090.

Kistler, R., Kalnay, E., Collins, W. et al., 2001. The NCEP/NCAR 50-year reanalysis: monthly means CD-ROM and documentation. Bulletin of the American Meteorological Society 82 (2), 247–267.

Le Callonec, L., Person, A., Renard, R., Létolle, R., Nebout, N., Ben Khelifa, L., Rubanov, I., 2005. Preliminary data on chemical changes in the Aral Sea during low-levels periods from the last 9000 years. Compte Rendus Geosciences (in press).

Létolle, R., Mainguet, M., 1996. Der Aral See. Eine ökologische Katastrophe. Berlin, Heidelberg, New York, Springer Verlag.

Létolle, R., Aladin, N., Filipov, I., Boroffka, N.G.O., 2005. The future chemical evolution of the Aral Sea from 2000 to years 2050. Mitigation and Adaptation Strategies for Global Change 10, 51–70.

Luterbacher, J., Rickli, R., Xoplaki, E., Tinguely, C., Beck, C., Pfister, C., Wanner, H., 2001. The Late Maunder Minimum (1675–1715) – A key period for studying decadal-scale climatic change in Europe. Climatic Change 49, 441–462.

Luterbacher, J., Xoplaki, E., Dietrich, D., Jones, P.D., Davies, T.D., Portis, D., González-Rouco, J.F., von Storch, H., Gyalistras, D., Casty, C., Wanner, H., 2002. Extending North Atlantic Oscillation reconstructions back to 1500. Atmospheric Science Letters 2, 114–124.

Luterbacher, J., Dietrich, D., Xoplaki, E., Grosjean, M., Wanner, H., 2004. European seasonal and annual temperature variability, trends, and extremes since 1500. Science 303, 1499–1503.

Lydolf, P.E., 1977. Climates of the Soviet Union. Elsevier, 443 pp.

Mac Donald, R.W., Harner, T., Fyfe, J., 2005. Recent climate change in the Arctic and its impact on contaminant pathways an interpretation of temporal trend data. Science of the Total Environment 342, 5–86.

Maev, E.G., Maeva, S.A., 1991. Bottom sediments of the Aral. In: Sevastyanov, D.V. (Ed.), History of lakes Sevan, Issyk-Kul, Balkhash, Zaisan and Aral, Russian Academy of Sciences, Leningrad, pp. 239–242. (in russian).

Maheras, P., 1983a. Les types de temps dépressionnaires perturbés au dessus de la mer d'Egée. Rivista di Meteorologia Aeronautica 43 (1–2), 13–22.

Maheras, P., 1983b. Les visages cycloniques des saisons et des mois au dessus de la mer d'Egée. Rivista di Meteorologia Aeronautica 43 (1–2), 23–30.

Maheras, P., Flocas, H.A., Patrikas, I., Anagnostopoulou, C., 2001. A 40-year objective climatology of surface cyclones in the Mediterranean region: spatial and temporal distribution. International Journal of Climatology 21, 109–130.

Mann, M.E., Bradley, R.S., Hughes, M.K., 1998. Global-scale temperature patterns and climate forcing over the past six centuries. Nature 392, 779–787.

Mann, M.E., Bradley, R.S., Hughes, M.K., 1999. Northern hemisphere temperatures during the past Millenium: Inferences, uncertainties and limitations. Geophysical Research Letters 26 (6), 759–762.

Mann, M.E., 2002. Large-scale climate variability and connections with the Middle East in the past. Climatic Change 55, 287–314.

Matthiessen, J., de Vernal, A. (Eds.), 2001. Dinoflagellate cysts and paleoceanography of high latitude marine environments. Journal of Quaternary Science (Special Issue) 16 (7), 595–751.
Micklin, P.P., Williams, W.D. (Eds.), 1996. The Aral Sea Basin. NATO Advanced Science Institute Series, Partnership Sub-Series 2, Environment 12. Berlin, Springer Verlag.
Moberg, A., Sonechkin, D.M., Holmgren, K., Datsenko, N.M., Karlén, W., 2005. Highly variable northern temperatures reconstructed from low- and high-resolution proxy data. Nature 433, 613–617.
Mokhov, I.I., Petukhov, V.K., 1999. Atmospheric centers of action and tendencies of their change. Izv. Acad. Sci. USSR, Atmos. Oceanic Phys. 36, 292–299.
Naurzbaev, M.N., Vaganov, E.A., Sidorova, O.V., Schweingruber, F.H., 2002. Summer temperatures in eastern Taimyr inferred from a 2427-year late Holocene tree-ring chronology and earlier floating series. The Holocene 12 (6), 727–736.
Neronov, V.V., 1997. Landscapes features of century changes in wetting of south-eastern Turkmenistan. Arid Ecosystems 3 (6–7), 141–150 (in Russian with summary in English).
Nowaczyk, N.R., 2001. Logging of magnetic susceptibility. In: Last, W.M., Smol, J.P. (Eds.), Tracking environmental change using lake sediments: Physical and chemical techniques, vol. 1. Kluwer Academic Publishers, Dordrecht, pp. 155–170.
Overpeck, J.K., Hughen, K., Hardy, D., Bradley, R., Case, R., Douglas, M., Finney, B., Gajewski, K., Jacoby, G., Jennings, A., Lamoureux, S., Lasca, A., Moore, G.M.J., Retelle, M., Smith, S., Wolfe, A., Zielinski, G., 1997. Arctic environmental change of the last four centuries. Science 278, 1251–1256.
Pauling, A., Luterbacher, J., Casty, C., Wanner, H., 2005. Five hundred years of gridded high-resolution precipitation reconstructions over Europe and the connection to large-scale circulation. Climate Dynamics, DOI: 10.1007/s00382-005-0090-8.
Pfister, C., 1999. Wetternachherage. 500 Jahre Klimavariationen und Naturkatasrophen, 1496–1995. Paul Haupt, Bern, Switzerland.
Price, C., Stone, L., Huppert, A., Rajagopalan, B., Alpert, P., 1988. A possible link between El Niño and precipitation in Israel. Geophysical Research Letters 25, 3963–3966.
Rimbu, N., Lohmann, G., Felis, T., Pätzold, J., 2001. Arctic Oscillation signature in a Red Sea coral. Geophysical Research Letters 28 (15), 2959–2962.
Röhl, U., Abrams, L.J., 2000. High-resolution, downhole, and non-destructive core measurements from Sites 999 and 1001 in the Caribbean Sea: application to the Late Paleocene Thermal Maximum. In: Leckie, R.M., Sigurdson, H., Acton, G.D., Draper, H. (Eds.), Proc. ODP, Sci. Res., vol. 165, Ocean Drilling Program, College Station, TX, pp. 191–203.
Rooley, J.R., Southworth, D., 1967. Deposition of sporopollenin on lamellae of unit membrane dimensions. In: Muir, M.D., Sarjeant, W.A.S., (Eds.), 1977. Palynology Part I: Spores and pollen. Dowden, Hutchinson & Ross, Inc, United Kingdom, 383 pp.
Serreze, M.C., Walsh, J.E., Chapin III, F.S., Osterkamp, T., Dyurgerov, M., Romanovsky, V., Oechel, W.C., Morison, J., Zhang, T., Barry, R.G., 2000. Observational evidence of recent change in the Northern high-latitude environment. Climatic Change 46, 159–207.
Shermatov, E., Nurtaev, B., Muhamedgalieva, U., Shermatov, U., 2004. Analysis of water resources variability of the Caspian and the Aral sea basins on the basis of solar activity. Journal of Marine Systems 47, 137–142.
Slonosky, V.C., Jones, P.D., Davies, T.D., 2000. Variability of the surface atmospheric circulation over Europe, 1774–1995. International Journal of Climatology 20, 1875–1897.
Slonosky, V.C., Jones, P.D., Davies, T.D., 2001. Atmospheric circulation and surface temperature in Europe from the 18th century to 1995. International Journal of Climatology 21, 63–75.
Snowball, I., 1993. Mineral magnetic properties of Holocene lake sediments and soils from the Karsa valley, Lappland, Sweden, and their relevance to palaeoenvironmental reconstruction. Terra Nova 5, 258–270.
Solanki, S.K., Usoskin, I.G., Kromer, B., Schüssler, M., Beer, J., 2004. Unusual activity of the Sun during recent decades compared to the previous 11,000 years. Nature 431, 1084–1087.
Stuiver, M., Braziunas, T.F., 1993. Modeling atmospheric ^{14}C influences and ^{14}C ages of marine samples to 10,000 BC. In: Stuiver, M., Long, A., Kra, R.S. (Eds.), Calibration1993. Radiocarbon 35 (1) , 137–189.
Takaya, K., Nakamura, H., 2004. Intra-seasonal amplification of the Siberian High. Geophysical Research Abstracts, vol. 6, 06248.
Tayanç, M., Karaca, M., Dalfes, H.M., 1997. March 1987 cyclone (blizzard) over the Eastern Mediterranean and Balkan region associated with blocking. Monthly Weather Review 126, 3036–3047.
Thompson, R., Battarbee, R.W., O'Sullivan, P.E., Oldfield, F., 1975. Magnetic susceptibility of lake sediments. Limnology and Oceanography 20, 687–698.
Thompson, D.W.J., Wallace, J.M., 1998. The Arctic Oscillation signature in the wintertime geopotential height and temperature fields. Geophysical Research Letters 25, 1297–1300.
Thompson, D.W.J., Wallace, J.M., 2000. Annular modes in the extratropical circulation Part I. Month-to-month variability. Journal of Climate 15, 1000–1016.

Thompson, D.W.J., Lee, S., Baldwin, M.P., 2003. Atmospheric processes governing the Northern Hemisphere Annular Mode / North Atlantic Oscillation. In: Hurrell, J.W., Kushnir, Y., Ottersen, G., Visbeck, M., (Eds.), The North Atlantic Oscillation: Climate significance and environmental impact. Geophysical Monograph Series 134. Washington DC, 81–112.

Tolstov, S.P., 1962. Po drevnim del'tam Oksa I Jaksarta. Moscow: Vostochnaja Literatura.

Touchan, R., Garfin, G.M., Meko, D.M., Funkhouser, G., Erkan, N., Hughes, M.K., Wallin, B.S., 2003. Preliminary reconstructions of spring precipitation in southwestern Turkey from tree-ring width. International Journal of Climatology 23, 157–171.

Trenberth, K.E., Branstator, G.W., Karoly, D., Kumar, A., Lau, N.C., Ropelewski, C., 1998. Progress during TOGA in understanding and modeling global teleconnections associated with tropical sea surface temperatures. Journal of Geophysical Research 103, 14291–14324.

Tsvetsinskaya, E.A., Vainberg, B.I., Glushko, E.V., 2002. An integrated assessment of landscape evolution, long-term climate variability, and land use in the Amu Darya Prisarykamish delta. Jouranl of Arid Environments 51, 363–381.

Ulbrich, U., Christoph, 1999. A shift of the NAO and increasing storm track activity over Europe due to anthropogenic greenhouse gas forcing. Climate Dynamics 15, 551–559.

Ulbrich, U., Christoph, M., Pinto, J.G., Corte-Real, J., 1999. Dependance of winter precipitation over Portugal on NAO and baroclinic wave activity. International Journal of Climatology 19, 379–390.

Verosub, K.L., Roberts, A.P., 1995. Environmental magnetism: past, present and future. Journal of Geophysical Research 100 (No. B2), 2175–2192.

von Storch, H., Zorita, E., Jones, J.M., Dimitriev, Y., González-Rouco, F.J., Tett, S.F.B., 2004. Reconstructing past climate from noisy data. Science 306, 679–682.

Wall, D., Dale, B., Lohman, G.P., Smith, W.K., 1977. The environmental and climatic distribution of dinoflagellate cysts in modern sediments from regions in the North and South Atlantic oceans and adjacent seas. Marine Micropaleontology 2, 121–200.

Wallace, J.M., Thompson, D.W.J., 2002. Annular modes and climate prediction. Physics Today, 28–33 [February].

Wanner, H., Brönnimann, S., Casty, C., Gyalistras, D., Luterbacher, J., Schmutz, C., Stephenson, D.B., Xoplaki, E., 2001. North Atlantic Oscillation – concept and studies. Survey in Geophysics 22, 321–381.

Wigley, T.M.L., Farmer, G., 1982. Climate of the Eastern Mediterranean and the Near East. In: Bintliff, J.L., Van Zeist, W. (Eds.), *Palaeoclimates, Palaeoenvironments and Human Communities in the Eastern Mediterranean Region in Later Prehistory,* B.A.R. International Series 133, British Archaeological Reports, pp. 3–37.

Williamson, D., Jelinowska, A., Kissel, C., Tucholka, P., Gilbert, E., Gasse, F., Massault, M., Taieb, M., Van Campo, E., Wieckowski, K., 1998. Mineral-magnetic proxies of erosion / oxidation cycles in tropical maar-lake sediments (Lake Tritrivakely, Madagascar): palaeoenvironmental implications. Earth and Planetary Science Letters 155, 205–219.

Xoplaki, E., González-Rouco, J.F., Luterbacher, J., Wanner, H., 2004. Wet season Mediterranean precipitation variability: influence of large-scale dynamics and trends. Climate Dynamics 23, 63–78.

Ziv, B., Dayan, U., Kushnir, Y., Roth, C., Enzel, Y., 2006. Regional and global atmospheric patterns governing rainfall in the southern Levant. International Journal of Climatology 26, 55–73.